PUBLISHED PAPERS IN RADIO AND SPACE PHYSICS

R.L. Dowden

submitted for the degree of
Doctor of Science at the
University of Tasmania.

PREFACE

The 34 published works (papers, notes and letters, all referred to here as "papers") presented here span a period of 16 years and four main topics or fields in radio and space physics:

Papers 1, 2	:	Ionospheric and related studies.
Papers 3-17, 28-34	:	VLF electron-cyclotron mode ("whistler mode") propagation and emission in the magnetosphere (called the "exosphere" in the earlier work).
Papers 18-20	:	Jupiter emission and related work.
Papers 21-27	:	Proton-cyclotron mode (variously called "micropulsation mode", "ordinary mode" and "hydromagnetic") propagation and emission in the magnetosphere.

The order of presentation and listing is chronological with two exceptions (papers 17 and 20) to provide a more logical grouping. The "early" (3-17) and "late" (28-34) VLF papers are separated by an eight-year gap.

The 30 papers for which I am the sole author are entirely my own work apart from help detailed in the *Acknowledgements* in each paper. Four other papers have a second author contributing in varying degrees. Mr Goldstone assisted in recording the event discussed in paper 3. Mr Emery assisted in data analysis in paper 22 and in construction of the device described in paper 23. Mr Allcock invented the basis of the technique described in paper 32. Papers for which I am not the senior author, or which have multiple authorship, have been omitted from this collection.

To the best of my knowledge, all 34 papers describe only original research except where specific reference is made in these papers to the work of others, and none of this work has been previously submitted for the purposes of the degree of Doctor of Science.

Richard L. Dowden
15 March 1974

PUBLISHED WORKS

1. R.L. Dowden, "Short-range echoes observed on ionospheric recorders", *J.Atmos.Terr.Phys.* 11, 111-117, (1957).

2. R.L. Dowden, "Ionospheric thermal radiation at radio-frequencies in the auroral zone" *J.Atmos.Terr.Phys.* 18, 8-19, (1960).

---

3. R.L. Dowden and G.T. Goldstone, "'Whistler-mode' echoes remote from the conjugate point", *Nature,* 183, 385-386, (1959).

4. R.L. Dowden, "L.F. Radio noise from the aurora", *Nature,* 184, 803 (1959).

5. R.L. Dowden, "Geomagnetic noise at 230 kc/s", *Nature,* 187, 677-678 (1960).

6. R.L. Dowden, "A theoretical model of electron density along a geomagnetic line of force in the exosphere", *J.Atmos.Terr.Phys.* 20, 122-130 (1961).

7. R.L. Dowden, "Simultaneous observations of V.L.F. noise ('hiss') at Hobart and Macquarie Island", *J. Geophys.Res.* 66, 1587-1588 (1961).

8. R.L. Dowden, "Wide band bursts of V.L.F. radio noise ('hiss') at Hobart", *Australian J.Phys.* 15, 114-119 (1962).

9. R.L. Dowden, "Doppler shifted cyclotron radiation from electrons: a theory of V.L.F. emissions", *J.Geophys.Res.* 67, 1745-1750 (1962).

10. R.L. Dowden, "Theory of generation of exospheric V.L.F. noise ('hiss')", *J.Geophys.Res.* 67, 2223-2230 (1962).

11. R.L. Dowden, "'Scale frequency' of the exosphere", *Nature,* 195, 984-985 (1962).

12. R.L. Dowden, "Cyclotron theory of V.L.F. discrete emissions", *Nature,* 195, 1085-1086 (1962).

13. R.L. Dowden, "Very-low-frequency discrete emissions received at conjugate points", *Nature,* 195, 64 (1962).

14. R.L. Dowden, "Authors reply to the preceding discussion" (of paper 9) *J.Geophys.Res.* 67, 4900-4902 (1962).

15. R.L. Dowden, "Method of measurement of electron energies and other data from spectrograms of V.L.F. emissions" *Australian J.Phys.* 15, 490-503 (1962).

16. R.L. Dowden, "Doppler shifted cyclotron generation of exospheric V.L.F. noise ('hiss')", *Plant.Space Sci.*, 11, 361-369 (1963).

17. R.L. Dowden, "Effect of Magnetic Anomalies on V.L.F. discrete emissions", *Australian J.Phys.* 16, 588-92 (1963).

---

18. R.L. Dowden, "A minimum reading phase sensitive detector", *Proc.I.R.E.* 51, 231 (1963).

19. R.L. Dowden, "Polarization measurements of Jupiter radio bursts", *Aust.J.Phys.* 16, 398-410 (1963).

20. R.L. Dowden, "A Jupiter model of pulsars", *Proc.Astron.Soc. Aust.* 1, 4, 159 (1968).

---

21. R.L. Dowden, "'Micropulsation mode' propagation in the magnetosphere", *Planet.Space Sci.* 13, 761-772 (1965).

22. R.L. Dowden and M.W. Emery, "The use of micropulsation 'whistlers' in the study of the outer magnetosphere", *Planet.Space Sci.* 13, 773-779 (1965).

23. R.L. Dowden and M.W. Emery, "An automatic dynamic spectrum analyser for tape recorded signals", *Nature*, 207, 493-495 (1965).

24. R.L. Dowden, "Ordinary mode whistlers observed in satellites", *Nature*, 207, 963-964 (1965).

25. R.L. Dowden, "Micropulsation 'nose whistlers'. A helium explanation", *Planet.Space Sci.*, 14, 1273-1280 (1966).

26. R.L. Dowden, "Possible helium ion effects in micropulsation spectrograms", *J.Geophys.Res.*, 72, 2029-2031 (1967).

27. R.L. Dowden, "Dotted pearl micropulsations", *J.Geophys.Res.*, 73, 2995-3003 (1968).

---

28. R.L. Dowden, "Location of generation regions (in L and λ) of midlatitude V.L.F. discrete emissions by dispersion analysis of ground station observations", *J.Geophys.Res.* 76, 1729-37 (1971).

29. R.L. Dowden, "Electron energy spectrum and structure deduced from analysis of V.L.F. discrete emissions by using the Helliwell criterion", *J.Geophys.Res.* 76, 3034-45 (1971).

30. R.L. Dowden, "V.L.F. discrete emissions deduced from Helliwell's theory", *J.Geophys.Res.* 76, 3046-54 (1971).

31. R.L. Dowden, "Distinctions between midlatitude V.L.F. hiss and discrete emissions", *Planet.Space Sci.*, 19, 374-76 (1971).

32. R.L. Dowden and G.McK. Allcock, "Determination of nose frequency and non-nose whistlers", *J.Atmos.Terr.Phys.*, 33, 1125-29 (1971).

33. R.L. Dowden, "Trigger delay in whistler precursors", *J.Geophys.Res.*, 77, 695-99 (1972).

34. R.L. Dowden, "Use of electron and proton beams for production of very low frequency and hydromagnetic emissions", *J.Geophys.Res.*, 78, 684-96 (1973).

Journal of Atmospheric and Terrestrial Physics, 1957, Vol. 11, pp. 111 to 117. Pergamon Press Ltd., London

Short-range echoes observed on ionospheric recorders

R. L. DOWDEN
Antarctic Division, Department of External Affairs, Melbourne

(*Received* 15 *May* 1957)

Abstract—Strong echoes from the 20–100 km region previously reported from several ionospheric stations near the sea have been examined at Macquarie Island and found to arrive from very low angles of elevation and with vertical polarization. It is shown that the echoes are therefore not ionospheric but are produced by coherent back-scatter of surface propagated waves by sea waves of length $L = \lambda/2$.

1. INTRODUCTION

VARIOUS investigators have reported pulse reflections from D-region heights on frequencies much greater than the critical frequency. ELLYETT (1947) reported strong echoes (voltage reflection coefficient $>10^{-2}$) at heights down to 20 km from Pitcairn, Raoul, and Christmas Islands. He suggested that these reflections might be characteristic of a tropical region. Similar reflections however, have been observed from Campbell Island ($52\frac{1}{2}°$ S) and Macquarie Island ($54\frac{1}{2}°$ S). MAJOR (1955) concluded that the reflections were peculiar to island observatories. An example of these "island echoes" is shown in Fig. 1.

Inland, weak reflections (voltage reflection coefficients around 10^{-4}) from the D-region of the ionosphere from 60 km and upwards have been described by DIEMINGER (1952), GARDNER and PAWSEY (1953) and others. The latter used simple direction-finding tests to establish that their "low" echoes were arriving from near overhead.

This paper describes similar direction-finding tests made by the author at the Australian National Antarctic Research Expedition's station at Macquarie Island at 7 Mc/s which demonstrate that the "low" island echoes were arriving, not from overhead, but at very low angles of elevation. An ionospheric mechanism is obviously ruled out.

At the observed ranges the only possible reflecting objects were tropospheric irregularities and the sea surface. From echo strength considerations the former is immediately rejected. However the latter mechanism is consistent with the strong echoes observed and also agrees with recent C.W. observations of sea reflections at 13 Mc/s made by CROMBIE (1955) in New Zealand.

This apparently clears up an anomaly of long standing, viz. the conflicting reports on low echoes as summarized by ELLYETT (1947). Instead of yielding data on the ionosphere it is probable that this type of observation could be developed to give information on sea waves and so provide a useful tool in oceanographical research.

2. OBSERVATIONS

The equipment used was the Macquarie Island ionospheric recorder described elsewhere (CALLOW, 1956). The transmitter "delta" aerial was used throughout the experiments and initially the usual receiver delta was used also. In addition three

half-wave dipoles—two horizontal and one vertical—were erected a quarter wavelength above the ground. The two horizontal aerials had their wire axes pointing approximately north–south and east–west respectively. Any one of these aerials could be quickly connected to the receiver of the ionospheric recorder by a rotary switch.

2.1. *Angle of arrival.* A large number of *A*-scope photographs of echoes received by each of the above aerials were taken. A typical series is shown in Fig. 2. The amplitudes and ranges of the strongest maxima of the short-range echo and the amplitude of the *F*2 echo were scaled from these photographs. The ratios of the echo amplitude on a horizontal aerial to that on the vertical aerial (i.e. H/V ratio) were then calculated. The mean ratios for each type of echo for both horizontal aerials are shown below in Table 1. The three range classifications of short-range echo are purely arbitrary.

Table 1

Echo	Mean range	H/V for N–S	H/V for E–W	No. of obs.
*F*2	—	6·0	6·7	24
<30 km	22 km	0·032	0·067	19
30–49 km	37 km	0·034	0·091	45
>49 km	58 km	0·036	0·067	24

Now the horizontal aerials have their maxima directed vertically upwards and the vertical one horizontally. Thus the high value of the H/V for the *F*2 is to be expected. But the values of H/V for the short-range echoes are about 1 per cent of those for *F*2 and are completely inconsistent with arrival from overhead. The short-range echoes must arrive from within a few degrees of the horizontal and must be vertically polarized.

Further the higher average intensity on the east-west aerial compared with the north-south one appears to indicate a preference for an easterly or westerly direction. The east-west aerial would have its maximum sensitivity for vertically polarized waves from the east and west. The transmitting delta aerial which is oriented about 30° west of north should radiate in the horizontal direction somewhat less in the E–W direction than N–S. Since the prevailing wind is E–W this direction of arrival is perpendicular to the dominant sea waves.

2.2. *Apparent reflection coefficient.* The "apparent reflection coefficient" for any echo mechanism can be defined in terms of an equivalent smooth infinite plane surface of voltage reflection coefficient ρ. The power of the received echo at a distance "R" from such a surface can be found from the "radar equation" to be (in the usual notation):

$$p = \frac{GPA}{8\pi^2} \cdot \frac{\pi\rho^2}{R^2}$$

$$= K \frac{\pi\rho^2}{R^2} \qquad (1)$$

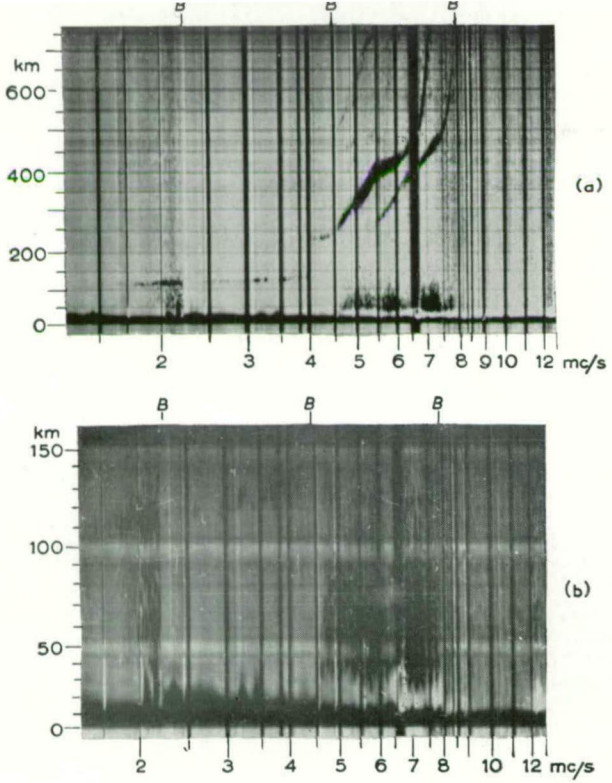

Fig. 1. (a) Typical $p'f$ record showing strong short-range echoes up to about 7·5 Mc/s. Band changes occur at points marked B. (b) Similar record using faster time base to expand range scale.

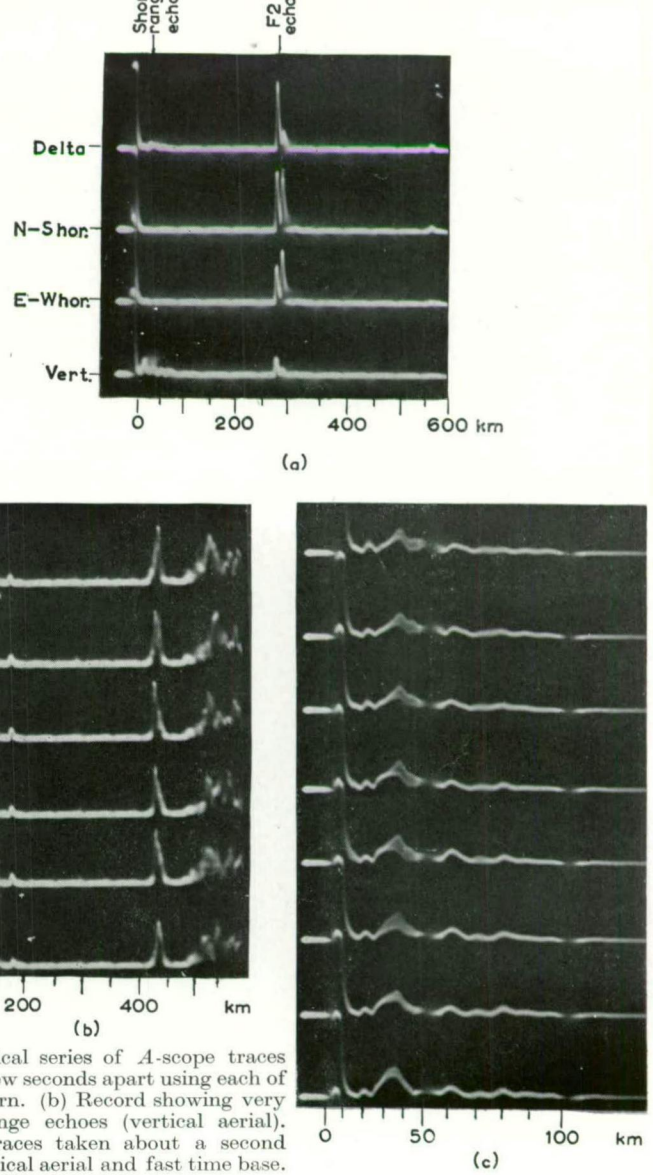

Fig. 2. (a) Typical series of A-scope traces taken about a few seconds apart using each of the aerials in turn. (b) Record showing very strong short-range echoes (vertical aerial). (c) Series of traces taken about a second apart using vertical aerial and fast time base.

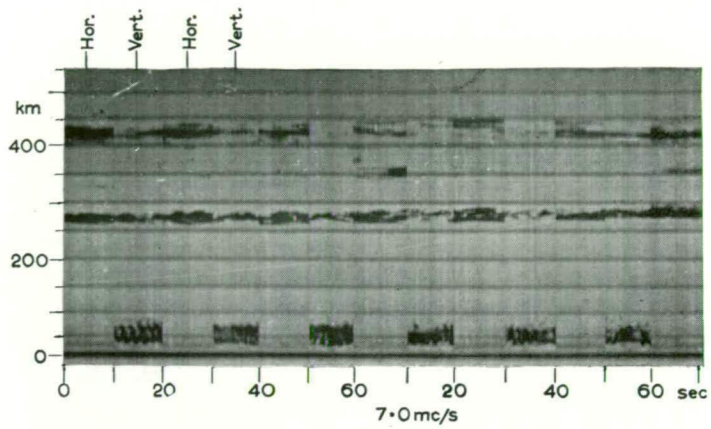

Fig. 4. *P't* record using vertical and horizontal aerials alternately. Note fading pattern in first sample using vertical aerial.

The reflection coefficient of a horizontal layer can be found experimentally (MITRA, 1952) using multiple reflections from some other layer. Since all echoes come from the same direction, the equipment and aerial constants (the K term above) cancel. At first the short range-echoes were presumed at vertical incidence and ρ was computed to be $1{\cdot}5 \times 10^{-2}$. As this is not the case, the apparent reflection coefficient is probably nearer 10^{-1}.

2.3. *Echo structure.* The amplitudes and ranges of 152 maxima from a series of 16 A-scope photographs taken over a period of about a minute on 14 August are shown plotted in Fig. 3. For ranges less than about 30 km it is likely that the receiver sensitivity is considerably reduced by ground pulse paralysis. Beyond this it is believed there is no strong variation of gain with range although this was not accurately checked. The spread of observations in Fig. 3 indicates no tendency to

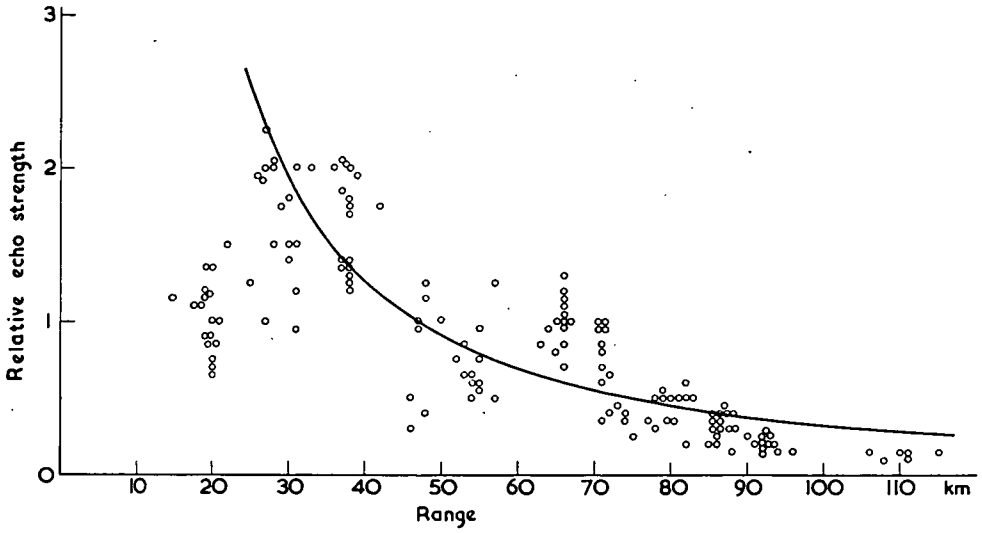

Fig. 3. Echo maxima from a series of A-scope photographs taken on 14 August. The full line is the $R^{-3/2}$ relationship expected for back-scatter from one-dimensionally extended objects (e.g. wave crests).

form layers. Also the echo amplitude falls fairly slowly with range up to about 70 or 80 km and then more rapidly.

2.4. *Fading.* Slow fading of the different peaks of the echo was often noticed and is clearly shown in Fig. 4, obtained at a constant frequency of 7·0 Mc/s on moving film in a similar manner to the routine $p'f$ records. The receiver has been alternately switched from the vertical dipole to the north-south horizontal dipole every 10 sec. The first sample using the vertical dipole in Fig. 4 shows this fading very clearly and the fading period is seen to be very nearly 2 sec. Unfortunately this was the only observation actually recorded.

2.5. *Apparent diurnal variation.* The intensity of the echo appearing on the standard $p'f$ records was visually estimated on an arbitrary 0–4 scale according to the area of $p'f$ record covered. The mean hourly intensities for each of the two months (January and February 1956) for which this was done showed that the echo was usually just detectable at night but apparently strengthened rapidly around

sunrise to an intensity such as that shown in Fig. 1. Around sunset the echo rapidly waned. This pattern is similar to that reported by ELLYETT and others.

This effect may be instrumental. The diurnal variation of the background of interference which is controlled by the absorption of the *D*-layer may have introduced a strong diurnal variation of effective receiver sensitivity. At the time it was not possible to check this.

3. DISCUSSION

We now consider possible objects of reflection in the observed ranges of 15 to 100 km. Obviously the echoes are non-ionospheric and, as the maximum dimension of the Island is about 30 km, they are equally obviously not due to fixed objects. This leaves back-scatter from tropospheric irregularities or back-scatter from sea waves as the only possible mechanisms.

3.1. *Tropospheric back-scatter.* A patchy plane surface (i.e. irregularities much smaller than a wavelength, 40 m) might conceivably give rise to our type of echo, the longer delay time components corresponding to lower angles of elevation. Echoes from higher angles would correspond to delay times well within the paralysis region and would not be seen.

To derive an upper limit for the echo strength due to this mechanism we might consider a layer of small spheres of saturated air in dry air and choose the diameter of the spheres to give maximum back-scatter. The apparent reflection coefficient can then be estimated from the RAYLEIGH scattering law for 30 km echoes to be about 10^{-7}. If the scatterers were somehow arranged to produce coherent scattering, then this value might be increased to about 10^{-4}, but this is still two or three orders of magnitude lower than the experimental value.

3.2. *Sea back-scatter.* Sea echoes on centimetre and decimetre wavelengths have been studied in detail (KERR, 1951). At such frequencies however, fine scale irregularities are important, so the mechanism cannot be considered similar to ours. Back-scatter of dekametre wavelengths by the sea have since been reported by CROMBIE (1955) and MCCUE (1956). The latter was concerned with fairly high angle back-scatter via the ionosphere and so his results are not readily comparable with ours.

By measuring the Doppler shifts of sea echoes at 13·56 Mc/s CROMBIE (1955) found a strong resonance effect for sea wavelengths equal to half the wavelength of his radio waves, i.e. for $L = \lambda/2$. He found a smaller effect for the $L = \lambda$ case. This suggests that resonant or coherent scattering is the most important mechanism: of the large spectrum of sea waves normally present the radio wave selects those exactly half its length and in a direction perpendicular to the direction of propagation to yield most of the back-scatter.

The intensity of the back-scattered radiation can be expressed as the product of two factors, one giving the scattering produced by a single sea wave and the other depending on the arrangement of the sea waves. For grazing incidence and back-scatter, neglecting multiple scattering, the latter factor is of the form (DITCHBURN, 1952):

$$F(L) = \frac{\sin^2 2\pi NL/\lambda}{\sin^2 2\pi L/\lambda}$$

where N is the number of sea waves contained in the distance corresponding to the transmitter pulse length. Since this is about 70 μsec, N is about $(2/L) \cdot 10^4$. Principal maxima are obtained for $L/\lambda = \frac{1}{2}, 1, \frac{3}{2}, 2, \ldots$ etc. Most of the echo is therefore due to sea waves of length $L = \lambda/2$, the intensity of the $L = \lambda$ component being about one quarter as much.

The scattering produced by a single wave is more difficult to calculate and only the order of magnitude is estimated. Since the height to wavelength ratio of sea waves is small ($\sim 1/20$) suppose we consider the waves to be triangular. As a further simplification we will neglect that part of the wave facing away from the transmitter, so that each sea wave becomes a "thin" ribbon, inclined (say) 6° to the horizontal towards the transmitter. Expressions for the scattering of waves by thin ribbons have been obtained by MORSE and RUBENSTEIN (1938) in terms of Mathieu functions. From these, the power of the received echo at a distance R from N such scatterers spaced $\lambda/2$ apart is found from the "radar equation" to be:

$$p = \frac{GPA}{8\pi^2} \cdot \frac{N^2 h}{R^3} \times 10^{-2}$$

$$= K \cdot \frac{N^2 h}{R^3} \times 10^{-2}$$

To find the "apparent reflection coefficient" we substitute in equation (1) (page 112):

$$\frac{\pi \rho^2}{R^2} = \frac{N^2 h}{R^3} \times 10^{-2}$$

For 30 km echoes, $L = \lambda/2 = 20$ m, $N \approx 10^3$, $H = 2$ m, we find $\rho \approx 0{\cdot}4$, in reasonable agreement with the experimental value of roughly 0·1.

This estimate is probably an overestimate since it includes end effects of the postulated ribbons which would be absent for real waves; further the wave height of 2 m is large for waves of a particular wavelength which need not be that of the principal waves. However it gives the right order of magnitude and the $R^{-3/2}$ law suggested by Fig. 3.

3.3. *Propagation.* To produce echoes from ranges of up to 100 km, the 7 Mc/s pulse must be confined to the earth's surface for about one degree of arc for both the outgoing and returning trip. We consider three mechanisms for this.

The average ray curvature given by the rate of change of refractive index with respect to height for the layer of air between the ground and the 900 mb level at Macquarie Island was calculated from radiosonde data (ANARE, 1955). That for the best day found on inspection of a number of months was only 15 min of arc in 100 km. Superrefraction if therefore ruled out.

There is evidence (FRIEND, 1941) of sharp tropospheric discontinuities in temperature and humidity which usually escape detection because of the slow response of radiosondes. Even at vertical incidence, FRIEND reports voltage reflection coefficients of up to 10^{-4} which would be considerably augmented for grazing incidence. However an attenuation of one or two orders of magnitude over that for free space would be introduced.

The ratio of the strength of the surface wave to that expected for a free wave (inverse distance) for various distances travelled over a smooth sphere of various surfaces is given in Table 2 below (obtained from curves after TERMAN, 1943) for a frequency of 5·0 Mc/s.

Table 2

Distance	Sea	Good earth	Poor earth
40 km	0·9	10^{-2}	2×10^{-3}
80 km	0·8	5×10^{-3}	6×10^{-4}
160 km	0·4	10^{-3}	10^{-4}

For echo ranges up to 70 or 80 km over sea the attenuation is scarcely more than the free space wave. This is in agreement with the more rapid decrease in amplitude for echoes beyond 70 or 80 km noticed in Fig. 3. This also explains the association of the echo with islands. Over land, ground objects are highly reflecting but the surface waves are attenuated some hundreds of times more.

3.4. *Fading.* As mentioned above, CROMBIE using C.W. observed a Doppler beat between the ground wave and the sea echo. Since the velocity v of a sea wave of length L is given by $v = \sqrt{\frac{g}{2\pi}L}$, g being the acceleration due to gravity, then the Doppler shift Δf produced by sea waves of length $L = \frac{\lambda}{2}$ travelling radially to the observer will be

$$\Delta f = \frac{2v}{\lambda} = \frac{2}{\lambda}\sqrt{\frac{g}{2\pi} \cdot \frac{\lambda}{2}} = \sqrt{\frac{g}{\pi} \cdot \frac{1}{\lambda}}$$

At 7 Mc/s, $\Delta f = 0{\cdot}27$ c/s and the observed fading of about $2\Delta f$ ($\approx 0{\cdot}5$ c/s) would fit the beat between reflections from opposite sides of the island.

3.5. *Apparent diurnal effect.* The observed diurnal variation is inconsistent with the sea-echo hypothesis. As mentioned above the effect is probably instrumental.

4. CONCLUSIONS

The short-range echoes observed on ionospheric recorders at Macquarie Island and other island observatories, and formerly attributed to reflections from the lower ionosphere have been shown to be due, not to ionospheric effects, but to back-scatter from the sea propagated along the surface.

Most of the back-scatter is produced by sea waves of length $L = \lambda/2$. The back-scatter and hence the relative amplitude of other sea wavelengths can be found by varying λ. Hence observations of this type should provide a useful tool in oceanographical research.

Acknowledgements—The author wishes to express thanks to the Ionospheric Prediction Service for the use of equipment, to Australian National Antarctic Research Expedition members for assistance with observations and to Drs. F. F.

GARDNER and J. L. PAWSEY of the Radiophysics Division, and Dr. G. H. MUNRO of the Research Board, C.S.I.R.O. for many valuable criticisms and suggestions to the draft paper.

REFERENCES

Australian National Antarctic Research Expedition	1955	*Meteorology* VI Series D.
CALLOW D. R. L.	1956	*Interim Report No.* 13. Australian National Antarctic Research Expedition.
CROMBIE D. D.	1955	*Nature, Lond.* **175,** 681.
DIEMINGER W.	1952	*J. Atmos. Terr. Phys.* **2,** 340.
DITCHBURN R. W.	1952	*Light* p. 175. Blackie, London.
ELLYETT C. D.	1947	*Terr. Magn. Atmos. Elect.* **52,** 1.
FRIEND A. W.	1941	*Bull. Amer. Met. Soc.* **22,** 53.
GARDNER F. F. and PAWSEY J. L.	1953	*J. Atmos. Terr. Phys.* **3,** 321.
KERR D. E.	1951	*Propagation of Short Radio Waves* p. 481. McGraw-Hill, New York.
MCCUE C. G.	1956	*Aust. J. Phys.* **9,** 454.
MAJOR G.	1955	*Nature, Lond.* **175,** 862.
MITRA S. K.	1952	*Upper Atmosphere* p. 249. Asiatic Society.
MORSE P. M. and RUBENSTEIN P. J.	1938	*Phys. Rev.* **54,** 895.
TERMAN F. E.	1943	*Radio Engineer's Hand Book* pp. 681–683. McGraw-Hill, New York.

Journal of Atmospheric and Terrestrial Physics, 1960, Vol. 18, pp. 8 to 19. Pergamon Press Ltd. Printed in Northern Ireland

Ionospheric thermal radiation at radio-frequencies in the auroral zone

R. L. DOWDEN
Ionospheric Prediction Service, Hobart, Tasmania

(*Received* 11 *August* 1959)

Abstract—Measurements of the temperature of the ionospheric *D*-region in the auroral zone from observations of 2 Mc/s radio noise are described and compared with measurements similarly made in the temperate region. The temperatures of the undisturbed and disturbed ionospheres at the two latitudes are found to be essentially similar, but the disturbing influence in the auroral zone is probably corpuscular rather than ultra-violet radiation.

1. INTRODUCTION

IN the absence of man-made interference and atmospherics, it has been found possible to measure radio-frequency radiation from the ionosphere at medium frequencies.

The temperature of the ionospheric *D*-region has been previously measured by this method at 2 Mc/s in temperate latitudes (PAWSEY *et al.*, 1951; GARDNER, 1954). In a companion paper (GARDNER and PAWSEY, 1953), the absorbing structure of the lower ionosphere was determined from *D*-region echoes to find the heights to which the temperature applied. However, it was felt that conditions might be very different in an auroral zone.

Noise level and echo experiments were carried out by the writer at the Australian National Antarctic Research Station at Macquarie Island as a member of the 1956 party. The apparent *D*-region echoes were found to be not from the ionosphere, however, but from sea waves (DOWDEN, 1957). The present paper describes the radio noise level experiments at 2 Mc/s using a half-wave dipole aerial to provide a direct comparison with GARDNER'S (1954) observations in a temperate latitude (30°S).

2. EXPERIMENTAL PROCEDURE

2.1. *Site and aerial*

The site of the experiment was near Hurd Point, Macquarie Island (55°S, 159°E, geomagnetic lat. −62°), on peat slopes at the foot of the plateau which forms most of the island. The nearest source of man-made interference of any kind was the Station, 20 miles north. Its noise was completely negligible at this distance. The nearest broadcast stations and atmospherics were several hundred miles to the north.

The aerial used for this part of the experiment was a half-wave dipole (2 Mc/s) suspended from wires attached to various crags. The aerial itself was about 20° off horizontal, about a quarter-wave above the ground (120 ft) and more than a wavelength from the cliffs of the plateau. The aerial passed directly over the recording hut from which it was fed by an 80 Ω shielded twin line. Far less trouble

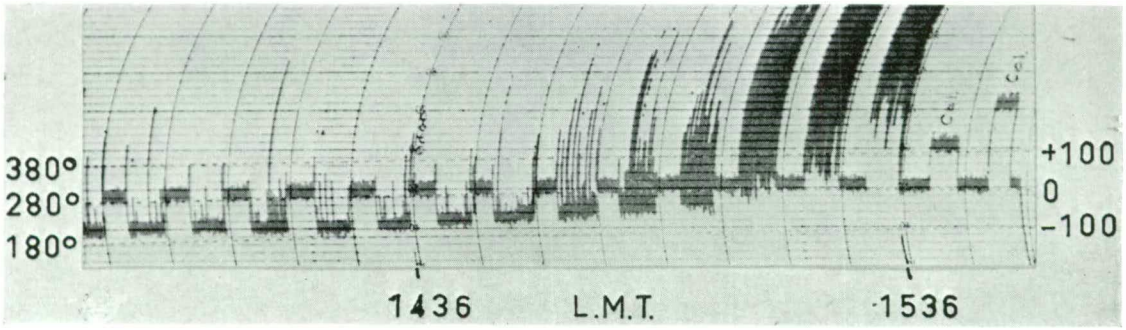

Fig. 1. Typical record showing onset of atmospherics (June observations).

from winds was encountered than expected, the mean wind velocity at the site being only about half that recorded at the Main Station.

2.2. *Determination of ionospheric temperature*

The equipment used and the recording technique was similar to that described by GARDNER (1954). The receiver was automatically connected to a dummy aerial for 3 min every 7·5 min by a chronometer operated relay. The sensitivity of the recording system was checked with a diode noise generator three times a day. The impedance of the aerial was accurately rematched to that of the dummy usually once a day.

The difference t between the noise level produced by the aerial and that by the dummy was read from the record in arbitrary units. A typical record showing this difference is in Fig. 1. The temperature T_i of the relevant part of the ionosphere can be found from this by an expression of the form: $T_i = At + T_d$. The scale factor A is the reciprocal of the product of the sensitivity of the receiving system (in recorder units per degree K), the attenuation of the aerial feed and matching unit, and the "efficiency" of the aerial. T_d is the ambient temperature of the dummy aerial, provided this is not greatly different from that of the matching unit, feed and ground. It was found that the temperature in the recording hut was usually within a degree Kelvin of that of the outside air and ground.

The efficiency of the half wire dipole was calculated from the SOMMERFELD and RENNER (1942) analysis using measured values of ground conductivity and aerial height. The figure obtained was also checked by the impedance method (GARDNER, 1954). Fortunately, for an aerial height of about a quarter wavelength, the efficiency is nearly unity and varies only slowly with height and ground constants. The adopted value was $0{\cdot}90 \pm 0{\cdot}05$. The total attenuation of matching unit and aerial feed was easily measured by the noise generator.

The errors of reading, sensitivity calibration and matching and those due to errors in aerial efficiency and attenuation measurement could be expected to give both systematic errors and random errors of about 5°K.

3. OBSERVATIONS

3.1. *General*

The seven observing periods from May to November (1956) are shown in Table 1.

Table 1. Observing periods

Period	Interval	Duration (days)
May–June	30 May–15 June	17
June–July	26 June–16 July	21
July	20 July–30 July	11
August	23 Aug.–31 Aug.	9
Sept.–Oct.	26 Sept.–17 Oct.	22
Oct.–Nov.	24 Oct.–3 Nov.	11
November	13 Nov.–20 Nov.	8

The observations made in the second period (June–July), showed strong interference from natural sources and so were not used for temperature measurement. During daylight hours random thermal noise was usually the only component seen on the "aerial" trace—similar in all respects except level to the "dummy" trace.

Occasionally, local cloud discharges produced small isolated spikes. Atmospherics propagated by the ionosphere from tropical latitudes were usually not

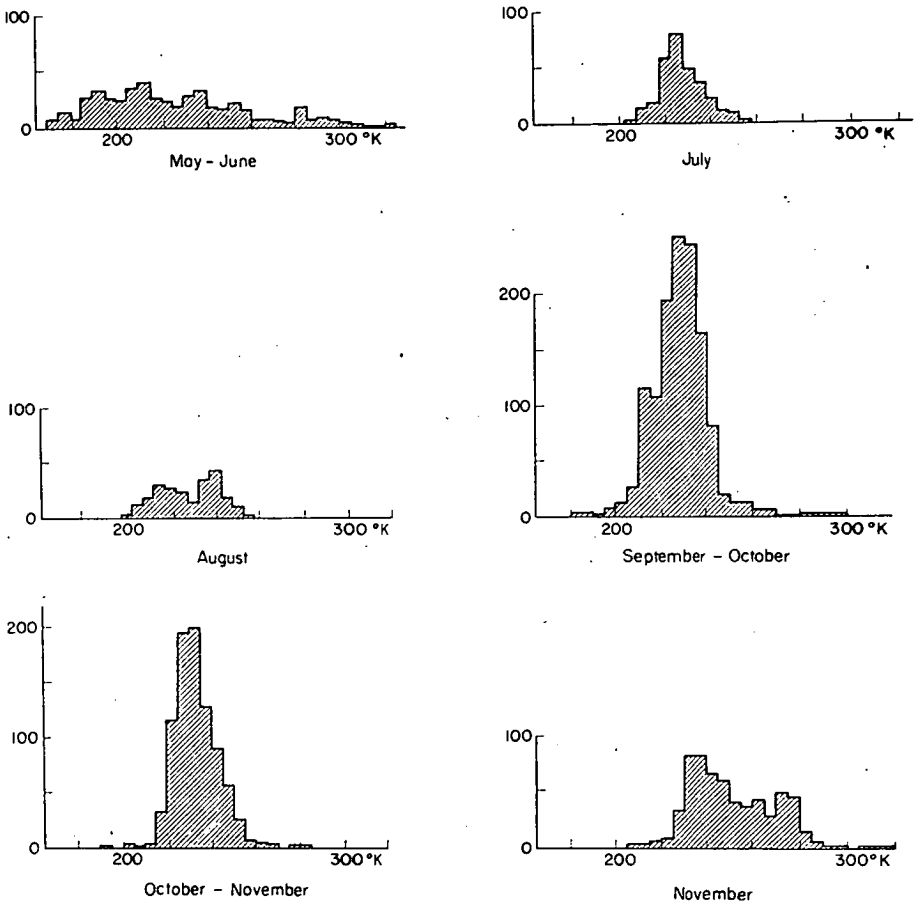

Fig. 2. Histograms of all observations of noise levels for the different observing periods. Only those obviously affected by atmospherics or precipation static were excluded. The average atmospheric free time (length of observing time) in a day was much larger in the summer months than in the winter (see Fig. 3).

observed until near sunset. Within an hour of their first appearance they were usually sufficiently strong to hold the recorder pen off scale continuously. A typical record showing this is Fig. 1. The length of observing time (about sunrise to sunset) varied from about 8 hr in May–June to 16 hr in November.

3.2. *Observed temperatures*

Histograms of the observed temperatures in each of the observing periods are shown in Fig. 2. All observed temperatures have been incorporated except those

obviously affected by atmospherics or precipitation static. These can be directly compared with temperate latitude observations (GARDNER, 1954). For the undisturbed months both sets of observations show distributions of temperatures starting from about 200°K, rising to a maximum around 220–230°K, then a slower tailing off to around 260–280°K. This undisturbed component of the distribution persists in most of the histograms. The temperatures of these first maxima (usually

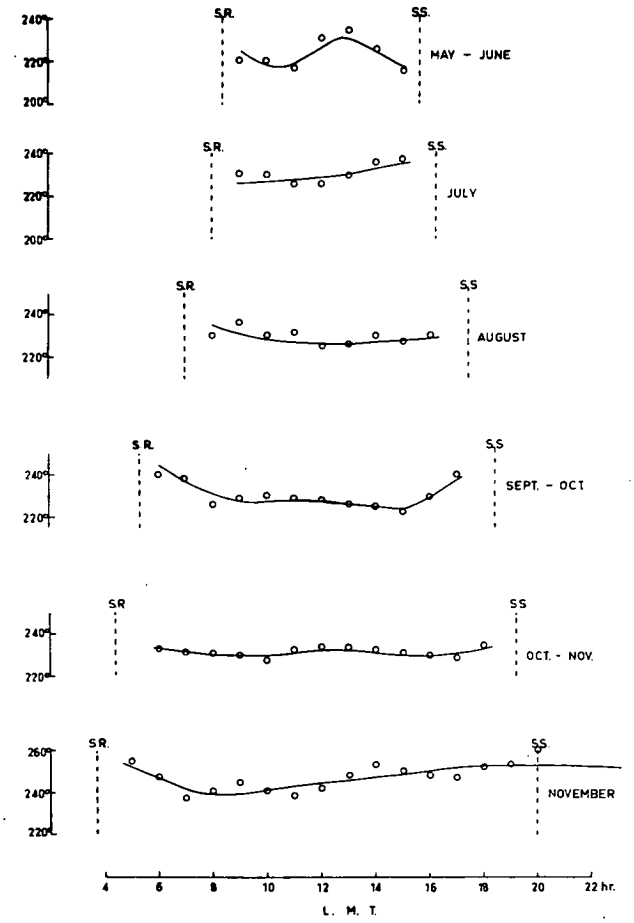

Fig. 3. Diurnal variation of ionospheric temperature for the different observing periods. Only observations unaffected by atmospherics have been considered. Times of sunrise and sunset are as indicated. The spread in observations can be gauged from the corresponding histograms (Fig. 2).

the modes), for each period in the Macquarie Island observations are usually within five or ten degrees of those for the corresponding periods in the Urisino (GARDNER, 1954) data. Again in agreement with lower latitude results, the temperatures observed in the winter periods are lower than those observed towards summer.

Hourly mean temperatures for each observing period are shown plotted in Fig. 3. Only observations unaffected by atmospherics, as gauged by the repetition rate and amplitude of the atmospherics, have been used in calculating these means.

The spread of observations in each period can be gauged from the corresponding histogram in Fig 2. The diurnal variations shown are on the verge of significance. This can also be judged from the corresponding histograms. The Sept.–Oct. and

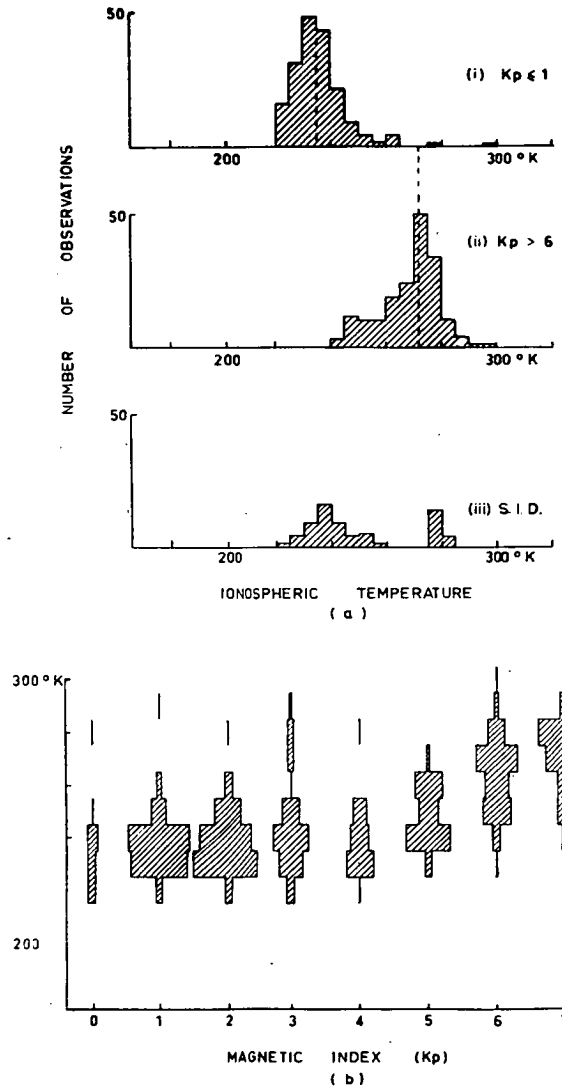

Fig. 4. (a). Histograms showing ionospheric temperatures during (i) three hourly periods for which $K_p < 1$, (ii) periods for which $K_p > 6$ and (iii) periods of s.i.d.s.
Fig. 4. (b). Histograms of temperatures for each value of K_p.

the Oct.–Nov. periods were fairly undisturbed and also a large number of observations were made and so the slight diurnal effect for these two periods is probably significant. A slight rise in temperature of about five degrees occurs about noon. The temperatures near sunrise and sunset appear higher than those during the day by some ten degrees. This may be due to an error in judgement of the effect of

weak atmospherics on temperature levels. Another possibility is that, as mentioned in a later section, on disturbed days, observed temperatures are higher and the absorption of the D-layer is higher so that the onset of atmospherics occurs later. Hence on these days values unaffected by atmospherics can be made nearer sunrise and sunset (as happens in the November period) so that at these times the means may not be truly representative.

A much larger effect of higher temperatures during early morning and late afternoon (about 50°) at Urisino and a still larger one at Rankin Springs (GARDNER, 1954) has been attributed to man-made interference propagated via the ionosphere. Consequently, the effect should be less at a site more remote from this interference as at Macquarie Island.

3.3. *Temperatures observed during disturbed periods*

During the November period some severe magnetic storms occurred. Two maxima are seen in the histogram (Fig. 2), suggesting a disturbed component. To separate this component histograms were computed of temperatures observed during quiet periods (three hourly periods for which the magnetic planetary index (K_p) was $\leqslant 1$), three hourly periods for which $K_p > 6$, and during sudden ionospheric disturbances (s.i.d.s). This is shown in Fig. 4(a). The correlation of observed ionospheric temperature with K_p is quite significant and sufficient to show up in a temperature–K_p plot as shown by the plotted histograms in Fig. 4(b). Up to about $K_p = 5$ the temperatures appear undisturbed but are increased by a further increase of K_p.

The effect of s.i.d.s, however, does not appear significant. This may partly be due to competition with magnetic disturbances occurring at about the same time. Also by an unhappy chance the equipment was not operating during many of the large s.i.d.s so that information is limited. At the Urisino site, GARDNER (1954) reported "a very definite rise of about 40°K during an s.i.d." This is not observed at Macquarie Island.

3.4. *Non-thermal noise*

As mentioned above, owing to the remoteness of the site, no trouble was experienced with man-made interference and comparatively little from atmospherics. The other forms of atmospheric noise listed by GARDNER were observed, viz. rain static, cloud static and wind static. In addition snow static was occasionally observed. This is aurally similar to rain static, but the intensity can be several orders of magnitude greater. The noise from sufficiently distant snow storms appeared quite random or "white" and at low enough intensities to appear as slowly varying increases of apparent temperatures (100°K) lasting for an hour or so.

The above spurious noise was easily recognized and ignored. A more serious type of non-thermal noise occurred in mid-winter. This produced an excess temperature of 50°K to 100°K or more for several days at a time. Because of this, the May–June histogram (Fig. 2) is strongly spread and shows temperatures above 300°K. In the June–July series (which was not used for temperature measurement for this reason) the apparent temperature was above ambient (280°K) all day for 10 days out of the 16 days observed.

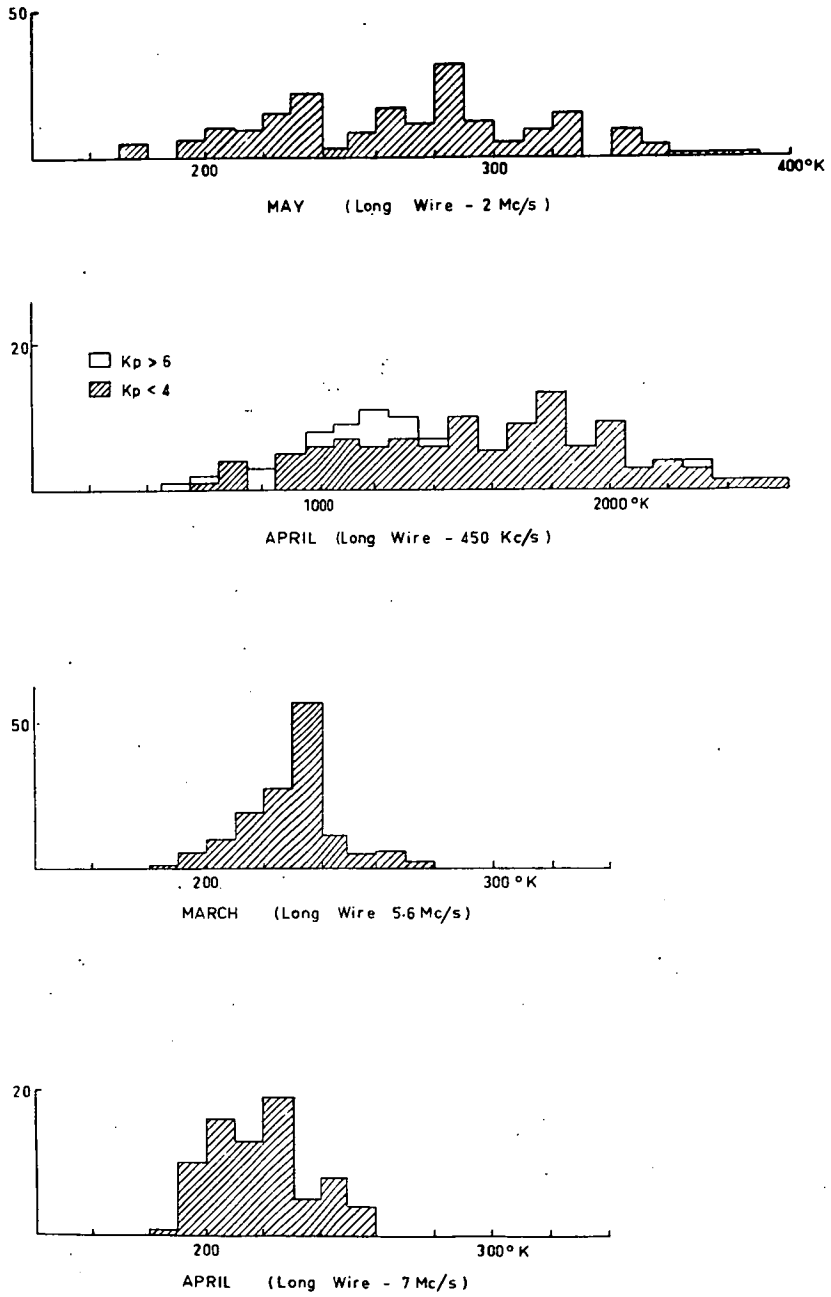

Fig. 5. Histograms of observations of apparent temperatures made using 400 m "long wire" aerial tilted 34° to the south.

Measurements carried out at 2·0 Mc/s and 450 kc/s using a southerly directed "long wire" aerial showed that this excess noise came from the south and that it was much stronger (2000°K) at 450 kc/s (Fig. 5). At 450 kc/s a weak negative

correlation with the magnetic index (K_p) was found indicating that the noise is *reduced* during disturbed periods. During mid-winter at Macquarie Island, the elevation of the sun is only 12° at noon. Consequently at this time of the year, the night side of the earth is never more than about 1250 km distant. It is suggested then that intense radiation incident on the night side of the earth might travel beneath the ionosphere to Macquarie Island with sufficiently weak attenuation to produce the observed noise levels. The stronger noise at 450 kc/s might be due to less attenuation at this frequency and the reduction of noise during disturbed conditions (high K_p) suggests increased attenuation.

At a frequency of 2 Mc/s the equivalent temperature of cosmic noise is of the order of 10^7 °K (ELLIS, 1957). Near the edge of the night hemisphere the ionosphere would probably be transparent to this noise. For frequencies much below 1 Mc/s ELLIS (1956) has shown that observations of cosmic noise are unlikely. However, REBER (1956) reports night-time temperatures of about 10^5 °K at 520 kc/s. Hence intense radiation is incident at night at both frequencies, so we now consider attenuation for propagation beneath the ionosphere. ELLIS (1958) has considered such trapping of noise and its subsequent propagation by hop transmission for large horizontal distances. The attenuation with distance for several ionosphere power reflection coefficients is given in his Fig. 11. If we now take the reasonable reflection coefficients of 0·01 at 2 Mc/s and 0·5 at 450 kc/s and the initial noise temperatures of 10^7 °K we can expect excess noise at Macquarie Island during mid-winter days of about 10^2 °K at 2 Mc/s and 10^3 °K at 450 kc/s.

3.5. *Observations at 5·6 Mc/s and 7·0 Mc/s*

These measurements were made with the long wire aerial mentioned above. The 5·6 Mc/s histogram (Fig. 5) is not significantly different from the 2 Mc/s dipole one for Sept.–Oct. (Fig. 2). At 7 Mc/s the temperatures appear about ten degrees lower, which is barely significant. Cosmic noise was apparent at 7 Mc/s when the critical frequency of the F-layer (f_0F2) went below 7 Mc/s. The very high intensity of cosmic noise made it easily recognizable, so that it has not been included in the noise levels scaled for temperature measurement.

4. DISCUSSION

Although a considerable volume of the ionosphere contributes to the measured temperature, it can be shown (PAWSEY *et al.*, 1951) that only a small range of heights, about 10 km, contributes appreciably. Physically, the ionosphere is too opaque for the aerial to "see" beyond this range of heights and too transparent for it to "see" any ionosphere below it. To a first approximation, therefore, the measured temperature may be taken as that of a certain level of the ionosphere corresponding to the "optimum opaqueness" of the ionosphere which depends on the electron density N and collision frequency ν. If either N or ν is increased the optimum opaqueness will occur at a lower level. Rocket measurements (Rocket Panel, 1952) show that the temperature of the ionosphere varies with height so that we would expect a variation of N or ν to produce a variation in measured temperature.

The diurnal variation of the height of the D-region has been investigated by

BRACEWELL *et al.* (1951), with reflections of very long radio waves and found to fit the formula:

$$h_\chi = h_{\chi=0} + A(t) \ln \sec \chi$$

where χ is the altitude of the sun and $A(t)$ is a constant having the value of about six during the equinoxes. They also found a difference between the summer and winter noon heights and a sharp decrease in height during an s.i.d. (sudden phase anomaly). Using this, the expected diurnal height variation during an equinox at Macquarie Island together with summer and winter and s.i.d. effects is shown in Fig. 6. The temperature scale on the right was taken from the Rocket Panel (1952)

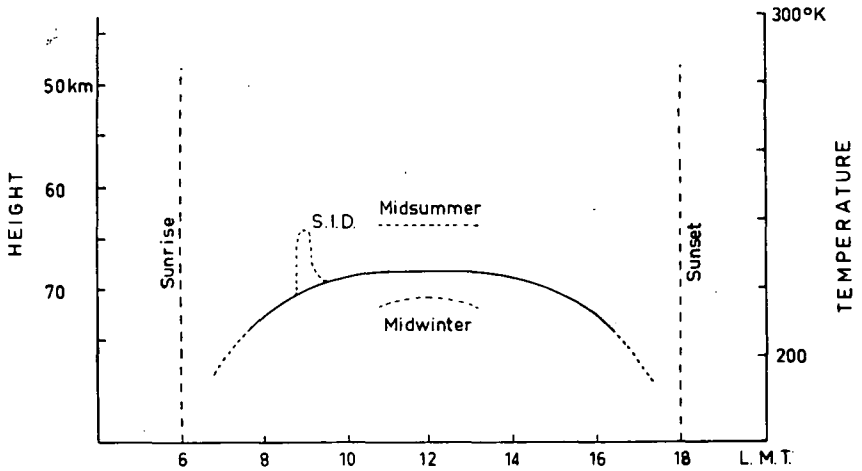

Fig. 6. Diurnal variation of the height of the D-layer at the equinoxes. Midday summer and winter heights are shown dotted. The temperature scale on the right was compiled from the Rocket Panel curve. The height decrease during a sudden phase anomaly indicates the temperature rise expected from an s.i.d.

temperature–height curve which is approximately linear in the height range 53 km to 74 km (210°K to 270°K).

Consider the possibility that all the variation of observed temperature is due to variation in electron density (as indicated by height measurements at very low frequencies) alone. The predictions of this hypothesis and the experimental results are compared in Table 2. The general agreement here is quite good. The predicted diurnal variation barely shows up probably owing to the atmospheric effect discussed in Section 3. A somewhat stronger temperature rise occurs during disturbed periods than that predicted. This was also the case during s.i.d.s at Urisino (40°K). For large increases of ionization, however, the optimum opaqueness level, being a function of N and ν, is depressed more than the isopyc* since the collision frequency ν increases exponentially with decrease in height, giving a stronger rise in measured temperature.

At 5·6 and 7 Mc/s the temperatures were much the same (within the expected error) as the 2 Mc/s measurements. However, at these frequencies the D-region

* *isopyc*: surface through points of equal electron density.

is much more transparent so that there is no longer a thin layer of "optimum opaqueness" responsible for most of the temperature contribution. This situation is apparent from the principle of detailed balancing. Suppose the aerial is radiating power towards the ionosphere. At 2 Mc/s the absorption is very high and most of the power will be absorbed in a relatively thin layer. At 7 Mc/s though, probably

Table 2

Fixed temperature–height hypothesis	Experiment
Mid-summer temp. : 240°K Equinox temp. : 225°K Mid-winter temp. : 215°K	November : 235°K Sept.–Oct. : 227°K July : 225°K
Noon temperatures, some 10–15° higher than early morning and late afternoon.	About 5° difference (Oct.–Nov. series)
Rise of 15–20° during an s.i.d.	40–50° during strong magnetic activity

only about half of this power would be absorbed on the ray's first trip through the D-region. If we assume that the reflection coefficients of the F-layer and "ground" (in this case the Southern Ocean) are both unity, then all the power will ultimately be absorbed in the D-region but the depth of ionosphere responsible for (say) 90 per cent of the absorption might include the entire D-region. The temperature measured would then represent an average one for the whole region.

Large increases in measured temperature and anomalously high absorption are strongly correlated with high K_p values. Both of these effects are probably due to large overall increases of D-region ionization produced by auroral particle bombardment. The apparent temperature increases have been explained above. If we make the simplifying assumptions that most of the absorption occurs in a relatively thin stratum, and that the various factors governing the absorption do not vary appreciably within this stratum, we find the total absorption ρ in nepers at frequencies greater than the collision frequency ν and the gyro-frequency f_L is given by:

$$\rho = CN_e\nu(f + f_L)^{-2}$$

where C is constant.

Since the absorption decreases rapidly with frequency it is often measured on ionospheric soundings in terms of the lowest frequency for which echoes are received ($f_{\min}$). During daylight hours $f_{\min}$ is around 2 Mc/s on undisturbed days but rises to around 10 Mc/s or more during highly disturbed conditions. Since the gyro-frequency f_L is about 1·5 Mc/s it is seen that at any given frequency the absorption and thus the product $N_e\nu$ must increase by a factor of about 10.

The collision frequency at any given height is unlikely to change by more than some per cent (since $\nu \propto T^{1/2}$), but as a function of height we find an exponential relation, so that at a height 20 km lower the collision frequency is some ten times higher. In order to explain increases of apparent temperature of from 40° to 50° during strong magnetic activity we required a height depression of isopycs of some 15 km (see Fig. 6). Owing to the limited region for which the slope of the temperature–height curve (Rocket Panel) is negative a further height decrease would not have given a further temperature increase. Hence during severe magnetic activity we might suppose that the overall ionization of the *D*-region is increased sufficiently to depress the lower isopycs by some 20 km. For each isopyc then, the collision frequency effectively increases some ten times so that the total absorption increases by about this amount.

5. CONCLUSIONS

The temperature of the lower ionosphere has been measured in an auroral zone, using similar techniques to those used by GARDNER (1954) in a temperate region. The temperature range and seasonal variation of temperatures have been found to be the same as in a temperate region. Owing to the much lower intensity of atmospherics and complete freedom from man-made noise, temperatures have been measured from sunrise to sunset, and the higher temperatures during early morning and late afternoon in GARDNER's results were not apparent. The observed temperature variations can be similarly explained in terms of a fixed temperature height scale.

No large increases in temperature have been observed during s.i.d.s, but during strong magnetic activity temperatures have been found up to 50° above normal. This, and the very large increase in absorption ("polar blackout") experienced in auroral latitudes during magnetic storms is thought to be due to bombarding auroral particles causing a strong increase in ionization and thus a descent of the region of absorption to levels of much greater collision frequency rather than a direct heating effect caused by these particles producing higher collision frequencies.

For temperature measurements by this method the optimum frequency appears to be around 2 Mc/s. At much lower frequencies measurements can be contaminated by noise trapped from the night hemisphere and at much higher frequencies the *D*-region becomes too transparent for temperature measurements in a narrow height range.

Acknowledgements—The writer wishes to express thanks to the Radiophysics Division, CSIRO, for loan of the basic equipment; to the Antarctic Division, Department of External Affairs, for finance and auxiliary equipment; to Drs. J. L. PAWSEY and F. F. GARDNER of the Radiophysics Division, CSIRO, and Professor G. NEWSTEAD of the University of Tasmania for valuable criticisms and suggestions, and to the Australian National Antarctic Research Expedition members, particularly Mr. K. D. COLE, without whose co-operation this work would have been impossible.

References

Bracewell R. N., Budden K. G., Ratcliffe J. A., Straker T. W. and Weekes K.	1951	*Proc. Instn. Elect. Engrs.* III **98,** 221.
Dowden R. L.	1957	*J. Atmosph. Terr. Phys.* **11,** 111.
Ellis G. R.	1956	*J. Atmosph. Terr. Phys.* **9,** 51.
Ellis G. R.	1957	*J. Geophys. Res.* **62,** 229.
Ellis G. R.	1958	*J. Atmosph. Terr. Phys.* **13,** 61.
Gardner F. F.	1954	*J. Atmosph. Terr. Phys.* **5,** 298.
Gardner F. F. and Pawsey J. L.	1953	*J. Atmosph. Terr. Phys.* **3,** 321.
Pawsey J. L., McCready L. L. and Gardner F. F.	1951	*J. Atmosph. Terr. Phys.* **1,** 261.
Reber G.	1956	*Proc. Radio Astronomy Symposium,* 1956. CSIRO, Sydney.
Sommerfeld A. and Renner F.	1942	*Wireless Engr* **19,** 357, 409, 457.
The Rocket Panel	1952	*Phys. Rev.* **88,** 1027.

(*Reprinted from Nature, Vol.* 183, *pp.* 385–386, *Feb.* 7, 1959)

'Whistler Mode' Echoes remote from the Conjugate Point

ECHOES of very low frequency radio signals from station *NDT* on 17·44 kc./s. in Tokyo (25° N. geomagnetic latitude) with delays of about 0·2 sec. have been detected at Hobart, Tasmania (51° S. geomagnetic latitude). The Eckersley–Storey theory of 'whistler' propagation predicts that 'whistler mode' signals from Tokyo would return to the Earth's surface at a point (the geomagnetic conjugate point to Tokyo) near Darwin, Northern Territory, some 3,500 km. from Hobart.

The signals used were ½-sec. pulses sent every second for a 4-min. period. These transmissions were specially arranged by the Australian National Committee of the International Geophysical Year for a conjugate point experiment. The receiving equipment consisted of a single-turn, crossed-loop system, 70 ft. high, fed through a goniometer into a made-up receiver having four tuned radio-frequency stages and two tuned intermediate-frequency stages. The enclosed area of each loop was about 900 m.², the receiver intermediate frequency was 750 c./s. and the overall band-width was about 15 c./s. The signals were recorded on tape. The null direction of the crossed-loop system was adjusted so as to reduce considerably the direct signal since the *NDT* transmitter radiated a strong residual signal in between the pulses.

The direct signal from *NDT* was received with a strength of about 150 μV./m. during the day. All measurements were made at about 1250 local time. A series of distinct echoes were heard on only one of the five periods observed (1251½ E.A.S.T., September 30). On analysis these were found to have an average time delay of 0·21 sec. and a strength of 3 μV./m. Four direct pulses, each followed by an echo of about this delay, are shown in Fig. 1.

As only a few echoes were heard it was not possible to locate the source by direction-finding methods. It seems most likely from the delay times, however, that the echoes travelled via the 'whistler mode' from

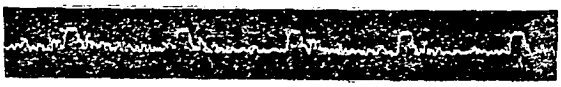

Fig. 1

Tokyo to somewhere around Darwin and to Hobart via the Earth – ionosphere wave-guide mode. The observed 0·2-sec. delay is in agreement with observed whistler dispersions (from 30 to 50) for this geomagnetic latitude[1] and with a similar whistler mode echo experiment[2], using the station *NPM*, which is also on about this same geomagnetic latitude. The actual time spent in the whistler mode is found by adding the travel time for the direct pulse from Tokyo to Darwin (0·02 sec.). This time is then 0·23 sec.

Use can be made of these results to estimate the minimum electron density on the line of force originating from the transmitter. Whistler mode echoes of very low-frequency stations have an advantage over natural lightning flash whistlers in that the position of the transmitter is readily and accurately known. As borne out by this experiment, the assumption that short whistlers originate near one's conjugate point could lead to an error of more than thirty degrees of latitude.

The whistler mode delay time for a signal of frequency f travelling along a line of force in a medium of plasma frequency f_p and gyro frequency f_H is given by Storey's[3] equation (15) provided $f_H \gg f$ and $f_p^2 \gg f f_H$:

$$t = \frac{1}{2c}\int f_p (f f_H)^{-1/2}\, ds$$

If we assume a dipole field and a constant electron density along the line of force (neglecting, for the moment, the effect of the lower ionosphere), we can get the approximate expression:

$$t \approx \frac{R_0}{c} f_{p_0} (f f_{H0})^{-1/2} \int_0^{x_g} (1-x^2)^{3/2} (1\ 3x^2)^{1/4}\, dx$$

$$\approx \frac{R_0}{c} f_{p_0} (f f_{H0})^{-1/2}\, x_g(1-\tfrac{1}{4}x_g^2) + \text{terms in } x_g^5 \qquad (1)$$

where R is the distance from the Earth's centre (in units of the Earth's radius) and x is the sine of the geomagnetic latitude angle. The subscripts 0 and g refer to values in the geomagnetic equatorial plane and at the Earth's surface respectively. The maximum value of x is $x_g = \sin 25° = 0{\cdot}4$, so to within an accuracy of a few per cent we may neglect terms in x^4.

To this must be added a correction to take account of retardation through the lower ionosphere. Considering only the F' region and assuming a parabolic layer of semi-thickness y_m, critical frequency f_{pc} and magnetic dip angle φ and assuming all other quantities to be constant within the integra-

tion limits, we find the correction to be applied is:

$$\Delta t = \tfrac{1}{4}\pi f_{pc} (f f_H)^{-1/2} y_m \operatorname{cosec} \varphi \qquad (2)$$

We can apply equations (1) and (2) to find f_{p_0} at R_0. On substitution of $x_g = \sin 25°$ and $t + \Delta t = 0{\cdot}23$ sec. we find $\Delta t = 0{\cdot}04$ sec. $R_0 = 1{\cdot}22$ radii and $f_{p_0} = 1{\cdot}75$ Mc./s. This suggests an electron density of about 20,000 cm.$^{-3}$ at a height of about 1,400 km.

We wish to thank Dr. G. R. Ellis, Upper Atmosphere Section, Commonwealth Scientific and Industrial Research Organization, for his useful suggestions.

R. L. Dowden
G. T. Goldstone

Commonwealth Ionospheric Prediction Service,
Hobart, Tasmania.
Nov. 28.

[1] Maeda, K., and Kimura, T., *Rep. Ionosph. Res. Japan*, **10**, No. 3, 105 (1956).
[2] Allcock, G. McK., A.N.Z.A.A.S. Conference, Adelaide (1958).
[3] Storey, L. R. O., *Phil. Trans. Roy. Soc.*, A, 246, 908 (1953).

Printed in Great Britain by Fisher, Knight & Co., Ltd., St. Albans.

(Reprinted from Nature, Vol 811 pp. 803, September 12, 1959)

Low-frequency (100 kc./s.) Radio Noise from the Aurora

EXTRATERRESTRIAL radio 'noise' has been intensively studied during the past decade. The steady background radiation or 'cosmic noise' from interstellar space has been observed[1] at frequencies down to about 1 Mc./s. and an intensity of about 10^{-19} watts per square meter per cycle per second (W.m.$^{-2}$ (c./s.)$^{-1}$). Ellis[2] later showed that cosmic noise at lower frequencies could not penetrate the earth's magneto-ionic upper atmosphere. Reber[3], however, reported observations of steady noise of intensity 10^{-22} W.m.$^{-2}$ (c./s.)$^{-1}$ at frequencies of 520 kc./s. and 140 kc./s. This appeared to be correlated with sidereal time and so was claimed to be cosmic noise.

Recently[4] extraterrestrial continuous ('white') noise has been studied in the audio-frequency band. This normally shows peak intensity (10^{-16} W.m.$^{-2}$ (c./s.)$^{-1}$) at around 4 kc./s. It appears to be generated in the upper atmosphere by auroral particles[5], it is highly correlated with auroral airglow[6], and it has been designated 'hiss'.

I have also carried out observations of 'hiss' at Hobart, Tasmania, to provide a comparison with those of Ellis at Sydney. Results appeared broadly similar but the intensity at Hobart is much higher (10^{-15} W.m.$^{-2}$ (c./s.)$^{-1}$). In view of Reber's observations (and similar observations of mine[7] at 450 kc./s. at Macquarie Island) it was decided to operate on five frequency channels simultaneously, covering the gap from the normal 'hiss' frequencies to the controversial 100 kc./s. band. The centre frequencies of these channels were 4·6, 9·6, 27, 70 and 180 kc./s. For the loop antenna and amplifiers used the sensitivity increased with frequency, so at the lower two channels it was about 10^{-17} W.m.$^{-2}$ (c./s.)$^{-1}$ and for the higher two it was around 10^{-21} W.m.$^{-2}$ (c./s.)$^{-1}$. It was found that the intensity of both the 'back-ground' radiation and the usual 'bursts' showed a general decrease with frequency so that normally nothing was observed at 70 and 180 kc./s.

On one occasion, however (April, 1959) a number of bursts were observed which showed deep fading. When the records of the five channels were examined together it was found that strong noise was present on all channels. Moreover, the fades on each channel showed a strong one-to-one correspondence and were

simultaneous to the limit of reading ($\sim$ 10 seconds). The noise level of these bursts at the lower frequencies was fairly typical of the more usual bursts (10^{-15} W.m.$^{-2}$ (c./s.)$^{-1}$ at 4·6 kc./s.) but at 70 and 180 kc./s. the noise power was at least two or three orders of magnitude greater than normal (to about 10^{-19} W.m.$^{-2}$ (c./s.)$^{-1}$).

Unfortunately it is not known exactly on what day this occurred nor whether a notable geomagnetic event took place at the same time, for the research station together with the equipment and records was destroyed by fire on May 24, 1959. It is probably a rare event as it only occurred on one occasion in about two months observing. It is none the less established that 'hiss' can sometimes occur at frequencies up to 180 kc./s. at least, suggesting that extraterrestrial noise much below a megacycle might be 'hiss' (that is generated in the upper atmosphere) rather than 'cosmic noise'.

My thanks are due to Mr. G. T. Goldstone, who built and operated much of this equipment and assisted in the observations, and to Dr. G. R. A. Ellis, Upper Atmosphere Section, C.S.I.R.O., who provided part of the equipment and circuits and who suggested the 4·6 kc./s. and 9·6 kc./s. observations.

R. L. DOWDEN

Commonwealth Ionospheric Prediction Service,
Hobart, Tasmania.
Aug. 19.

[1] Reber, G., and Ellis, G. R., *J. Geo. Res.*, **61**, 1 (1956).
[2] Ellis, G. R., *J. Atmos. Terr. Phys.*, **9**, 51 (1956).
[3] Reber, G., *J. Geo. Res.*, **63**, 109 (1958).
[4] Ellis, G. R., Plan. Space Sci. (in the press).
[5] Ellis, G. R., *J. Atmos. Terr. Phys.*, **10**, 302 (1957).
[6] Duncan, R. A., and Ellis, G. R., *Nature*, **183**, 1618 (1959).
[7] Dowden, R. L., *J. Atmos. Terr. Phys.* (in the press).

Printed in Great Britain by Merritt & Hatcher Ltd., London & High Wycombe

(*Reprinted from Nature, Vol.* 187, *No.* 4738, *pp.* 677–678, *August* 20, 1960)

Geomagnetic Noise at 230 kc./s.

GEOMAGNETIC radio noise or 'hiss' usually occurs only in the audio region. During severe magnetic storms it has been reported up to 30 kc./s. on a sweep frequency analyser[1] and at 70 and 180 kc./s. on fixed tuned channels[2]. The latter report[2] was written after the records had been destroyed in a fire. New observations at up to 230 kc./s. are described here.

Observations were made simultaneously at the four frequencies 4, 9, 70 and 230 kc./s. (using two dual-beam cathode-ray oscillographs and photographic recording) over the period mid-September to mid-November, 1959. Geomagnetic noise was observed on three occasions only: 2245 U.T., October 31; 0430 U.T., November 3; and around 0330 U.T., November 6. The planetary magnetic index (k_p) ranged from 4 to 6 at these times. The noise burst observed on November 6 is reproduced in Fig. 1. This shows 9 and 230 kc./s. only, since the camera recording 4 and 70 kc./s. jammed on this occasion.

The general appearance of the noise burst—relatively gradual rise and decline of intensity (as distinct from the sharp 'on' and 'off' of man-made interference) and impulsive noise component superimposed on a steady or 'white' noise-level—is typical of geomagnetic noise bursts observed at audio-frequencies. The maximum noise-levels are seen to be $0{\cdot}8\,\mu V.m.^{-1}\,(c./s.)^{-\frac{1}{2}}$ at 9 kc./s. and 16 $m\mu V.m.^{-1}\,(c./s.)^{-\frac{1}{2}}$ at 230 kc./s., corresponding to intensities of about 10^{-15} $W.m.^{-2}\,(c./s.)^{-1}$ at 9 kc./s. and 3×10^{-19} $W.m.^{-2}\,(c./s.)^{-1}$ at 230 kc./s. The intensities observed at 4 and 9 kc./s. at these times were typical of strong bursts at these frequencies. The 70 and 230 kc./s. intensities were of the same order as previously reported[2]. A striking feature of Fig. 1 is the close correspondence of amplitude fluctuations at the two frequencies. These appear simultaneous to the limit of reading of the time scale (~ 10 sec.).

A probable mechanism for generation of this noise is Čerenkov radiation from small clouds of charged particles travelling through the ionosphere and exosphere[1,3,6]. Radiation is produced at all frequences for which the velocity of the particle clouds exceeds the group velocity of the radiation (Čerenkov condition). The close correspondence between the two

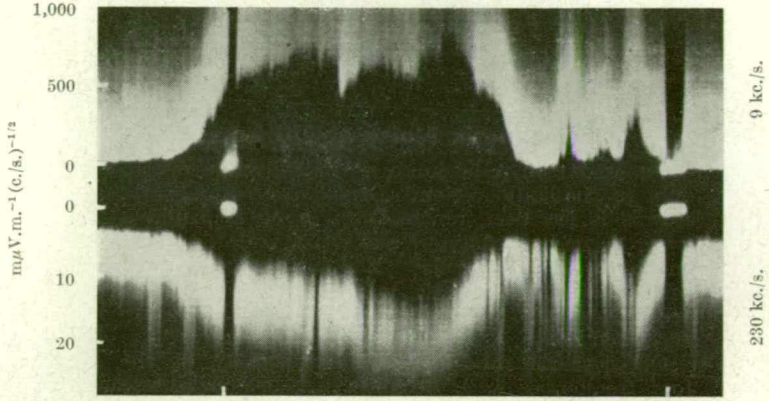

Fig. 1

frequency components observed suggests production by the same particle clouds and in the same geomagnetic tube of force since moving charged particles are effectively constrained to a tube of force.

Accordingly the tube of force ending at Hobart (geomagnetic lat. 52° S.) was considered, and the group velocities of 9 and 230 kc./s. radiation call culated[4] as a function of distance along this tube of force. Electron density as a function of radia- distance was obtained from whistler data[5]. The assumption was made that the electron density in the exosphere is spherically distributed. At 9 kc./s. it was found that the group velocity would be every- where less than 0·12 c. from the ionosphere to the equatorial plane (total distance 15,000 km.). At 230 kc./s. only radiation produced below the gyro-level is observable on the ground. From the ionosphere to the gyro-level (a distance of about 5,000 km.) the 230 kc./s. group velocity would be everywhere less than 0·17 c. Consequently, particle clouds travelling down this tube of force at 0·2 c. (say) could produce Čerenkov radiation at both frequencies. Since the travel-time even of 9 kc./s. radiation produced at 15,000 km. would be less than a second, bursts of radiation at the two frequencies would arrive at the ground simultaneously to our limit of reading.

Estimates of absolute intensities to be expected from the Čerenkov process depend too strongly on unknown factors (for example, size and number of clouds and cloud density) to be meaningful. But we can make an order-of-magnitude estimate of the

relative intensities based on reasonable assumptions. If these unknown factors were the same for both frequencies we would find that the ratio of intensities produced at 9 and 230 kc./s. would be proportional to the path-length in wave-lengths for which the Čerenkov condition holds[3]. This indicates that the intensity produced at 230 kc./s. should be nearly ten times that at 9 kc./s. However, this ratio will be modified by the ear trumpet effect of the converging tube, giving enhancement proportional to the tube cross-section, which is in turn inversely proportional to the field-strength or gyro-frequency. For the tube of force under consideration this will enhance the ratio in favour of 9 kc./s. by a factor of five. Also if the attenuation in regions of high collision frequency is taken into account (from Helliwell's curves[4]) we find that 230 kc./s. will be attenuated by about eight times as many decibels as 9 kc./s. Agreement with the ratio of intensities observed at Hobart (3×10^3 or 35 db.) is reached for an assumption of about 5 db. for 9 kc./s. and hence about 40 db. for 230 kc./s.

Consideration of tubes of force ending farther south of Hobart require attenuations of 9 kc./s. considerably less than this, in keeping with observations of multi-echo whistler trains. Thus estimates based on this mechanism give reasonable agreement with observations of wide-band noise bursts for frequencies from a few kc./s. to a few hundred kc./s.

It is interesting to note that for this mechanism wide-band bursts will only be observed if the electron density distribution along a line of force is such that the plasma frequency is always greater than the gyro frequency for the range of frequencies observed. Since the electron density in the equatorial plane is obtained from whistler data this gives a lower limit to electron density at each point along the line of force.

My thanks are due to Mr. G. T. Goldstone, who built much of the equipment and assisted in the observations, and to Mr. P. S. Bowling who provided housing for the equipment in the field.

R. L. Dowden

Commonwealth Ionospheric Prediction Service,
Hobart, Tasmania. June 10.

[1] Ellis, G. R., *Plan. Space Sci.*, **1**, 253 (1959).
[2] Dowden, R. L., *Nature*, **184**, 803 (1959).
[3] Marshall, L., *Astrophys. J.*, **124**, 469 (1956).
[4] Helliwell, R. A., "Low Frequency Propagation Studies, Part 1", ASTIA Document No. *AD*110184 (1958).
[5] Maeda, K., and Kimura, I., *Rep. Ionos. Res. Japan*, **10**, 105 (1956).
[6] Ellis, G. R., *J. Atmo. Terr. Phys.*, **10**, 302 (1957).

Printed in Great Britain by Fisher, Knight & Co., Ltd., St. Albans.

Journal of Atmospheric and Terrestrial Physics. 1961, Vol. 20, pp. 122 to 130. Pergamon Press, Ltd. Printed in Northern Ireland

A theoretical model of electron density distribution along a geomagnetic line of force in the exosphere

R. L. DOWDEN
Ionospheric Prediction Service, Hobart, Tasmania, and the University of Tasmania

(*Received* 17 *August* 1960)

Abstract—By consideration of charged particles spiralling in geomagnetic tubes of force, particle densities are derived for a source of particles filling the tubes at (i) the equatorial plane or (ii) the earth's surface (ionosphere). The first case gives a distribution of roughly constant density for geomagnetic latitudes (λ) up to 60° and the second to one of density roughly proportional to magnetic field strength for $\lambda < 60°$ and $R < 1{\cdot}25$ earth's radii.

1. INTRODUCTION

OVER the last few years whistler and micropulsation studies have yielded information about electron densities in the exosphere out to several earth's radii. So far this information has not been sufficient to determine whether or not the electron density varies with latitude. In studies of propagation of radio and hydromagnetic waves along the geomagnetic lines of force and of the generation of v.l.f. radio noise, dawn chorus, etc., it is necessary to assume a distribution of electron density along the line of force. The assumption usually made is that electron density is distributed with spherical symmetry about the centre of the earth. This would be logical in the absence of a magnetic field as any local discontinuities would tend to diffuse over a sphere. In the presence of a magnetic field, however, charged particles are mainly confined to a tube of force so that diffusion would take place along the magnetic field lines.

This paper is an attempt to take this effect into account and derive the distribution along a line of force on the assumption that the tubes of force are supplied with charged particles (electrons, protons, etc.) from near the earth's surface (e.g. the upper ionosphere). The particles will move in helical orbits along the line of force. Since the cross-section of the tube of force rapidly increases towards the equatorial plane and since the pitch of the helices decreases (i.e. opens out) in this direction we would expect the density to decrease. Collisions are neglected except in the source regions near the earth's surface. Here down-coming particles which are "lost" are replaced (assuming equilibrium) by an equal number of up-going ones.

The density distribution of the faster particles which produce v.l.f. radio noise and possibly aurora during magnetic storms is also derived on the assumption that these particles are injected into the tubes in regions farthest from the earth, that is near the equatorial plane.

Finally the electron density at any point in space is derived on the rough assumption that the electron density in the source regions (ionosphere) varies with geomagnetic latitude (λ) as cos λ.

In all cases symmetry about the geomagnetic axis is assumed. Hence the relatively slow drift of charged particles in longitude has been neglected.

2. Theory

The various equations describing the dipole magnetic field, a line of force and a tube of force are given (Alfvén, 1950; Chapman and Sugiura, 1956):

$$R = R_0 \cos^2 l$$

$$R_0 = \sec^2 \lambda$$

$$H = \eta H_0$$

$$HA = H_0 A_0 \text{ hence } A = A_0/\eta$$

$$\frac{ds}{dl} = R_0 \phi \cos l$$

where:

R = radius vector in earth radii
l = latitude angle
} polar coordinates

λ = geomagnetic latitude at which the line of force cuts the earth's surface
H = intensity of the earth's magnetic field
$\eta = \phi \sec^6 l$
$\phi = (1 + 3 \sin^2 l)^{1/2}$
A = cross section area of tube of force
s = distance along line of force

Subscript "0" denotes values for which $l = 0$ (i.e. in equatorial plane) and subscript "λ" values for which $l = \lambda$ (earth's surface). We note immediately that:

$$\eta_0 = \phi_0 = 1.$$

We consider one of the particles spiralling along the line of force determined by λ. At the point determined by "l", let its pitch angle be ψ and its speed v. Equations governing its motion (Gold, 1959) are:

$$v = v_0 \text{ (constant)}$$

$$H/\sin^2 \psi = H_0/\sin^2 \psi_0$$

Hence $\sin^2 \psi = \eta \sin^2 \psi_0$.

The velocity of the "guiding centre" of the spiralling particle is:

$$\frac{ds}{dt} = v \cos \psi = v(1 - \sin^2 \psi)^{1/2}$$

$$= v(1 - \eta \sin^2 \psi_0)^{1/2}.$$

The probability of finding this particle at position "l" is proportional to dt/dl. Now,

$$\frac{dt}{dl} = \frac{dt}{ds} \cdot \frac{ds}{dl} = R_0 \phi \cos l [v(1 - \eta \sin^2 \psi_0)^{1/2}]^{-1}.$$

If we consider a large number of such particles (l, ψ_0, v) the density (cm^{-3}) will be given by

$$n(\psi_0, v) \propto \frac{dt}{dl}/A = \frac{KR_0}{A_0 v} \cdot \eta\phi \cos l \,(1 - \eta \sin^2 \psi_0)^{-1/2}$$

where K is a constant of proportionality.

In the equatorial plane:

$$n_0(\psi_0, v) = \frac{KR_0}{A_0 v}(1 - \sin^2 \psi_0)^{-1/2} = \frac{KR_0}{A_0 v \cos \psi_0}.$$

Hence

$$n(\psi_0) = n_0(\psi_0)\eta\phi \cos l \cos \psi_0 (1 - \eta \sin^2 \psi_0)^{-1/2}. \tag{1}$$

We first consider the simpler case of a source of particles in the equatorial plane. If the source is isotropic (no preferred particle direction) simple geometrical considerations show that the distribution of pitch angles will be given by

$$dN_0(\psi_0) = N_0 \sin \psi_0 \, d\psi_0 \tag{2}$$

where the expression on the left hand side represents the density (at $l = 0$) of particles having pitch angles in the range ψ_0 and $\psi_0 + d\psi_0$. Substituting this for $n_0(\psi_0)$ in (1):

$$dN(\psi_0) = N_0 \eta\phi \cos l \sin \psi_0 \cos \psi_0 (1 - \eta \sin^2 \psi_0)^{-1/2} \, d\psi_0.$$

The total density at point l, λ is given by integration over all allowable values of ψ_0 from $\psi_0 = 0$, to $\psi_0 =$ its maximum value Ψ_0 given by $\eta \sin^2 \Psi_0 = 1$. Particles which had pitch Ψ_0 will have pitch $\psi = \pi/2$ at this point (magnetic mirror point). Particles of greater pitch will have been removed by magnetic reflection before reaching this point.

Hence

$$N = N_0 \eta\phi \cos l \int_0^{\Psi_0} \sin \psi_0 \cos \psi_0 (1 - \eta \sin^2 \psi_0)^{-1/2} \, d\psi_0.$$

Putting $x^2 = 1 - \eta \sin^2 \psi_0$,

$$N = N_0 \eta\phi \cos l \frac{l}{\eta} \int_0^1 dx = N_0 \phi \cos l. \tag{3}$$

The expression $\phi \cos l$ is unity at $l = 0$ and at $\sin^2 l = 2/3$ ($l \sim 55°$). It has its maximum value (1·15) for $\sin^2 l = 1/3$ ($l \sim 35\frac{1}{2}°$). Simple computation shows it to be within 15 per cent of unity for $l < 60°$.

Hence this distribution which probably applies to the case of solar particles injected into the tube of force during magnetic storms gives a practically constant density along a line of force for all lines (λ) up to $\lambda = 60°$.

The thermal particles which make up the background medium are probably supplied where ionization is taking place, i.e. in the ionosphere. Accordingly we

consider an isotropic source at $l = \lambda$. The distribution of pitch angles is given [as in (2)] by

$$dN_\lambda(\psi_\lambda) = N_\lambda \sin \psi_\lambda \, d\psi_\lambda. \tag{4}$$

We relabel these same particles by the pitch angles (ψ_0) they would have on reaching the equatorial plane, where

$$\sin^2 \psi_\lambda = \eta_\lambda \sin^2 \psi_0. \tag{5}$$

Differentiating:

$$2 \sin \psi_\lambda \cos \psi_\lambda \, d\psi_\lambda = 2\eta_\lambda \sin \psi_0 \cos \psi_0 \, d\psi_0.$$

Hence

$$\sin \psi_\lambda \, d\psi_\lambda = \eta_\lambda \frac{\sin \psi_0 \cos \psi_0}{\cos \psi_\lambda} d\psi_0$$

$$= \eta_\lambda \sin \psi_0 \cos \psi_0 (1 - \eta_\lambda \sin^2 \psi_0)^{-1/2} \, d\psi_0.$$

Relabelling (4) and substituting:

$$dN_\lambda(\psi_0) = N_\lambda \eta_\lambda \sin \psi_0 \cos \psi_0 (1 - \eta_\lambda \sin^2 \psi_0)^{-1/2} \, d\psi_0. \tag{6}$$

From (1) we have:

$$n_0(\psi_0) = n_\lambda(\psi_0) \frac{(1 - \eta_\lambda \sin^2 \psi_0)^{1/2}}{\phi_\lambda \eta_\lambda \cos \psi_0 \cos \lambda}.$$

Replacing $n_0(\psi_0)$ by $dN_0(\psi_0)$ and $n_\lambda(\psi_0)$ by $dN_\lambda(\psi_0)$ as given in (6):

$$dN_0(\psi_0) = \frac{N_\lambda \sin \psi_0}{\phi_\lambda \cos \lambda} d\psi_0.$$

Integrating from $\psi_0 = 0$ to $\psi_0 = \Psi_0$ where $\sin^2 \Psi_0 = 1/\eta_\lambda$ [hence $\cos \Psi_0 = (1 - 1/\eta_\lambda)^{1/2}$]:

$$N_0 = \frac{N_\lambda}{\phi_\lambda \cos \lambda} \int_0^{\Psi_0} \sin \psi_0 \, d\psi_0$$

$$= \frac{N_\lambda}{\phi_\lambda \cos \lambda} \left[1 - \left(1 - \frac{1}{\eta_\lambda} \right)^{1/2} \right]$$

$$= \frac{N_\lambda}{\phi_\lambda \cos \lambda} \zeta \left(\frac{1}{\eta_\lambda} \right). \tag{7}$$

Hence

$$dN_0(\psi_0) = \frac{N_0}{\zeta\left(\frac{1}{\eta_\lambda}\right)} \sin \psi_0 \, d\psi_0. \tag{8}$$

We can now find N at any point "l" as in the previous argument by replacing the pitch distribution given in (2) by that in (8) except that the upper limit is now given by $\sin^2 \Psi_0 = 1/\eta_\lambda$.

That is

$$N = \frac{N_0}{\zeta(1/\eta_\lambda)} \phi \cos l \, [(1 - \eta \sin^2 \psi_0)^{1/2}]_{\Psi_0}^0$$

$$= N_0 \phi \cos l \, \zeta \left(\frac{\eta}{\eta_\lambda} \right) \Big/ \zeta \left(\frac{1}{\eta_\lambda} \right) \tag{9}$$

where $\zeta \left(\frac{\eta}{\eta_\lambda} \right) = 1 - \left(1 - \frac{\eta}{\eta_\lambda} \right)^{1/2}$ and use has been made of (5).

An approximation can be obtained by noting

$$\zeta(\delta) \approx \tfrac{1}{2}\delta + \tfrac{1}{8}\delta^2.$$

Hence for $\eta_\lambda \gg 1$ and $\eta_\lambda \gg \eta$:

$$N = N_0 \eta\phi \cos l. \tag{10}$$

This approximation is good to within about 10 per cent provided $\eta_\lambda/\eta > 2\frac{1}{2}$ or $\sec^6\lambda/\sec^6 l > 2$ or $R > 1{\cdot}25$.

The distributions derived have been expressed in terms of N_0 since this quantity (as a function of R_0 or λ) is the one most readily found from whistler and pulsation studies. However, the $N_0(\lambda)$ distribution is derivable if we assume a distribution for N_λ, the electron density in the upper ionosphere.

Suppose

$$N_\lambda = N_E \cos \lambda.$$

Substituting in (7)

$$N_0 = \frac{N_E}{\phi_\lambda}\zeta\left(\frac{1}{\eta_\lambda}\right)$$

$$\approx \frac{N_E}{2\phi_\lambda\eta_\lambda} \text{ for } \lambda > 25°$$

Or in terms of $R_0 (R_0 > 1{\cdot}25)$:

$$N_0 \approx \frac{N_E}{2R_0^3(4 - 3/R_0)}. \tag{11}$$

3. Discussion

3.1. *Assumptions*

The theory is valid provided (i) that the geomagnetic field is approximately dipole, (ii) that collisions and (iii) gravitational forces can be neglected, and (iv) that the electrons (and protons) are supplied mainly from near the earth's surface. We will consider each of these assumptions separately.

3.1.1. *Dipole field.* Recent data from the space probe Pioneer V (Coleman *et al.*, 1960) indicates that the field extends out to about 14 earth's radii. Vestine and Sibley (1959) find that the field lines connecting the auroral zones ($R_0 \sim 6$) are not seriously distorted by solar streams, even during auroral displays. This indicates the dipole field is valid out to about 10 radii.

3.1.2. *Collisions.* As pointed out in the Introduction, collisions in the regions of highest collision frequency, the source regions, are effectively taken into account by the theory. In an exosphere of protons and electrons only collisions of electrons with protons are important since elastic collisions between like particles involve only velocity exchange and the much heavier protons are not greatly effected by collisions with electrons. Assuming a temperature of about 10,000°K in the source regions, the thermal velocity of an electron would be around 10^8 cm/sec. The time taken for one trip along the line of force $\lambda = 70°$ (say) would be about 100 sec. The effective average density $\bar{N}$ ($\bar{N}s \equiv \int N ds$) along this line is about 80 cm^{-3} so that at this temperature the effective average collision frequency will be about 2×10^{-4} sec^{-1}. Thus the probability of an electron suffering a collision during a single trip would be about 1 in 50. Collisions would involve pitch changes and so

change the theoretical pitch distribution slightly. In the equilibrium condition this effect could be allowed for by a weak source in the equatorial plane giving rise to a small and essentially constant additive term (equation 3).

3.1.3. *Gravitational forces.* These can be neglected if the maximum gravitational potential energy is much less than the kinetic energy of the particles. This condition is met for temperatures in the source regions of ~2°K for electrons and ~4000°K for protons. CHAPMAN (1959) suggests that the temperature of the exosphere

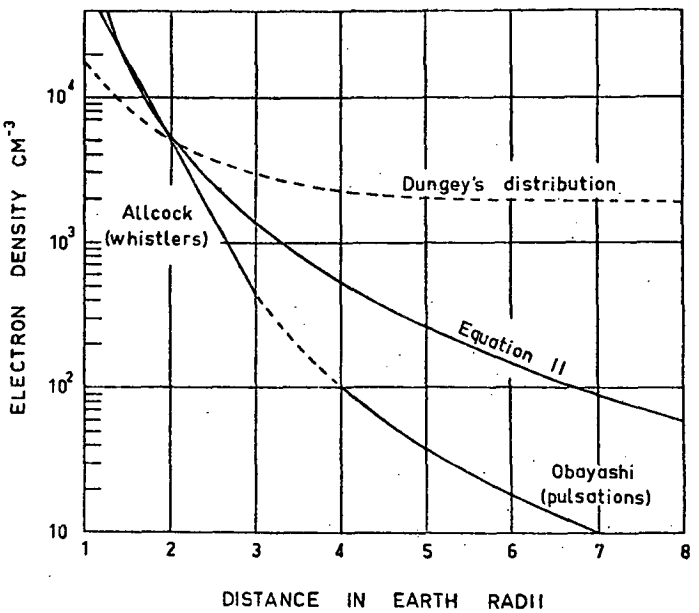

Fig. 1. Electron density along a radius in the equatorial plane.

ranges from 30,000°K at heights around 1000 km to about 200,000°K where the exosphere merges into interplanetary space. Thus it is likely that the condition is met for both electrons and protons.

3.1.4. *Source points.* JOHNSON (1959) has shown that the electrons etc. making up the exosphere must be of telluric (terrestrial) rather than solar origin. Hence the source will be the ionosphere where appreciable ionization is taking place. The theory developed above strictly requires that the "surface of the earth" be the ionosphere and so the "radius of the earth" be the radius of the ionosphere. This will effect slightly the units of R and R_0 and the definition of λ.

3.2. *Computed distributions*

The electron density in the equatorial plane (N_0) as a function of radial distance (R_0) was computed from (11) for $N_E = 2 \times 10^5$ cm^{-3}. This value of N_E, the average electron density of the source region above the equator, is consistent with experimental measurements of the noon maximum density of the ionosphere (N_{max}) at the equator (CROOM *et al.*, 1960) of ~20×10^5 cm^{-3} and values N/N_{max} ~0·2 at ~800 km (presumably the source region) found by satellite experiments (GARRIOTT, 1960). This is shown in Fig. 1 together with DUNGEY'S (1954) theoretical

distribution $N \propto \exp(2{\cdot}5/R)$ scaled to give agreement at 2 earth's radii and the experimental distribution of ALLCOCK (1959) from whistler studies for the range 1·2–3 earth's radii, and by OBAYASHI (1958) from pulsation studies for the range 4–7 earth's radii. When compared with the experimental curve we find a discrepancy which is small for $R_0 < 2$, nearly a factor of ten for $R_0 \sim 7$, but decreasing at greater distances [using OBAYASHI's extrapolation $N = \exp(17{\cdot}5/R_0)$].

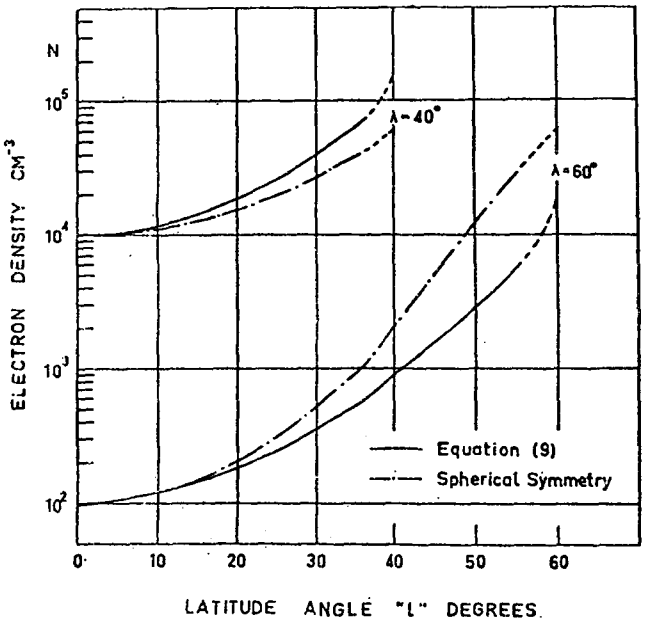

Fig. 2. Electron density along a line of force.

The distributions along lines of force $\lambda = 40°$ and $\lambda = 60°$ were computed from (9) using values of N_0 of 10,000 cm^{-3} and 100 cm^{-3} respectively taken from the whistler–pulsation experimental curve. These are shown in Fig. 2 together with distributions computed from the experimental curve on the assumption that the electron density is distributed with spherical symmetry about the earth. The dashed portions of the curves correspond to extrapolations into regions within 1000 km. The fact that the discrepancies between the two types of distribution change sign between $\lambda = 40°$ and $\lambda = 60°$ suggest that the spherical symmetry distribution may be a reasonable approximation for longitudinal propagation studies within this range of λ. However, for $\lambda < 60°$, $\phi \cos l \approx 1$ and so provided also $R > 1{\cdot}25$, we have from (10) $N \approx \eta N_0$ or $N \propto H$. Hence in this region the "whistler" mode (longitudinal extraordinary mode at frequencies much less than the gyro frequency) refractive index, being proportional to N/H, is approximately constant.

Values of electron density (N) were computed for a large number of points (λ, l) for lines up to $\lambda = 80°$ from values of N_0 taken from the experimental $N_0(R_0)$ whistler–pulsation curve. For $\lambda > 65°$ values of *effective* N_0 were obtained by

extrapolation. For the longer lines of force ($\lambda > 70$) it was assumed that the theory would remain a reasonable approximation for $R < 10$ even though the line of force equations may not hold for $R > 10$. Contours of electron density or *isopycs* are shown in a plane containing the geomagnetic axis in Fig. 3. The line of force $\lambda = 70°$ is shown for reference. Presumably the contours close over the axis poles. This suggests considerable extensions of electron density in the direction of the axis.

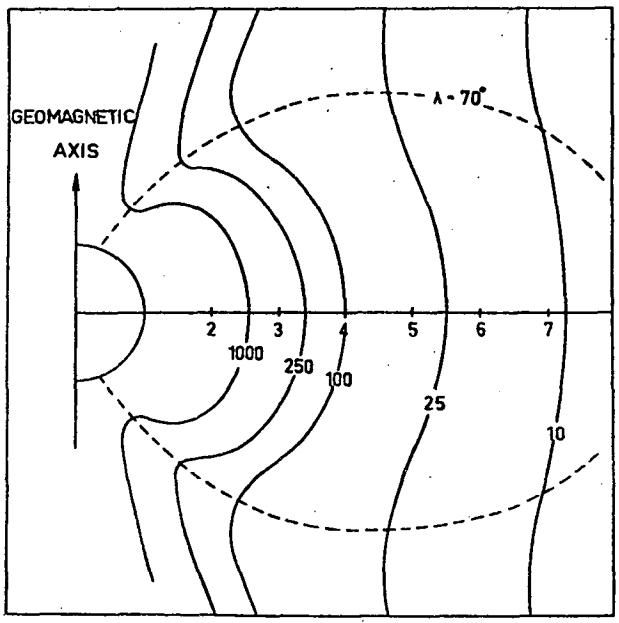

Fig. 3. Contours of electron density (isopycs) in a plane containing the geomagnetic axis.

4. Conclusions

The distribution of electron (and proton) density along a line of force has been derived (equation 9). At latitudes less than 60° and heights greater than about 2000 km ($R > 1{\cdot}25$) the electron density is approximately proportional to the magnetic field strength ($N/N_0 = H/H_0$). The density distribution of "aurora" or "magnetic storm" particles has also been derived (equation 3). The latter expression approximates to $N = N_0$ for latitudes less than about 60°. The electron density distribution in polar coordinates has been derived graphically (Fig. 3). At low latitudes the distribution is approximately spherically symmetrical, but at high latitudes departures from this are great, tending towards constancy along radii. This suggests considerable extensions of electron density above the geomagnetic poles.

Acknowledgements—The writer expresses his appreciation to Professor G. Newstead of the Department of Electrical Engineering and Dr. K. B. Fenton of the Department of Physics, University of Tasmania, and to Dr. W. G. Baker, Officer in Charge, Ionospheric Prediction Service, for helpful discussions and suggestions.

NOTE ADDED IN PROOF

IT HAS SINCE been pointed out to the writer by Dr. J. H. PIDDINGTON and Dr. F. S. JOHNSON that satellite orbit data give temperatures of 1000–1500°K at heights around 400–700 km (HARRIS and JASTROW, 1959) so that the assumption of 10,000°K in the source regions is around seven or eight times too high. If these low temperatures applied throughout the exosphere, collision frequencies would be some twenty times greater. The electron density distribution will be largely controlled by the distribution of the much heavier protons which may not be seriously affected by electron collisions, but at these low temperatures thermal protons would have insufficient energy to neglect gravitional and geocentrifugal effects. This difficulty might be resolved by placing the source regions at a much greater height where the effective gravitional potential energy is lower and where the temperature may be much higher. The same equations derived above will describe this case provided quantities are redefined as discussed in Section 3.1.4.

On the other hand the writer has also been informed since (by Professor R. A. HELLIWELL) of a distribution of electron density out to 5 earth radii obtained from nose whistler measurements (SMITH, 1960). This distribution was found to fit a "gyrofrequency" model: $N = Kf_H\phi_\lambda^{-1}$, where K is constant. Our distribution can be put in this form from (10) and (11) where

$$K = \frac{N_E\phi \cos l}{2(f_H)_\lambda} \approx \frac{N_E}{2(f_H)_\lambda}.$$

For $R_0 > 1{\cdot}25$ and l and $\lambda < 60°$, K is "constant" to within about 50 per cent. The two distributions can be closely matched throughout this region if the value of N_E suggested in Section 3.2 is reduced by a factor of about three.

REFERENCES

ALFVEN H.	1950	*Cosmical Electrodynamics*, p. 4. Clarendon Press, Oxford.
ALLCOCK G. McK.	1959	*J. Atmosph. Terr. Phys.* **14**, 185.
CHAPMAN S.	1959	*J. Atmosph. Terr. Phys.* **15**, 43.
CHAPMAN S. and SUGIURA M.	1956	*J. Geophys. Res.* **61**, 485.
COLEMAN P. J., SONNETT C. P., JUDGE D. L. and SMITH E. J.	1960	*J. Geophys. Res.* **65**, 1856.
GROOM S., ROBBINS A. and THOMAS J. O.	1960	*Nature, Lond.* **185**, 902.
DUNGEY J. W.	1954	*The Physics of the Ionosphere*, p. 229. Physical Society London.
GARRIOTT O. K.	1960	*J. Geophys. Res.* **65**, 1139.
GOLD T.	1959	*Nature. Lond.* **183**, 355.
HARRIS I. and JASTROW R.	1959	*Planet. Space Sci.* **1**, 20.
JOHNSON F. S.	1959	*Nature, Lond.* **184**, 1787.
OBAYASHI T.	1958	*Rep. Ionos. Res. Japan* **12**, 301.
SMITH R. L.	1960	Stanford Electronics Laboratory, Techn. Rept. No. **6**
VESTINE E. H. and SIBLEY W. L.	1959	*Planet. Space Sci.* **1**, 285.

Simultaneous Observations of VLF Noise ('Hiss') at Hobart and Macquarie Island

R. L. DOWDEN

Ionospheric Prediction Service and the University of Tasmania
Hobart, Tasmania, Australia

Ellis [1960] showed that individual bursts of LF radio noise associated with geomagnetic isturbances (also called 'hiss' or 'geomagnetic oise') are often fed into the ionosphere-earth aveguide structure at fairly well defined points. he geographical position of these virtual sources an be located by comparing noise intensities of ree different stations [*Ellis*, 1961]. For each air of stations there will exist a family of curves efined by

$$(r_2/r_1) \exp [-\alpha(r_1 - r_2)] = R$$

here R (a constant of each curve) is the ratio the power intensities observed from a noise ource distant r_1, r_2, respectively, from stations and 2, and where α is the attenuation coefficient. Data were obtained for the pair of stations obart–Macquarie Island at the two frequencies 3 and 9.3 kc/s for the 10 weeks from December 26, 1959, to March 3, 1960. Bursts recorded at both stations are listed in Table 1. It should be noted that the sensitivity of the receiver at Macquarie Island was much lower than that at Hobart, particularly at 9 kc/s. Only those bursts observed at both stations were considered. This tended to exclude 4-kc/s components that were not stronger at Macquarie Island and 9-kc/s components which were not very much stronger at Macquarie Island.

A map of the area showing Hobart and Macquarie Island, the auroral zone (hatched arc), and constant R curves for attenuation coefficients of 10 db/1000 km (full line curves) and 2 db/1000 km (dashed) corresponding to 4 kc/s and 9 kc/s propagation, respectively, is given in Figure 1. A 4-kc/s source occurring on the Hobart–Macquarie Island line would appear 10 db weaker at both stations if it were shifted

TABLE 1. Simultaneous Noise Bursts

Date	Universal Time	4 kc/s Intensity $Wm^{-2}(c/s)^{-1} \times 10^{16}$			9 kc/s Intensity $Wm^{-2}(c/s)^{-1} \times 10^{16}$		
		Hobart	M. I.	Ratio	Hobart	M. I.	Ratio
Jan 14	0500–1000	30	650	22			
15	2040	30	14	0.5			
Feb 1	1630	1.2	4.8	4			
2	1630–1715	1.2	1.2	1			
3	0450–1400	8.5	170	20	1.2	480	400
3	2125	13	120	3			
4	0200–1900	4.8	330	70	0.5	330	660
5	0530	2.1	19	9	<0.5	210	>400
6	0130	2.1	19	9	0.3	270	900
6	2330	0.5	19	36			
9	1315	3.3	480	140	0.3	270	900
19	2045	0.3	13	45	<0.13	120	>1000
19	2100	0.8	30	36	0.2	210	1000
26	1600	0.3	2.1	7	1.1	<3.3	<3
29	2235–2310	2.1	8.4	4			
Mar 1	2130	2.1	19	9			

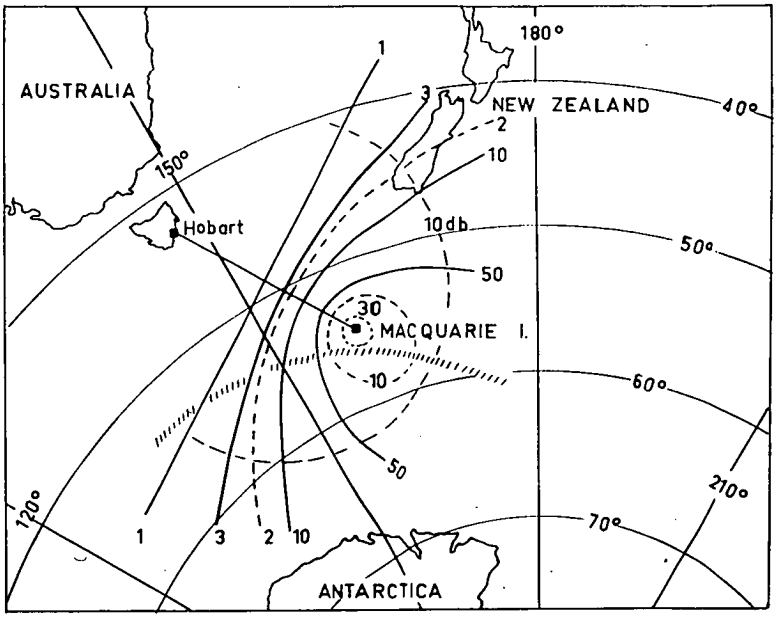

Fig. 1. Map of area showing constant intensity ratio curves for attenuation coefficients of 10 db per 1000 km (full-line curves) for 4 kc/s, and of 2 db per 1000 km (dashed) for 9 kc/s. The hatched arc is the auroral zone. Coordinates are geographic.

along a curve of constant intensity ratio to the dash semicircle marked '10 db.'

Independent 'fixes' of individual bursts are not possible without data from another pair of stations. All but one of the observed 9-kc/s components must have occurred well inside the R = 30 ring (Fig. 1). Little can be said about the positions of the 4-kc/s components except that they occurred on the appropriate curves and probably within the 10-db semicircle. However, two important points emerge. First, at 9 kc/s only sources of a few kilometers in extent could produce intensity ratios of 1000 even if the sources occurred overhead at Macquarie Island. This shows that some sources at least have very narrow dimensions. Second, it is immediately apparent from Figure 1 that for all but one (February 26) of the eight bursts observed at both frequencies, the source positions for the two components could not have coincided. In fact, the distances between these two source positio varied from at least 100 to 500 km.

Acknowledgments. This work also represent part of the research program of the Australi National Antarctic Research Expeditions at Ma quarie Island. I wish to thank Mr. R. Levick f operating the Macquarie Island equipment, Mr. G. Goldstone for operating the Hobart equipmer and Professor G. R. A. Ellis, Physics Departmer University of Tasmania, for much criticism a stimulating discussion.

References

Ellis, G. R. A., Directional observations of 5 kc radiation from the earth's outer atmosphere, *Geophys. Research, 65*, 839–843, 1960.

Ellis G. R. A., Spaced observations of the low fr quency radiation from the earth's upper atmo phere, *J. Geophys. Research, 66*, 19–23, 1961.

(Received January 16, 1961.)

WIDE-BAND BURSTS OF V.L.F. RADIO NOISE (HISS) AT HOBART*

By R. L. DOWDEN†

[*Manuscript received August* 15, 1961]

Summary

Wide-band bursts of radio noise from the upper ionosphere or exosphere have been observed at frequencies from 100 c/s to 250 kc/s. The observed intensity [Wm^{-2} $(c/s)^{-1}$] ranges from nearly 10^{-9} at 100 c/s to 10^{-19} at 250 kc/s. However, the intensity at the source (above the ionosphere), deduced by subtracting the losses suffered in the ionosphere and below the ionosphere, shows a relatively flat spectrum at a level of the order of 10^{-10} Wm^{-2} $(c/s)^{-1}$.

I. INTRODUCTION

V.L.F. noise, also known as " hiss " or geomagnetic noise, is audio-frequency radio noise originating in the upper ionosphere or exosphere which tends to occur at times of aurora and geomagnetic activity (Ellis 1959). It usually occurs in bursts of minutes or hours' duration. These bursts are usually narrow band (a few kilocycles bandwidth) centred at around 5 kc/s (Ellis 1959). Sometimes, particularly at times of strong geomagnetic disturbance, very wide-band bursts occur (Ellis 1959 ; Dowden 1960). Some very wide-band bursts have been observed covering a range of from less than 5 kc/s to more than 200 kc/s (Dowden 1960). Later observations (this paper) have followed these wide-band bursts down to less than 100 c/s so it seems likely that occasionally bursts spread over the range from 100 c/s or less to a few hundred kc/s—a frequency ratio of several thousand.

This paper examines the ground level intensities recorded at several spot frequencies (125, 240, 410, 760 c/s, 1·8, 4·3, 9·0, and 230 kc/s) during wide-band bursts observed at Hobart. The corresponding intensities at an arbitrary level above most of the ionosphere (550 km) are deduced from considerations of the losses affecting the wave from that level to the observing point.

II. EXPERIMENTAL

(*a*) *Techniques*

The receiving systems were broadly similar to those described elsewhere (Ellis 1959). A vertical loop antenna fed a wide-band amplifier followed by a narrow-band pass amplifier for each channel. Special techniques were used to avoid spurious effects of atmospherics and other impulsive noise.

In one recording system the detected outputs were applied to the vertical deflection plates of a C.R.O. During an impulse the C.R.O. spot would be deflected well off scale but between impulses the spot would be deflected only by

* Presented at the Conference on the Sun-Earth Environment, Brisbane, May 24–26, 1961.

† Ionospheric Prediction Service, University of Tasmania, Hobart.

continuous signal. When such a display is photographed by slowly moving film the continuous level between impulses is readily apparent.

The second system was developed by Ellis (1959) for recording on a pen recorder. This also records only the continuous level between impulses. In this method the detected outputs were applied to a partially unidirectional integrator. This had a long time constant of many tens of seconds for increases in signal but a very short time constant of some milliseconds for signal decreases. The system is thus the reverse of a peak-reading voltmeter.

Both systems give strong discrimination (of about 40 dB) against atmospherics even when the " mark-space " ratio of atmospherics is very high. In some cases both recording systems were used on the one frequency channel.

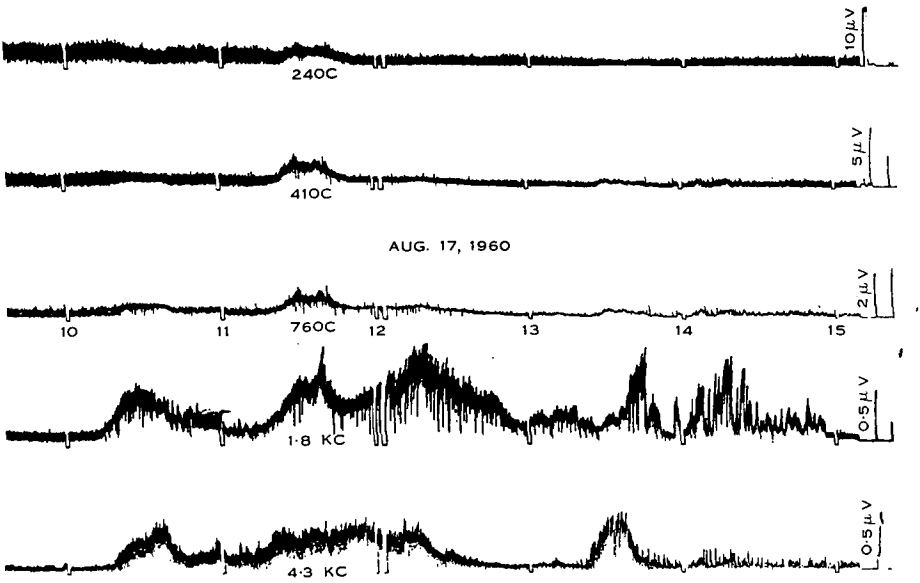

Fig. 1.—Typical wide-band (*c.* 1130 L.T.) and narrow-band bursts.

Further discrimination from any spurious effects follows from the nature of the phenomena studied. That shown in Figure 1 is fairly typical. The smooth rise and fall of amplitude during bursts, the duration of bursts (order of an hour), and the relative infrequency of bursts (around 10 per month), make the phenomena readily distinguishable from steady background noise or man-made bursts of interference.

Two basic methods of intensity calibration were used. In the first the loop antenna was replaced by a signal generator or noise generator of the same impedance. Burst intensities were then deduced from this receiver sensitivity calibration and the effective height of the loop antenna calculated from measurement of its physical dimensions. The second method gave direct calibration by generating a known field strength in the vicinity of the antenna from a remote auxiliary loop. Both methods gave consistent results. The calibration and reading accuracy (about 10%) was more than adequate for the argument presented in this paper.

Only six recording channels were available so that simultaneous recordings were not made at all eight frequencies mentioned above. However, there was sufficient frequency overlap to suggest that the wide-band bursts measured mainly at the higher frequencies were similar to those measured mainly at the lower frequencies.

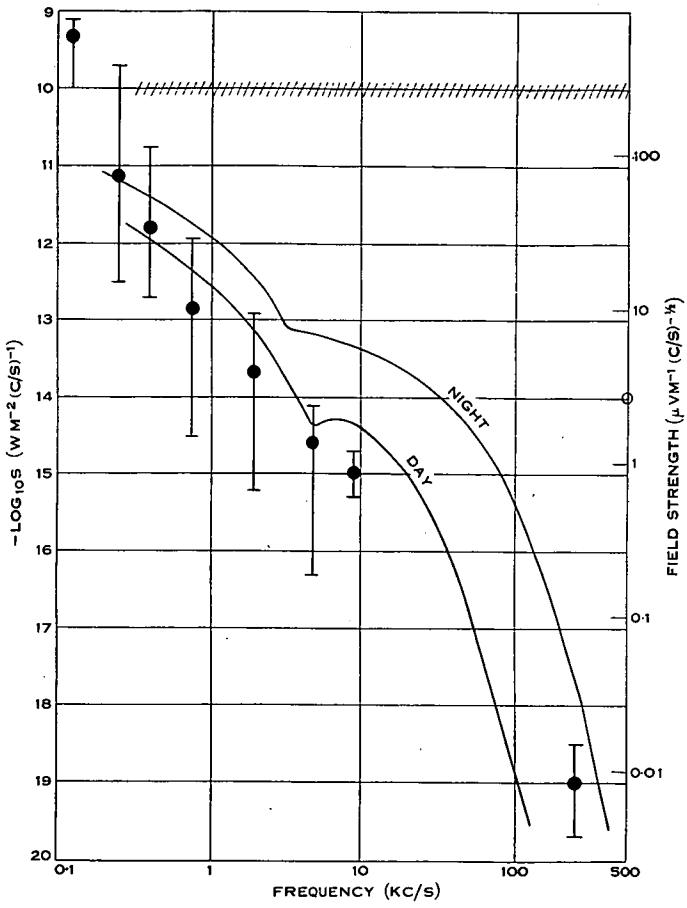

Fig. 2.—Medians and spread of peak intensities of observed wide-band bursts. Curves are expected ground intensities for a " white " source above the ionosphere at the hatched level [10^{-10} Wm^{-2} $(c/s)^{-1}$]. The right-hand ordinate is field strength.

Two sweep-frequency analysers covering the ranges 40–500 c/s and 400 c/s to 6 kc/s, though of less sensitivity and of restricted use for intensity measurement, were used to check the interpretation of the fixed-frequency records.

(*b*) *Observations*

Twenty-five wide-band bursts recorded over a period of about 15 months are considered here. Figure 1 shows one of these recorded on the five frequencies operating at the time. Other narrow-band bursts at around 2 and 5 kc/s are

seen on the same record. The median intensities and the spread of intensities recorded is shown plotted in Figure 2. Medians for 125 c/s and for 9·0 and 230 kc/s may not be truly representative, as less than five values were obtained for each. The burst signal to background noise ratio was best around the middle of the band (20 dB at 5 kc/s) but worsened in both directions to about 5 dB at 100 c/s and 10 dB at 200 kc/s.

III. Discussion

Although there is no strong evidence to indicate the level at which V.L.F. noise is produced, we will assume here that it is above most of the ionosphere, that is, above (say) 550 km. Directional and spaced observations (Ellis 1960; Dowden 1961) show that V.L.F. noise bursts often appear to be coming from virtual sources of quite small areas on the Earth's surface. Consequently we adopt the model that the burst is generated in a relatively narrow tube of force somewhere above the ionosphere, is then piped down through the ionosphere in the " whistler mode ", and radiated out under the ionosphere in the two-surface (Earth or ocean and ionosphere) waveguide to the observer. We require, then, the losses suffered in these two modes.

The Earth-ionosphere waveguide losses have been calculated by Watt and Maxwell (1957) for frequencies from .1 to 100 kc/s. Curves are given of field strength versus frequency for propagation over day-time and night-time sea-water paths of various distances for a unit " white " point source. In our case the distance between the virtual source and the observing point is not known for each burst but a typical median value can be estimated along the following lines.

Suppose all sources were point sources and that they were randomly distributed about Hobart. We consider an annular area centred on Hobart at distance r, width $\mathrm{d}r$, and area $\mathrm{d}A$. We define the probabilities: $p_s(r, \mathrm{d}r)$ of a source occurring within this annular area; $p_0(r, \mathrm{d}r)$ of it being observed at Hobart if it did occur; and $p_{0s}(r, \mathrm{d}r)$ of an *observable* source occurring within this area (within r and $r+\mathrm{d}r$). It follows:

$$\begin{aligned} p_s(r,\mathrm{d}r) &\propto \mathrm{d}A \propto r.\mathrm{d}r \\ p_0(r,\mathrm{d}r) &\propto \text{intensity on arrival at Hobart} \\ &\propto \mathrm{e}^{-\alpha r}/r \end{aligned}$$

where α = attenuation coefficient for the Earth-ionosphere waveguide mode.

$$\begin{aligned} p_{0s}(r,\mathrm{d}r) &= p_s(r,\mathrm{d}r)\cdot p_0(r,\mathrm{d}r) \\ &= \mathrm{e}^{-\alpha r}\cdot \mathrm{d}r. \end{aligned}$$

We define a median range $\bar{r}$ such that

$$\int_0^{\bar{r}} p_{0s}(r,\mathrm{d}r) = \int_{\bar{r}}^{\infty} p_{0s}(r,\mathrm{d}r),$$

that is

$$\frac{1}{\alpha}[\mathrm{e}^{-\alpha r}]_{\bar{r}}^{0} = \frac{1}{\alpha}[\mathrm{e}^{-\alpha r}]_{\infty}^{\bar{r}}.$$

Hence

$$\mathrm{e}^{-\alpha\bar{r}} = \tfrac{1}{2}.$$

The attenuation coefficient, α, is strongly frequency dependent, but typical values are around 3 dB per 1000 km (Watt and Maxwell 1957) so that the typical range ($\bar{r}$) will be around 1000 km.

Suppose instead the sources were very large so that everywhere in the vicinity of Hobart was essentially uniformly illuminated by each burst. We consider the same annular area described above. The total power intercepted by this annulus is proportional to its area,

$$dP_s(r) \propto r.dr,$$

Transmission over distance r to Hobart would decrease this by a factor $e^{-\alpha r}/r$, so that the power observed at Hobart from this area (from ranges r to $r+dr$) is then

$$dP_{0s}(r) = K.e^{-\alpha r}.dr,$$

K being a constant of proportionality. We define the median range $\bar{r}$ as that range within which half of the observed power occurs. Then

$$K\int_0^{\bar{r}} e^{-\alpha r}.dr = K\int_{\bar{r}}^{\infty} e^{-\alpha r}.dr.$$

Hence the same argument as that above leads to $\bar{r} \approx 1000$ km.

Selection of the $\bar{r}=1000$ km day and night curves of Watt and Maxwell gives us the below-ionosphere losses for the frequency range 1–100 kc/s. Those for frequencies outside this range are estimated by extrapolation.

The attenuations for whistler mode propagation through the ionosphere were obtained from curves by Helliwell (1958) using a model day-time ionosphere from 80 to 550 km given by Francis and Karplus (1960). Night-time attenuations were estimated from this model by disregarding the ionosphere below 100 km. The values found are roughly consistent with whistler mode echo observations (Dowden 1959) at 17 kc/s and observations of 512 kc/s signals from the ground made by a receiver carried in a rocket to a height of over 400 km (Mechtly and Bowhill 1960).

The losses for propagation through the ionosphere (whistler mode) and below the ionosphere (waveguide) are combined and plotted in Figure 2 for day and night conditions. We have assumed a " white noise " source of intensity 10^{-10} Wm^{-2} $(c/s)^{-1}$ at a level of 550 km. The curves thus represent the expected intensity at an observing station on the ground about 1000 km from the point immediately below the source. The accuracy of these curves deteriorates towards both ends of the frequency scale. The treatment used above breaks down at the low end because the distances involved approach a wavelength. At the high frequencies the attenuations are so large that small errors in the estimation of parameters become important. Both ends will suffer from the extrapolations.

It is seen from Figure 2 that the expected " ground level " spectrum resulting from this flat or " white " source spectrum fits the observed intensities to an order of magnitude or so, although an intensity proportional to wavelength

might give a better fit at the low frequency end. The main point emerging from this study is that much of the very strong frequency dependence of observed intensities is accounted for by attenuation.

Intensities of over 10^{-14} Wm^{-2} $(c/s)^{-1}$ at 512 kc/s have been observed at a height of 400 km by Mechtly and Bowhill (1960). This is a lower limit (receivers overloaded) and so consistent with our results. On the other hand, at frequencies above 900 kc/s, at times when the ionosphere above Hobart is transparent, ground level intensities (due to cosmic noise) of only 2×10^{-19} Wm^{-2} $(c/s)^{-1}$ are observed (Ellis 1957). This is some nine orders of magnitude less than our value. However, it must be remembered that very wide-band bursts are rare and occur only during very severe disturbances, whereas the ionosphere is transparent at low frequencies only during very quiet conditions. Nevertheless, this does show that, at least at the higher frequencies, a continuous high background level does not exist.

IV. Acknowledgments

The author is indebted to Professor G. R. A. Ellis of the Physics Department, University of Tasmania, for many interesting discussions, criticisms, and suggestions, and to Mr. G. T. Goldstone of the Ionospheric Prediction Service, Hobart, for building, operating, and maintaining the equipment.

V. References

Dowden, R. L. (1959).—*Nature* **183**: 385–6.
Dowden, R. L. (1960).—*Nature* **187**: 677–8.
Dowden, R. L. (1961).—*J. Geophys. Res.* **66**: 1587–8.
Ellis, G. R. A. (1957).—*J. Geophys. Res.* **62**: 229–34.
Ellis, G. R. A. (1959).—*Planet. Space Sci.* **1**: 253–8.
Ellis, G. R. A. (1960).—*J. Geophys. Res.* **65**: 839–43.
Francis, W. E., and Karplus, R. (1960).—*J. Geophys. Res.* **65**: 3593–600.
Helliwell, R. A. (1958).—Low frequency propagation studies, Part I. ASTIA Document No. AD110184 (Stanford University).
Mechtly, E. A., and Bowhill, S. A. (1960).—*J. Geophys. Res.* **65**: 3501.
Watt, A. D., and Maxwell, E. L. (1957).—*Proc. Inst. Radio Engrs., N.Y.* **45**: 787–94.

Doppler-Shifted Cyclotron Radiation from Electrons: A Theory of Very Low Frequency Emissions from the Exosphere

R. L. DOWDEN

Ionospheric Prediction Service and University of Tasmania
Hobart, Tasmania, Australia

Abstract. Cyclotron radiation from electrons in the exosphere spiraling along a line of force *away* from the observer will appear at a frequency less than the local gyrofrequency. An electron traveling from the observer's hemisphere to the opposite hemisphere will radiate a decreasing frequency until it crosses the equator, and thence an increasing frequency. Propagation conditions and various particle speeds give frequency-time spectra similar to those observed. A method of scaling electron speeds and the field lines in which they occur from observed data is described. Tests of the theory are discussed.

troduction. Very low frequency emissions r in the audiofrequency region and show ciation with magnetic disturbance. It is rally thought that they are generated in the phere or upper ionosphere by fast charged icles. Two main types occur: 'hiss,' a conous white noise that can occur in broad or ow bands; and 'chorus,' which is made up sing and falling tones or whistles. Only the us type is considered here. This phenomenon etimes occurs as quite separate discrete tles showing definite and repeatable forms frequency-time spectrographs. These have described by many workers as 'falling s,' 'hooks,' 'risers,' and 'pseudo noses.' mples of these are shown in Figure 1 (after *iwell and Carpenter* [1961]).

he first theory explaining the frequency-time e of some of these was given by *Gallet and iwell* [1959]. They suggested that, when the icle speed $\beta_d c$ was equal to the wave velocity at some frequency, energy from the particle d be fed to the wave in a process analogous hat of the traveling wave tube (TWT).

hus from the condition

$$n\beta_d = 1$$

the refractive index

$$n^2 = 1 + p^2/[f(h - f)]$$

$$n^2 \gg 1$$

found

$$f = \frac{h}{2}\left[1 \pm \left(1 - \frac{4\beta_d{}^2 p^2}{h^2}\right)^{1/2}\right]$$

where h is the gyrofrequency, p is the plasma frequency, and $\beta_d c$ is the component of particle velocity along the magnetic field line. (This is a more general form. They considered particles traveling exactly along the field line.)

This was applied to 'hooks' having a slowly descending frequency followed by a rapid rise. On this theory the first part would be produced in the exosphere and the rapid rise in the upper ionosphere.

MacArthur [1959] considered Doppler-shifted cyclotron radiation from protons. Protons gyrating at frequency H will appear at a much higher frequency f if they are rapidly approaching the observer, where

$$f = H/(1 - \beta_d n)$$

He showed that this approximated to the TWT expression. Essentially this is because for $H/f \ll 1$, $n\beta_d \simeq 1$. The same process was also considered by *Murcray and Pope* [1960*a*]. However, they used the refractive index at frequency H rather than that at f and consequently obtained a different expression. This was corrected in a later work [*Murcray and Pope*, 1960*b*].

Murcray and Pope [1960*a*, 1961] pointed out an advantage of the proton gyration theory over the TWT theory: a quantitative estimate of radiation can be made. On the other hand, such an estimate made by *Santirocco* [1960] indicated that *proton* radiation would be much too small for detection unless [*Murcray and Pope*, 1961] enormous numbers of protons radiate coherently.

However, the situation is different for radiation from gyrating *electrons*, since the emitted

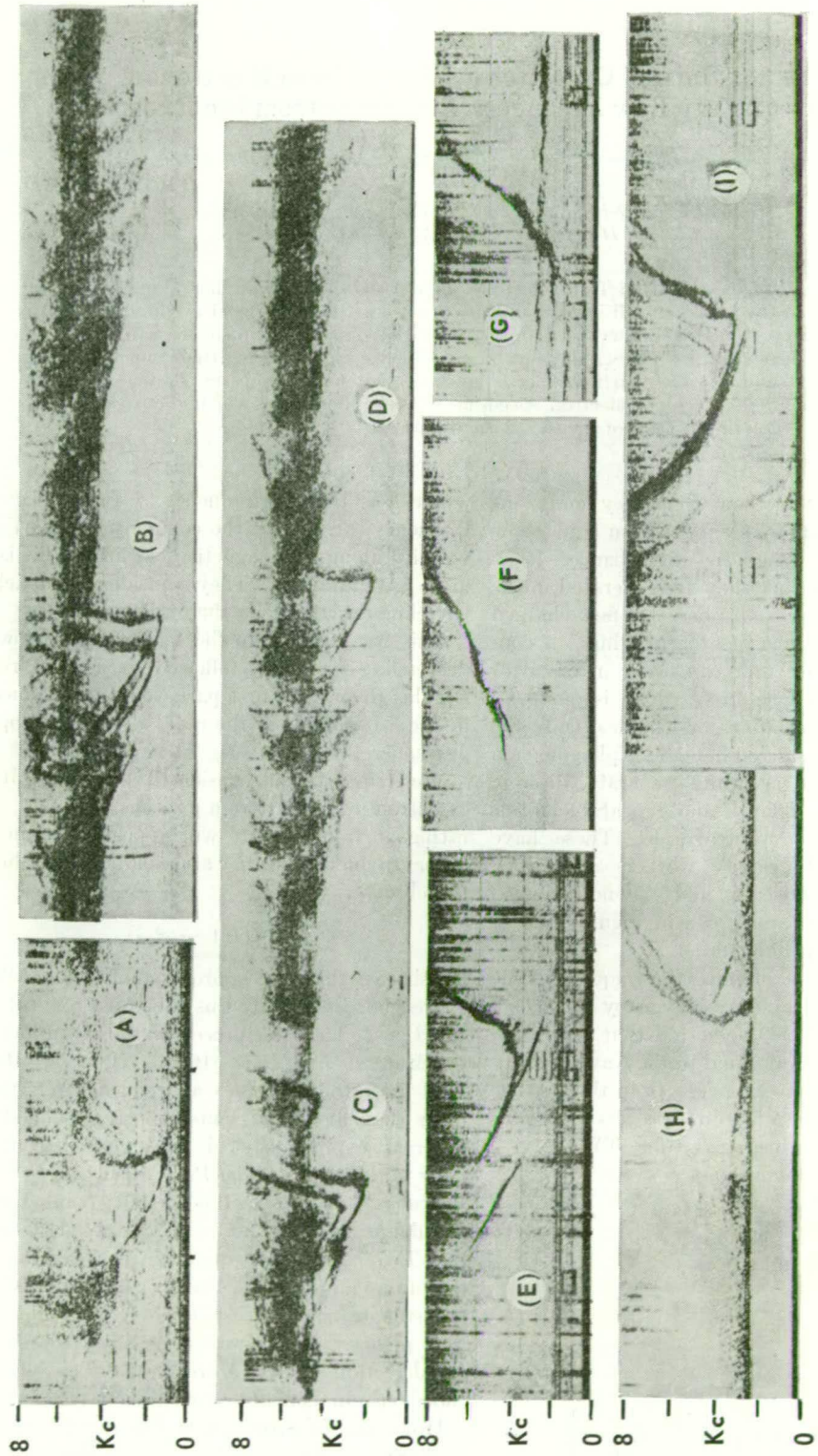

Fig. 1. Spectrograms of discrete VLF emissions (after *Helliwell and Carpenter* [1961]). Falling tones appear in *e*, quasi-constant tones in *g*, and risers in *f* and *g*. The other forms are probably all hooks.

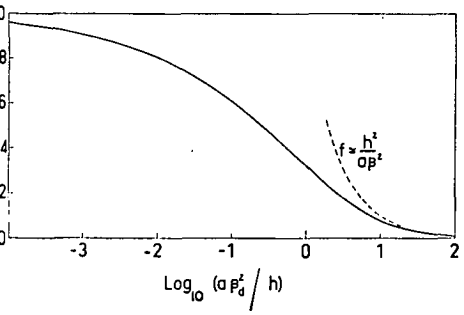

2. Graph of equation 3 for finding emitted frequency.

er is inversely proportional to the square he particle mass. Thus we would expect the ation power from electrons to be greater 3 million times that from protons, other ors being the same.

heory. Suppose that an electron (or rather mall bunch of electrons) is traveling in a about a line of force of the earth's magnetic . Suppose that it is traveling *away* from the rver's hemisphere with velocity component g the line of force of $\beta_d c$. Thus the rotating tron (or bunch) is an oscillator of frequency oving away from the observer at velocity in a medium for which the *observed* frequency vels at velocity c/n.

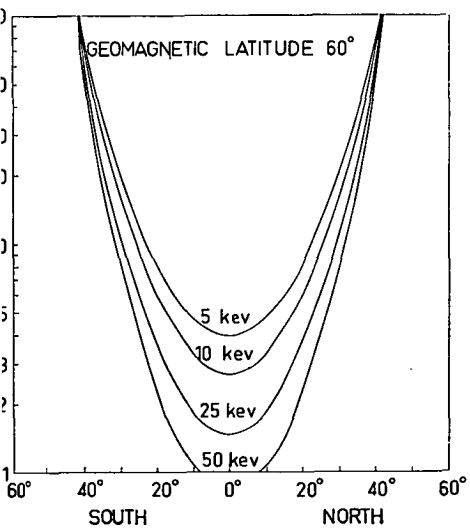

g. 3. Frequency emitted by an electron of energies shown as a function of position (latiangle). All four electrons have mirror points °.

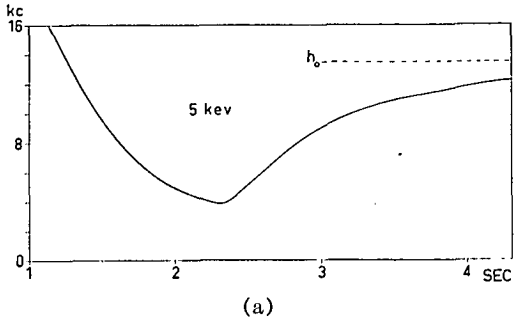

(a)

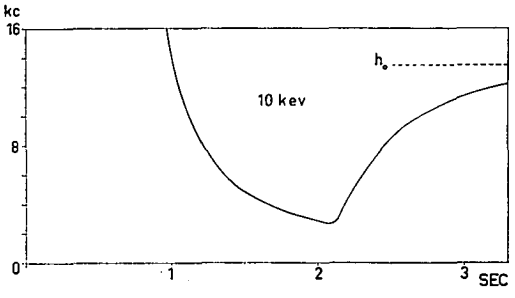

(b)

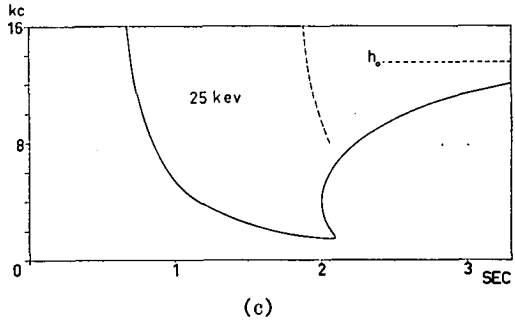

(c)

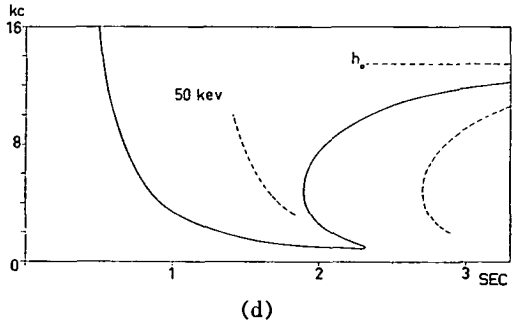

(d)

Fig. 4. Frequency-time (dispersions) curves for the electrons considered in Figure 3. These should be compared with the observed spectrograms in Figure 1.

TABLE 1. Mirror Oscillation Periods of the Electrons Considered in Figure 3

Energy, kev	Period, sec
5	2.56
10	1.82
25	1.28
50	0.81

Thus

$$f = h/(1 + \beta_d n)$$

where

$$n^2 \simeq p^2/[f(h - f)] \quad \text{for} \quad n^2 \gg 1$$

Hence

$$(h - f)^3 = p^2 \beta_d{}^2 f$$

Smith [1960] has shown that a model of electron density distribution in the exosphere for which the electron density is everywhere proportional to the gyrofrequency fits his nose whistler data rather well. Theoretical considerations by *Dowden* [1961] lead to a distribution that approximates to this gyrofrequency model.

Thus $p^2 = ah$, where $a \simeq 1$ Mc/s [*Smith*, 1960]

$$\therefore (h - f)^3 = a\beta_d{}^2 fh \qquad (1)$$

This is difficult to evaluate algebraically except for $f \ll h$, when

$$f \simeq h^2/a\beta_d{}^2 \qquad (2)$$

However (1) can be put in the form

$$\frac{(1 - f/h)^3}{f/h} = \frac{a\beta_d{}^2}{h} \qquad (3)$$

A plot of $a\beta_d{}^2/h$ versus f/h permits f to be found, given $\beta_d{}^2$ and h. This is shown in Figure 2. The approximation 2 is seen to be valid only for $a\beta_d{}^2/h > 20$.

Values of f have been found from Figure 2 for electrons of energies 5, 10, 25, and 50 kev traveling along the line of force terminating at geomagnetic latitude 60°. The position of a point on this field line is determined by the latitude angle l. The emitted frequency as a function of latitude angle is shown in Figure 3. The helical pitch (ψ_0) of all these electrons is 20° in the equatorial plane, so that mirror points occur in each hemisphere at $l = 41°$. The

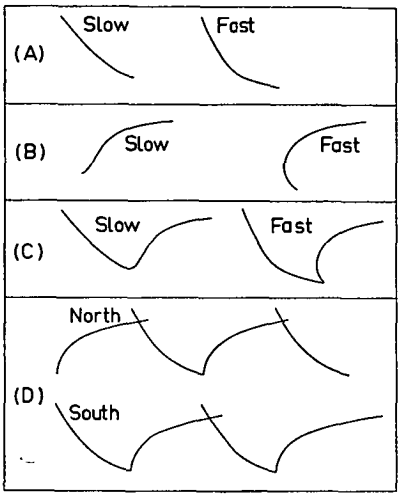

Fig. 5. Types of discrete emission that ca produced by this process. (*A*) Bunch inject midpoint (equatorial plane), mirrored in *ob er's* hemisphere, and scattered at midpoint (f tone or pseudo whistler). (*B*) Bunch inject midpoint and either absorbed near the mirr the *opposite* hemisphere or mirrored, and tered, at the midpoint (riser for slow b pseudo nose for fast). (*C*) Bunch injected at point, mirrored in observer's hemisphere, survived one transit through midpoint to into opposite hemisphere (hook). (*D*) Mec speed bunch injected at midpoint, mirrore southern hemisphere, then northern, sout northern, and finally scattered at the midpoi the northern hemisphere a riser, a hook, a falling tone are observed; in the southern hooks. Synchronized spectrograms from conj points would look like this.

parameter β_d is calculated for invarian magnetic moment:

$$\beta_d{}^2 = \beta^2(1 - \eta \sin^2 \psi_0)$$

where

$$\eta = (1 + 3 \sin^2 l)^{1/2} \sec^6 l$$

Suppose that these electrons make one from the mirror point in the observer's l sphere to the mirror point in the opposite l sphere. We need to find how frequency v vary with time as observed on the ea surface at the base of this line of force. frequency-time curves can be found by sum the time delay due to the finite velocity o electron (T_e) and that due to the finite g velocity of the wave (T_g).

$$T = T_e + T_g$$

TABLE 2. Hazards and Relative Occurrence

Class and Types	Hazards: Mirrors	Hazards: Source Region Transits	Observed* Relative Abundance
Chorus			403
3) Risers	0	0	178
psuedo noses			7
4) Falling tones	1	0	21
2) Hooks	1	1	15
0) Multiple forms	2 or more	1 or more	—

* From *McInnes* [1961].

here

$$'_g = \int \frac{ds}{V_g} = \frac{a^{1/2}}{2cf^{1/2}} \int \frac{h^{3/2}}{(h - f)^{3/2}} \cdot ds + \frac{D(\text{ionosphere})}{f^{1/2}}$$

nd

$$T_e = \int \frac{ds}{V_e} = \frac{1}{\beta c} \int \frac{ds}{(1 - \eta \sin^2 \psi_0)^{1/2}}$$

Integration is carried out over the path, and ne integrals were evaluated numerically. The esulting frequency-time curves are shown in igure 4. The time $T = 0$ is defined as that nstant when the electron passes through the quatorial plane toward the observer's hemi-phere. It could thus be the time of injection to the line of force. Note that for the 5-kev ectron the time scale starts 1 second after this.

Discussion. The frequency-time curves in igure 4 show good agreement with the ob-rved hooks in Figure 1. If the electron bunch nly makes half of the mirror-to-mirror trip, hich might happen if the source of the bunch robably near the equatorial plane) is also a nk, then only half of the full hooks will be bserved. If this half trip was confined to the bserver's hemisphere only, the falling part falling tone) would be observed. This might be istaken for a whistler in some circumstances. rips confined to the opposite hemisphere would ve rise to the other half: risers (f and g in Fig. and pseudo noses.

On the other hand, at times several complete ips might take place before the bunch is lost.

TABLE 3. Deduced Latitude and Energy of the Electrons Producing Nosed Hooks in Figure 1

Event in Figure 1	Latitude	Energy, kev
a	62°	7
d	62°	5
h	62°	25

This would give rise to a series of hooks of similar shape separated in time by the period of oscillation of the bunch between mirrors. For the faster particles in Figure 4 this is indicated by the curved broken lines. The oscillation periods are given in Table 1. An observer in the opposite hemisphere near the conjugate point would observe the same series of hooks, but since radiation is observed only when the bunch is traveling *away* from this observer he will observe this series shifted in time by half a period. Thus a northward-going bunch sends a hook to the southern observer, then, when returning on its southward trip, sends a hook to the northern observer. This conjugate point test of the theory was suggested to the author by G. R. A. Ellis.

The types of emission described above are illustrated in Figure 5. A bunch tends to be scattered by turbulent magnetic fields in the source region (probably near the equatorial plane) and to be absorbed by collisions near the mirror points. Thus we would expect the relative frequency of occurrence of the various types of emission to decrease with the number of mirrors and source-region transits required for each type. Thus 'quasi-vertical' or 'typical' chorus, and risers, which are required to survive no such hazards, should be the most common. In Table 2 the number of hazards for each type (as listed in Fig. 5) is compared with the observed relative frequency of occurrence (from *McInnes* [1961]). Nosed forms seem to be relatively rare, probably because low particle speeds occur more frequently than high. The observed order of abundance is otherwise as expected.

It can be seen from Figure 4 that when circumstances (fast particles, high latitudes) give rise to a nose similar to the nose whistler, the nose frequency is about one-third of the minimum gyrofrequency (h_0, shown by broken line). This allows calculation of the terminal latitude (λ) of the line of force along which the bunch is

guided:

$$\cos \lambda = (h_0/870)^{1/6} \qquad h_0 \text{ in kc/s}$$

The one-sixth power makes latitude evaluation reasonably accurate even for very rough estimates of h_0. The minimum frequency (f_0) can also be scaled from an observed hook. Substitution of h_0 and f_0 into equation 1 immediately gives the value of β_d^2 in the equatorial plane. The pitch will be smallest in the equatorial plane, so that, except for large pitch angles, $\beta_d^2 \simeq \beta^2$. The energy of the electrons in kev is then given by

$$E = 250\beta^2 \quad \text{kev}$$

Estimates of λ and E for the three hooks in Figure 1 showing well-developed noses (*a, d, h*) are given in Table 3.

It is interesting to compare this theory with that of the TWT. In the exosphere, for a gyrofrequency model of electron density and for fairly slow particles, the latter gives rise to a constant or slowly changing frequency. It is only when the particle (or bunch) penetrates the ionosphere that the frequency increases rapidly. Thus the TWT theory explains narrow-band hiss, 'quasi-constant tones,' and hooks having a fairly constant frequency first part and a rapidly increasing second part. A nose might be produced with this mechanism if the TWT hook is reflected back along the line of force and observed in the opposite hemisphere. The hook shown in Figure 1(*H*) might be of this type. On the other hand, the theory presented here produces all the forms entirely in the exosphere. In addition, it can explain the other hooks shown in Figure 1. The TWT theory will not produce multiple hooks from successive particle mirroring, since particles having mirror points in or below the ionosphere will not survive. It seems, then, that both mechanisms operate. The TWT theory produces some of the observed forms with relatively slow particles (1 kev or less) of small pitch angle (for hooks). Our theory produces other forms with faster particles, which may have greater pitch angles. In both theories noses are produced by propagation and so can be used to determine the line of force associated with the particles. The above comments on the TWT theory also apply to MacArthur's gyrating proton mechanism.

Conclusions. The qualitative frequency-time form of many exospheric emissions is explaine by this theory. Further, the theory does n require ionospheric effects to explain part this form, as does the TWT type mechanism. addition to explaining characteristics alread observed, it predicts further points that woul provide a test for the theory. Since radiation produced only from electrons traveling *awa* from the observer, local precipitation effec (aurora, absorption, X rays) will tend to occ in the hemisphere opposite that from which t radiation is observed. Observation of more tha one similar hook produced by bunches makin more than one trip would show that the hoo were generated in a region whose mirroring possible (exosphere) and would give an ind pendent measure of particle velocity to chec the theory. Simultaneous observations at bot ends of a line of force (conjugate point exper ment) would be useful for checking this.

Acknowledgment. I am indebted to Professo G. R. A. Ellis, Physics Department, University Tasmania, for many suggestions and discussions.

References

Dowden, R. L., A theoretical model of electro density along a geomagnetic line of force in th exosphere, *J. Atmospheric and Terrest. Phys 20,* 122–130, 1961.

Gallet, R. M., and R. A. Helliwell, Origin of ver low frequency emissions, *J. Research NBS, 63I* 21–27, 1959.

Helliwell, R. A., and D. L. Carpenter, Whistler west IGY-IGC synoptic program, *SEL Fin Rept.,* Stanford University, March 20, 1961.

MacArthur, J. W., Theory of the origin of the ver low frequency radio emissions from the earth exosphere, *Phys. Rev. Letters, 2,* 491–492, 195

McInnes, B. A., A study of ionospherics at Ma quarie Island, *Australian J. Phys., 14,* 218–23 1961.

Murcray, W. B., and J. H. Pope, Doppler shifte cyclotron frequency radiation from protons i the exosphere, *Phys. Rev. Letters, 4,* 5–6, 1960

Murcray, W. B., and J. H. Pope, Radiation fro protons of auroral energy in the vicinity of th earth, *J. Geophys. Research, 65,* 3569–357 1960*b*.

Murcray, W. B., and J. H. Pope, Energy fluxe from the cyclotron radiation model of V.L.I radio emission, *Proc. IRE, 49,* 811–812, 1961.

Santirocco, R. A., Energy fluxes from the cyclotro radiation model of V.L.F. radio emission, *Pro IRE, 48,* 1650, 1960.

Smith, R. L., The use of nose whistlers in th study of the outer ionosphere, *SEL Tech. Rep 6,* Stanford University, July 11, 1960.

(Manuscript received November 17, 1961.)

Theory of Generation of Exospheric Very-Low-Frequency Noise (Hiss)

R. L. DOWDEN

Ionospheric Prediction Service and University of Tasmania
Hobart, Tasmania, Australia

Abstract. The traveling wave tube amplification process proposed by Gallet and Helliwell is considered in greater detail. Account is taken of the spiral motion of particles traveling in the magnetic field, the interaction distance for which amplification at any one frequency can occur, and the slowing down of the stream particles by the wave amplification process. It is shown that narrow band bursts of hiss can be generated by weak electron streams of even very broad velocity and pitch distribution. The center frequency of such a band is characteristic of the terminating latitude of the line of force of generation. Stronger streams produce an overload effect giving rise to wide and very wide bands. Narrow bands can be produced at other frequencies by streams of narrow velocity and pitch distribution.

ntroduction. The phenomenon treated here that continuous type of exospheric emission iously called VLF noise, exospheric noise, geognetic noise, and hiss. It usually appears as nd-limited white noise in the frequency range about 1 to 10 kc/s. Hiss occurs in a broad nd or in one or more narrow bands. The nar- bands usually have bandwidths of around c/s, though narrower bands occur [*Helliwell Carpenter,* 1961]. Hiss occurs in bursts of main types [*Ellis,* 1959]. The most common e, 'isolated burst,' is typical of magnetically et conditions. These bursts are narrow band, ally 1–2 kc/s, centered at about 4 kc/s. ough detectable at relatively low latitudes the t majority of these have been shown to oc- at geomagnetic latitudes greater than 50° *lis,* 1960]. The center frequency, bandwidth, l intensity of the hiss remain remarkably con- nt over the duration of these bursts, which enerally about an hour. The second type oc- s as an extended series of hiss bursts or 'noise rms.' In contrast, these show considerable in- sity and bandwidth variations. All major gnetic storms are accompanied by noise rms [*Ellis,* 1959]. Generally, the bandwidth reases with magnetic activity. During severe urbances very wide band bursts covering the ge from about 100 c/s to over 200 kc/s can ur [*Dowden,* 1962*a*].

Hiss shows a strong correlation with airglow *uncan and Ellis,* 1959] and aurora [*Martin, Helliwell, and Marks,* 1960]. Rocket and satellite observations have shown that streams of electrons produce aurora [*McIlwain,* 1960] and airglow [*O'Brien, Van Allen, Roach, and Gartlein,* 1960]. It seems likely that these streams also produce hiss, though experiments to test this have yet to be reported.

Several mechanisms have been suggested [*Ellis,* 1957, 1959; *Allcock,* 1957; *MacArthur,* 1959; *Gallet and Helliwell,* 1959] capable of producing noise in this frequency range. However, none of these attempts to account for all the features outlined above. The most promising approach is the selective amplification process analogous to the traveling wave tube (TWT) proposed by Gallet and Helliwell. In this an electron stream provides amplification at frequencies for which the phase velocity of the amplified wave is equal to velocity of the stream. Both electrons and wave were assumed to travel exactly along the direction of the magnetic field.

Gallet's TWT process can be generalized by removing the restriction that the electrons travel exactly down the field line. In general, the electrons will spiral down the field lines. The pitch of the spiral at any position along the field line is determined by the principle of invariance of magnetic moment. For the low-energy particles required for this process (at most, a few kev) the radii of gyration will be much smaller than the extent of the wave front. Thus it is the component of particle velocity down the field

line or 'guiding center' velocity that must be equated to the longitudinal component of the wave phase velocity.

The analogy of this process with the traveling wave tube is perhaps closer than envisaged by Gallet and Helliwell. Since their work was published, it has been established by several people that field-aligned columns of ionization can occur in the exosphere [*Smith*, 1960], and these produce a strong wave guide action in the very-low-frequency range [*Smith, Helliwell, and Yabroff*, 1960]. A longitudinal magnetic field is often introduced into traveling wave tubes to focus the electron beams, and it is the guiding center velocity of the electrons that determines the amplification. As for the laboratory TWT, a (signal) longitudinal electric field is required for interaction with the stream. As was pointed out by Gallet and Helliwell, a substantial longitudinal component of electric field will exist in the exospheric TWT. It is the phase velocity of this component that is important, but for simplicity we will assume that this is c/n, where n is the refractive index of the medium for strict longitudinal propagation in the extraordinary mode below the gyrofrequency (whistler mode). Thus for guiding-center velocity $\beta_d c$ the condition for amplification is

$$n\beta_d = 1$$

In addition to this, we assume that, as for the laboratory TWT, the amplification in decibels or nepers is proportional to the distance in wavelengths along the field line for which amplification is possible at any one frequency. In the treatment given below the physical processes of amplification are not considered further.

Many of the writers referred to above described mechanisms for the production of chorus type phenomena rather than hiss. These discrete VLF emissions differ from the phenomenon considered here in ways other than their discreteness [*Helliwell and Carpenter*, 1961]. A mechanism for the production of these discrete emissions, very different from that considered here, is described by the writer elsewhere [*Dowden*, 1962*b*].

Amplified Frequencies. From the condition

$$n\beta_d = 1$$

and the refractive index for whistler-mode propagation

$$n^2 = 1 + p^2/f(h - f)$$

$$n^2 \gg 1$$

We find by solving for f

$$f = \frac{h}{2}\left[1 \pm \left(1 - \frac{4\beta_d{}^2 p^2}{h^2}\right)^{1/2}\right]$$

where

p is the plasma frequency,
h is the gyrofrequency,
f is the amplified frequency, and
n is the refractive index.

This is essentially the expression derived *Gallet and Helliwell* [1959]. If a model of t exosphere is assumed, this expression can be p in a form in which, for a given line of force, t latitude angle coordinate is the only variab To do this we assume that, at least along t lines of force considered here, the magnetic fi is a dipole and the electron density varies in way previously derived [*Dowden*, 1961]. Th

$$h = \eta h_0$$

$$p^2 = p_0{}^2 \eta\phi \cos l \quad \text{for} \quad R > 1.25$$

$$\beta_d{}^2 = \beta^2(1 - \eta \sin^2 \psi_0)$$

where

$\eta = \phi \sec^6 l$,
$\phi = (1 + 3 \sin^2 l)^{1/2}$,
l is the latitude angle coordinate,
R is the radius vector in earth radii,
ψ is the pitch angle, and
subscript 0 refers to values in the equato plane.

We assume here that the energy loss of a particle through amplification of the wave v be sufficiently small to regard the particle sp βc as constant. The effects of appreciable ene loss will be considered in a later section. S stituting these expressions, we find

$$f = \frac{\eta h_0}{2}$$

$$\cdot\left\{1 \pm \left[1 - \frac{4\beta^2 p_0{}^2}{h_0{}^2} \cos^7 l(1 - \eta \sin^2 \psi_0)\right]^{1}\right.$$

It will be seen later that the frequency gi by the minus sign is the more interesting. T

n be put in a form containing relatively slowly
rying functions, which is more suitable for
mputation. We define

$$a = 4\beta^2 p_0^2/h_0^2$$

$$x = a \cos^7 l(1 - \eta \sin^2 \psi_0)$$

$$\gamma = (2/x)[1 - (1 - x)^{1/2}]$$

hen

$$f^- = (\eta h_0/2)[1 - (1 - x)^{1/2}]$$

$$= \frac{\beta^2 p_0^2}{h_0} \gamma \cdot \phi \cos l(1 - \eta \sin^2 \psi_0) \qquad (2)$$

requencies as a function of the latitude angle l
ve been computed for particles of various
eeds and pitch angles traveling along the line
force that terminates at geomagnetic latitude
°. A smooth join to an ionosphere similar to
at used by *Gallet and Helliwell* [1959] has been
ade at a height of 2000 km above the surface
the earth. The results of this are shown in
gure 1. Except for the effect of the ionosphere,
e shape of these curves would be very similar
r lines of force terminating at other latitudes.
nly a change in frequency scale is required.
he important parameter affecting the shape is a.
is seen that in many cases the amplified
equency is fairly constant over great distances.
his follows from (2), for $\phi \cos l$ stays within 15
r cent of unity for $l < 60°$, γ rapidly ap-
oaches unity for small values of x, and the
rm containing the pitch angle is fairly constant
cept near the mirror points. Of even greater
terest are those regions for which variation of
ese terms nearly cancels out, producing very
early constant frequencies over great distances.
t these frequencies amplification will be great.
e will consider this in greater detail.

Interaction distance. For appreciable inter-
tion at any *one* frequency we require not only
at the wave phase and particle guiding center
locities be equal, but also that this condition
ould hold effectively over some appreciable
stance s.

Suppose that initially ($s = 0$) the condition
$\beta_d = 1$ holds exactly at some frequency, but
rther on, owing to changes in the guiding-
nter velocity of the medium, the particle stream
owly overtakes the wave. The stream (guiding-
nter) velocity relative to the wave is thus

$$\Delta v = \frac{c}{n}(n\beta_d - 1)$$

In time dt

$$d(\Delta s) = \Delta v \cdot dt \qquad ds = c/n \cdot dt$$

$$\therefore d(\Delta s) = (n\beta_d - 1)\, ds$$

Now

$$(n\beta_d - 1) = \int_0^s (n\beta_d)' \cdot ds$$

where

$$(n\beta_d)' = \frac{\partial}{\partial s}(n\beta_d)_{f\ const.}$$

Hence

$$\Delta s = \int_0^s \int_0^s (n\beta_d)' \cdot ds \cdot ds$$

In the region of interest, that is, on one of the curves defined by (1), the condition $n\beta_d = 1$ holds at all points, changes in the medium or stream velocity being exactly balanced by changes in frequency f.

Thus

$$\frac{d}{ds}(n\beta_d) = 0$$

Hence

$$\frac{\partial}{\partial s}(n\beta_d)_{f\ const.} = -\frac{\partial}{\partial s}(n\beta_d)_{f\ varying}$$

Now

$$n\beta_d = p\beta_d[f(h - f)]^{-1/2} \quad \text{for} \quad \beta^2 \ll 1 (n^2 \gg 1)$$

$$\therefore -\frac{\partial}{\partial s}(n\beta_d)_{f\ varying}$$

$$= \frac{\frac{1}{2}p\beta_d[f(h - f)]^{-1/2} \cdot \left(h \cdot \frac{df}{ds} - 2f \cdot \frac{df}{ds}\right)}{f(h - f)}$$

Hence

$$\frac{\partial}{\partial s}(n\beta_d)_{f\ const.} = \frac{1}{2f} \cdot \frac{h - 2f}{h - f} \cdot \frac{df}{ds}$$

since $n\beta_d = 1$. Since Δs must be small (at least $< \lambda/2$) throughout the interaction distance s, then s is given by the integration limits

$$\frac{\lambda}{2} > \Delta s = \int_0^s \int_0^s (n\beta_d)' \cdot ds \cdot ds$$

$$= \frac{1}{2} \int_0^s \int_0^s \left(\frac{1}{f} \cdot \frac{h - 2f}{h - f} \cdot \frac{df}{ds}\right) ds \cdot ds \qquad (3)$$

where λ is the wavelength.

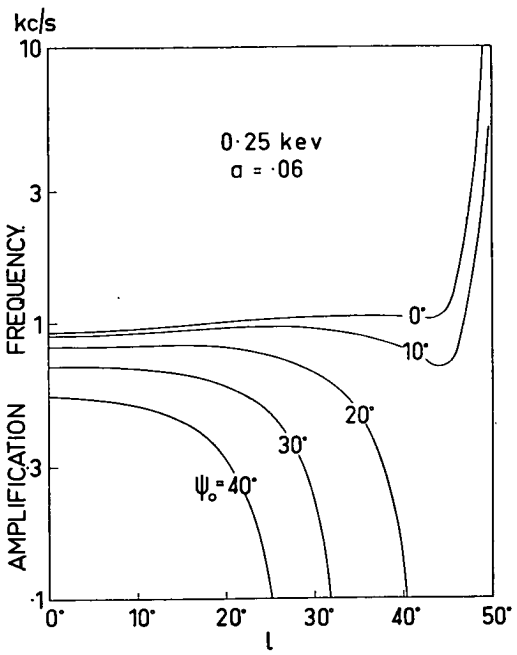

(a)

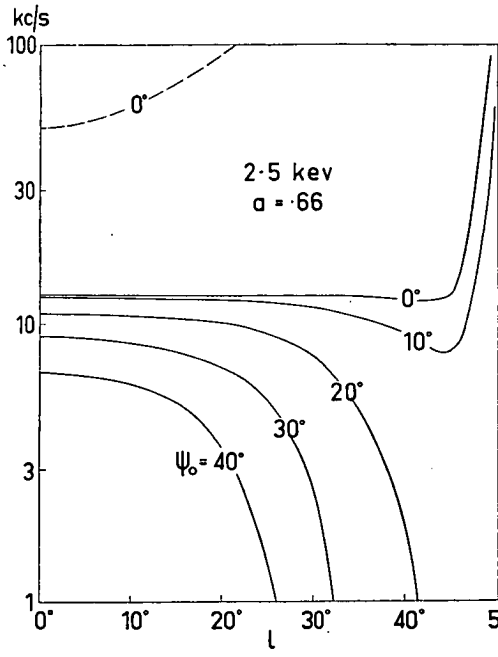

(b)

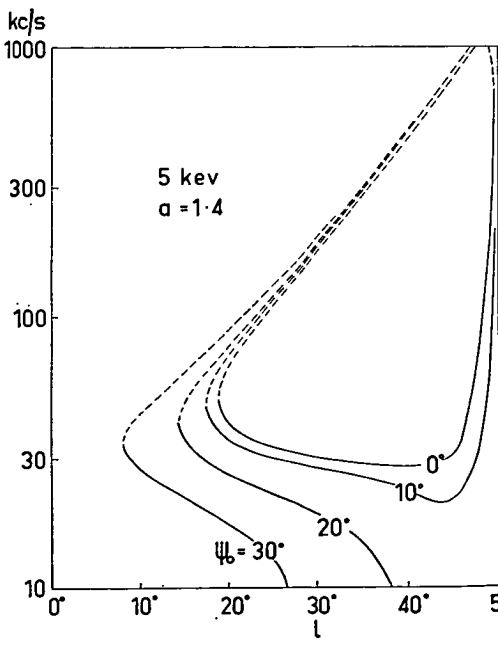

(c)

Fig. 1. Frequencies amplified by streams traveling along the field line that terminates at geomagnetic latitude 50°. These are plotted against the latitude coordinate angle l. The frequencies given by the negative sign in (1) are shown by the solid curves for several initial pitch angles ψ_0. Those for the positive sign are shown by broken curves. (*a*) Stream of 0.25 kev electrons. The shape of these curves is typical of $a \ll 1$. The upper frequency (f^+) approximates the gyrofrequency at all points and is thus well above the frequency scale shown here. (*b*) 2.5 kev electrons. This is typical of the 'resonance' condition for small pitch angles: $a \sim 0.6$. (*c*) 5 kev electrons. This is typical of $a > 1$. The 'noses' where the two branches meet occur at half the gyrofrequency.

This shows that amplification will not be preciable at the frequency given by the plus n (f^+) in (1) for two reasons; first, because ds is usually large (Fig. 1) and, second, ause $(h - f)$ is generally quite small. At the nts where the two curves join (Fig. 1c) $- 2f$ is zero, but also df/ds is infinite. nsequently, the high-frequency branch will be considered further.

Thus, considering only the low-frequency nch, we differentiate (1) with respect to l d make the γ substitution

$$\frac{df}{dl} = \tan l \left\{ 6 + \frac{3\cos^2 l}{\phi^2} - \frac{7 + \eta\left(\frac{3\cos^2 l}{\phi^2} - 1\right)\cdot\sin^2\psi_0}{(1 - \eta\sin^2\psi_0)(2 - \gamma)} \right\} = L \quad (4)$$

om the line of force equations for a dipole field

$$\frac{ds}{dl} = R_0\phi\cos l \quad (5)$$

e resulting expression containing s can be plified by noting that $\phi\cos l \sim 1$ for $l < 60°$, in the region of interest (high amplification) term

$$(h - 2f)/(h - f)$$

lso close to unity. Thus from (3), (4), and we have

$$\frac{2\,\Delta s}{R_0} \simeq \int_{l_1}^{l_2}\int_{l_1}^{l} L\,dl\,dl \quad (6)$$

$$s/R_0 \simeq l_2 - l_1$$

We assume that, as in the TWT process, the plification (in decibels or nepers) is proporal to the interaction distance measured in velengths, s/λ. In those cases for which s is iciently small, the integration range $l_2 - l_1$ lso small, so that over this range the integral n (6) will be approximately constant. Thus

$$\frac{2\,\Delta s}{R_0} \simeq L\cdot\tfrac{1}{2}(l_2 - l_1)^2 = \frac{\lambda}{R_0}$$

he limiting case ($\Delta s = \lambda/2$).

Then, since

$$\lambda = \frac{c}{nf} = \frac{\beta_d c}{f}$$

$$\left(\frac{s}{\lambda}\right)^2 \simeq \frac{2f}{\beta_d c}\cdot\frac{R_0\phi\cos l}{L} \quad (7)$$

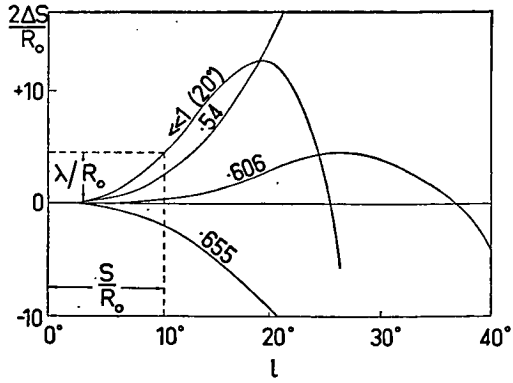

Fig. 2. Calculation of s/λ. Equation 6 is plotted for three values of a near 0.6 for $\psi_0 = 0$, and for $a \ll 1$ for $\psi_0 = 20°$.

However, in the more interesting cases where s is large, (6) must be integrated. Curves giving $2\Delta s/R_0$ as a function of l are shown in Figure 2 for some of the cases which give relatively large values of s. For a given curve the value s/λ is found by selecting a range of l that has a range of $2\Delta s/R_0$ equal to λ/R_0. This range of l is then s/R_0, as is shown in Figure 2. It is seen that for very small pitch angles the highest values of s/λ are found for $a \sim 0.6$. For larger pitch angles these are found at lower values of a. No particles of pitch angle ψ_0 much greater than 20° have large s/λ values.

The parameter s/λ as a function of frequency for particles of very small pitch angle traveling along the line of force terminating at geomagnetic latitude 60° is shown in Figure 3. Particles of greater pitch angle will have a s/λ curve showing a smaller and broader maximum occurring at lower frequencies. For other lines of force the essential change in the s/λ curve is the frequency scale, the maximum occurring (from equation 2) at

$$f \simeq ah_0/4 \simeq 0.15h_0$$

This relation is also shown in Figure 3.

The theory derived so far shows that, if a particle stream is confined to a narrow tube of force and if this stream is 'weak' so that very high amplification is required, a narrow band of noise (hiss) can be produced even though the stream contains a wide spectrum of particle velocities and pitch angles. This occurs because only a very narrow range of particle velocities and pitches can give the necessary amplification.

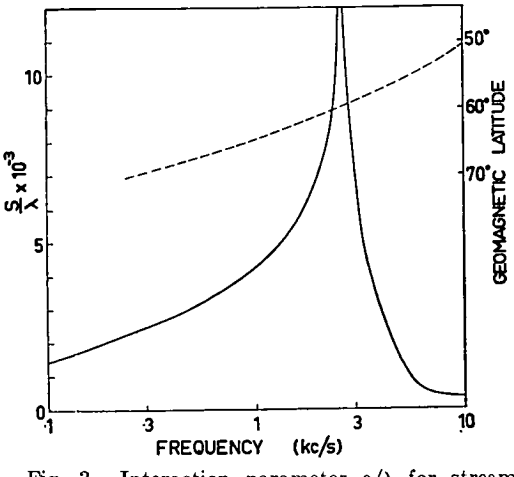

Fig. 3. Interaction parameter s/λ for stream particles of small pitch guided along the field line terminating at geomagnetic latitude 60°. At other latitudes frequencies will scale so that maximum s/λ occurs at the frequency given by the dashed curve.

Thus we have explained the observed occurrence of narrow band, 'quiet,' isolated bursts. The theory further predicts that the frequency at which these bursts occur is a function of the terminating latitude of the line of force. There is not sufficient experimental evidence as yet to prove this one way or the other: some observations indicate that lower frequencies occur at higher latitudes as has been predicted by *Gustafsson, Egeland, and Aarons* [1960]; others [*Outsu and Iwai*, 1961] seem to indicate the reverse.

Energy loss. As for the laboratory TWT, we expect the amplification (in nepers) to be proportional to s/λ. Thus the amplified power is

$$P = b \exp(\alpha s/\lambda) \qquad (8)$$

where b and α are constants. The constant b is thus the power before amplification, or at least that generated at the beginning of the amplification process. The constant α controls the rate of amplification. This must be some function of the properties of the stream.

If b (in Wm^{-2} c/s^{-1}) is not a strong function of frequency, then, from (8), the s/λ curve in Figure 3 has the shape of a logarithmic plot of generated noise intensity with frequency. However, from (2) the noise power in any given small band of frequency is produced by particles of a corresponding small range of velocities and pitches. Clearly, the noise power produced this band cannot exceed the kinetic power (of the corresponding particles. Thus

$$P < K$$

This 'overload' condition is probably mo restrictive than this, so we write it as

$$P \leq P_m = AK \qquad (7)$$

where A is a factor as yet undetermined. Th in general there will be an overload plate region of relatively constant intensity, provid of course, that neither A nor K is a stro function of frequency. This will be reached fo given value of α when the intensity given by reaches that given by (9). Then for all values s/λ as given in Figure 3 greater than the criti value (from equations 8 and 9)

$$(s/\lambda)_{crit} = 1/\alpha \log_e (AK/b) \qquad (10)$$

the intensity will be given by (9).

Consequently 'weak' streams for which rate of amplification (α) is small will prod narrow band hiss, and 'strong' streams (large will produce wide or very wide band hiss. T peak intensity for all will be given by (9), that unless A or K is a strong function of the main effect of varying degrees of amplifi tion rate should appear in the bandwidth rat than in intensity. If α is related to magn activity, then this explains why the peak tensity of hiss bursts occurring during m netically quiet periods is of the same order that during disturbed conditions, but in gene the bandwidth increases with magnetic activ from around 1 kc/s for 'isolated bursts' [*El* 1959] to over 100 kc/s during severe disturban [*Dowden*, 1962*a*].

It is difficult to make quantitative estima since little is known of the relevant quantit We can get some idea of the amplificat required in the following way. The obser peak intensities of hiss after allowing for pro gation losses [*Dowden*, 1962*a*] are of the orde $AK = 10^{-10}$ Wm^{-2} (c/s)$^{-1}$. If the amplificat is large we require only a very crude idea of initial noise intensity b. For Cerenkov emiss [*Ellis*, 1957] this would be of the order of $b = 1$ Wm^{-2} (c/s)$^{-1}$. Then from (8) it is seen t about 20 nepers of amplification would required. From (10) and Figure 3, $\alpha = 2 \times 1$ would be required for a narrow band burst

ss and $\alpha = 2 \times 10^{-2}$ for a wide band burst. lthough this amplification is very high com- ıred with laboratory TWT practice, the values amplification rate α required here are very nservative.

We also need to see if the kinetic energy of ectron streams is adequate to explain the served hiss intensities, that is, if the required lues of A in (9) are reasonable. Rocket meas- ements [*McIlwain*, 1960] have been made in electron stream that produced a quiescent ıroral glow and so might be taken as typical. ithin the range of measurement (3 to 30 kev) e stream kinetic energy flux in watts per uare meter per unit energy interval (kev) was und to fit the expression

$$K = 5 \times 10^{3} E \exp(-E/5) \qquad (11)$$

in kev. At around 2 kc/s, from (2), amplifi- tion will be produced by 0.5 kev electrons, d an energy interval of 1 ev will correspond a frequency interval of about 4 c/s. So suming that the above expression (11) is valid wn to 0.5 kev, the stream kinetic 'intensity' is

$$K \simeq 6 \times 10^{-7} W m^{-2} (\mathrm{c/s})^{-1}$$

om (9) and the observed intensity quoted ove, $A \sim 10^{-4}$. Even if this extrapolation of 1) is a very crude approximation, it seems at there will be sufficient energy, that is, $A < 1$. or the laboratory TWT the efficiency is around per cent; that is, $A \sim 0.1$. However, we ould expect much lower values for the exo- here because, within the much longer iteration stances of several thousand wavelengths quired, a relatively small loss of kinetic energy ould destroy synchronism.

Discussion. The theory explains the main aracteristic of hiss: that it appears as band- nited white noise. The expression (9) suggests at within this band the intensity will be latively uniform but outside the band the tensity (8) drops exponentially. Bandwidths om very narrow to very wide are possible ithout requiring special velocity and pitch stributions of the stream particles. The band- dth of the noise increases with the 'strength' the stream, which seems in agreement with e observation that bandwidth increases with agnetic activity. Very strong streams requiring ly short distances of interaction to reach over- ad power could produce noise at all the frequencies in Figure 1 simultaneously and so produce the very wide band bursts. Short streams some 1000 km long in the direction of the field. having high values of α and a narrow spectrum of velocities, would amplify the frequencies along one of the curves in Figure 1 in sequence. These could produce the 'quasi-constant tones' and the TWT 'hooks' as proposed by *Gallet and Helliwell* [1959].

We would expect 'isolated bursts' to be produced by weak streams. If these generally occur in geomagnetic latitudes from about 50° to 65° then the corresponding center frequencies (broken curve in Figure 3) should range from about 1 to 10 kc/s. Thus 4-kc/s bursts should occur at around 55° to 60°. The experimental evidence so far obtained seems to allow this, though there is not sufficient data to provide a test.

On the other hand, narrow band noise not conforming to this frequency-latitude relation could be produced by streams of narrow energy (velocity) and pitch distributions. *McIlwain* [1960] found that a stream which produced a strong visible aurora consisted of practically monoenergetic electrons. A stream having more than one such energy distribution could produce more than one narrow band of noise. Multiple narrow bands could also be produced by weak streams of uniform velocity distribution if several occurred in slightly different latitudes simultaneously. Thus, as seen from Figure 3 (broken curve), center frequencies differing by a factor of 2 can be produced by streams less than 5° of latitude (~500 km) apart. In the same way the finite width of streams would set a limit to the narrowness of the amplified band. However, satellite measurements at a height of a few hundred kilometers [*O'Brien, Van Allen, Roach, and Gartlein*, 1960] show that some streams are as narrow as 25 km (traversed by the satellite in 3 sec).

It may appear to the reader that this theory rests on the assumption that detailed expressions can be extracted from a theoretical model which might not be truly representative of the real exosphere. However, provided the electron density *along the field line* varies *smoothly* in a manner not greatly different from the model used, the essential qualitative results of this theory should still hold. Similarly the qualitative results may not be greatly affected should

subsequent study of the exospheric TWT mechanism require some modification to the amplification condition $n\beta_d = 1$.

Acknowledgment. I am indebted to Professor G. R. A. Ellis of the Physics Department, University of Tasmania, for suggesting this work initially and for giving many helpful criticisms and suggestions.

References

Allcock, G. McK., A study of the audio-frequency radio phenomenon known as 'dawn chorus,' *Australian J. Phys., 10,* 286–298, 1957.

Dowden, R. L., A theoretical model of electron density along a geomagnetic line of force in the exosphere, *J. Atmospheric and Terrest. Phys., 20,* 122–130, 1961.

Dowden, R. L., Wide band bursts of V.L.F. radio noise ('hiss') at Hobart, *Australian J. Phys., 15,* 114–119, 1962*a*.

Dowden, R. L., Doppler-shifted cyclotron radiation from electrons: a theory of very-low-frequency emissions from the exosphere, *J. Geophys. Research, 67*(5), 1962*b*.

Duncan, R. A., and G. R. Ellis, Simultaneous occurrence of subvisual aurorae and radio noise bursts on 4.6 kc/s, *Nature, 183,* 1618–1619, 1959.

Ellis, G. R., Low frequency radio emission from aurorae, *J. Atmospheric and Terrest. Phys., 10,* 302–306, 1957.

Ellis, G. R. A., Low frequency electromagnetic radiation associated with magnetic disturbances, *Planetary and Space Sci., 1,* 253–258, 1959.

Ellis, G. R. A., Directional observations of 5 kc/s radiation from the earth's outer atmosphere, *J. Geophys. Research, 65,* 839–843, 1960.

Gallet, R. M., and R. A. Helliwell, Origin of v low frequency emissions, *J. Research NBS, 6* 21–27, 1959.

Gustafsson, G., A. Egeland, and J. Aarons, Aud frequency electromagnetic radiation in the roral zone, *J. Geophys. Research, 65,* 2749–27 1960.

Helliwell, R. A., and D. L. Carpenter, Whistle west IGY-IGC synoptic program, *SEL Fi Rept.,* Stanford University, March 20, 1961.

MacArthur, J. E., Theory of the origin of the v low frequency radio emission from the eart exosphere, *Phys. Rev. Letters, 2,* 491–492, 19

McIlwain, Carl E., Direct measurement of p ticles producing visible auroras, *J. Geophys. search, 65,* 2727–2747, 1960.

Martin, L. H., R. A. Helliwell, and K. R. Mar Association between aurorae and V.L.F. hiss served at Byrd Station, Antarctica, *SEL Te Rept. 1,* Stanford University, April 29, 1960.

O'Brien, B. J., J. A. Van Allen, F. E. Roach, a C. W. Gartlein, Correlation of an auroral and a subvisible monochromatic 6300 A arc w outer-zone radiation on November 28, 1959, *Geophys. Research, 65,* 2759–2766, 1960.

Outsu, J., and A. Iwai, SEA and hiss associa with great bursts of solar radio emission in N vember, 1960, 3, Hiss, *Proc. Research Inst. Atmospherics, Nagoya Univ., 8,* 13, 1961.

Smith, R. L., The use of nose whistlers in the stu of the outer ionosphere, *SEL Tech. Rept.* Stanford University, July 11, 1960.

Smith, R. L., R. A. Helliwell, and I. W. Yabr A theory of trapping of whistlers in field-alig columns of enhanced ionization, *J. Geoph Research, 65,* 815–823, 1960.

(Manuscript received December 11, 1961; revised March 22, 1962.)

(*Reprinted from Nature, Vol.* 195, *No.* 4845, *pp.* 984–985, *September* 8, 1962)

'Scale Frequency' of the Exosphere

WHISTLER measurements of nose frequency (f_n) and time delay at this frequency (t_n) give a f_n, t_n distribution well fitted by a 'gyrofrequency' model of electron density in the exosphere[1]: one for which the electron density is everywhere proportional to the magnetic field strength or gyrofrequency (f_H). Since the electron density is directly proportional to the square of the plasma frequency (f_0) and uniquely determined by it we can express this model by the relation:

$$f_0^2 = f_a f_H$$

The constant of proportionality, f_a, has the dimensions of frequency and so might be called the 'scale frequency' of the exosphere. It is typically around one megacycle per second (as deduced from Smith's work[1]).

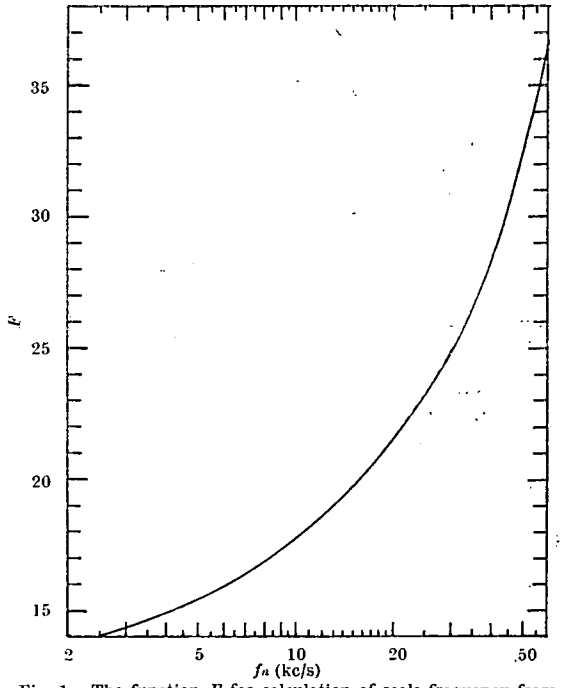

Fig. 1. The function F for calculation of scale frequency from nose frequency and nose delay time

To the extent that the gyrofrequency model fits the real exosphere the scale-frequency is constant. But the point I wish to make in this communication is that, regardless of this fit, the parameter, 'scale frequency', is a very useful one in exospheric studies. It is in the same form (frequency) as the other parameters (f_0, f_H, f) describing emission and propagation in the exosphere. The low-frequency dispersion $D_0 = f^{1/2}t$ becomes $D_0 = s f_a^{1/2}$ where s is the half-length of the field line in light-time units (light-seconds). For f_a constant along a field line the nose whistler integral can be solved analytically[1]. Since whistler data show that the scale frequency is at least quasi-constant then variations in space and time can be sensitively expressed by it. This would be particularly useful in discussing magnetic disturbance effects.

Scale frequencies are readily deduced from f_n, t_n data from nose whistlers. A recent extension of whistler analysis[2] makes it possible to obtain f_n and t_n from perhaps all well-defined whistlers even when the nose is not directly observable. In this work[2] it was shown that the nose frequency dispersion (D_n) is related to the low-frequency dispersion (D_0) as:

$$D_n = 1{\cdot}456\ D_0$$

Thus:

$$t_n f_n^{1/2} = 1{\cdot}456\ s f_a^{1/2}$$

Since the field line (and length s) is uniquely determined by the nose frequency, a function of f_n can be substituted for s. Thus:

$$f_a = F\, t_n^2\, f_n^{5/3} \text{ kc/s}$$

$$F = (1{\cdot}456\, s f_n^{1/3})^{-2}$$

where t_n is measured in seconds, f_n in kc/s and the slowly varying function F is shown in Fig. 1.

It is interesting to note that a theoretical model[3] of electron density in the exosphere based on the premise that the electrons are controlled by the Earth's magnetic field rather than gravity gives a quasi-constant scale frequency. Thus, this is largely a consequence of geomagnetic control of exospheres just as a quasi-constant scale height in the Earth's atmosphere is a consequence of gravity control.

R. L. Dowden

Ionospheric Prediction Service,
University of Tasmania,
Hobart.

[1] Smith, R. L., Ph.D. dissertation, July 11, 1960, *S.E.L. Tech. Rep.* 6, Stanford University.
[2] Smith, R. L., and Carpenter, D. L., *J. Geophys. Res.*, 66, 2582 (1961).
[3] Dowden, R. L., *J. Atmos. Terr. Phys.*, 20, 122 (1961).

Printed in Great Britain by Fisher, Knight & Co., Ltd., St. Albans.

(*Reprinted from Nature, Vol.* 195, *No.* 4846, *pp.* 1085–1086, *September* 15, 1962)

Cyclotron Theory of Very-Low-Frequency Discrete Emissions

It was recently shown[1] that the Doppler shifted cyclotron radiation from receding electrons would give the observed frequency-time shape of discrete very-low-frequency emissions. A further development enables information about these electrons to be deduced from this shape. Thus, electron energy (E), initial helical pitch angle (ψ_0), geomagnetic field line of occurrence (λ), and the exosphere electron density parameter[2], 'scale frequency' (f_a), are obtained from four parameters (two frequencies and two times) scaled from a spectrogram of the emission. Full details of this process will be published elsewhere.

As a demonstration, consider the 'hook' shown in Fig. 1*a*. The location of three points in the frequency-time plane unambiguously requires $E = 150$ keV, $\psi_0 = 68{\cdot}6°$, $\lambda = 61{\cdot}4°$ and $f_a = 527$ kc/s. To test the theory, 25 points were calculated from first principles using this information. The curve through these points is shown in Fig. 1*b*. Comparison shows excellent agreement.

The theory[1] explains other types of discrete emissions as special cases of 'hooks'. In particular, the theory predicted a repetitive type of emission not previously recognized. This occurs when the electron bunch survives several hemisphere to hemisphere traverses or 'bounces' between magnetic mirror points. The emission appears as a succession of similar hooks separated by the bounce period of the electrons. It is readily distinguished from whistler mode echoes of a single hook since successive hooks are not progressively more dispersed according to their order in the sequence. Since the observable radiation is unidirectional the hooks are received in opposite hemispheres alternately, that is, the sequence observed in one hemisphere is displaced half a bounce period from that observed in the other. This effect distinguishes the predicted emission from some other effect such as periodic injection of electrons.

Observation of this predicted emission showing a bounce period consistent with E, ψ_0, and λ scaled from the shape would be a crucial test of the theory both qualitatively and quantitatively.

A sequence which was probably of this predicted type was recently discussed[3]. It appeared as two

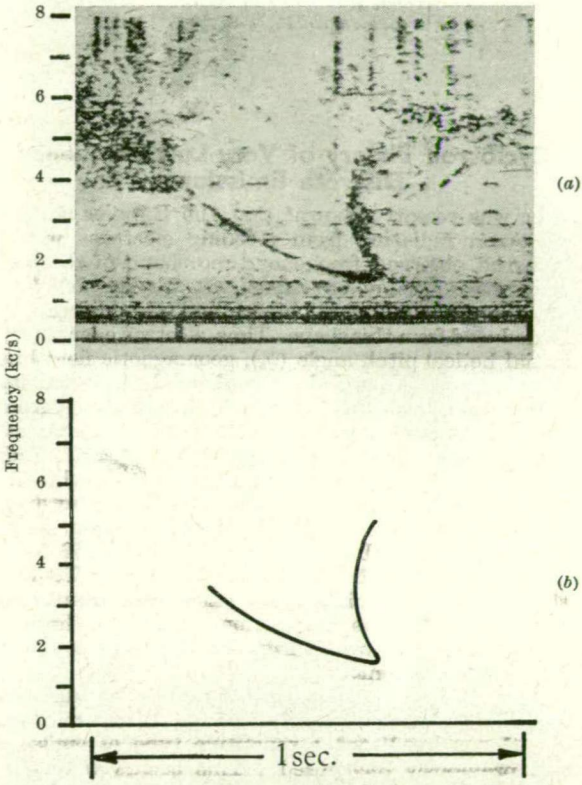

Fig. 1. *a*, 'Hook' recorded at Seattle, on September 23, 1957, at 2035 : 28 U.T. (after Helliwell and Carpenter, ref. 6) ; *b*, as calculated from the theory (ref. 1) for $E = 150$ keV, $\psi_0 = 68{\cdot}6°$, $\lambda = 61{\cdot}4°$ and $f_a = 527$ kc/s

bursts of 5–6 kc/s noise (presumably parts of a single hook) seen three times. It was observed in both hemispheres, not simultaneously, but alternately as explained here. Since only a narrow frequency band was observed the progressive dispersion criterion could not be applied. However, the recurrence period was consistent with a bounce period for electrons of typical energies as deduced from other hooks, but only a half to a third of typical whistler mode echo, delay times at this frequency. On the other hand, in a reply[4], Helliwell pointed out that whistler delay times can be sufficiently small during magnetic storms so that in this case the echo possibility cannot be ruled out.

I have since noticed four clear-cut examples published by Gallet[5]. In each of these there was a striking lack of progressive dispersion despite the

Table 1. COMPARISON OF OBSERVED RECURRENCE PERIOD (P_0) WITH THAT CALCULATED (P_c) FROM E, ψ_0 AND λ DEDUCED FROM THE FREQUENCY-TIME SHAPE

Sequence No.	No. of hooks in each sequence	Energy (E) (keV)	Helical pitch ψ_0	Geomagnetic latitude λ	Calculated period P_c (sec.)	Observed period P_0 (sec)
1	3	14	70°	59°	1·2	1·6
2	6	8	62°	59°	1·7	1·6
3	2	15	72°	59°	1·1	1·6
4	3	5	48°	59°	2·1	1·6

considerable frequency extent of the hooks and the relatively large number of separate hooks (six, in one sequence). Gallet[5] remarked on this at the time. Table 1 shows E, ψ_0 and λ deduced from the shape of one of the hooks for each sequence. The expected bounce periods calculated from E, ψ_0 and λ are shown as P_c and the observed periods (as measured by Gallet) are shown as P_0. The spectrograms as published[5] are rather small for accurate scaling so that the probable error in P_c is rather large. However, the general agreement is quite good.

The electron cyclotron theory gives excellent agreement with the observed frequency-time shape of discrete emissions. In addition, the predicted periodic emission is shown to occur and with periods reasonably close to those predicted. Verification of the theory not only clears up a mystery of long standing but also justifies the use of spectrograms of emissions for finding information about the electrons which produce them. Large numbers of such spectrograms were recorded during the International Geophysical Year.

I thank Prof. G. R. A. Ellis for advice.

R. L. DOWDEN

Ionospheric Prediction Service,
University of Tasmania,
Hobart, Tasmania.

[1] Dowden, R. L., *J. Geophys. Res.*, **67**, 1745 (1962).
[2] Dowden, R. L., *Nature* (in the press).
[3] Dowden, R. L., *Nature*, **195**, 64 (1962).
[4] Helliwell, R. A., *Nature*, **195**, 64 (1962).
[5] Gallet, R. M., *Proc. Inst. Rad. Eng.*, **47**, 211 (1959).
[6] Helliwell, R. A., and Carpenter, D. L., *Whistlers-West I.G.Y.-I.G.C. Synoptic Program* S.E.L., Final Rep., March 20, 1961 (Stanford University).

Printed in Great Britain by Fisher, Knight & Co., Ltd., St. Albans.

(*Reprinted from Nature, Vol.* 195, *No.* 4836, *p.* 64 *only.*
July 7, 1962)

Very-Low-Frequency Discrete Emissions received at Conjugate Points

In a recent article[1] describing a geomagnetic conjugate point experiment an accurately synchronized pair of spectrograms was shown. As shown in Fig. 1 of that article a sequence of six noise bursts in the 5–6 kc./s. frequency region was observed at both Knob Lake, Canada (68° N., geomagnetic), and at Byrd Station, Antarctica (70° S., geomagnetic); but the sequence began at Knob Lake 0·8 ± 0·1 sec. before it began at Byrd.

However, close inspection of Fig. 1 indicates that in each case the sequence is not six separate bursts but a pair of bursts seen three times. In support of this it will be noticed that the shapes and separation of the two bursts in each pair are similar and in each case the first burst occurs at a slightly higher frequency than the second. Furthermore, the time separation between successive pairs (using the time-scale provided) is 1·6 ± 0·1 sec., which is just twice the delay between Knob Lake and Byrd. Thus at intervals of 0·8 sec. this pair of bursts appeared alternately at Knob Lake and Byrd.

This phenomenon cannot be due to successive reflexions in opposite hemispheres of electromagnetic energy because the observed time delays are too short. Whistler observations in these latitudes show 5 kc./s. propagation times between 1·5 and 2·5 sec. for a single hemisphere to hemisphere trip[1]. Even then these times refer to lower latitudes because geomagnetic field lines terminating at latitudes greater than about 62° do not allow 5 kc./s. propagation of this type[2]. Thus if this phenomenon were due to whistler type echoes the delays would be several times longer.

However, such a sequence of alternate reception at conjugate points was predicted in a theory proposed by me[3] for the production of very-low-frequency discrete emissions. In fact such a conjugate point experiment was suggested as a test for the theory.

According to this theory Doppler-shifted cyclotron radiation is emitted by a small cloud or bunch of electrons spiralling along a field line. Only the downward-shifted frequency can propagate so that radiation is only emitted backwards. If the bunch should survive several trips along the field line from hemisphere to hemisphere, being reflected at the ends by

magnetic mirror effect, then an observer at each end of the field line would receive an emission each time the bunch was travelling away from him. Thus for each observer the time between successive emissions would be the complete (there and back) oscillation period of the cloud and the delay between the sequences observed in opposite hemispheres would be half this period[3].

The complete oscillation period of 1·6 sec. from Fig. 1 (ref. 1) would correspond to 60 keV. electrons (for minimum helical pitch angles of 20°) if the guiding field line was that connecting the two observing stations or 15 keV. electrons if the guiding field line was typical of those (around 60°) producing nose whistlers observed at Byrd[2]. These electron energies deduced from the oscillation period (15–60 keV.) are close to those (5–25 keV.) required by my theory to produce the detailed frequency-time shape of observed discrete emissions[3].

I thank Prof. G. R. A. Ellis, of the Physics Department, University of Tasmania, for advice.

R. L. Dowden

Ionospheric Prediction Service
and Department of Physics,
University of Tasmania,
Hobart.

[1] Lokken, J. E., Shand, J. A., Wright, Sir C. S., Martin, L. H., Brice, N. M., and Helliwell, R. A., *Nature*, **192**, 319 (1961).

[2] Smith, R. L., *The Use of Nose Whistlers in the Study of the Outer Ionosphere* (Stanford Electronics Laboratory, 1960).

[3] Dowden, R. L., *J. Geophys. Res.*, **67**, 1745 (1962).

Printed in Great Britain by Fisher, Knight & Co., Ltd., St. Albans.

Author's Reply to the Preceding Discussion

R. L. DOWDEN

Ionospheric Prediction Service, Hobart, Tasmania

Brice has devised a method of testing one of he features of my [*Dowden*, 1962*a*] electron yclotron theory of discrete VLF emissions: hat the sequence of emitted frequencies is patially symmetric about the top of the magetic field line (geomagnetic equatorial plane). Ie has derived testing parameters which should e equal to unity for any sequence of successive histler mode echoes of a hook beginning with he zero order or nonreflected hook. When this est was applied to four such sequences this arameter was of the order of three, quite sigificantly not unity. Brice concludes that my heory therefore cannot explain these hooks.

Now, using Brice's notation, it can easily be hown from his equation 2 that for symmetrial generation the theory predicts:

$$T_n - T_n' = (2n + 1)(T_0 - T_0') \qquad (1)$$

f these difference times are calculated from his Table 1, it will be seen that they are clearly not n the predicted ratio 1:5:9 for the first sequence and 1:3 for the other three.

On the other hand, it is rather striking that hese ratios are none the less in a logical order. They are quite close to 3:7:11 for the first sequence and 3:5 for the other three. This suggests that in each sequence the first trace observed by Brice was not the zero-order, or non-reflected, hook but the first-order, or once-reflected, hook. Then each of Brice's tabulated values of n should be increased by one. Now we can resolve this by measuring the times between any two traces in a sequence at f_t and f_0. These are the propagation times for the appropriate number of complete hemisphere to hemisphere hops. Thus, using the first and third of the traces in Brice's Figure 1 we find $8\tau_0 = 4.10$ sec and $8\tau_1 = 3.72$ sec. Thus from Brice's equation 1, $T_0 - T_0' = 2(\tau_0 - \tau_1) = 0.095$ sec. This is approximately one-third the value tabulated by him. Consequently, for the first sequence at least we have clearly demonstrated that the first trace observed is the first-order, or once-reflected, hook. Thus, for this sequence Brice's tabulated values of n should be increased by one, and his testing parameters should be calculated from his equation 4. This is shown in Table 1.

Without having recourse to the original

TABLE 1

n	T_n, sec	T_n', sec	$T_n - T_n'$, sec	Predicted $T_n - T_n'$ Ratios	$\frac{n-1}{3}\cdot\frac{T_1 - T_1'}{T_n - T_1}$	$\frac{n-1}{3}\cdot\frac{T_1 - T_1'}{T_1' - T_n'}$
0	Not observed		0.095	1		
1	0.39	0.05	0.34	3		
3	0.57	−0.14	0.71	7	1.3	1.2
5	0.75	−0.31	1.06	11	1.3	1.3
0	Not observed		*	1		
1	0.16	0.03	0.13	3		
2	0.22	−0.03	0.25	5	0.7	0.7
0	Not observed		*	1		
1	0.35	0.02	0.33	3		
2	0.42	−0.07	0.49	5	1.6	1.2
0	Not observed		*	1		
1	0.17	0.02	0.15	3		
2	0.22	−0.03	0.25	5	1.0	1.0

* These missing values could be obtained from the original spectrograms.

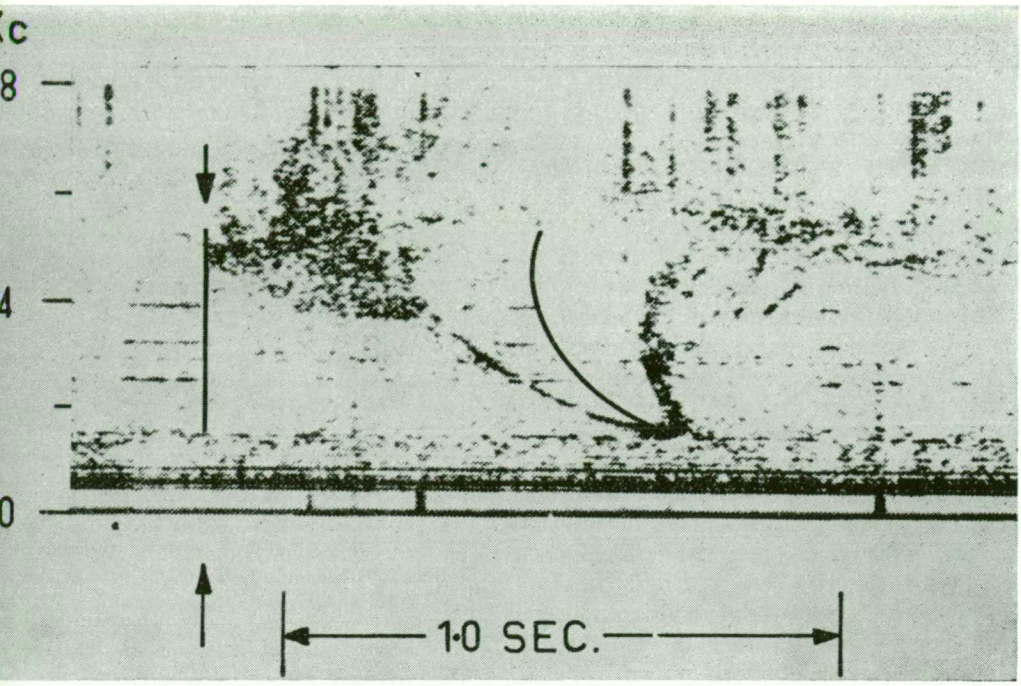

Fig. 1. Hook recorded at Seattle on September 23, 1957, at 20h 35m 28s UT (after *Helliwell and Carpenter* [1961]). Superimposed on this is a computed nose whistler originating from a hypothetical impulse at the top of the field line at the time shown by the arrow. Note that this computed curve is in the center of the hook at all frequencies.

ectrograms for the other three sequences, we nnot here make similar statements about these ıer three. Brice's statement that 'this amguity is removed if the hook and echo are served at conjugate stations' is not strictly ıe. Although the zero order signals must ve been reflected somewhere near one of the njugate stations, they could have been miss- from the spectrograms or at least not recogzed as such for a variety of reasons.

However, we can say that Brice's first sence unambiguously demonstrates the symtry aspect of my theory in both the predicns that the $T_n - T_n'$ ratios should be close to 3:7:11 (from equation 1) and that his test- parameters should be close to unity. The ıer three sequences fit the theory if the same erpretation of n applies to these also (Table . Furthermore, this can easily be checked ɔm the spectrograms as shown above for the st sequence. It should be noted that the reining discrepancies in $T_n - T_n'$ and his testing rameter values are easily accounted for by rors in scaling the times T_n and T_n' of about 0.01 to 0.02 sec. This is quite reasonable since the widths of the traces are some 0.05 to 0.1 sec., as is seen in his Figure 1.

Another test of the symmetry aspect of my theory is now presented. It is a consequence of this symmetry feature [*Dowden*, 1962*b*] that the observed frequency-time distribution of a hook should be symmetrically spaced (in time) about a half-dispersed nose whistler. In other words, at any frequency the midpoint in time between the two branches of a hook should lie on a curve corresponding to the whistler mode dispersion of a hypothetical wide-band impulse originating at the top of the field line at the instant of generation of the lowest frequency. This is also the instant at which the emitting electron bunch passes through this point.

Consider the hook shown in Figure 1. Superimposed on this is the nose whistler originating from a hypothetical impulse at the top of the field line at the instant shown by the arrow. The frequency-time shape of this nose whistler was calculated from a function given by *Smith and Carpenter* [1961] which they have shown accu-

METHOD OF MEASUREMENT OF ELECTRON ENERGIES AND OTHER DATA FROM SPECTROGRAMS OF V.L.F. EMISSIONS

By R. L. DOWDEN*

[*Manuscript received August* 8, 1962]

Summary

It has been shown that the detailed frequency-time shape of discrete very low frequency emissions from the exosphere can be closely fitted on the electron-cyclotron theory by suitably choosing the electron parameters. Additional support for the theory has since been obtained in the verification of its prediction. It is shown here that the fitting process can be reversed so that these parameters can be deduced from the observed spectrograms. These are: the energy and helical pitch of the emitting electrons, the field line which guides them, the instant of their passing through the equatorial plane, and the electron density of the medium. Nomograms are given allowing calculation of these with occasional use of a slide rule and simple arithmetic.

I. INTRODUCTION

In a recent paper (Dowden 1962*a*) it was pointed out that the cyclotron radiation from an electron spiraling along a geomagnetic field line *away* from the observer will be Doppler shifted to a frequency appreciably less than the frequency of gyration of the electron. An electron (or rather a small bunch of electrons) travelling from the observer's hemisphere to the opposite hemisphere will radiate at a decreasing frequency until it crosses the equatorial plane, and thence at an increasing frequency. Consideration of electron travel times and wave-group propagation times gives the frequency-time (spectrogram) shape of a " hook " for such a hemisphere to hemisphere traverse.

Other types of discrete emissions (" chorus ", " risers ", " pseudo noses ", " falling tones ", etc.) are produced by incomplete traverses. In particular the theory predicted a repetitive type emission when the electron bunch survives several hemisphere to hemisphere traverses or " bounces " between magnetic mirror points. Occurrences of this type have since been shown (Dowden 1962*b*) and the observed bounce periods (hook repetition period) agreed well with those calculated from electron parameters deduced (by the method to be discussed here) from the frequency-time shape of the individual hooks.

The parameters which affect the frequency-time shape, scale, and position of the complete transverse emission (" hook ") as observed on the Earth are: the energy E and helical pitch ψ of the emitting electrons, the terminal geomagnetic latitude λ of the field line which guides them, the instant ($\frac{1}{2}t_0$) of their passing through the top of this field line, and the " scale frequency " a of the electron density of the medium. If these are suitably chosen a theoretical frequency-time trace can be calculated to give an effectively exact fit to any

* Ionospheric Prediction Service, University of Tasmania, Hobart.

observed hook. This has been demonstrated with a relatively complex hook (Dowden 1962*b*). This and the later verification of the prediction mentioned above effectively establish the theory. In addition the observed trace contains the effects of these parameters so that it may be possible to deduce these parameters from the observed trace.

It will be shown here that the scaling of only two frequencies (f_n and f_0) and two times (T^+ and T^-) is sufficient for complete and unambiguous evaluation of the parameters cited above.

II. Energy

The general expression for the Doppler-shifted cyclotron frequency from an electron spiraling along a field line is (Eidman 1958)

$$f=h[\gamma(1\pm\beta_d n\cos\theta)]^{-1}, \tag{1}$$

where h is the local gyro frequency, γ is the relativistic correction $(1-\beta^2)^{-1/2}$, n is the refractive index of the medium at the frequency f, β_d is the longitudinal component of velocity in units of the velocity of light, and θ is the angle between the field and the direction of emission.

The minus sign in (1) refers to forward Doppler shift and so need not be considered here. The angle θ in (1) also appears in the general Appleton-Hartree expression for the refractive index. For the terrestrial case of backward Doppler-shifted emission the general expression for f obtained by substituting this refractive index $n(\theta)$ into (1) is found (Ellis 1962) to be almost independent of θ. If it were otherwise we would not expect such narrow-band V.L.F. emissions as are observed. Consequently we consider only the case $\theta=0$.

The whistler mode refractive index is given by

$$n^2=1+p^2[f(h-f)]^{-1}, \tag{2}$$

where p is the plasma frequency of the medium. This latter can be expressed in the form

$$p^2=ah,$$

where a is the " scale frequency " (Dowden 1962*c*). For a gyro frequency model (electron density everywhere proportional to magnetic field or gyro frequency), as suggested by whistler data (Smith 1960), a is constant.

From (1) and (2), making the appropriate substitutions discussed above, and for $n^2\gg1$, we have

$$(h-f)(h/\gamma-f)^2=a\beta_d^2hf. \tag{3}$$

This more general expression reduces to that obtained previously (Dowden 1962*a*) for $\gamma=1$. If ψ is the helical pitch angle we have

$$\beta_d=\beta\cos\psi.$$

The helical pitch at any point is determined by its value at any other point by the principle of invariance of magnetic moment. Thus, specifying quantities in the equatorial plane by subscript zero, we have

$$\beta_d^2=\beta^2[1-\eta\sin^2\psi_0], \tag{4}$$

where η is the ratio of the magnetic field or gyro frequency at the point in question to that at the equatorial plane. For a dipole field

$$\eta=(1+3\sin^2 l)^{1/2}\sec^6 l,$$

where l is the latitude coordinate angle.

At the equatorial plane ($l=0$) we have from (3) and (4)

$$(h_0-f_0)(h_0/\gamma-f_0)^2=a\beta^2\cos^2\psi_0 h_0 f_0. \tag{5}$$

Making the substitution $x=h_0/f_0$ and $\beta^2=(\gamma^2-1)/\gamma^2$ we get

$$\frac{\gamma^2-1}{\gamma^2}=\frac{f_0}{a\cos^2\psi_0}\,\frac{[x-1]^3}{x}\left[\frac{x/\gamma-1}{x-1}\right]^2. \tag{6}$$

The kinetic energy of an electron is given by

$$E=500(\gamma-1)\text{ keV}. \tag{7}$$

As we will find later, nearly all emissions are produced by electrons of energies for which relativistic effects are very small ($\gamma\simeq 1$).

For these we can write

$$E'=250\beta^2=(250f_0/a\cos^2\psi_0)(x-1)^3/x\text{ keV}. \tag{8}$$

From (6), (7), and (8) we find

$$E'=E(1+E\times 10^{-3})[(x-1)/(x-\gamma)]^2. \tag{9}$$

From (8) we would generally expect high energies to be associated with large values of x, in which case the term containing x is close to unity and (9) is in a convenient form for applying relativistic corrections to a nomogram energy scale. This is shown in Figure 4.

Of the quantities in (8) required for evaluation of the electron energy only f_0 is measurable in an obvious manner from spectrograms of complete emissions (" hooks "). This is the minimum or cusp frequency of the hook (for $\gamma\simeq 1$) as shown previously (Dowden 1962*a*). We now consider methods of deducing the other parameters.

III. Latitude λ and Parameter x

Suppose we assume that the energy lost (radiated) by the bunch during one hemisphere to hemisphere traverse is negligible. Then the observed emission frequencies will be symmetric with respect to the geomagnetic equatorial plane. That is, the frequency produced by the bunch at latitude angle l in the northern hemisphere will be the same as that produced when this bunch is at the same latitude angle in the southern hemisphere.

Consider the hook in Figure 1 as observed in the northern hemisphere. We require the times T_1 and T_2 for some frequency f. These times, which define the shape of the hook, are made up of group propagation times (t_g) of waves of frequency f and f_0 and electron bunch travel times (t_e). We can specify a point on a given line of force by the gyro frequency at that point. Suppose that at the two points (one in each hemisphere) where the frequency f is produced, the

gyro frequency is h. The equatorial plane is then denoted by h_0 and the Earth's surface by h_λ. Propagation times along the surface of the Earth to the observer do not involve dispersion and so do not change the shape of the hook.

Consequently the time T_1 is the time taken for the electron bunch to travel from the point h_N in the northern hemisphere where frequency f is produced to the equatorial plane (h_0) plus the difference between the propagation times for

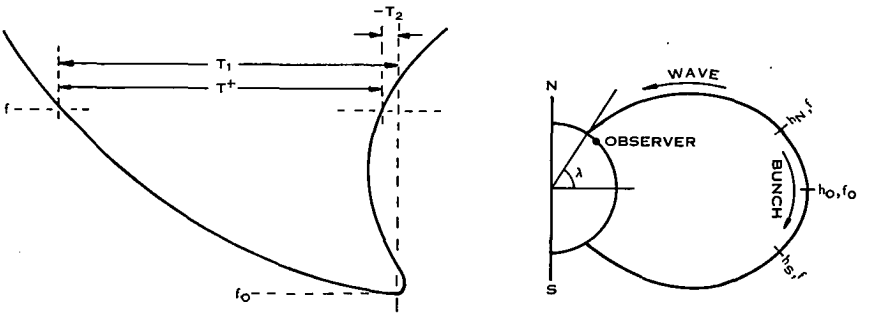

Fig. 1.—A tracing of a frequency-time spectrogram of a hook and the path of the electron bunch which generated it.

frequency f_0 to travel from the equatorial plane (h_0) to the Earth's surface ($h_{\lambda N}$) in the northern hemisphere and that for frequency f to travel from point h_N to $h_{\lambda N}$. Putting this in symbolic form,

$$T_1 = t_e(h_N \to h_0) + t_g(f_0, h_0 \to h_{\lambda N}) - t_g(f, h_N \to h_{\lambda N}).$$

In a similar way we find

$$\begin{aligned} T_2 &= t_e(h_0 \to h_S) + t_g(f, h_S \to h_{\lambda N}) - t_g(f_0, h_0 \to h_{\lambda N}) \\ &= t_e(h_0 \to h_S) + t_g(f, h_S \to h_0) + t_g(f, h_0 \to h_N) \\ &\quad + t_g(f, h_N \to h_{\lambda N}) - t_g(f_0, h_0 \to h_{\lambda N}). \end{aligned}$$

We can drop the N, S subscripts if we always refer to the shortest distance. Taking the sum and difference times T^+ and T^- we find:

$$T^+ = T_1 + T_2 = 2t_e(h_0 \to h) + 2t_g(f, h_0 \to h), \tag{10}$$

$$T^- = T_1 - T_2 = 2t_g(f_0, h_0 \to h_\lambda) - 2t_g(f, h_0 \to h_\lambda). \tag{11}$$

We will discuss (10) later. Consider now the difference time T^- given by (11). This contains only wave propagation times. Furthermore, if we consider T^- as a function of frequency f, then (11) is the general (nose) equation of a " short " whistler centred on the time ($T^- = 0$) for which $f = f_0$. The frequency for which T^- is maximum is then the nose frequency f_n of the equivalent nose whistler. Measurement of f_n defines the line of force in which the hook is produced and along which the electron bunch is guided. A function given by Smith (1960) enables h_0 and λ to be found from f_n.

A simple but accurate way of measuring f_n is shown in Figure 2. The frequency-time shape of the hook is traced on transparent paper. This tracing is turned over onto the original hook so that the frequency scales still correspond.

By moving the tracing in the time direction a position will be found where the descending part of the traced hook just touches the ascending part of the original hook and vice versa. The frequency at which this occurs is then the " true " nose frequency f_n. Note that this is always higher than the pseudo nose which sometimes appears on the ascending part of the hook (Fig. 2).

The nose frequency difference time (T_n^-) can be found at the same time, as shown in Figure 2. We have shown that $T^-(f)$ defines the exact shape of a whistler and so should provide electron density information. Smith and Carpenter (1961) have shown that if the time delays (t) and frequencies (f) of

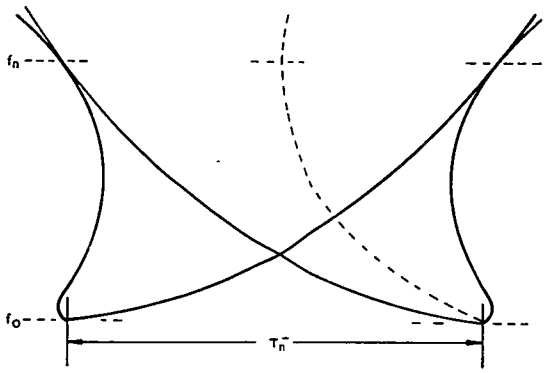

Fig. 2.—Method of scaling the nose frequency and difference time at this frequency. The midpoint locus (broken curve) has the shape of a nose whistler.

whistlers are normalized to nose values (t_n and f_n) then the resulting curves of t/t_n versus f/f_n all closely fit a single " universal whistler dispersion function " which they have calculated. Our T_n^- is then

$$T_n^- = t_0 - t_n,$$

that is,

$$T_n^-/t_n = S(f_0/f_n) - 1, \tag{12}$$

where t_0 is the short whistler time delay at frequency f_0, and S is the Smith-Carpenter dispersion function. The double-sided scale shown in Figure 3, which has been constructed from this function, allows calculation of t_n. Note that we can also find the time $\frac{1}{2}t_0$, which is the time between the instant the electron bunch passes through the equatorial plane (where frequency f_0 is emitted) to the instant of reception on the Earth of the cusp or minimum frequency of the hook.

It is interesting to consider here an alternative method of finding f_n and T_n^- which illustrates some of the points made above. The mid point of a line drawn from some frequency f on one branch of the hook to the same frequency on the other branch is given by

$$T_1 - \tfrac{1}{2}T^+ = \tfrac{1}{2}T^-.$$

Thus the locus of the mid point is the whistler which would be observed if a wide-band impulse occurred at the instant the electron bunch passed through the equatorial plane. This "half whistler" is shown in Figure 2. This alternative method is useful for finding f_n when the hook does not extend to this frequency by using the Smith-Carpenter techniques, particularly if the scale frequency (discussed below) is known from other data.

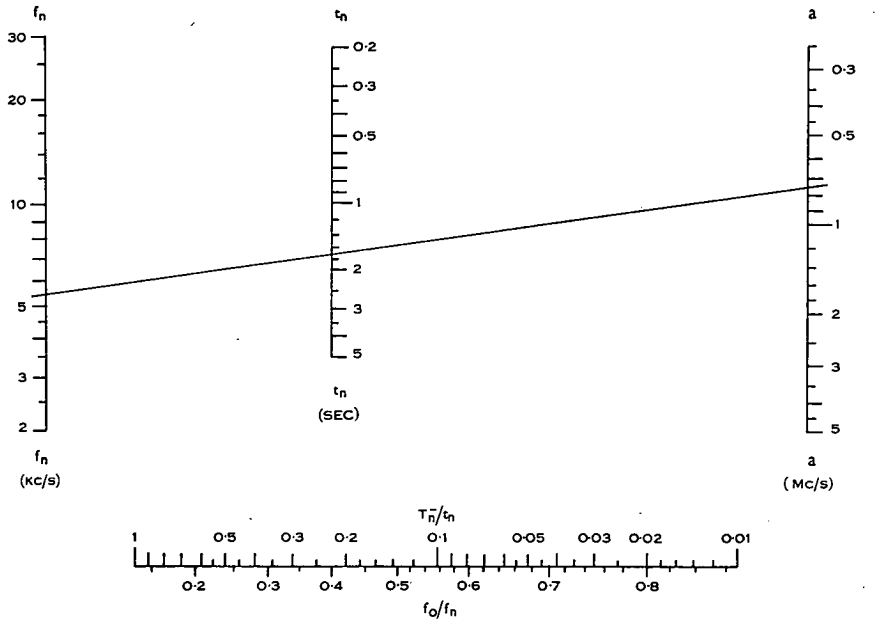

Fig. 3.—Nomogram for calculation of scale frequency a.

Having found t_n, f_n by the methods outlined above, or more accurately perhaps by the use of real nose whistlers we can now find the scale frequency a. This is given by (Dowden 1962*c*)

$$a = N(f_n) f_n^{5/3} t_n^2,$$

where N is a slowly varying function. A nomogram for solving this equation is given in Figure 3. The function N has been built into the f_n scale.

IV. Helical Pitch

The sum time T^+ is the time width of the hook at any given frequency, as shown in Figure 1. From equation (10) we see it contains both wave propagation times and electron bunch travel times. Thus T^+ will be dependent on ψ_0 so that it should be possible to use T^+ as a measure of ψ_0.

Suppose we measure T^+ at frequency $f = 2f_0$. For a dipole field we have

$$2t_e = 2\int_0^l \frac{R_0 \cos\psi_0 \cdot \eta \cos^7 l \, dl}{\beta c[1 - \eta \sin^2 \psi_0]^{1/2}}.$$

The radial distance to the top of the field line (R_0) can be expressed in terms of h_0, β is given by (8) and $h_0=f_0x$. Thus

$$2t_e=12\cdot82a^{1/2}f_0^{-5/6}\cos\psi_0x^{1/6}(x-1)^{3/2}\int_0^l\frac{\eta\cos^7 l\,dl}{[1-\eta\sin^2\psi_0]^{1/2}} \tag{13}$$

in seconds, where a is in Mc/s and f_0 in kc/s.

For the propagation time we have

$$2t_g=\frac{2}{2c\sqrt{(2f_0)}}\int_0^l\frac{phds}{[h-2f_0]^{3/2}},$$

where s is the distance along the field line and p is the plasma frequency of the medium. Smith (1960) has shown that this integral is only slightly dependent

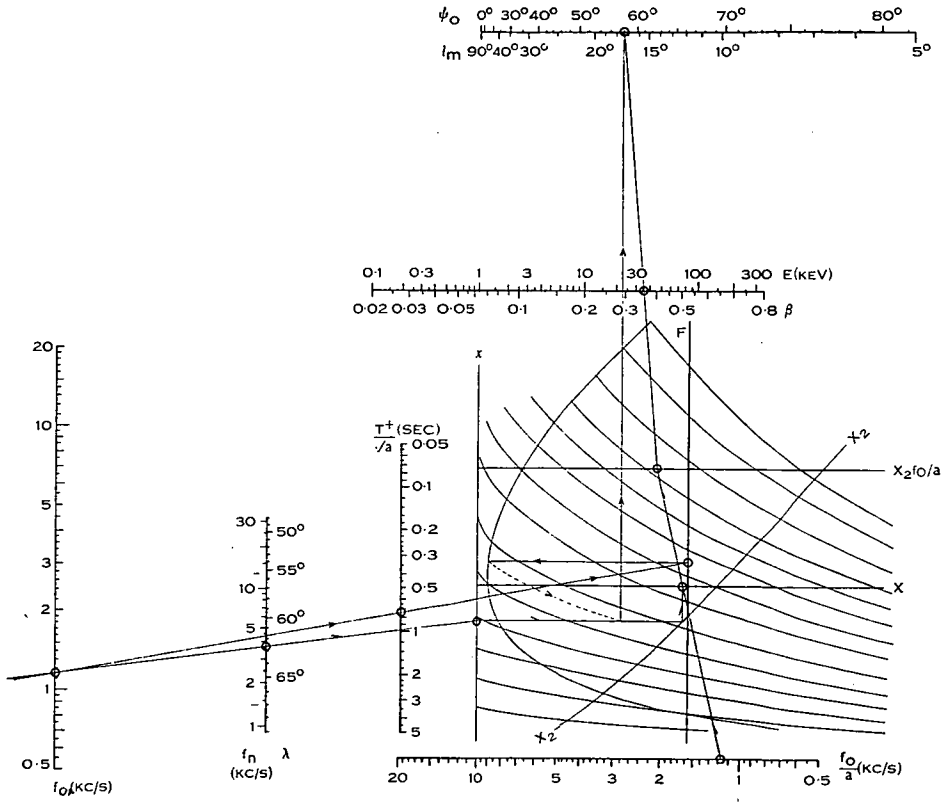

Fig. 4.—Nomogram for complete calculation of λ, ψ_0, and E, when T^+ is measured at the frequency $2f_0$. The scale frequency a must be in units of Mc/s as given in Figure 3. In the example calculation shown, meaningful intercepts are marked with circles.

on the model of electron density variation along the field line, even when integration is taken right down to the Earth's surface. Consequently we will use the quasi-constant model given by Smith (1960) which gives an algebraic solution. Thus

$$2t_g=4\cdot28a^{1/2}f_0^{-5/6}x^{7/6}\frac{\eta^{1/2}[1-1/\eta]}{x-2}[\eta x-2]^{-1/2}. \tag{14}$$

In (13) and (14) the integration limits l and η refer to values at the level for which $f=2f_0$ (and $h=\eta h_0$). At this level we have from (3) and (4) for the non-relativistic case

$$[\eta h_0-2f_0]^3=a\beta^2\cdot 2f_0\cdot\eta h_0[1-\eta\sin^2\psi_0].$$

At the equatorial plane ($f=f_0$) we have

$$[h_0-f_0]^3=a\beta^2 f_0 h_0\cos^2\psi_0.$$

Dividing and making the x substitution

$$[(\eta x-2)/(x-1)]^3=2\eta[1-\eta\sin^2\psi_0]/\cos^2\psi_0. \tag{15}$$

We can now find η from (15) and l from η and substitute these into (13) and (14). Then from (10) we have

$$T^+=a^{1/2}f_0^{-5/6}F(x,\psi_0), \tag{16}$$

where F is a function of x and ψ_0 but not of η. For a given value of F, which can be calculated from observed values of T^+, a, and f_0, then ψ_0 is a function of x only. This is shown by the family of curves of constant F in Figure 4. In this nomogram (Fig. 4) a point on the x scale is found from f_0 and f_n and a point in the F scale from f_0 and T^+ (for $a=1$ Mc/s). With the help of the nose-shaped curve the appropriate F curve is selected. This curve will intercept the previously found x value at the ψ_0 value given by the top scale.

The highest frequency observed on the rising part of a hook is about $0{\cdot}5$–$0{\cdot}6h_0$. This effect is well known in whistler studies (Smith 1960) and is caused by high attenuation in the vicinity of the gyro frequency. Thus measurement of T^+ at $f=2f_0$ is not possible for hooks of $x<3$ or 4. Also it will be noted from Figure 4 that the F curves become nearly horizontal for low values of x. For such hooks we use an alternative method based on T^+ measurement at $f=f_n$ or in general at $f=gh_0$.

Equation (15) becomes

$$[(\eta-g)/(x-1)]^3=\eta g[1-\eta\sin^2\psi_0]/x^2\cos^2\psi_0.$$

Rearranging,

$$x^2/[x-1]^3=\eta g[1-\eta\sin^2\psi_0]/[\eta-g]^3\cos^2\psi_0=X_1. \tag{17}$$

From (8) and (17) we find

$$\beta^2=\frac{h_0}{a}\cdot\frac{[\eta-g]^3}{\eta g[1-\eta\sin^2\psi_0]}.$$

Substituting this into the integral for $2t_e$ we find

$$2t_e=8\cdot 4a^{1/2}h_0^{-5/6}\cdot\frac{\eta^{1/2}}{[\eta-g]^{3/2}}\cdot[1-\eta\sin^2\psi_0]^{1/2}\int_0^l\frac{\eta\cos^7 l\,dl}{[1-\eta\sin^2\psi_0]^{1/2}}.$$

Note that this does not contain x. Also to the extent that

$$\frac{[1-\eta\sin^2\psi_0]^{1/2}}{l}\int_0^l\frac{\eta\cos^7 l\,dl}{[1-\eta\sin^2\psi_0]^{1/2}}=1, \tag{18}$$

and using the approximation for small values of l,

$$l \approx \frac{\sqrt{2}}{3}[\eta - 1]^{1/2}.$$

we have

$$2t_e = 3 \cdot 96 a^{1/2} h_0^{-5/6} \eta^{1/2} \cdot [\eta - 1]^{1/2} / [\eta - g]^{3/2}. \tag{19}$$

Using the same quasi-constant model of electron density and referring all frequencies to h_0, we find

$$2t_g = \frac{6 \cdot 06}{g^{1/2}[1-g]} a^{1/2} h_0^{-5/6} \frac{\eta - 1}{\eta^{1/2}} [\eta - g]^{-1/2}. \tag{20}$$

So that from (10) we have

$$T^+(g) = a^{1/2} h_0^{-5/6} G(g, \eta), \tag{21}$$

where G is given by (19) and (20).

The error introduced into t_e by assuming the validity of (18) is very small at low frequencies (near f_0) where $t_e > t_g$. It becomes larger at the higher frequencies, but there $t_g > t_e$ so that the resulting error in T^+ is never appreciable. It may seem surprising then that G, which does not contain ψ_0 explicitly, can be used to find ψ_0. However, we can obtain η by inverting G and then, solving (17) for ψ_0, we have

$$\sec^2 \psi_0 = \frac{1}{\eta - 1}\left[\eta - \frac{X_1(\eta - g)^3}{\eta g}\right]. \tag{22}$$

V. Use of Nomograms

We have obtained expressions for the electron parameters E, ψ_0, λ, t_0, and a in terms of the quantities f_0, f_n, T_n^-, and T^+ which can be scaled from spectrograms of hooks as explained above. We now discuss techniques of evaluation of these parameters using the nomograms of Figures 3, 4, and 5.

The scale frequency a is found from the nomogram of Figure 3. The f_n, t_n data may be taken from (i) the hook to which one is to apply the scale frequency value for calculation of other parameters, (ii) a nearby hook, or (iii) a nose or " near-nose " whistler. In the first two cases t_n is deduced from f_0, f_n, and T_n by use of the double-sided scale in Figure 3. It will be seen from this scale that for reasonable accuracy we require a hook for which $f_n \gtrsim 2f_0$. In general, whistler measurements will be more accurate. However, in both cases (ii) and (iii) we may be measuring scale frequency in a different field line (if f_n is different). This could introduce an error of 40% (Smith 1960).

For evaluation of the other parameters T^+ is measured at $f = 2f_0$ and the nomogram of Figure 4 is used, provided $f_n \gtrsim 2f_0$. Otherwise T^+ is measured at $f = f_n$ or $f = \frac{3}{4}f_n$ and Figure 5 is used. In both cases the terminating geomagnetic latitude of the field line is immediately obtained from the f_n–λ scale.

Consider the first case (Fig. 4). The f_0 scale is graduated and scaled logarithmically in f_0. The f_n–λ scale is scaled (but not graduated) logarithmically in h_0. A straight line through appropriate values of f_0 and f_n gives the position of x on the x reference line. This scale is not graduated as the actual value is

not required. Similarly the position of F on the F reference line can be found from f_0 and $T^+/\sqrt{a}$. The curve labelled X_2 is the function

$$X_2=(x-1)^3/x.$$

The position of X_2 on the X_2 reference line, corresponding to x found above, is obtained by drawing a horizontal line through the x point and a vertical line through the X_2 point such that these intersect on the X_2 curve. A horizontal line drawn through the F point will intersect the nose-shape curve at a point which lies on the appropriate constant F curve of the family. This curve will intersect the horizontal line through x at the value of ψ_0 given by (vertical line) the ψ_0–l_m scale at the top of Figure 4. This scale is graduated in degrees for

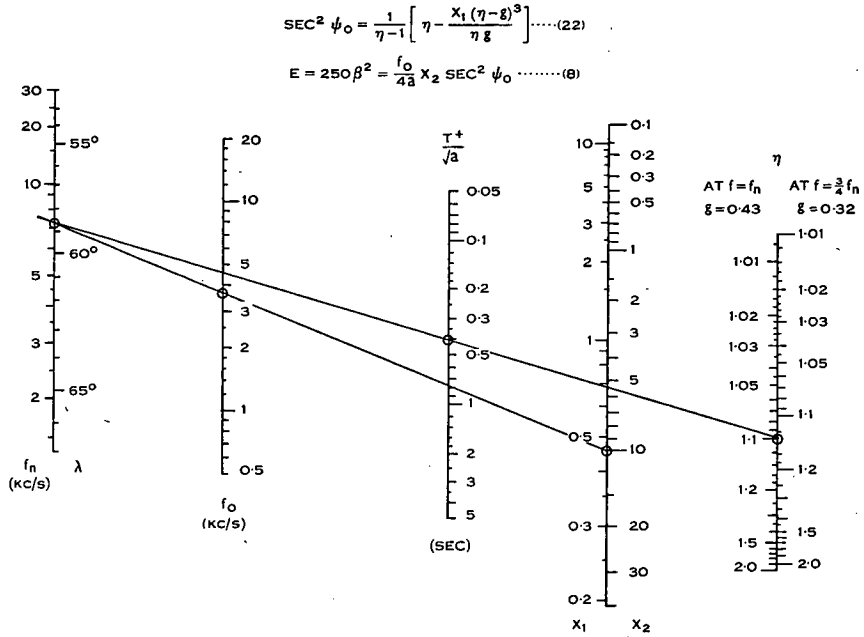

Fig. 5.—Nomogram for calculation of η, X_1, and X_2 for T^+ measured at the nose frequency or three-quarters of this frequency. Energy and helical pitch are then obtained from the expressions (8) and (22). This method entails some simple arithmetic and slide rule calculations.

ψ_0 and l_m (latitude angle of mirror point) but scaled logarithmically in $\sec^2\psi_0$. The energy (E) and β are then found from f_0/a, the position X_2 and $\sec^2\psi_0$ nomographically. This part of the nomogram expresses equation (8). The E–β scale is scaled logarithmically in E' but graduated according to the relativistic correction given in equation (9).

This procedure is illustrated by the example shown in Figure 4. Only certain combinations of scales bear nomographic relationships so meaningful intercepts are marked with small circles. It is, of course, unnecessary to draw any of these lines or curves. All scales and reference lines are parallel or perpendicular so that set squares can be used for the graphical parts. It should

be noted that the scale frequency must be used in units of Mc/s as obtained in Figure 3.

If $f_n < 2f_0$, measurement at $f = 2f_0$ may be impossible. In this case the nomogram of Figure 5 is used. The value of η is found from the f_n and $T^+/\sqrt{a}$ scales. The η scale is logarithmically scaled in the function G of equation (21) but graduated in η for two values of g. As will be seen later, the terminal latitudes (λ) of the field lines in which hooks are generated appear to be confined to a narrow range about 60°. For this range these two values correspond to $f = f_n$ and $f = \frac{3}{4}f_n$. The time T^+ can be measured at either of these frequencies provided the corresponding side of the η scale is used. The X_1–X_2 scales are scaled logarithmically in x and so these values are obtained from the f_n and f_0 scales as shown in Figure 5. Then E, β, and ψ_0 must be calculated from equations (22) and (8). Since this case ($f_n < 2f_0$) corresponds to low values of x, which are generally associated with low energies, we do not require a relativistic correction. The simpler form of this nomogram is offset by the necessity of additional slide rule and arithmetical calculations.

The discussion so far has been limited to " original " or non-echoed hooks. However, the electromagnetic energy or signal may be reflected near the Earth back along the field line once (and so be observable near the conjugate point) or perhaps several times. Such echoed hooks can also be used for evaluation of electron parameters. The frequencies f_0 and f_n will be unchanged. From (10) we see that T^+ also will be unchanged. On the other hand the midpoint locus $\frac{1}{2}T^-$ for a non-echoed hook is the dispersion of a single trip from the equatorial plane to the Earth's surface. For a once-echoed hook the dispersion path is three times this so that T_n^- for such a hook is three times that of the original hook. Since a once-reflected hook is not easily recognized as such, calculation of scale frequency from T_n^- by Figure 3 would lead to a value nine times too large. Fortunately, however, such an ambiguity can usually be resolved. Carpenter (1962) measured f_n, t_n of over 250 whistlers. If these are converted to scale frequencies, about 75% lie in the range 0·5–2 Mc/s. The highest was about 4 Mc/s and for nose frequencies less than about 10 kc/s there was none above 2 Mc/s. Consequently, apparent values of $a > 2$ or 3 as obtained from T_n^- are evidence of echoed hooks. This ambiguity is completely removed if more than one echo is observed, as t_n can then be measured directly.

In general, the treatment given above can only be applied to complete emissions or hooks. Incomplete forms such as " falling tones " and " risers " only provide f_0, and T_1 or T_2. If the nose and scale frequencies are known from other data the missing parts could be supplied from the midpoint locus $\frac{1}{2}T^-$. This would be the case if identifiable echoes were observed.

The theory of this treatment is based on the assumption of a dipole magnetic field and a constant scale frequency along the field line within the region of generation of the observed frequencies. Some departures in the T^+ curve over that calculated from the theory have been noticed. As these occur at the high frequency end it is perhaps advisable to measure T^+ at the lower of the frequencies f_n and $2f_0$. These departures do not seem to occur in the T^- curve, indicating that any perturbations are symmetrical about the equatorial plane.

VI. Some Examples

As an example of the method 14 hooks were scaled from spectrograms published by Gallet (1959) and by Helliwell and Carpenter (1961). These published spectrograms had the usual aspect ratio of 10 kc/s range being equivalent to 1 second interval, which is ideal for our purposes. The size, contrast, and definition of these spectrograms as published were not really suitable for accurate scaling but useful results were obtained, as shown in Table 1. The first five of these hooks were taken from Gallet and the remaining nine from Helliwell and Carpenter.

The sum time T^+ was measured at $2f_0$ for each hook and at f_n as well for six of these hooks. These times are shown in Table 1 as T^+_{20} and T^+_n respectively. For these six hooks both methods were used for energy and helical pitch calcu-

Table 1

ELECTRON DATA DEDUCED FROM HOOKS

No.	Measured					Deduced						
	f_0 (kc/s)	f_n (kc/s)	T^-_n (sec)	T^+_n (sec)	T^+_{20} (sec)	$\frac{1}{2}t_0$ (sec)	a* (Mc/s)	λ	ψ_0	E (keV)	ψ_0†	E† (keV)
1	3·3	9·6	0·40	0·57	0·33	0·85	1·3	57°	64°	85	62°	78
2	3·3	5·7	0·22	0·56	0·70	1·3	1·8	60°	74°	47	70°	31
3	3·7	7·1	0·23	0·70	0·75	1·0	1·5	59°	58°	23	63°	29
4	2·7	5·3	0·35	0·78	0·80	1·5	1·7	60°	64°	26	66°	26
5	3·9	10·4	0·40	—	0·53	1·0	2·1	57°	56°	37	—	—
6	1·6	4·6	0·48	—	0·31	1·0	0·50	61°	68°	150	—	—
7	4·2	8·0	0·28	0·42	0·49	—	(2·8)	58°	50°	47	57°	60
8	2·7	7·5	0·28	—	0·43	0·65	0·53	58°	38°	55	—	—
9	1·6	6·5	0·61	—	0·36	0·95	0·59	59°	41°	70	—	—
10	2·0	6·5	0·44	—	0·42	0·85	0·56	59°	48°	68	—	—
11	2·3	6·5	0·44	—	0·38	1·0	0·82	59°	58°	83	—	—
12	2·1	6·5	0·35	—	0·38	0·70	0·40	59°	56°	80	—	—
13	3·2	7·1	0·28	0·56	0·48	0·95	1·1	59°	52°	51	56°	57
14	1·9	6·3	0·50	—	0·38	0·95	0·63	59°	55°	88	—	—

* Deduced from the hook. The value used for energy and pitch calculation may differ from this.

† Calculated by the alternative method (Fig. 5).

lation. The two sets of these values are shown in Table 1. There is reasonable agreement between them. What discrepancies there are could be explained by either scaling errors or the simplifying assumptions used in deriving the alternative (f_n) method.

The scale frequency a as calculated from Figure 3 for each hook is shown in Table 1. However, for the value adopted for energy and pitch calculation, use was made of the fact that hooks often occur in groups. For instance, the last seven hooks all occurred within 30 seconds or so of 0135 U.T. on October 6, 1959. Also hooks 2 and 3 both occurred at 0635 U.T. on February 15, 1958. It seems reasonable to assume that the scale frequency would not change in such a short time. Thus a weighted average value was adopted in such cases.

This sample is too small for statistical analysis. It seems that relatively few spectrograms of hooks have been actually published, though since 7 of the 14 considered here occurred in an interval of half a minute one would expect that enormous numbers would have been recorded during the I.G.Y. However, some interesting preliminary conclusions can be drawn from the few we have here.

Table 1 shows that the generation of these hooks was confined to a narrow range of field line latitudes. The last seven were observed at Seattle (geomagnetic latitude 54° N.) but barely or not at all at Stanford (44° N.), as shown in Helliwell and Carpenter (1961). This indicates an observing range for any one event (produced by propagation under the ionosphere) of some 10° of latitude. Thus we would predict from this that the occurrence rate of observations as a function of receiving station latitude should show a broad maximum in the vicinity of 59°. The observed (Helliwell and Carpenter 1961) occurrence rate of "chorus" for days of $K_p \geqslant 4$ shows such a maximum at approximately 58°. Although the average latitude of the field lines of generation can be deduced from such analyses of occurrence rate of observations, the method given here for the first time gives the latitude of *individual* emissions. The method also gives the time of generation of the centre (f_0) of the hooks. From Table 1 we see that this occurred about 1 second before observation.

If the electron bunches which produce these hooks were all injected into the field line near the equatorial plane and if there were no preferred direction of injection, one would expect the median of the equatorial pitch angle ψ_0 values of a large number of bunches to be 60°. This is approximately so for the 14 hooks in Table 1. The latitude angles of the mirror points (l_m) corresponding to these values of ψ_0 range from about 8° to 30° as seen from the top scale of Figure 4. The latitude angles of the points at which the frequency f_n was generated was found from η for the six hooks for which T_n^+ was scaled. These ranged from 7° to 14°. Thus most of the observed frequency range is generated within some 10–20° of the equatorial plane. It is important to note that, since f_n is the highest frequency at which measurements are made, the assumptions of constant scale frequency and dipole magnetic field need only apply within this region.

Probably the most important parameter is the electron energy. The energies shown in Table 1 are of the order of a few tens of kilo-electron-volts. Thus

typical values of β are around 0·3–0·5. Relativistic effects are very small at these velocities, so that the approximate correction formula (9) which was applied to the energy scale of Figure 4 should be sufficiently accurate.

VII. Acknowledgment

I am indebted to Professor G. R. A. Ellis of the Physics Department, University of Tasmania, for advice, criticism, and encouragement.

VIII. References

Carpenter, D. L. (1962).—*J. Geophys. Res.* **67**: 135–45.

Dowden, R. L. (1962*a*).—*J. Geophys. Res.* **67**: 1745–50.

Dowden, R. L. (1962*b*).—*Nature* **195**: 1085–6.

Dowden, R. L. (1962*c*).—*Nature* **195**: 984–5.

Eidman, V. Ia. (1958).—*J. Exp. Theor. Phys.* (*U.S.S.R.*) **34**: 131–8.

Ellis, G. R. A. (1962).—*Aust. J. Phys.* **15**: 344–53.

Gallet, R. M. (1959).—*Proc. Inst. Radio Engrs.* **47**: 211–31.

Helliwell, R. A., and Carpenter, D. L. (1961).—Whistlers—West I.G.Y.–I.G.C. Synoptic Program. S.E.L. Report March 20, Stanford University.

Smith, R. L. (1960).—The use of nose whistlers in the study of the outer ionosphere. S.E.L. Report No. 6, Stanford University.

Smith, R. L., and Carpenter, D. L. (1961).—*J. Geophys. Res.* **66**: 2582–6.

Planet. Space Sci., 1963, Vol. 11, pp. 361 to 369. Pergamon Press Ltd. Printed in Northern Ireland

DOPPLER SHIFTED CYCLOTRON GENERATION OF EXOSPHERIC VERY-LOW-FREQUENCY NOISE ("HISS")

R. L. DOWDEN
Ionospheric Prediction Service and University of Tasmania, Hobart, Australia

(*Received* 20 *November* 1962)

Abstract—Cyclotron radiation from a receding electron in the exosphere can be doppler shifted to a frequency much less than the local gyrofrequency. A discrete bunch of electrons will produce a discrete emission as shown previously.[1] A stream of electrons will produce band limited white noise or hiss. The low frequency limit of this band is an emission cut off and the upper limit is a propagation cut off. Narrow, wide and very wide bands of hiss can be produced by electron streams of even very broad velocity and pitch distribution. Tests of this theory and of the TWT theory[2] are suggested.

1. INTRODUCTION

Very low frequency exospheric noise or "hiss" occurs in the audiofrequency region usually in association with magnetic disturbance. In this and many other respects it is similar to the discrete emissions such as "hooks", "risers", "falling tones", etc. The most important difference is that the latter appear as separate discrete falling and rising tones whereas hiss appears as band limited white noise.

Several theories have been advanced to explain these emissions, but most of these do not attempt to account for the detailed features that are observed. Recently, however, two theories were advanced, one for hiss and the other for the discrete emissions, which do account for the detailed features of the two types of emissions.

The first[2] explains hiss as amplified Čerenkov emission from electron streams by analogy with the travelling wave tube (TWT process). It was shown that an electron stream in the exosphere acts as narrow band amplifier if the stream is "weak" but as an overloaded amplifier for "stronger" streams. Largely as a consequence of this it was possible to explain the following characteristics of hiss: that it occurs mostly in the 1 to 10 kc/s region; that the vast majority of hiss originates at geomagnetic latitudes[3] greater than 50°; that the bandwidth varies from about[4] 750 c/s to over[5] 200 kc/s, though bandwidths of 1 or 2 kc/s are more usual[6]; and that in general the bandwidth increases with the degree of magnetic activity.[6] Several other features of hiss, such as the occasional occurrence of multiple narrow bands of hiss and the long term (minutes and hours) frequency and amplitude variations of hiss, could be explained in terms of this theory, but these features are determined by the properties of the sources of the electron streams and so not relevant to the actual hiss generation process.

The second theory[1] explained the discrete emissions by a very different process. It was shown that a single discrete bunch of electrons spiralling along a field line *away* from the observer will radiate the doppler shifted frequency (f) given by:

$$(h - f)^3 = a\beta^2 hf \cos^2 \psi \qquad (1)$$

where h is the local gyro frequency, a is the electron density parameter[7] "scale frequency", β is the electron velocity in units of the velocity of light, and ψ is the helical pitch angle of the electrons. Consideration of electron travel times and wave group propagation times gives the frequency-time shape of a "hook" for a complete hemisphere to hemisphere

traverse. A family of hooks calculated in this way is shown in Fig. 1. A half traverse (bunch lost at mirror point or at re-entry of injection region) gives only half a hook. This may be a "falling tone," a "riser" or a "pseudo nose" as seen in Fig. 1.

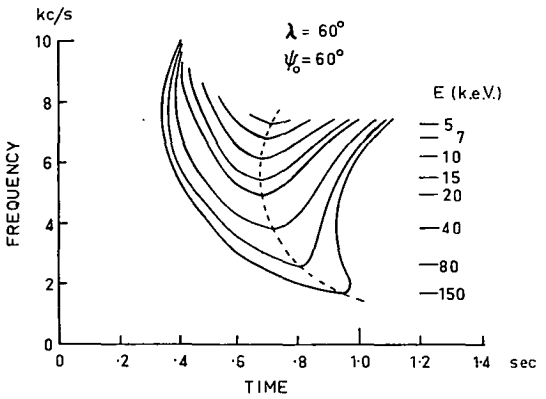

FIG. 1. A FAMILY OF HOOKS CALCULATED FOR ELECTRON BUNCHES OF MINIMUM PITCH ANGLE $\psi = 60°$ AND SEVERAL ENERGIES AS SHOWN TRAVELLING IN AN EXOSPHERE OF SCALE FREQUENCY $a = 500$ kc/s ALONG THE (DIPOLE) FIELD LINE $\lambda = 60°$. AT TIME $t = 0$ EACH BUNCH PASSED THROUGH THE EQUATORIAL PLANE FROM THE OBSERVER'S HEMISPHERE TO THE OPPOSITE HEMISPHERE. THE BROKEN CURVE (WHICH HAS A NOSE WHISTLER SHAPE[13]), DIVIDES THE HOOKS INTO FALLING AND RISING PARTS GENERATED IN THE OBSERVER'S AND THE OPPOSITE HEMISPHERES RESPECTIVELY. THESE PARTS MAY OCCUR SEPARATELY GIVING "FALLING TONES", "RISERS", ETC. THE RISING PART IS CUT OFF AT THE FREQUENCY $0{\cdot}55h_0$. THE HIGHEST FREQUENCY OF THE FALLING PART IS f_m GIVEN BY (3).

This theory also includes "dawn chorus". This is a continuous emission made up of discrete emissions (hooks, risers, etc.) often overlapping in time. At times this discreteness or fine structure may only be apparent when observed aurally or on fast spectrograms.[4] Thus we have a well-known and very common class of emissions which are explained in terms of the cyclotron theory and which can be very similar to hiss. This suggests that perhaps hiss is only a type of unresolved dawn chorus produced by the cyclotron process by a sufficiently large number of small electron bunches or a continuous stream of electrons. This merely explains the continuous or white noise nature of hiss. However it will be shown in this paper that all of the other characteristics of hiss which are explained by the TWT process can be equally well explained by the doppler shifted electron–cyclotron process.

2. FREQUENCY BAND LIMITS

It is clear that a sufficiently large number of overlapping and unresolved "discrete emissions" could produce white noise. However an essential feature of hiss is that it is band limited and that the band width is often quite small, whereas at first sight one might expect only broad band noise from unresolved "discrete emissions" produced by the cyclotron process. But two effects limit the upper and lower frequencies respectively.

For electrons of given energy and minimum pitch angle, the minimum frequency occurs at the geomagnetic equatorial plane. Using subscript zero to denote values at this point the minimum frequency or low frequency cut off (f_o) is given by:

$$(h_o - f_o)^3 = a\beta^2 h_o f_o \cos^2 \psi_o \tag{2}$$

The highest frequency *emitted* (from (1)) is the gyro frequency at the mirror point.

However there is a propagation cut off much below this limit caused by attenuation near the local gyro frequency. It is very sharp: Liemohn and Scarf[8] found that in the vicinity of this cut off the attenuation increased from 5 dB to 50 dB in a three per cent interval of frequency. Smith[9] found that the upper cut off frequency of all nose whistlers he analysed never exceeded 0·55 to 0·6 times the minimum gyro frequency along the whistler path. Choosing the lower frequency, for example, the highest observable frequency from emissions generated in the hemisphere opposite that of the observer will be $0{\cdot}55\ h_o$. For emissions generated in the observer's hemisphere, however, the lowest gyro frequency along the path from the emission point to the observer occurs at the emission point. Thus the highest observable frequency (f_m) will be $0{\cdot}55h_m$ where h_m is the gyro frequency at the point at which f_m is generated. Substituting into (1).

$$(h_m - 0{\cdot}55h_m)^3 = 0{\cdot}55a\beta^2 h_m{}^2 \cos^2 \psi_m.$$

From the principle of invariance of magnetic moment we can express the pitch (ψ) in terms of its value at the equator:

$$\cos^2 \psi = 1 - (h/h_o) \sin^2 \psi_o.$$

Consequently:

$$f_m = 0{\cdot}55h_m = 0{\cdot}55\ [0{\cdot}17/a\beta^2 + \sin^2 \psi_o/h_o]^{-1}. \tag{3}$$

These points are illustrated in Fig. 1. The rising parts (right hand side of broken curve) are produced in the hemisphere opposite that of the observer and so are limited to $0{\cdot}55h_o = 7{\cdot}4$ kc/s. The upper limits of the falling parts are given by (3). At any given frequency only energies above some limit can produce radiation. At frequencies below the whistler cut off ($0{\cdot}55h_o$) radiation from both hemispheres can be observed. If the stream is confined to the hemisphere opposite that of the observer the upper limit will be the whistler cut off. This is another way of saying that if the hiss consists entirely of unresolved "risers" and "pseudo noses" (no unresolved "hooks" or "falling tones") the upper frequency limit will be $0{\cdot}55h_o$. This is perhaps likely at times since rising type discrete emissions are about ten times as common as hooks and falling tones.[10]

The upper and lower limits as a continuous function of energy for discrete pitch angles and of pitch angle for discrete energies are shown in Figs. 2 and 3. These are drawn for the field line terminating at latitude $\lambda = 60°$. The same curves can be applied at any other latitude if the frequencies and energies are scaled in proportion to h_o. A constant scale frequency of 500 kc/s has been assumed but a definite model of magnetic field is not required (provided it is monotonic) except for obtaining field line latitude λ from minimum gyro frequency h_0. Note that narrow band noise can be produced by a range of energies for any given pitch angle, but for large pitch angles this energy range is larger. Wide and very wide band noise will be produced by electrons of low pitch and high energy. During magnetic storms electron streams reach down to the ionosphere to produce aurorae[11]. At high latitudes ($\sim 60°$) this requires pitch angles (ψ_0) less than about 5°. We might also expect higher energies during storms and thus wide and very wide band noise as observed[5].

3. AMPLITUDE—FREQUENCY SPECTRA

In considering bandwidths of hiss produced by streams of electrons of various energies and minimum pitch angles we have assumed mono-energetic, mono-pitched streams. This is not an unreasonable assumption since it is observed that the bandwidths of individual discrete emissions rarely exceed 150 c/s at any instant[4]. This could not happen

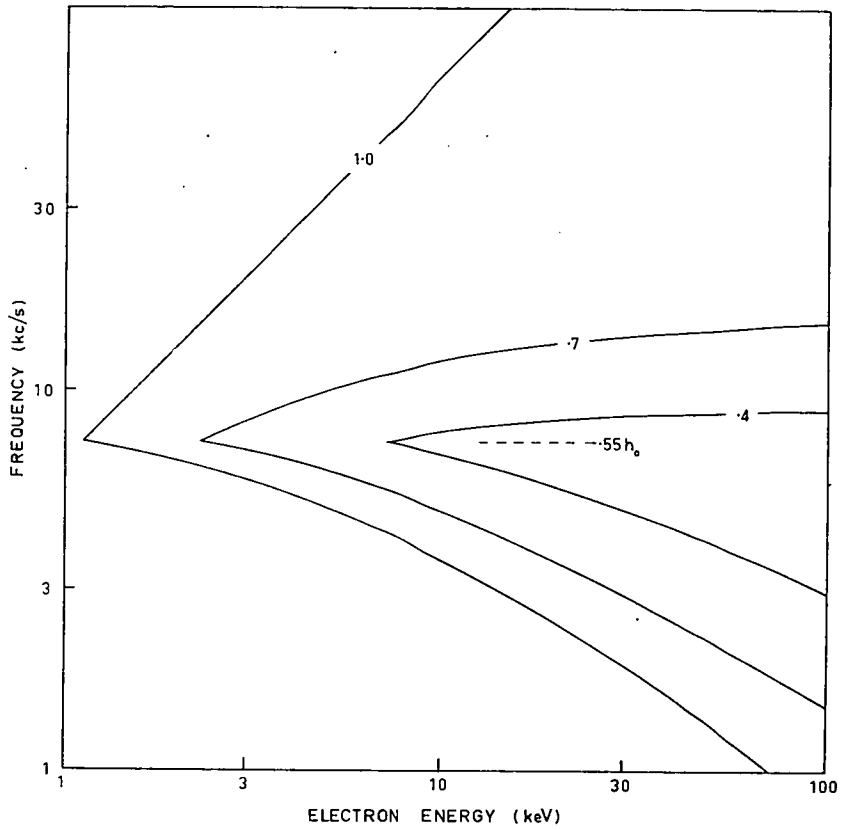

FIG. 2. UPPER AND LOWER BAND LIMITS OF HISS GENERATED IN THE FIELD LINE $\lambda = 60°$ AS A FUNCTION OF THE ENERGY OF THE ELECTRONS GENERATING IT. CURVES ARE SHOWN FOR THREE DISCRETE VALUES OF MINIMUM PITCH ANGLE (cos ψ_o)

unless the electrons in the bunches which produce these emissions had narrow ranges of energy and pitch. One would expect the same to hold true of streams. Also mono-energetic electron streams have been observed[11]. Pitch angle measurements of electrons *in streams* have not been reported. However we will show that the main features of hiss can be produced even if the electrons of the streams have wide energy and pitch distributions.

Two energy spectra of electron streams as measured by McIlwain[11] will be considered. Both were measured by rockets fired into visible aurora. The first was observed inside a quiescent auroral glow of intensity I. It showed an integral number energy spectrum proportional to exp $(-E/5)$ electrons/sec cm^2 over the range 3 to 30 keV. The second was observed in a bright active auroral arc. This stream consisted of practically mono energetic electrons of energy 6 keV.

We will consider a pitch angle distribution produced by isotropic injection at the equatorial plane. It can be shown by simple geometrical considerations that the fraction of pitch angles between ψ_0 and $\psi_0 + d\psi_0$ is given by

$$dN(\psi_o)/N = \sin \psi_o \, d\psi_o. \tag{4}$$

Satellite measurements[12] of the low energy ($\ll 500$ keV) electrons in the outer radiation zone indicate such a pitch distribution. Preliminary measurements from hooks[13] indicate

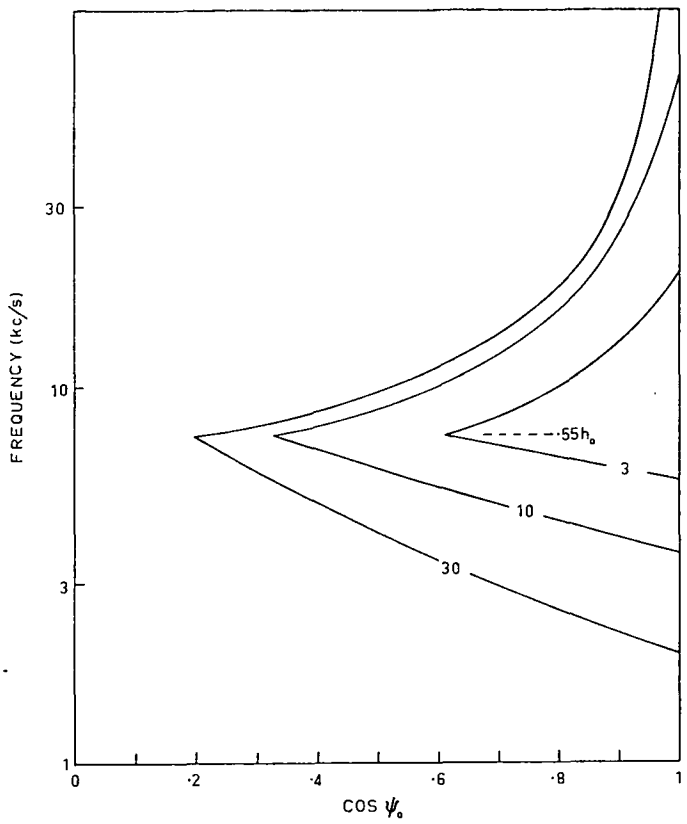

FIG. 3. BAND LIMITS OF HISS GENERATED IN THE FIELD LINE $\lambda = 60°$ BY ELECTRONS OF ENERGY 3, 10 AND 30 keV RESPECTIVELY, AS A FUNCTION OF THE MINIMUM PITCH ANGLE ψ_o OF THESE ELECTRONS

that the pitch distribution of the electron *bunches* (but not of the electrons in an individual bunch) is also of this type.

The power radiated by an electron travelling along a helical path in a plasma with superimposed magnetic field has been given by Eidman[14]. A much simpler expression will suffice for our purpose since the spectrum shape is mainly controlled by the pitch and energy distributions. That is:

$$p = kf^{3/2}E \tag{5}$$

where k is assumed constant. This is the power radiated by a single electron. From Figs. 2 and 3 we see that a given frequency f requires electrons of energy equal to or greater than some minimum value $E_n(\psi_o)$, which is a function of ψ_o. We will assume that the power radiated by the electron stream at this frequency is proportional to the number of electrons fulfilling this condition, weighted by their energy as in (5). If the number of electrons having energies within dE of E is $dN(E)$ and if the pitch distribution is given by (4), then the power radiated by the stream at frequency f is given by (arbitrary units):

$$P = f^{3/2} \int_0^{\psi_0} \int_{E_n}^{\infty} E\, dN(E) \sin \psi_o\, d\psi_o. \tag{6}$$

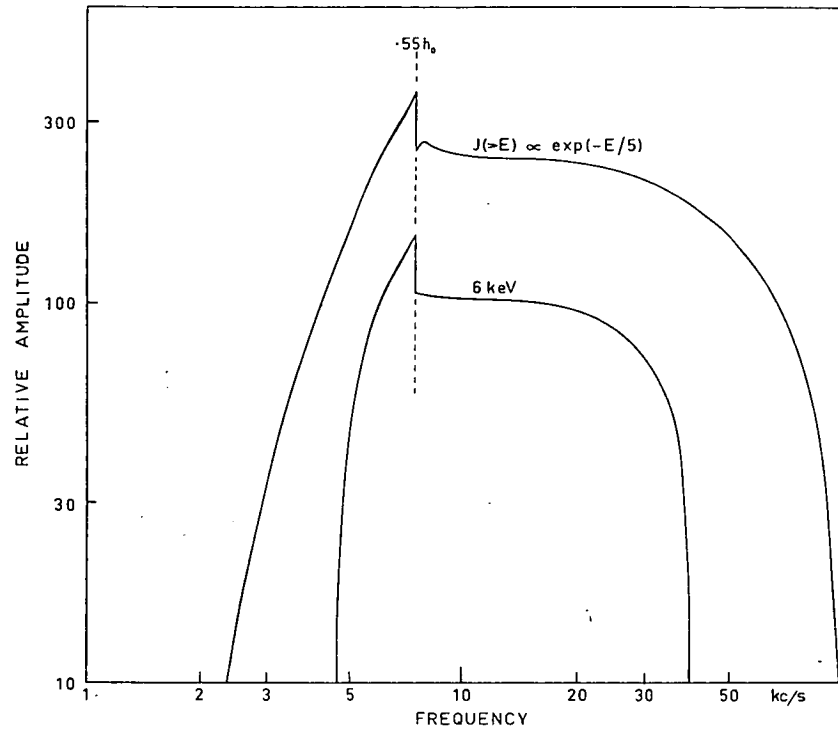

FIG. 4. AMPLITUDE–FREQUENCY SPECTRA OF HISS GENERATED IN THE FIELD LINE $\lambda = 60°$ BY ELECTRONS HAVING THE PITCH DISTRIBUTION GIVEN BY (4) AND ENERGY DISTRIBUTIONS AS IN THE STREAMS OBSERVED BY MCILWAIN. A FINITE STREAM WIDTH WOULD SMOOTH OUT THE DISCONTINUITY AT $0.55h_o$.

For McIlwain's first stream the integral number energy spectrum is given by

$$J(>E) \propto \exp(-E/5) \text{ electrons/sec cm}^2.$$

The number energy spectrum per energy interval in then:

$$\frac{dJ}{dE} \propto \exp(-E/5)$$

The density of the electrons in this energy interval dE is given by:

$$dN(E) \propto dJ/\beta c \propto E^{-1/2}\, dJ$$

$$\propto E^{-1/2} \exp(-E/5)\, dE.$$

For McIlwain's monoenergetic stream we take:

$$dN(E) = \begin{cases} 1 & \text{for } E = 6 \text{ keV} \\ 0 & \text{for all other values of } E. \end{cases}$$

Amplitude-frequency spectra of hiss generated by these two streams as calculated from (6) for streams confined to the field line terminating at latitude $\lambda = 60°$ are shown in Fig. 4.

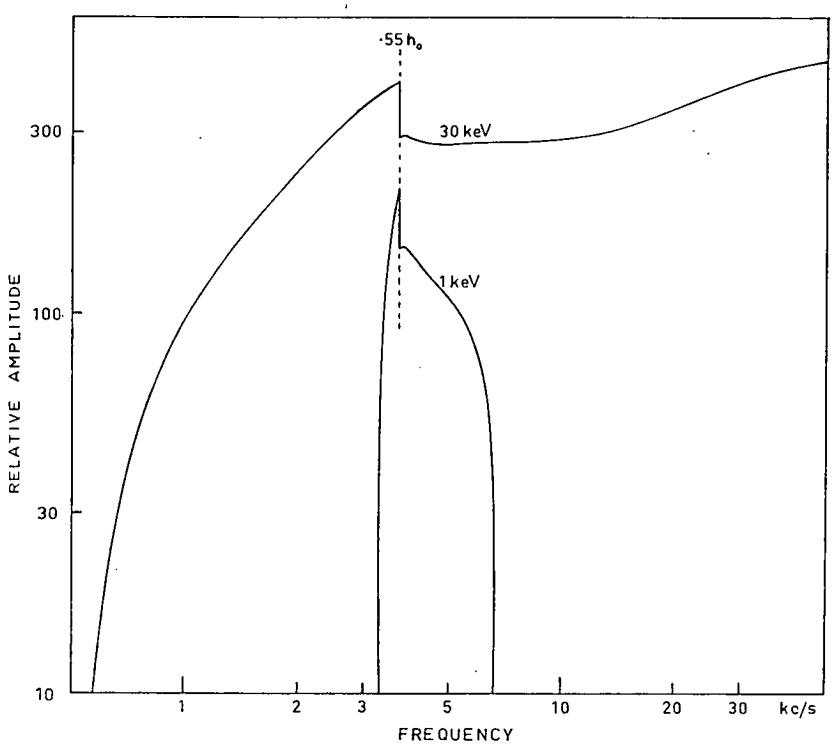

FIG. 5. AMPLITUDE–FREQUENCY SPECTRA OF HISS GENERATED IN THE FIELD LINE $\lambda = 63{\cdot}5°$ BY TWO MONO-ENERGETIC ELECTRON STREAMS HAVING PITCH DISTRIBUTIONS GIVEN BY (4).

Note the similarity in shape of the two spectra. The peak or average amplitudes are not comparable, they have been arbitrarily chosen for best clarity. The band limit of the hiss generated by the monoenergetic stream are approximately given by the cos $\psi_0 = 1$ curve of Fig. 2. Thus the hiss spectrum from the first stream (exponential energy distribution) could be approximated in shape, amplitude and band width by one generated by a mono energetic stream of 15 keV electrons. Hiss spectra from two hypothetical mono energetic streams at latitude $\lambda = 63{\cdot}5°$ are shown in Fig. 5. From what has been said above we would expect similar spectra from streams having energy distributions $J(>E) \propto \exp(-E/E_c)$ if E_c is appropriately chosen.

An amplitude discontinuity occurs at the whistler cut off frequency $0{\cdot}55h_o$. Above this frequency only hiss generated in the observer's hemisphere can be observed, whereas below this frequency hiss from both hemispheres can be observed (see Fig. 1). For hiss consisting entirely of unresolved "hooks", or of "hooks" plus equal amounts of "risers" and "falling tones" the discontinuity will be a factor of two in power or of root two in amplitude as shown here. If the hiss consists entirely of "falling tones" the discontinuity will disappear, but if it consists entirely of "risers" and "pseudo noses" the high frequency side ($f > 0{\cdot}55\ h_o$) will not be observed at all. In all cases the low frequency side could be further augmented by whistler mode reflections near the earth of previously generated hiss. In any case the sharpness of the discontinuities will be considerably rounded by finite attenuation at cut off and finite stream width (field line latitude ranges of a few tenths of a degree would suffice).

Figure 6 shows amplitude-frequency spectra of hiss observed by Watts[15] during a magnetic storm. These show similar shapes to those of Figs. 4 and 5 if the discontinuities are rounded off. The observed spectra will have been modified by attenuation in propagation through and under the ionsphere. This increases with frequency[5]. As it is the comparison indicates that the frequency $0{\cdot}55h_o$ is about 2 kc/s. This would correspond to a field line of generation of about latitude 65°.

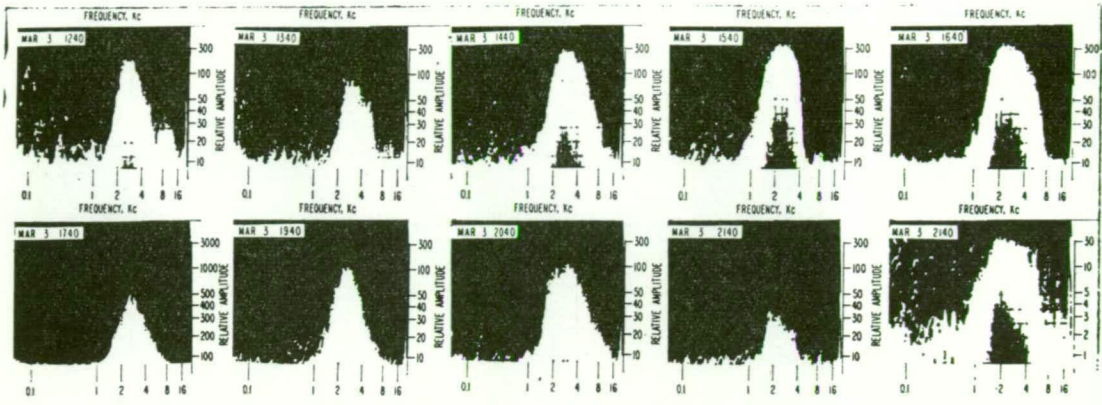

FIG. 6. HISS SPECTRA OBSERVED BY WATTS (NOTE CHANGE OF AMPLITUDE SCALE). THESE SHOULD BE COMPARED WITH THOSE CALCULATED IN FIGS. 4 AND 5. (AFTER WATTS[15]).

4. DISCUSSION

This cyclotron theory of hiss can account for the observed characteristics of hiss listed in Section 1. From Figs. 4 and 5 and equations (2) and (3) we see that narrow and medium band width hiss occurring at frequencies less than 10 kc/s would be produced at geomagnetic latitudes of 60° or higher. Very wide to narrow band widths can be produced by this process even for wide pitch angle and energy distributions provided the high energies are fairly sharply cut off (power law or exponential) as observed[11]. Wide band widths will be produced by higher energy electrons which we might expect to be associated with magnetic activity.

From our present state of knowledge, the cyclotron process explains the observed features of hiss as well as does the TWT process. In addition the cyclotron process already explains the much more detailed features of the discrete emissions and dawn chorus. However the two processes are not mutually exclusive. Both may operate, possibly even at the same time and in the same electron stream, though one may dominate. It should be possible to distinguish between these three possibilities (cyclotron, or TWT, or both), if not from present data, at least from new experiments based on predictions of the two theories.

The TWT process requires a stream travelling towards the observer whereas the cyclotron process requires the reverse. Unfortunately hemisphere to hemisphere electron and wave travel times are of the order of seconds whereas time variations of hiss are of the order of minutes or hours[6]. Thus whistler mode reflections of hiss and magnetic reflections of electrons would make the original stream and emission direction very difficult to detect.

Although both theories predict that the centre frequency of narrow band bursts will be proportional to the minimum gyro frequency (h_o), the constants of proportionality are different. For the TWT theory this frequency is $0{\cdot}15h_o$, whereas for the cyclotron theory it

is $0{\cdot}55h_0$. For typical 4 kc/s narrow band hiss the corresponding field line latitudes are 55·5° and 63·5°. In addition the TWT process can produce narrow band hiss not obeying this relation if the stream is mono energetic and narrow pitched[2]. This effect is difficult to detect on the earth because propagation under the ionosphere allows observation of hiss generated in a wide range of field line latitudes. On the other hand a satellite travelling just above the ionosphere (or higher) will receive only radiation generated in the field line through which it is passing. In addition, since there would be no ionospheric losses to contend with, the intensity would be several orders of magnitude greater[5] and the observed amplitude-frequency spectra would be as generated[5]. For similar reasons such a satellite would be very useful for work on discrete emissions and whistlers.

5. CONCLUSIONS

Doppler shifted cyclotron radiation from receding electrons which already explains the detailed frequency-time shapes of discrete emissions can also explain the observed characteristics of hiss. However the amplified Čerenkov (TWT) process also explains these characteristics and it is difficult to distinguish between the two theories for hiss on present data. Observations from a satellite of the variation of frequency of narrow band hiss with geomagnetic latitude could resolve this.

Acknowledgements—The author would like to thank Professor G. R. A. Ellis for many criticisms and suggestions concerning both the theory and the manuscript.

REFERENCES

1. R. L. Dowden, *J. Geophys. Res.*, **67**, 1745 (1962).
2. R. L. Dowden, *J. Geophys. Res.*, **67**, 2223 (1962).
3. G. R. A. Ellis, *J. Geophys. Res.*, **65**, 839 (1960).
4. R. A. Helliwell and D. L. Carpenter, *S. E. L. Final Dept.*, Stanford University, March 20 (1961).
5. R. L. Dowden, *Aust. J. Phys.*, **15**, 114 (1962).
6. G. R. A. Ellis, *Planet Space Sci.*, **1**, 253, (1959).
7. R. L. Dowden, *Nature Lond.*, **195**, 984 (1962).
8. H. B. Liemohn and F. L. Scarf, *J. Geophys. Res.*, **67**, 1785 (1962).
9. R. L. Smith, *S. E. L. Tech. Dept.* 6, Stanford University, July 11 (1960).
10. B. A. McInnes, *Aust. J. Phys.*, **14**, 218 (1961).
11. C. E. McIlwain, *J. Geophys. Res.*, **65**, 2727 (1960).
12. T. A. Farley and N. L. Sanders, *J. Geophys. Res.*, **67**, 2159 (1962).
13. R. L. Dowden, *Aust. J. Phys.*, **15**, No. 4 (1962).
14. V. Ia. Eidman, *Zh. Eksp. Teor. Fiz.*, **34**, 131 (1958).
15. J. M. Watts, *J. Geophys. Res.*, **62**, 199 (1957).

Резюме—Циклотронное излучение от отступающего электрона в эксосфере может получить сдвиг Допплера до частоты, которая гораздо меньше местной гирочастоты. Как было показано раньше[1], дискретный пучек электронов создает дискретную эмиссию. Поток электронов создает белый шум или шипение с ограниченной полосой. Низкочастотная граница этой полосы—эмиссионное ограничение, а высокочастотная граница—ограничение распространения. Узкая, широкая и очень широкая полосы шипения могут быть созданы электронными потоками с равномерным, очень широким распределением скорости и угла между скоростями электронов и магнитными силовыми линиями. Предложены испытания этой теории и TWT[2].

Short Communications reprinted from the Australian Journal of Physics,
Volume 16, Number 4, pp. 588–92, December 1963

EFFECT OF MAGNETIC ANOMALIES ON VERY LOW FREQUENCY DISCRETE EMISSIONS

By R. L. Dowden

EFFECT OF MAGNETIC ANOMALIES ON VERY LOW FREQUENCY DISCRETE EMISSIONS*

By R. L. Dowden†

The author has suggested (Dowden 1962) that the spectrogram (frequency *v.* time) shapes of V.L.F. discrete emissions can be explained as Doppler-shifted cyclotron radiation from electrons spiralling along a geomagnetic field line *away* from the observer. The emission frequency is given by Eidman (1958),

$$f = \gamma h[1+\beta n \cos\theta \cos\psi]^{-1},$$

where h is the gyro frequency, $\gamma^2 = 1-\beta^2$, β is the electron velocity in units of the velocity of light, n is the refractive index of the medium at the frequency f and direction θ, θ is the angle between the field and the direction of emission, and ψ is the pitch angle of the spiralling electrons.

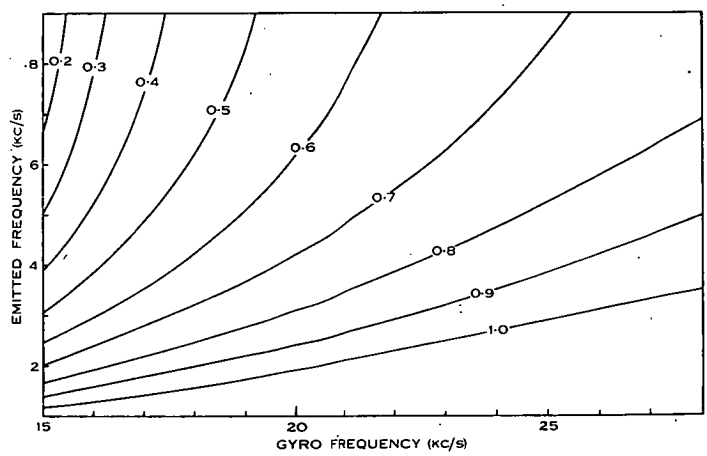

Fig. 1.—Doppler-shifted cyclotron frequency emitted by electrons of energy 75 keV in a medium of scale frequency $a = 500$ kc/s shown as a function of gyro frequency for several values of cos ψ_0.

It is reasonable to assume that γ and β are constant, that the electron density in the exosphere is everywhere proportional to the magnetic field, that θ is either constant or a function of h only, and that ψ is given by the invariance of magnetic moment:

$$\sin^2\psi/\sin^2\psi_0 = h/h_0,$$

where subscript zero can refer to any known point such as the equatorial plane or point of minimum magnetic field. In this case the variation of frequency emitted by an electron spiralling along a field line is produced entirely by the variation of

* Manuscript received September 4, 1963.

† Physics Department, University of Tasmania, Hobart.

magnetic field (or gyro frequency) along the path. This is shown in Figure 1 for small θ, for electrons of energy 75 keV, and for several values of cos ψ_0 defined at the arbitrary level $h_0 = 15$ kc/s.

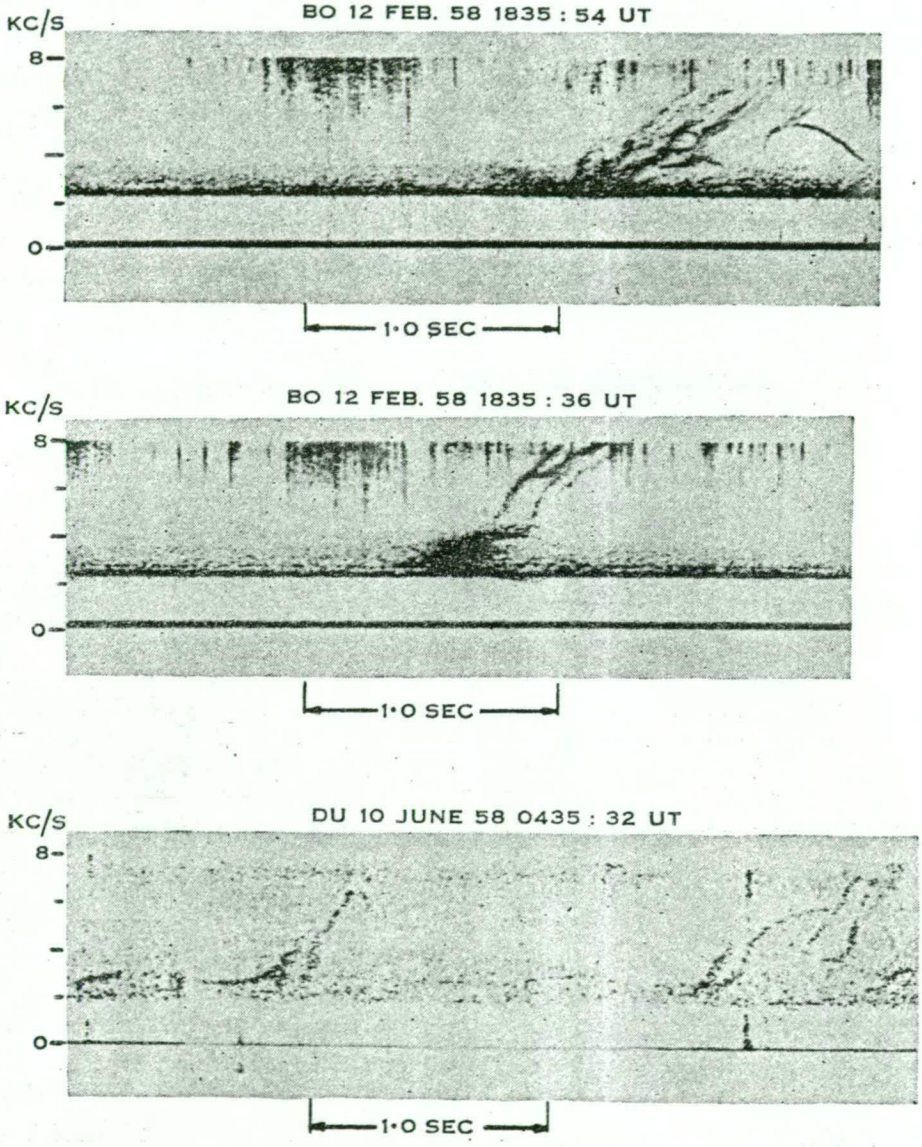

Fig. 2.—"Unusual events" recorded at Boulder and Dunedin (after Helliwell and Carpenter 1961).

For a dipole magnetic field, consideration of electron travel times and wave group propagation times gives the spectrogram shapes of "hooks" for hemisphere to hemisphere traverses and those of "falling tones", "risers", and "pseudo noses"

for incomplete traverses (Dowden 1962). However, many discrete emissions have distorted spectrograms which cannot be explained by the theory, if a dipole field is assumed. Examples of these are shown in Figure 2.

The following points suggest that these distorted emissions are produced by magnetic anomalies in a predominantly dipole magnetic field. An atlas of spectrograms of V.L.F. emissions (Jones *et al.* 1963) observed at times of quiet conditions, moderate disturbance, and severe disturbance, indicates that the degree of distortion increases with the degree of disturbance. Reference to Figure 1 shows that the emitted frequency can be quite sensitive to small changes in magnetic field or gyro frequency, particularly for large pitch angles. Anomalies observed by satellites and space probes appear to have significant amplitudes. These are shown in Table 1 (the last two entries refer to hydromagnetic fluctuations).

TABLE 1

SATELLITE OBSERVATIONS OF MAGNETIC ANOMALIES

Region (Earth radii)	Amplitude (gammas)	Remarks	Reference
7	−50	(ring current?)	Smith *et al.* (1960)
5½	+15	quiet period	Heppner *et al.* (1963)
—	800	disturbance	Dolginov *et al.* (1960)
—	140	disturbance	Dolginov & Pushkov (1962)
7	10	H.M. (100–500 s)	Judge & Coleman (1962)
10	100	H.M. (0·3 c.p.s.)	Sonett *et al.* (1960); Coleman *et al.* (1960)

It is not clear what anomalies should be taken as typical during disturbed periods in the region of interest ($L \sim 4$ Earth radii or $h \sim 15$ kc/s). However, to demonstrate the effect a number of hypothetical anomalies of 54 gamma ($\Delta h = 1{\cdot}5$ kc/s) were assumed. These models are shown in Figure 3 together with the resulting distorted hooks calculated from the integrals for electron travel times and wave group propagation times given previously (Dowden 1962). Field lines were chosen so that the minimum gyro frequency $h_0 = 15$ kc/s. The first model is a purely dipole field. In the remaining models the undisturbed dipole field is shown by the broken curve. Two hooks have been computed for each model corresponding to $\cos \psi_0 = 0{\cdot}5$ and $0{\cdot}4$ respectively. Both are produced by electrons of 150 keV moving in a medium of scale frequency 500 kc/s along a field line terminating at about 59° geomagnetic latitude.

In each case the total fields (dipole plus anomalies) are taken as symmetrical about the geomagnetic equatorial plane. This is not particularly likely (especially for cases 4, 5, and 6) but was chosen to show the different effects of the anomalies on the predominantly falling and rising parts of the hooks respectively. A more realistic approach would be to consider different models for opposite hemispheres. Since very little of the distortion arises from propagation effects (as discussed later), the resultant hooks from a combination of any two field models shown here can be

synthesized by connecting (at the point of minimum emitted frequency f_0) the falling part of one hook with the rising part of another. It should also be remembered that, in the majority of cases, some or all of the falling branch will be missing, as discussed previously (Dowden 1962). Thus the observed events shown in Figure 2 appear to correspond to those shown for model 5 of Figure 3.

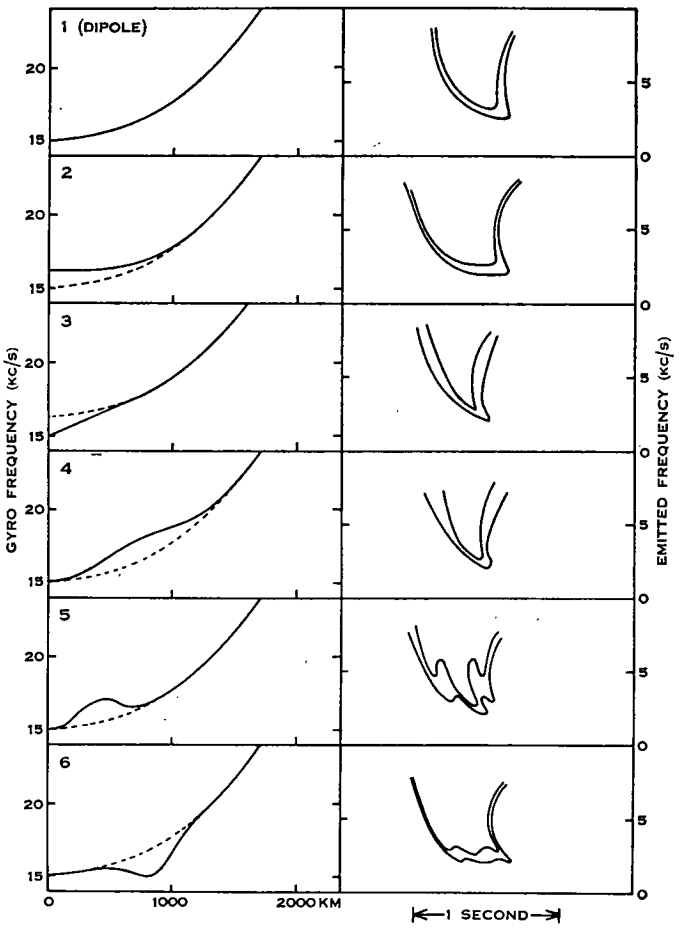

Fig. 3.—Hooks calculated for electron bunches of energy 150 keV, pitch cosines of 0·4 (inner) and 0·5 (outer) respectively, moving in a medium of $a = 500$ kc/s along the field line $\lambda = 59°$. The magnetic field models are shown on the left as gyro frequency versus distance along the field line measured from the equatorial plane.

An electron bunch emitting Doppler-shifted cyclotron radiation acts as a naturally occurring magnetometer in orbit in the exosphere. As in the case of a man-made orbiting magnetometer, unambiguous magnetic data can be deduced if the orbit parameters (energy, pitch, field line) are known. It may be possible to deduce both these and the magnetic anomalies from a single distorted hook. However, qualitative measurements are possible even without knowing these

parameters. In Figure 3 we see that the distortions of the hooks relative to the undistorted or "dipole" hook are roughly similar to the distortions of the anomalous fields relative to the pure dipole field. Thus, for any emission which is recognizable as a distorted form of a standard or dipole hook, we can get some idea of the shape and the sign of the anomaly.

It has been shown above (see Figs. 1 and 3) that the frequency-time shape of some V.L.F. emissions is remarkably sensitive to small field anomalies: changes of a few percent over a few hundred kilometers would be detectable. Whistlers, on the other hand, are quite insensitive to anomalies along the propagation path. Indeed, in an investigation into the effects of much larger anomalies on whistlers, Spreiter and Briggs (1962) found that, although there might be an appreciable change in the nose frequency and nose time delay, there is very little change in shape; i.e. the frequency-time plot of a nose whistler produced in a highly anomalous field could be closely fitted to one produced in a dipole field by suitably changing the field line latitude and the scale frequency or electron density.

I am indebted to Professor G. R. A. Ellis, Physics Department, University of Tasmania, for many criticisms, suggestions, and discussions.

References

COLEMAN, P. J., SONETT, C. P., JUDGE, D. L., and SMITH, E. J. (1960).—*J. Geophys. Res.* **65**: 1856–7.

DOLGINOV, S. SH., EROSHENKO, E. G., ZHUZGOV, L. N., PUSHKOV, N. V., and TYORMINA, L. O. (1960).—*Artificial Earth Satellites* **5**: 490.

DOLGINOV, S. SH., and PUSHKOV, N. V. (1962).—Proc. Intern. Space Sci. Symp. 3, Washington.

DOWDEN, R. L. (1962).—*J. Geophys. Res.*, **67**: 1745–50.

EIDMAN, V. IA. (1958).—*J. Exp. Theor. Phys.* (*U.S.S.R.*) **34**: 131–8.

HELLIWELL, R. A., and CARPENTER, D. L. (1961).—Whistlers—West IGY–IGC synoptic program, *SEL Final Rept.*, Stanford University, March 20, 1961.

HEPPNER, J. P., NESS, N. F., SCEARCE, C. S., and SKILLMAN, T. L. (1963).—*J. Geophys. Res.* **68**: 1–46.

JONES, D. L., GALLET, R. M., WATTS, J. M., and FRAZER, D. N. (1963).—N.B.S. Tech. Note 166, Boulder.

JUDGE, D. L., and COLEMAN, P. J. (1962).—*J. Geophys. Res.* **67**: 5071–89.

SMITH, E. J., COLEMAN, P. J., JUDGE, D. L., and SONETT, C. P. (1960).—*J. Geophys. Res.* **65**: 1858–61.

SONETT, C. P., JUDGE, D. L., SIMS, A. R., and KELSO, J. M. (1960).—*J. Geophys. Res.* **65**: 55–68.

SPREITER, J. R., and BRIGGS, B. R. (1962).—*J. Geophys. Res.* **67**: 3779–90.

Minimum-Reading Phase-Sensitive Detector*

Many of the powerful techniques of radio astronomy make use of a device which measures only the *difference* signal between two inputs or situations. Well-known examples:[1] the Dicke system for suppression of receiver fluctuations, the phase-switched interferometer for suppression of galactic background and the pencil-beam Mill's Cross. The effect is produced by rapidly switching between the two inputs or situations and recording the difference signal with a phase-sensitive detector (PSD).

A very different technique, the minimum reader, has been used in LF radio astronomy and in exospheric VLF noise studies for the suppression of atmospherics and other impulsive interference.[2] This is a partially unidirectional integrator having a long time constant for signal increases and a very short one for signal decreases. Thus only the slowly varying signal component *between* impulses is recorded. If the receiver (local oscillator) frequency is rapidly swept over a short range (a few times the receiver bandwidth), communication transmissions become impulsive interference so these are also suppressed.[3,4]

In LF radio astronomy both techniques may be required: a switched system with a minimum-reading PSD. In a simple Dicke system one input is connected to a dummy antenna or a calibration noise source. Impulses can only occur in the other (signal) input so that at the output of the PSD these will always appear with the same polarity. These can then be suppressed with a minimum reader as is done in the riometer.[3] However, in other systems in which the impulses can appear in *either* input (interferometer, Mill's Cross), this is no longer true. A method of overcoming this is discussed below.

Fig. 1 shows a complete system, input-switching and minimum-reading PSD, using only two twin triodes and six solid-state diodes. As well as alternately switching the receiver to the RF inputs through diodes D_1 the multivibrator T_1 alternately applies a positive potential to the "earth" end of the detector loads R_1. The potential at point A is then alternately the detected signal from input 1 (top half of T_1 cutoff) and the always higher potential of the multivibrator cathode. The minimum reader, comprising the unidirectional Miller integrator D_2, C_2 and T_2, sees only the least of these, the detected signal from input 1. Thus the outputs 1 and 2 are the respective detected minimums of the inputs 1 and 2. The difference signal appears *across* outputs 1 and 2. Impulses appearing in either or both of the inputs are suppressed. The output impedance is of the order of 1000 ohms so that a recording milliammeter can be connected directly across the output terminals. Terminal 3 is a fixed backing-off voltage. Three recorders connected respectively between 1 and 3, 2 and 3, 1 and 2, will allow separate recording of signal 1 only, signal 2 only and the difference signal only.

With the circuit values as shown, the multivibrator frequency is about 12 cps.; the detector time-constant (R_1C_1) is about 1 msec; and the upward time-constant of the minimum reader is about 15 sec. This latter is adjusted through the capacitors C_2. The output zero can be adjusted with the potentiometer shown and the gain equalized by adjusting the plate loads R_2. This system is being used for polarization measurements at 10.1 Mc with a local oscillator sweep of 12 kc, a sweep rate of about 20 per sec, and a receiver bandwidth (rectangular) of about 4 kc. However, this system could also be used as a phase-switching interferometer or a Mill's Cross.

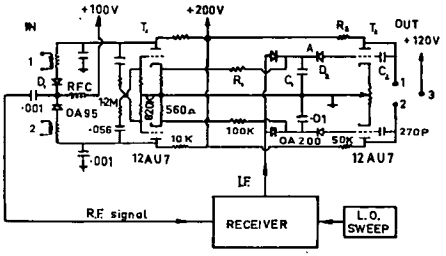

Fig. 1—Minimum-reading phase-sensitive detector. This circuit is symmetrical so that components are labeled in one half only.

R. L. DOWDEN
Ionospheric Prediction Service
University of Tasmania
Hobart, Tasmania, Australia

* Received June 18, 1962.

[1] J. L. Pawsey and R. N. Bracewell, "Radio Astronomy," The Clarendon Press, Oxford, England; 1955.

[2] G. Reber and G. R. Ellis, "Cosmic radio-frequency radiation near one megacycle," *J. Geophys. Res.*, vol. 61, pp. 1–10; March, 1959.

[3] C. G. Little and H. Leinbach, "The riometer—a device for the continuous measurement of ionospheric absorption," PROC. IRE, vol. 47, pp. 315–320; February, 1959.

[4] R. H. Lee, "Solar-flare detection for I.G.Y.," *Electronics*, vol. 30, pp. 162–165; March, 1957.

Reprinted from the PROCEEDINGS OF THE IEEE
VOL. 51, NO. 1, JANUARY, 1963

PRINTED IN THE U.S.A.

POLARIZATION MEASUREMENTS OF JUPITER RADIO BURSTS AT 10·1 Mc/s

By R. L. DOWDEN*

[*Manuscript received May* 1, 1963]

Summary

At 10·1 Mc/s Jupiter bursts of both senses of circular polarization are readily observed. The algebraic mean axial ratio is a strong function of Jovian longitude. This is almost entirely due to variation with longitude of the relative proportion of bursts of opposite sense of polarization. If bursts of the two senses (L.H. and R.H.) are analysed separately the two mean axial ratios show little or no variation with longitude and are equal and opposite in sign. The axial ratio distribution and other observations are compared with the predictions of the Doppler-shifted cyclotron theory.

I. INTRODUCTION

Decametre radio bursts from Jupiter are elliptically polarized, usually in the right-handed (R.H.) sense. Observations by Bollhagen (Carr, personal communication) show that at 22 Mc/s, 99·4% of bursts are R.H. and 0·6% L.H., while at 16 Mc/s, 67% are R.H. and 33% L.H. No systematic variation of these ratios with longitude has been reported though "there are slight but apparently significant differences in the average polarizations" of bursts from the three main longitudes of emission (Carr *et al.* 1961). In contrast the measurements at 10·1 Mc/s described here show that, while the average for all longitudes is about 63% R.H. and 37% L.H., this ratio is strongly dependent on longitude,† varying from 95% R.H. at 270° to 17% R.H. at 85°.

II. INSTRUMENTATION

Jupiter bursts were received on a horizontal array of twenty pairs of crossed half-wave dipoles arranged in a 10×2 configuration with the long axis in the north-south direction. The half-power cone of the antenna beam cuts the celestial sphere in a banana-shaped curve which enclosed Jupiter for some two or three hours either side of transit throughout the period of observation. For symmetry (and minimum number of support poles) the two sets of dipoles were positioned in the NE.–SW. and NW.–SE. directions respectively, that is, both at 45° to the long axis of the antenna.

The transmission lines from the two orthogonal linear polarizations were interconnected by a quarter-wave line and matched to identical preamplifiers. The outputs of these, which were the amplified L.H. and R.H. components respectively, were sampled

* Ionospheric Prediction Service and the University of Tasmania; present address: Physics Department, University of Tasmania, Hobart.

† The longitude system used in this paper is the original System III of period 9h 55m 28·8s (Carr *et al.* 1958). To convert to the I.A.U. revised System III of period 9h 55m 29·37s (Carr *et al.* 1961), subtract 30° from the longitudes quoted in the text and the longitude scales of Figures 5, 6, and 7.

by a commercial communications receiver through a diode switch as shown in Figure 1. C.W. (e.g. communication and broadcast transmissions) interference was completely suppressed by using a "rectangular" i.f. band-pass filter of 4 kc/s bandwidth and by rapidly sweeping the second local oscillator through a range of about 12 kc/s. This

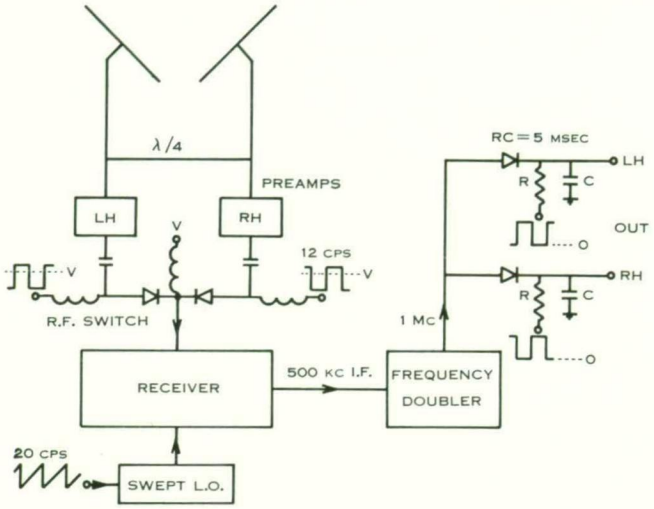

Fig. 1.—Block diagram of polarimeter.

converted c.w. interference to impulsive interference which could be suppressed, as explained later. Power linear detected outputs were obtained by doubling the intermediate frequency and using linear detectors. Voltage or field-strength linear outputs were also obtained by linear detection of the intermediate frequency before doubling

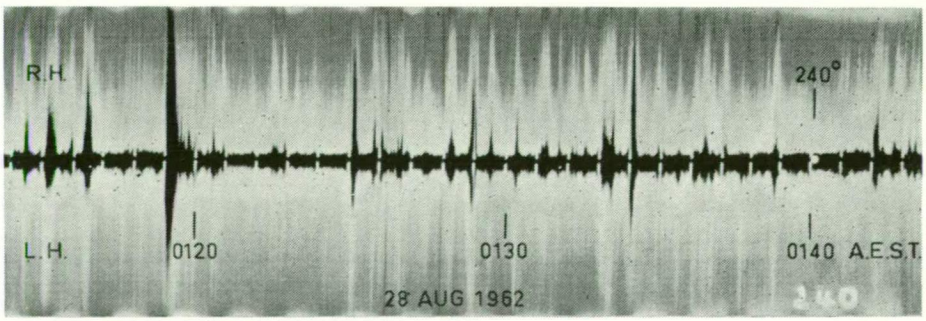

Fig. 2.—Typical C.R.O. record of 10·1 Mc/s Jupiter bursts.

(not shown). At each output the unwanted component of circular polarization was suppressed by applying a positive pulse to the "earthy" end of the detector load during the time the receiver sampled the unwanted component, as shown in Figure 1.

The wanted circular polarization component of Jupiter and Galactic radiation is separated from unwanted c.w. interference, wide-band impulsive interference (such as

atmospherics), and the unwanted polarization component by using a system which records only the least signal occurring in a period of a few tens of milliseconds. The record shown in Figure 2 was obtained by connecting the L.H. and R.H. outputs to the deflection plates of a twin-beam cathode-ray oscilloscope. It is seen that all unwanted signals have been converted to unresolved pulses (filled-in white areas). Jupiter bursts appear as resolved (black) pulses and the Galactic component appears as a small steady level just above the zero level indicated by the one-minute time and zero marks. Pen recorders were also used by employing minimum reading circuits. This

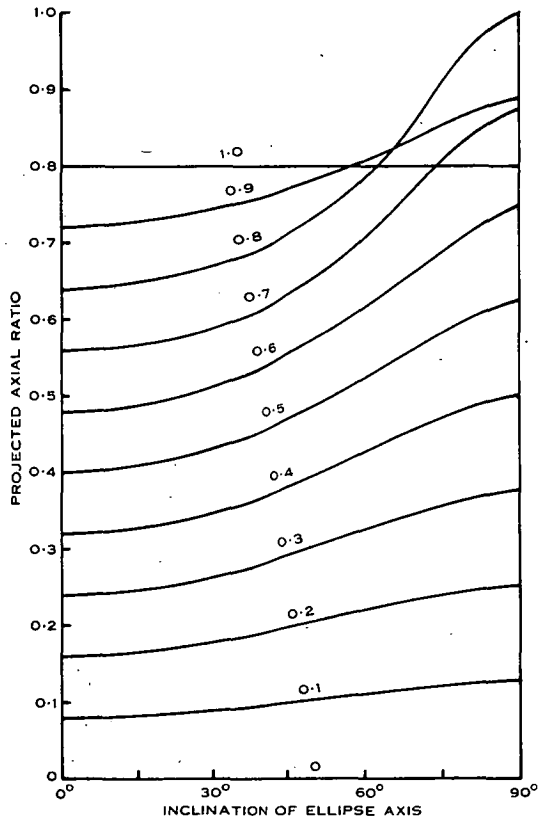

Fig. 3.—Apparent or projected axial ratio as a function of the inclination of the ellipse minor axis for various actual ratios and for an angle of incidence of 37°.

system is discussed in more detail elsewhere (Dowden 1963). A total of eight pen-recorder channels and six C.R.O. channels recording L.H., R.H., and L.H. minus R.H. components, using both power linear and voltage linear recording and different paper and film speeds were operated simultaneously. However, the two power linear C.R.O. channels recorded on 35-mm film moving at 6 in. per hour produced the best records, and only these are discussed here.

III. Axial Ratio Measurement

If Jupiter bursts are completely elliptically polarized and if the peak powers of the two components of a single burst are obtained, the apparent axial ratio is given by $\gamma = (r^{\frac{1}{2}}-1)/(r^{\frac{1}{2}}+1)$, where r = Peak power of L.H. component/Peak power of R.H. component.

However, with a horizontal antenna system as described above, the axial ratio measured is that of the horizontal components of the electromagnetic field, and thus that of the polarization ellipse projected onto the horizontal plane. The apparent or projected axial ratio γ is related to the true axial ratio Γ by the expression:

$$\gamma = [(P+Q-R)/(P+Q+R)]^{\frac{1}{2}},$$

where
$P = \sin^2\theta\,(1+\Gamma^2\cot^2\theta)$,
$Q = \sec^2 i\,\cos^2\theta\,(1+\Gamma^2\tan^2\theta)$,
$R = (P-Q)^2+4H^2$,
$H = \sec i\,(1-\Gamma^2)\sin\theta\,\cos\theta$,
θ = angle between the major axis of the ellipse and the horizontal plane (or inclination of the minor axis),
i = angle of incidence of Jupiter radiation.

Figure 3 shows this relation for an angle of incidence of 37° which was typical for the observations reported here. Faraday rotation along the path will cause the inclination of the ellipse (θ) at the antenna to differ from that at the point of emission on Jupiter by some hundreds of radians. A small change in the total electron content along the path will produce a large change in θ so that in general θ will be changing continuously. If θ changes slowly in time so that it is essentially constant during a burst, then a large number of bursts of a given axial ratio will be observed as a distribution of projected axial ratios which can be calculated from the appropriate curve in Figure 3 by assuming that all values of θ are equally probable. Slight complications arise if θ varies during a burst, but this is automatically overcome, as we will see later.

Faraday rotation is also frequency dependent. If the differential rotation over the bandwidth of the receiver is greater than 180° all values of γ for a given Γ will be averaged. The mean projected axial ratios ($\bar{\gamma}$) as a function of incidence angle (i) for several values of true axial ratio (Γ) are shown in Figure 4.

An expression for the Faraday rotation fading rate is given by Aitchison and Weekes (1959). If longitudinal propagation is assumed and a typical effective value of total electron content (I) of about 30×10^{12} cm^{-2} is substituted, this becomes

$$2\frac{\partial\theta}{\partial t} = 4\times10^4(If^2)^{-1}\frac{\partial}{\partial t}(I\sec i),$$

where θ is measured in revolutions and the frequency (f) in megacycles per second. Substituting f = 10 Mc/s, the average fading rate caused by the variation of incidence angle (i) over the 5-hr observing periods centred on transit would produce a fading rate of about one per minute. A 30% change in I (at constant i) spread over the same period would produce a similar rate. This fading period is much longer than typical

Jupiter bursts. An expression for the rate of change of rotation with frequency can be similarly derived:

$$\partial\theta/\partial t = -8\times10^4 f^{-3}\sec i \qquad \text{rev/(Mc/s)}.$$

For $f = 10$ Mc/s and $\sec i = 1\cdot25$ we find that θ will change by 180° over a bandwidth of 5 kc/s.

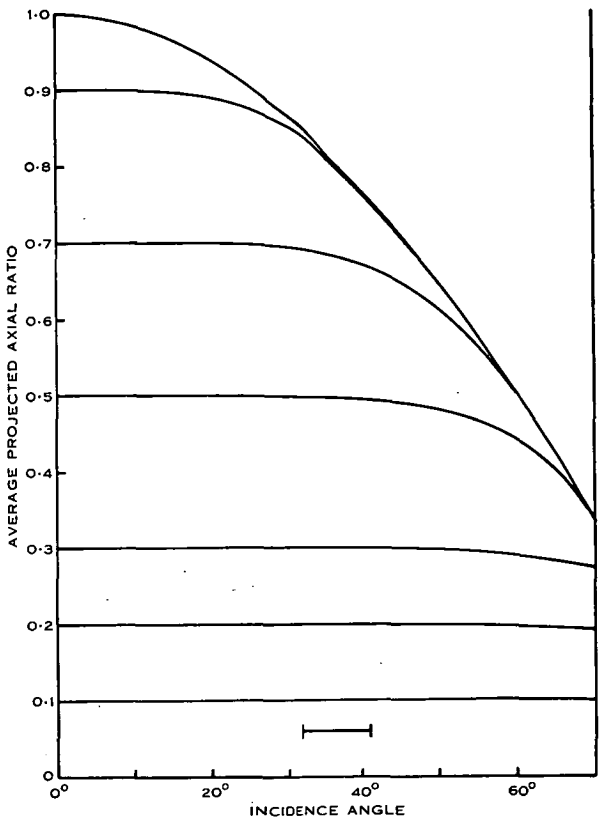

Fig. 4.—Projected axial ratio averaged over all ellipse inclinations as a function of the angle of incidence for various actual axial ratios.

Since the receiver bandwidth was about 4 kc/s, the projected axial ratios will be averaged by the receiver, giving the corrections indicated in Figure 4. Over the range of incidence angles which apply to these observations (as indicated by the limit bar in Fig. 4), and for $\Gamma<0\cdot7$ we find $\bar{\gamma}\approx\Gamma$ to within the limit of the scaling errors. This also applies if the amount of Faraday rotation has been underestimated. If it has been overestimated values of γ will not be completely averaged by the receiver. This will produce a broadening effect, since each value of Γ produces a range of γ. However, for the distribution as shown in Figure 11 the total corrections would be less than the statistical errors.

Apart from projection effects, the observed axial ratio will be smaller than those emitted on Jupiter if some bursts of opposite polarization are superimposed on the record. In this way apparent ratios near zero could be produced by coincident and oppositely polarized bursts of relatively high axial ratio.

A similar and potentially more serious effect may be irrelevant. Roberts (1963) has pointed out that polarizations deduced from measurement of only the two circular components could be interpreted in two ways: pure elliptical polarization or a mixture

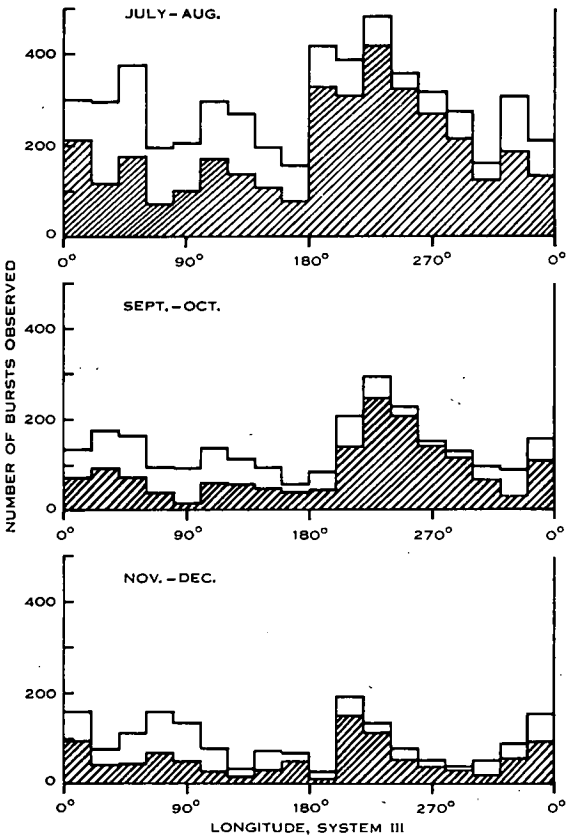

Fig. 5.—Histograms of Jupiter bursts for three observing periods. The shaded portions correspond to bursts polarized in the right-handed sense.

of pure circular plus random polarization. He pointed out that this could be resolved by measuring the random component as well. However, this is difficult at decametre wavelengths because the Faraday rotation is large and is both frequency and time dependent. Thus, at 10 Mc/s, for the Faraday rotation estimated above, the orientations of ellipses would be completely randomized over a bandwidth of about 5 kc/s or a time constant of about 1 min. Thus physically realizable polarimeters would tend to see only circular plus random polarization when pure elliptical polarization was

incident. In view of this, one or other interpretation must be chosen on other grounds. The former (pure elliptical) is chosen here.

An alternate method of studying polarization variations is to count the relative proportions of L.H. and R.H. bursts. This method does not suffer from any of the effects mentioned above, since none of them can reverse the sense of polarization. It has the additional advantage of involving only simple counting instead of two measurements and a calculation for each burst. Much of the following discussion is based on this method. The effect of imbalance between the L.H. and R.H. channels, which can occur both in the equipment and in the Earth's ionosphere, leading to a zero shift in axial ratio, will be discussed later.

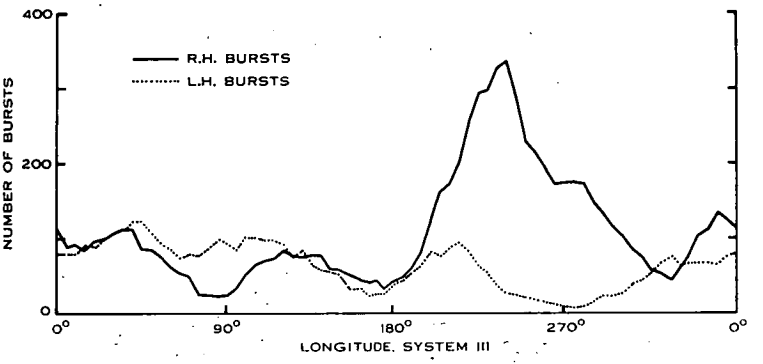

Fig. 6.—Smoothed occurrence rate of right-handed and left-handed bursts in September-October.

IV. Observations

Polarimeter records of Jupiter bursts were obtained from July to December 1962. This period was divided into three periods of from July 4 to August 28, August 28 to October 8, and November 21 to December 22. Histograms of burst occurrence in 20° intervals of longitude are shown for the three periods in Figure 5. The number of R.H. bursts is indicated by the shaded areas while that for L.H. bursts is superimposed as white areas. The histograms for the three periods are similar, bearing in mind the statistical error and the different lengths of the observing periods. Thus the bursts occurring in the September–October period, which were scaled in greater detail, should be reasonably typical. For this period the L.H. and R.H. power components of circular polarization were measured, and the (apparent) axial ratio calculated, for each burst. Intervals of five degrees of longitude were used, but to reduce statistical fluctuations centred running means over 25° were calculated.

Figure 6 shows the occurrence rate of L.H. and R.H. bursts for the September–October period. The occurrence rate of R.H. bursts shows a pronounced variation with longitude with peak occurrence at 240°. Nearly half (48%) of all R.H. bursts occurred within 40° of this peak. The occurrence rate of L.H. bursts shows less variation and a number of subsidiary peaks, the largest occurring at about 40°.

The sum of the peak powers of all bursts occurring within 25° ranges of longitude are plotted (dots) at 5° intervals in Figure 7. The L.H. and R.H. components have been added. The burst occurrence rate is plotted in a similar way (crosses) on the same graph. In general the two curves follow the same trends though the "total power" seems to be more sensitive to longitude than burst occurrence rate and has a greater maximum to minimum ratio.

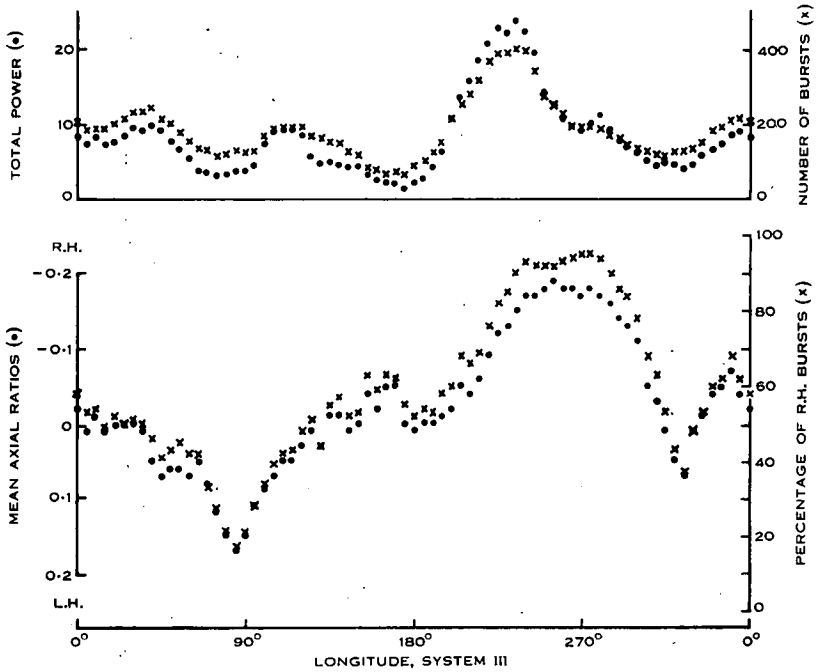

Fig. 7.—Smoothed longitude variation of total power and mean axial ratio (dots), and of the burst occurrence rate and the proportion of bursts which were polarized in the right-handed sense (crosses).

Also shown in Figure 7 are the mean algebraic (positive and negative) axial ratios (dots) of bursts occurring within 25° ranges of longitude and the percentage of these bursts which were polarized in the R.H. sense (crosses). Both show a pronounced and very similar variation with longitude. We would expect some relation between the two for the following reason. The mean algebraic axial ratio is defined as

$$\bar{\Gamma} = \frac{\Sigma \Gamma}{N},$$

where N is the number of bursts observed. If the bursts are separated into L.H. and R.H., we have:

$$\bar{\Gamma} = \frac{\Sigma \Gamma_{\mathrm{L}} + \Sigma \Gamma_{\mathrm{R}}}{N_{\mathrm{L}} + N_{\mathrm{R}}}$$

$$= \frac{N_{\mathrm{L}} \bar{\Gamma}_{\mathrm{L}} + N_{\mathrm{R}} \bar{\Gamma}_{\mathrm{R}}}{N_{\mathrm{L}} + N_{\mathrm{R}}}.$$

Variation of $\bar{\Gamma}$ can be produced by variation of either (or both) N_L/N_R or $\bar{\Gamma}_L/\bar{\Gamma}_R$. It is quite clear from Figures 6 and 7 that N_L/N_R is not constant, so we will consider $\bar{\Gamma}_L = -\bar{\Gamma}_R = \bar{\Gamma}_A$. Then

$$\bar{\Gamma} = \frac{N_L - N_R}{N_L + N_R} \cdot \bar{\Gamma}_A = \left(1 - 2\frac{N_R}{N}\right) \cdot \bar{\Gamma}_A.$$

Thus, if the distribution of absolute values (signs disregarded) of axial ratio is not

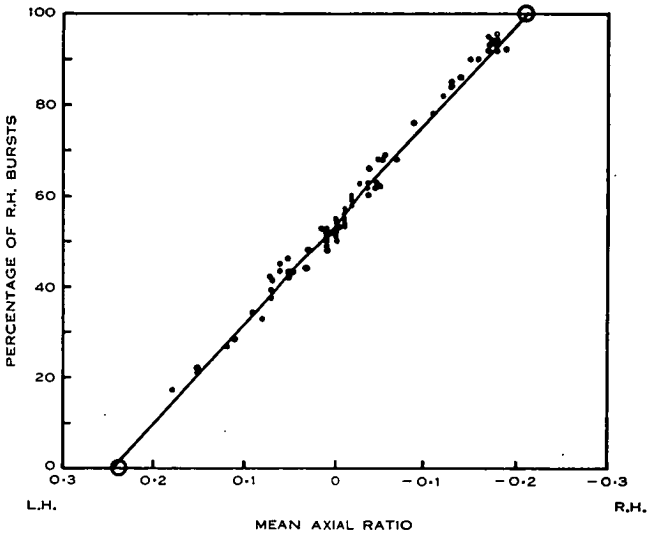

Fig. 8.—Correlation of the mean axial ratios and the percentage of right-handed bursts. The circles at 0% and 100% are the mean axial ratios of left-handed and right-handed bursts respectively.

TABLE 1

MEAN AXIAL RATIOS OF L.H. AND R.H. BURSTS

Longitude	Left Hand			Right Hand		
	$\Sigma\Gamma$	N	$\bar{\Gamma}$	$-\Sigma\Gamma$	N	$-\bar{\Gamma}$
0°– 60°	63·25	237	0·27	51·20	230	0·20
60°–120°	51·00	210	0·24	20·45	110	0·185
120°–180°	27·95	120	0·23	29·25	141	0·21
180°–240°	31·15	157	0·20	81·15	423	0·19
240°–300°	8·70	41	0·21	104·15	459	0·225
300°–360°	34·55	148	0·235	40·90	193	0·21
0°–360°	216·60	913	0·237	327·10	1556	0·210

dependent on longitude, the algebraic mean axial ratio will be a linear function of the percentage of R.H. bursts (N_R/N).

The correlation of these two quantities is shown in Figure 8. A linear relationship is a good fit. Mean axial ratios of L.H. and R.H. bursts considered separately and for six longitude intervals of 60° are shown in Table 1.

It is seen that there is little or no systematic variation of average axial ratio with longitude for bursts of either sense of polarization. The cyclotron theory (Ellis and McCulloch 1963) predicts a slight tendency for $\bar{\Gamma}$ to follow N according as

$$\Sigma \Gamma \propto N^{1\cdot05}.$$

The relation is tested in Figure 9 by plotting the information given in Table 1. The

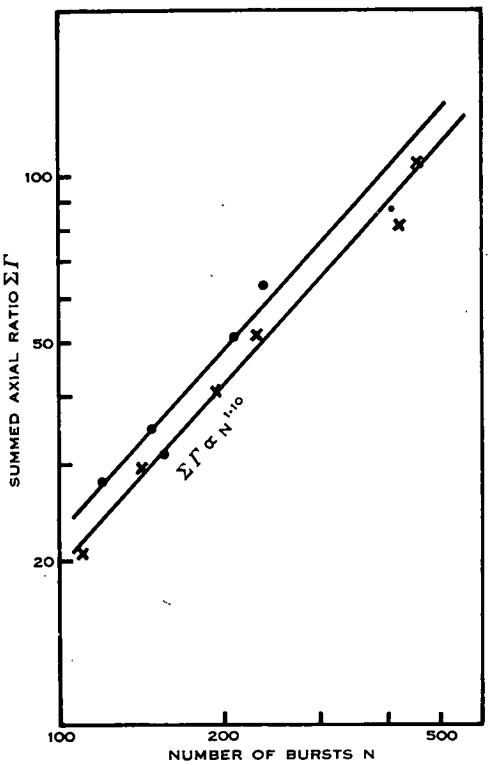

Fig. 9.—Correlation of summed axial ratio and occurrence rate of bursts. Left and right-handed bursts are plotted as dots and crosses respectively. For the small dot both scales should be reduced by a factor of ten.

exponent for best fit appears to be 1·10, which is probably not significantly different from that predicted. A similar prediction of the cyclotron theory is that the total power (Σ P) be related to the number of bursts by the relation

$$\Sigma P \propto N^{1\cdot3}.$$

The exponent for best fit of the data in Figure 7 is seen in Figure 10 to be 1·51. The

difference, if significant, could be due to the increased probability of coincidence of bursts when the occurrence rate is large.

It will be noted from Figure 1 that not all the amplification of the signals from Jupiter was common to both polarization components. Gain balance was measured by automatic hourly noise generator calibrations, though no special precautions were taken to maintain exact balance. Since the relation between measured axial ratio

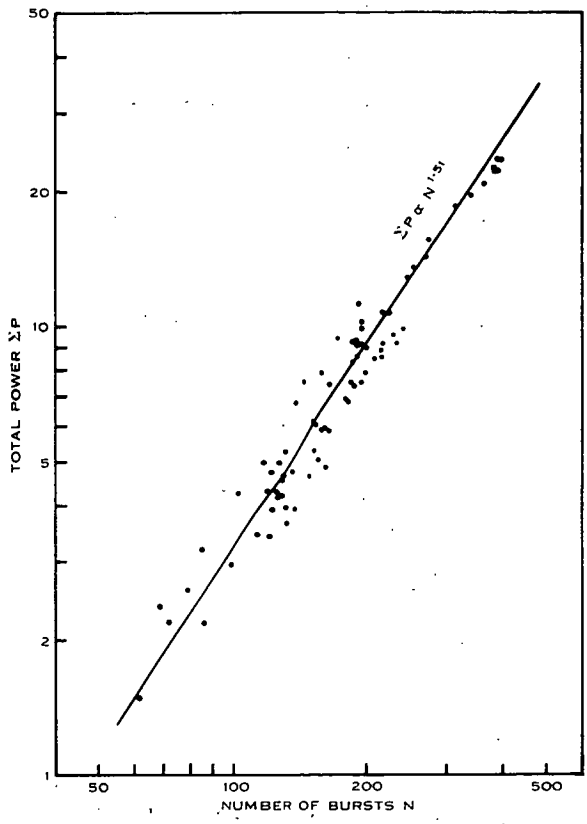

Fig. 10.—Correlation of the total power and the occurrence rate of bursts.

and power ratio (r) is quite closely logarithmic for values of r between 0·1 and 10, a small amount of imbalance would affect nearly all values of measured axial ratio by an algebraically additive constant. That is, it would shift the zero of the axial ratio scale. The zero chosen was deduced from the noise calibrations. For this zero the Galactic noise has an apparent axial ratio of about 0·043. This suggests a small amount of differential absorption in the Earth's ionosphere, assuming that Galactic noise is completely randomly polarized. The absorption is not necessarily the same for Jupiter radiation, since the brightest parts of the Galaxy were lower in the sky than Jupiter during these observations.

It is interesting to note that if a correction of 0·025 is used we find that, averaged over all longitudes, $\bar{\Gamma}_L = -\bar{\Gamma}_R = 0{\cdot}212$. Also the regression line in Figure 8 now passes through the point $\bar{\Gamma} = 0$, $N_R/N = 50\%$, and the two regression lines in Figure 9 (for L.H. and R.H. bursts respectively) coincide. This zero correction has been applied in the histogram of absolute values of axial ratio shown in Figure 11. The absolute axial ratio distribution does not appear to be a function of longitude, so this histogram was compiled from values from all longitudes. The projection correction has not been applied, as it would have very little effect. The observed distribution is similar in shape to that predicted by Ellis and McCulloch, if it is assumed that apparent axial ratios below about 0·2 are produced by superimposition of bursts of higher axial ratio but of opposite sense of polarization. The position of the predicted distribution on the axial ratio scale depends on the model used rather than on the theory.

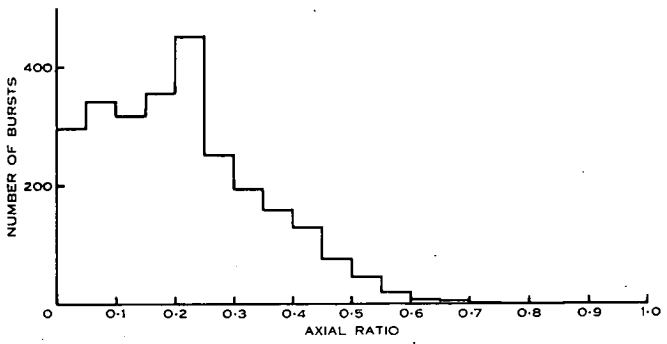

Fig. 11.—Histogram of absolute values (both left and right taken positively) of axial ratio. The zero correction has been applied but the shape of the distribution makes the projection correction unnecessary.

V. Discussion

On the cyclotron theory (Ellis and McCulloch 1963) the configuration of the Jupiter magnetic field in longitude can be deduced from observations of the longitudinal variation of burst occurrence, preferably at a number of frequencies. Much additional information is provided by polarization measurements. Thus, by considering the L.H. and R.H. burst occurrence rates separately, as in Figure 6, both the regular or dipole component and the anomalous components can be resolved into hemispheres. It is felt that the polarization data obtained so far are not sufficient for a detailed analysis of field configuration. Intercomparison of the three histograms in Figure 5 shows that much of the fine structure of the occurrence rates is statistical error. However, some conclusions can be drawn from the broad features which persist through these three histograms.

The main features of the occurrence rates in Figure 6 are a large and fairly narrow peak for R.H. bursts at about 240° and a smaller and broader peak for L.H. bursts at about 40°. The L.H. peak is somewhat larger and more prominent in the July–August histogram of Figure 5. If the occurrence rates are not masked by anomalous

peaks, this would give the positions of the north-seeking and the south-seeking poles respectively. Decimetre observations by Morris and Berge (1962) show that the longitudes of the poles are $230 \pm 10°$ for the pole in the northern hemisphere and $50 \pm 10°$ for that in the southern hemisphere, after conversion to the longitude system used here. Observations by Roberts and Komesaroff (Bolton 1963) show these poles at 215° and 35° respectively. Both of these are in reasonable agreement with the positions deduced from Figure 6, and further indicate that the sense of the magnetic field of Jupiter is opposite that of the Earth, for the north-seeking magnetic pole is located in the northern hemisphere.

The fact that the R.H. or northern hemisphere peak is two to three times the L.H. or southern hemisphere peak may be significant. The large R.H. peak could be a combination of a "polar" peak at about 220° and an anomalous peak at about 260°. The data considered by Ellis and McCulloch support this interpretation. On the other hand an asymmetry in the polar peaks (without localized anomalies) of about this amount would be produced if the magnetic dipole is displaced along its axis towards the northern hemisphere by an amount (0·05 times the planet's radius) similar to that of the Earth. This asymmetry would increase with frequency and produce different cut-off frequencies for the two polarizations. The observed cut-off frequencies are around 38 Mc/s (Barrow 1963) for R.H. radiation and around 22 Mc/s (Carr *et al.* 1961) for L.H. radiation.

Such displacements of the dipole are not inconsistent with the decimetre observations. In particular, it should be noted that the decimetre observations only locate the longitudes of the poles if the magnetic and rotation axes are coplanar. Thus, if the dipole is displaced about 0·05 radii in a direction perpendicular to both axes, the longitudes of the poles (using the Morris and Berge data) would be 214° and 34° (or 246° and 66°) and thus only 148° apart. More data are required for accurate location of the dipole position. Polarization measurements at a low frequency (such as 5 Mc/s), where contributions from dip anomalies are very small (Ellis and McCulloch 1963), may resolve this.

VI. Acknowledgments

The author is indebted to Professor G. R. A. Ellis for many helpful discussions and suggestions, to Mr. M. L. Urquhart for deriving the axial ratio projection expression, and to Mr. G. T. Goldstone for building and operating the polarimeter.

VII. References

Aitchison, G. J., and Weekes, K. (1959).—*J. Atmos. Terr. Phys.* **14**: 236–48.
Barrow, C. H. (1963).—*Nature* **197**: 580.
Bolton, J. G. (1963).— *Proc. Inst. Radio. Engrs. Aust.* **24**: 106–12.
Carr, T. D., Smith, A. G., Pepple, R., and Barrow, C. H. (1958).—*Astrophys. J.* **127**: 274.
Carr, T. D., Smith, A. G., Bollhagen, H., Six, N. F., Jr., and Chatterton, N. E. (1961).—*Astrophys. J.* **134**: 105–25.
Dowden, R. L. (1963).—*Proc. Inst. Radio. Engrs., N.Y.* **51**: 231.
Ellis, G. R. A. (1962).—*Aust. J. Phys.* **15**: 344–53.
Ellis, G. R. A., and McCulloch, P. M. (1963). *Aust. J. Phys.* **16**: 380–97.
Morris, D., and Berge, G. L. (1962). *Astrophys. J.* **136**: 276.
Roberts, J. A. (1963).—*Planet. Space. Sci.* **11**: 221–59.

(Reprinted from the Proceedings of the Astronomical Society of Australia, Vol. 1, No. 4, pp. 159, December, 1968)

A Jupiter Model of Pulsars

R. L. DOWDEN

Department of Physics, University of Otago, New Zealand

A precedent to the recently-discovered pulsed radio sources or 'pulsars' exists in our own solar system. Jupiter could be thought of as a very slow 'pulsar' having a period of about 10 h or 35 000 s. Like pulsars, this emission period is known to a high order of accuracy (about 1 in 10^6). One difference is that Jupiter emission is received over an appreciable part of this period ($\frac{1}{4}$ to $\frac{1}{2}$ or more) compared with about 1/30 of a typical pulsar period (about 40 ms in 1.3 s). Both pulsar and Jupiter bursts have a microstructure of the order of milliseconds, suggesting similar sizes of instantaneous emission regions. In both, the intensity observed varies from period to period. Emissions from both have relatively strong circular-polarization components at times.

There is good evidence, which I will not detail here, that the decametric radiation from Jupiter is Doppler shifted cyclotron radiation from electrons.[1] This idea came from a theory of VLF emissions in the Earth's magnetosphere,[2] so it is appropriate, particularly at this conference, to see if these 'solar system' ideas might work for pulsars also.

I suggest then, that a pulsar is a star rotating with the observed emissions period ($\sim$1 s), with a fairly strong dipole or radial magnetic field and that the magnetic axis is inclined to the rotation axis. Unlike Jupiter, there is no special reason to expect the rotation axis to be nearly normal to the line of sight to the Earth, so that in general we would expect to observe radiation from only one magnetic hemisphere, perhaps only during brief intervals when the angle between the magnetic axis and line of sight is relatively small ($\sim 10°$, say).

The purpose of this paper is to compare the received power from a pulsar with what we might expect if the radiation process (cyclotron) is similar to that for Jupiter. The model outlined above is generally less extreme than many suggested in recent papers in *Nature*. Some further details will be filled in below.

The peak power flux received from the pulsars is typically 10^{-24} Wm^{-2} Hz^{-1} compared with about 10^{-20} Wm^{-2} Hz^{-1} from Jupiter. On the other hand our distance from a pulsar is about 2×10^6 times that from Jupiter so the effective (excluding beaming) radiated power from a pulsar is about 4×10^8 times that from Jupiter. On the model outlined above we might take the rather small on-off ratio ($\sim 1/30$) of pulsar reception to indicate beaming (a 'lighthouse' theory). If this is effective over two dimensions we gain a factor of 100 or 1000 in comparing Jupiter with a pulsar. So we need now to justify a pulsar radiating at least 10^6 times the power of Jupiter.

The decametric radiation from Jupiter and the radiation from pulsars show broadly similar energy spectra. The upper cut-off frequency for Jupiter is about 30 MHz whereas that for pulsars is about 1000 MHz. If this is indicative of the highest magnetic fields in the regions of emission, the ratio of magnetic field in the corresponding regions in pulsars and on Jupiter is ~ 30.

The radiated power from similar volumes on Jupiter and pulsars may be proportional to a relatively high power of the magnetic field B. The radiated power per electron is proportional to B^2. For incoherent radiation the power per unit volume is proportional to the electron kinetic energy density which is itself limited to the magnetic energy density ($\propto B^2$). Hence, if the Jupiter and pulsar ratios of kinetic to magnetic energy densities are similar, we might expect the total radiated power ratio to be proportional to the fourth power of the ratio of B.

Taking the ratio of B as 30 we might expect a pulsar to radiate 10^6 times the power of Jupiter as required. This calculation, which might be out by a few orders of magnitude either way, may not stand detailed examination, but it at least provides a degree of plausibility to a Jupiter type model and indicates that a closer examination might be worthwhile.

[1] Ellis, G. R. A. and McCulloch, P. M., *Aust. J. Phys.*, **16**, 380 (1963).
[2] Dowden, R. L., *J. Geophys. Res.*, **67**, 1745 (1962).

Planet. Space Sci. 1965, Vol. 13, pp. 761 to 772 Pergamon Press Ltd. Printed in Northern Ireland

"MICROPULSATION MODE" PROPAGATION IN THE MAGNETOSPHERE

R. L. DOWDEN
Physics Department, University of Tasmania, Australia

(*Received* 8 *March* 1965)

Abstract—Propagation of extremely low frequency (~1 c/s) waves along field lines in the magnetosphere in the "micropulsation mode" is considered. Expressions for phase and group refractive index for any wave normal direction are derived. Although wave normal angles are likely to be large, longitudinal expressions can be used with reasonable accuracy in calculating travel times and dispersion. The medium produces strong guiding without field aligned columns. The maximum deviation of the ray path from a field line is shown to be small.

1. INTRODUCTION

Certain types of micropulsations give rise to a dynamic spectrum of rising tones of frequency of the order of 1 c/s and repetition rates of the order of one per minute. An example recorded at Hobart is shown in Fig. 1. In private communications to Jacobs and Watanabe,[1] Obayashi and Lokken independently suggested that the sequence of rising tones might be an expression of dispersion in the propagation of a hydromagnetic wave packet guided by a magnetic field line in a manner similar to the falling tones of atmospheric whistlers. Jacobs and Watanabe[1] showed that, of the two modes which can propagate in the magnetosphere at these frequencies, one (called here the "micropulsation mode") is strongly guided by the Earth's magnetic field, is propagated more slowly at higher frequencies, and has a cut-off near the ion gyro-frequency. By calculating travel times as a function of frequency of hydromagnetic wave packets echoing between the conjugate joints along the field line terminating at latitude 65° they obtained a dynamic spectrum. This showed good agreement with an observed dynamic spectrum. Particularly so when it is remembered that only the field line could be chosen to fit the data as the plasma density model is already determined by VLF whistler studies.

The essence of this idea is that "ray" features applicable when relevant dimensions are large compared with a wave length are more important than "wave" features applicable when the reverse is true. This is due to long path lengths and a refractive index of the order of a thousand.

This paper considers the propagation relations in greater detail to provide a basis for further work. Where appropriate, a ray approach has been used. Much use has been made of ideas developed for VLF whistlers as discussed by Smith.[2]

2. REFRACTIVE INDEX

Astrom[3] has shown that the refractive index n for propagation in a magneto-ionic medium with wave normal direction θ is given by the roots of the equation:

$$\tan^2\theta = -\left[\left(\frac{1}{n^2}-\frac{1}{\varepsilon_1}\right)\left(\frac{1}{n^2}-\frac{1}{\varepsilon_2}\right)\right]\Big/\left[\left(\frac{1}{n^2}-\frac{1}{\varepsilon_3}\right)\left(\frac{1}{n^2}-\frac{1}{\varepsilon_4}\right)\right] \qquad (1)$$

For a neutral medium of electrons and protons the dielectric coefficients become:

$$\varepsilon_1 = 1 + \frac{a}{Mg - f} + \frac{a}{g + f} \simeq \frac{a}{g + f} \qquad (f < g)$$

$$\varepsilon_2 = 1 + \frac{a}{Mg + f} + \frac{a}{g - f} \simeq \frac{a}{g - f} \qquad (f < g)$$

$$\varepsilon_3 = 1 - \frac{aMg}{f^2} - \frac{ag}{f^2} \simeq -\frac{aMg}{f^2} \qquad (f < g)$$

$$\varepsilon_4 = \frac{2\varepsilon_1\varepsilon_2}{\varepsilon_1 + \varepsilon_2} \simeq \frac{a}{g} \qquad (f < g)$$

where f is the wave frequency, g is the proton gyro-frequency, M is the proton–electron mass ratio ($M = 1838$) and a is the scale frequency[4] or ratio between the plasma frequency squared and the gyro frequency. Use has been made of the fact that the two gyro frequencies are opposite in sign and that for a neutral medium the two scale frequencies are equal and opposite in sign. The approximations apply in the region of interest (i.e. at frequencies less than the proton gyro frequency) to an accuracy of about one part in M. Consistent with this accuracy we can neglect $1/\varepsilon_3$ in comparison with $1/n^2$ so that (1) becomes (for $f < g$)

$$\tan^2\theta = -\left[\left(\frac{1}{n^2} - \frac{g+f}{a}\right)\left(\frac{1}{n^2} - \frac{g-f}{a}\right)\right] \Big/ \left[\frac{1}{n^2}\left(\frac{1}{n^2} - \frac{g}{a}\right)\right]$$

Giving:
$$\sec^2\theta . \frac{1}{n^4} - \frac{2g}{a}(1 + \tfrac{1}{2}\tan^2\theta) . \frac{1}{n^2} + \frac{g^2 - f^2}{a^2} = 0$$

and thus:
$$n^2 = \frac{a}{g}[1 - \tfrac{1}{2}\sin^2\theta \pm \sqrt{(\tfrac{1}{4}\sin^4\theta + \lambda^2\cos^2\theta)}]^{-1} \qquad (2)$$

where:
$$\lambda = \frac{f}{g}$$

A few special cases are of interest. For the positive sign before the radical:

$$n^2 = \frac{a}{g}\frac{1}{1+\lambda} \qquad \theta = 0$$

$$= \frac{a}{g} \qquad \theta = 90°$$

$$= \frac{a}{g} \qquad f = 0, \text{ all } \theta$$

At micropulsation frequencies this mode is quasi-isotropic in θ. The first solution corresponds to $n^2 = \varepsilon_2$ obtained directly from (1) by equating the r.h.s. to zero. If we use approximations for ε_2 appropriate to $f \gg g, f < Mg$ we get, for $\theta = 0$:

$$n^2 = 1 + \frac{aMg}{f(Mg - f)} = 1 + \frac{f_0^2}{f(f_H - f)}$$

in more familiar notation. This identifies this mode with the "whistler mode".

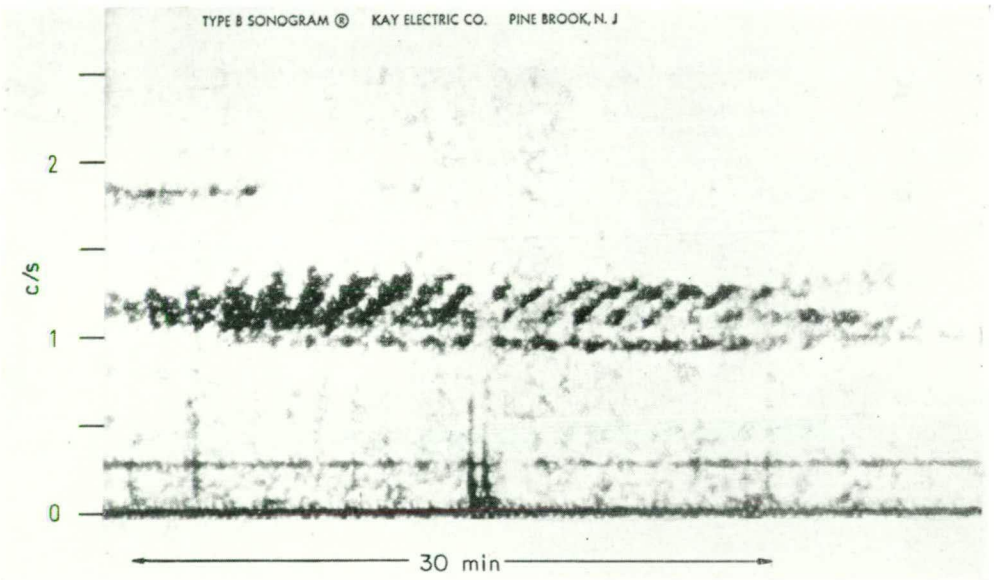

FIG. 1. DYNAMIC SPECTRUM OF A MICROPULSATION EVENT RECORD AT HOBART (1800 U.T. 10TH APRIL 1964).

For the negative sign, it is the component of refractive index in the direction of the magnetic field $n_{\|}$ which is quasi-isotropic

$$n_{\|}^2 = n^2 \cos^2\theta = \frac{a}{g}\frac{1}{1-\lambda} \qquad \theta = 0$$

$$= \frac{a}{g}\frac{1}{1-\lambda^2} \qquad \theta = 90°$$

$$= \frac{a}{g} \qquad f = 0, \text{ all } \theta$$

The mode corresponding to the positive sign is right-hand polarised which is the direction of rotation of the electrons. This mode is responsible for VLF whistlers. It is strongly anisotropic in θ for $f \gg g$ (VLF region) but in the region of interest ($f < g$) it is almost isotropic as shown above and by Jacobs and Watanabe.[1] Its behaviour is "ordinary" in the region of interest (Aström[3] referred to it as the ordinary mode) but "extra-ordinary" in the VLF whistler region. To avoid confusion it will be called the "whistler mode" in this paper.

The mode corresponding to the negative sign which has the interesting properties

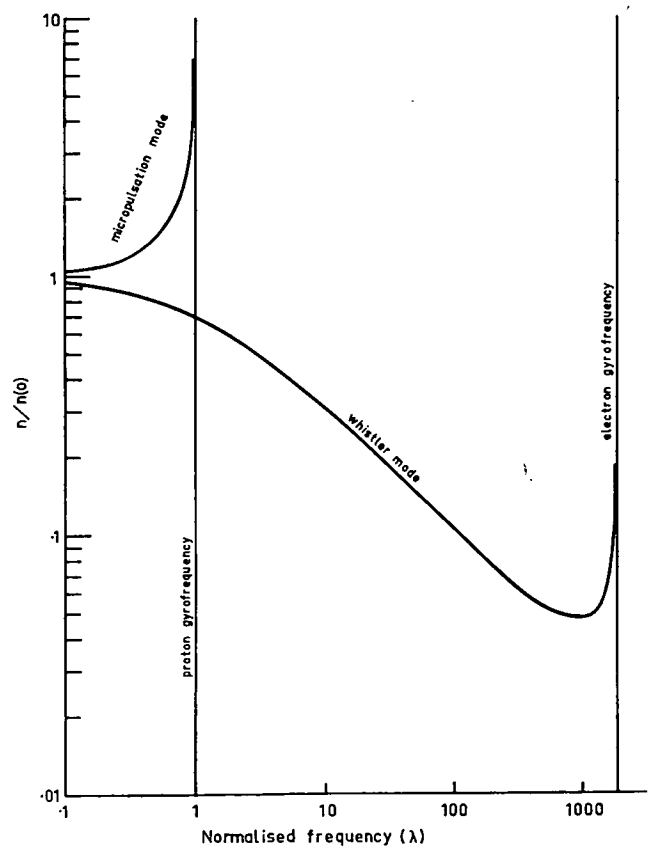

FIG. 2. NORMALISED REFRACTIVE INDEX AS A FUNCTION OF NORMALISED FREQUENCY (λ) FOR STRICT LONGITUDINAL PROPAGATION IN BOTH MODES.

discussed above and by Jacobs and Watanabe[1] will concern us here. The electric and magnetic vectors rotate in the direction of the protons (left-handed). It is thus the proton counterpart of the whistler mode. It will be referred to here as the "micropulsation mode".

The refractive index for longitudinal ($\theta = 0$) propagation in the two modes as a function of frequency is shown in Fig. 2. The refractive index has been normalised to its value at zero frequency $n(0)$ where

$$n(0) = \frac{a}{g} = \frac{c}{v}$$

where v is the Alfvén velocity. The frequency has been normalised to the proton gyrofrequency.

3. GUIDING

A polar diagram of normalised refractive index (radial) versus the angle θ for various values of λ is shown in Fig. 3. The ray direction (ϕ) is given by the normal to these curves as shown. It is seen that for all values of θ and λ the ray direction is close to the direction of the magnetic field, as pointed out by Jacobs and Watanabe.[1] The angle ϕ is given by:[2]

$$\tan(\phi - \theta) = -\frac{1}{n}\frac{dn}{d\theta}$$

By expansion of the L.H.S. and differentiation of (2) if can be shown:

$$\tan\phi = [\tfrac{1}{2}\tan\theta\,(\tfrac{1}{4}\sin^4\theta + \lambda^2\cos^2\theta)^{1/2} - \tfrac{1}{4}\sin^4\theta(\tan\theta + \cot\theta) - \tfrac{1}{2}\lambda^2\sin\theta\cos\theta]/[(\tfrac{1}{4}\sin^4\theta + \lambda^2\cos^2\theta)^{1/2} - \tfrac{1}{2}\lambda^2(1 + \cos^6\theta)] \quad (3)$$

Values of ϕ calculated from this expression (3) are shown plotted in Fig. 4 as a function of θ for selected values of λ. It seems likely from analogy with VLF whistlers that the highest frequencies propagated correspond to $\lambda = 0{\cdot}6$ or so. However even for a maximum of $\lambda = 0{\cdot}8$ we see that for all frequencies the angle between the ray and the magnetic field must be less than 11·4° everywhere along the path. A similar, though less pronounced, effect occurs for VLF whistlers which has been described as magneto-ionic ducting.[5]

In order to find the ray path we can assume that ray is always fairly close to the field line on which it started. Thus values calculated for the field line will apply reasonably accurately to the appropriate points of the ray path. Accordingly we will find θ and thus ϕ as a function of latitude "ℓ" along the field line and then use these to find the deviation of the ray from this field line.

The values of wave normal angle θ (and thus ϕ) to be expected in the magnetosphere depend on the mechanism which initiates these micropulsations. There is some evidence that they are initiated by particle (probably proton) emissions.[1] Theoretical work[6] on VLF emission from single electrons (neglecting stream effects) indicates emission at fairly large angles θ. On the other hand, recent satellite observations show[7] both "micropulsation mode" and "whistler mode" whistlers initiated by common atmospheric impulses. For micropulsations initiated by atmospheric impulses we might expect small angles θ, since, to the extent that a ray approach is valid, waves from a lightning stroke entering the ionosphere will be refracted to the vertical (field direction in high latitudes) because of the high refractive index.

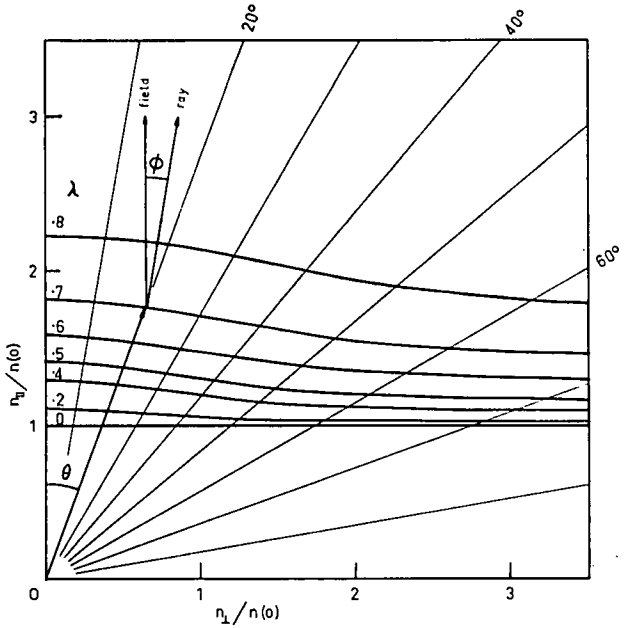

FIG. 3. POLAR DIAGRAM OF NORMALISED REFRACTIVE INDEX VERSUS WAVE NORMAL ANGLE θ PARAMETRIC IN NORMALISED FREQUENCY λ. THE RAY DIRECTION (ϕ) IS NORMAL TO THESE CURVES AS SHOWN.

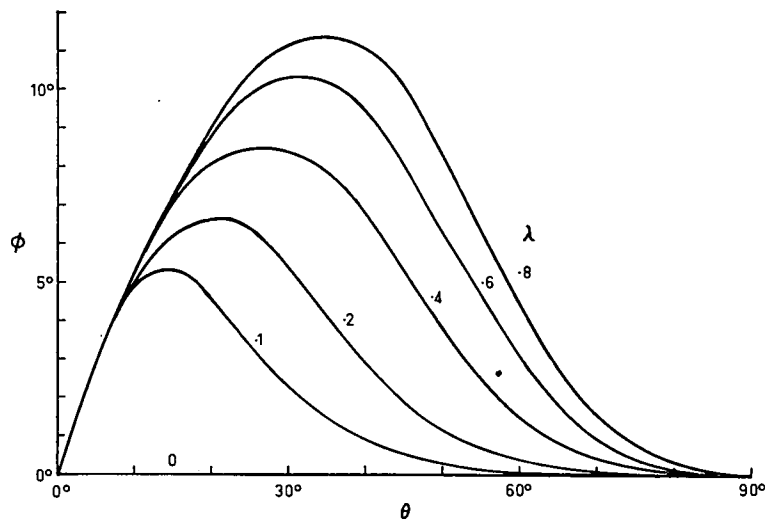

FIG. 4. RAY DIRECTION (ϕ) AS A FUNCTION OF WAVE NORMAL ANGLE θ FOR VARIOUS NORMALISED FREQUENCIES λ.

We take up our consideration of the micropulsation wave packet as it passes through the equatorial plane. We will take the field line which passes through this point as reference and denote quantities (θ, λ, g) at this point ($\ell = 0$) by subscript zero.

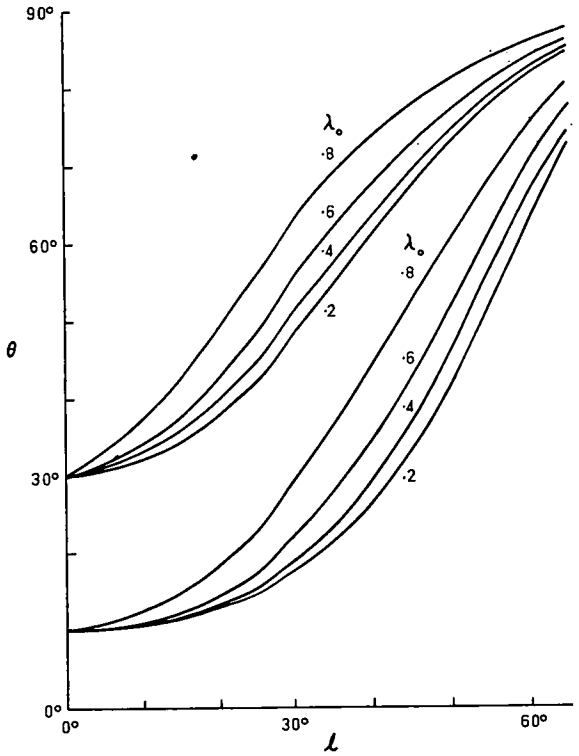

FIG. 5. VARIATION OF WAVE NORMAL ANGLE ALONG THE FIELD LINE (DEFINED BY THE LATITUDE ANGLE ℓ) CALCULATED FROM (4). INITIAL VALUES OF θ ARE $\theta_0 = 10°$ AND $\theta_0 = 30°$. INITIAL VALUES OF NORMALISED FREQUENCY (λ_0) ARE AS SHOWN.

The wave normal angle at any point along the field line is given by Snell's Law:

$$n(\theta) \sin \theta = n(\theta_0) \sin \theta_0$$

Thus

$$\frac{\tan \theta}{\tan \theta_0} = \frac{n_{\parallel}(\theta_0)}{n_{\parallel}(\theta)}$$

As shown above

$$n_{\parallel}(\theta) \simeq n_{\parallel}(0) = \frac{a}{g} \frac{1}{1 - \lambda}$$

to within 20% or 30%,

i.e.

$$\tan \theta \simeq \tan \theta_0 \left(\frac{g}{g_0} \frac{1 - \lambda}{1 - \lambda_0} \right)^{1/2} \tag{4}$$

Values of θ calculated from (4) are shown in Fig. 5 as a function of ℓ. Note that the wave normals are almost perpendicular to the field when the wave packet is near the bottom of the magnetosphere even for fairly small initial values of θ.

For any given initial values θ_0, λ_0, we can find θ, λ along the field line and thus the ray

direction ϕ. This is shown in Fig. 6 for selected values of θ_0 and λ_0. It appears that the path of the ray corresponding to $\lambda_0 = 0{\cdot}8$, $\theta_0 = 30°$ would deviate from the reference field line about as much as any other. We will estimate this deviation by approximating the relevant curve in Fig. 6 to one giving $\phi = 10°$ for $\ell < 20°$ and $\phi = 0$ for $\ell < 20°$. Then at a distance

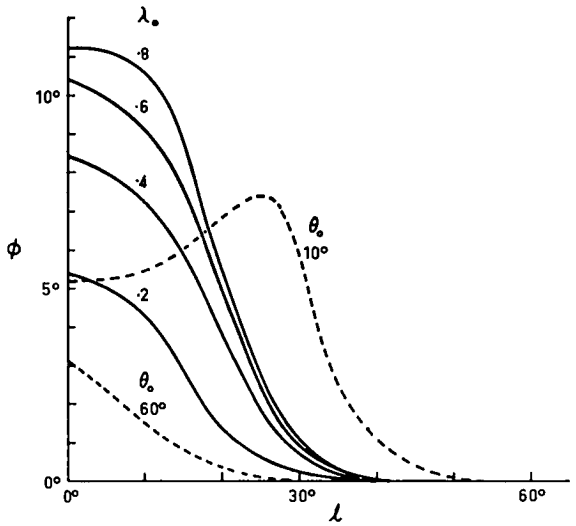

FIG. 6. VARIATION OF RAY DIRECTION (ϕ) ALONG THE PATH AS DETERMINED BY THE LATITUDE ANGLE ℓ. FOR THE SOLID CURVES, $\theta_0 = 30°$, λ_0 IS AS SHOWN. FOR THE BROKEN CURVES, $\lambda_0 = 0{\cdot}6$, θ_0 IS AS SHOWN.

s along the reference field line corresponding to $\ell = 20°$ the lateral deviation of the ray path will be approximately:

$$\Delta R \simeq s \tan \phi = s \tan 10°$$

where R is the distance from the Earth's centre (in Earth radii) of the corresponding point on the reference field line

$$R = R_0 \cos^2 \ell = R_0 \cos^2 20°$$

Beyond this point ($\ell = 20°$) the ray path will be along a new field line defined by

$$R \pm \Delta R = (R_0 \pm \Delta R_0) \cos^2 20°$$

Hence

$$\Delta R_0 = \frac{s \tan \phi}{\cos^2 \ell}$$

$$= \pm 0{\cdot}07\, R_0 \qquad (5)$$

Thus all rays starting from the equatorial plane on the field line terminating at geomagnetic latitude 65° (say) would reach the Earth within one degree of this latitude. Since the lateral deviation of the ray paths is small the differences in total path length are likely to be negligible.

Guiding might also be produced by field aligned columns of excess ionisation. This effect is important for VLF whistlers and is usually referred to as "trapping". If we can assume that the relevant dimensions such as the width of the column and distance over which medium changes appreciably are large compared with a wavelength, then we can show that trapping

can occur for quite a small ratio of excess plasma density inside the column (ΔN) to the ambient density outside (N). These assumptions imply that the space gradient of refractive index is normal to the magnetic field direction so that by Snell's Law, $n_\parallel$ is constant. If the wave normal angle at the centre of the column is θ, it will be zero at the point where the plasma density has fallen from $N + \Delta N$ to N:

$$n_\parallel(\theta, N + \Delta N) = n_\parallel(0, N)$$

For all θ:

$$n_\parallel^2(N + \Delta N) = \frac{N + \Delta N}{N} n_\parallel^2(N)$$

so that

$$\frac{\Delta N}{N} = \frac{n_\parallel^2(0)}{n_\parallel^2(\theta)} - 1$$

Trapping would be most useful where the magneto-ionic ducting effect is least. Thus, taking $n_\parallel$ from Fig. 3, we would require an excess density of about 12% for $\lambda = 0{\cdot}8$ and $\theta = 30°$. However in view of the apparent effectiveness of magneto-ionic ducting this effect will not be discussed further.

4. TRAVEL TIME

For the purposes of calculating the travel time of a wave packet along its ray path we will assume that this path is exactly along a dipole field line. The group refractive index in the direction of the field is given by

$$n_G = \cos\theta \frac{d}{d\lambda}(n\lambda)$$

$$= \left(\frac{a}{g}\right)^{1/2} \frac{1 - \frac{1}{2}\sin^2\theta - (\frac{1}{4}\sin^4\theta + \lambda^2\cos^2\theta)^{1/2} + \frac{1}{2}\lambda^2\cos^2\theta(\frac{1}{4}\sin^4\theta + \lambda^2\cos^2\theta)^{-1/2}}{[1 - \frac{1}{2}\sin^2\theta - (\frac{1}{4}\sin^4\theta + \lambda^2\cos^2\theta)^{1/2}]^{3/2}}$$

This simplifies in two special cases:

$$\theta = 0 \qquad n_G(0°) = \left(\frac{a}{g}\right)^{1/2}(1 - \tfrac{1}{2}\lambda)(1 - \lambda)^{-3/2}$$

$$\theta = 90° \qquad n_G(90°) = \left(\frac{a}{g}\right)^{1/2}(1 - \lambda^2)^{-3/2}$$

It will be convenient to express $n_G(\theta)$ in terms of the strictly longitudinal case ($\theta = 0$):

$$n_G(\theta) = \alpha(\lambda, \theta)\, n_G(0°)$$

The function α is shown plotted in Fig. 7. For given values of θ_0 and λ_0, subsequent θ and λ are determined as discussed above which can be used to calculate α at all points along the field line. Values of α calculated in this way for $\theta_0 = 30°$, and $\lambda_0 = 0{\cdot}6$ and $0{\cdot}8$ are shown superimposed as broken curves in Fig. 7. These curves suggest that it might be a reasonable approximation to use the simple expression for $n_G(0°)$ in calculating travel times. If this were so it would also avoid having to decide what values of θ_0 are applicable. The travel time for a "half-hop" (i.e. equatorial plane to the Earth's surface) becomes

$$t(\theta_0) = \frac{1}{c}\int_0^s n_G(\theta)\, ds$$

The percentage error in assuming strictly longitudinal propagation given by

$$\left(1 - \frac{t(\theta_0)}{t(0°)}\right) 100\%$$

is shown in Fig. 8 as a function of θ_0 for $\lambda_0 = 0{\cdot}6$. This value of λ_0 may well correspond with the upper observable limit. In the worst case ($\theta_0 = 90°$) the travel time is about 23% less

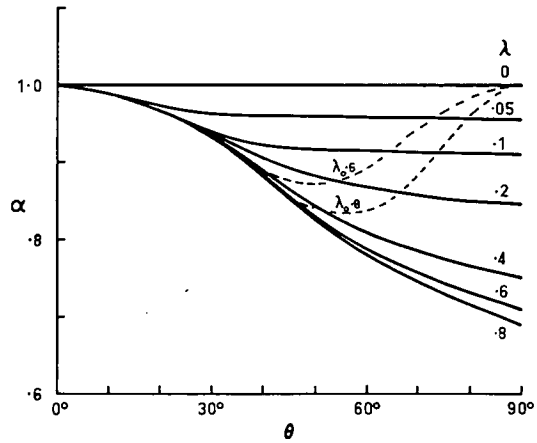

FIG. 7. THE RATIO (α) OF GROUP REFRACTIVE INDEX AT WAVE NORMAL ANGLE θ TO THAT AT $\theta = 0$ AS A FUNCTION OF θ PARAMETRIC IN λ. THE SEQUENCE OF VALUES α OCCURRING ALONG A FIELD LINE PATH IS SHOWN BY THE BROKEN CURVES FOR $\lambda_0 = 0{\cdot}6$ AND $\lambda_0 = 0{\cdot}8$.

than that for $\theta_0 = 0$. However there may well be some restriction on the maximum allowable values of θ, particularly in the lower regions of the magnetosphere, which does not appear in this analysis. Thus the error would be less than 2% if we need consider only wave normal angles less than, say, 75°. The following discussion will be restricted to the longitudinal case.

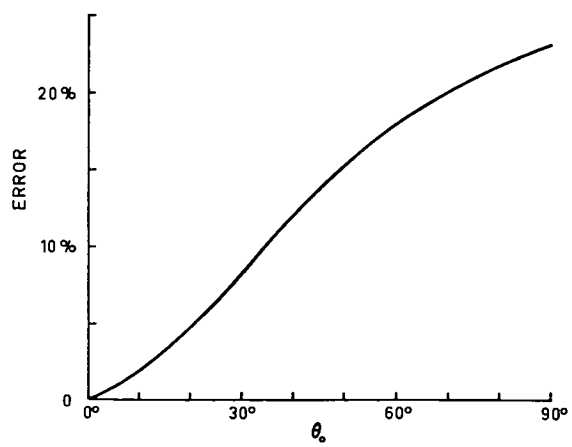

FIG. 8. PERCENTAGE ERROR INCURRED BY ASSUMING STRICT LONGITUDINAL PROPAGATION IN CALCULATING TRAVEL TIME SHOWN AS A FUNCTION OF INITIAL WAVE NORMAL ANGLE θ_0 FOR $\lambda_0 = 0{\cdot}6$.

The one-hop (hemisphere to hemisphere) travel time is then

$$t(\lambda_0) = \frac{2}{c}\int_0^s n_G(\lambda_0, 0°)\, ds = \frac{2R_0R_e}{c}\left(\frac{a}{g_0}\right)^{1/2}\int_0^L \left(\frac{g}{g_0} - \tfrac{1}{2}\lambda_0\right)\left(\frac{g}{g_0} - \lambda_0\right)^{-3/2} \sigma d\ell \qquad (6)$$

where R_e is the radius of the Earth, R_0 is in Earth radii, and L is the terminating latitude of the field line. We have assumed a model of the magnetosphere for which the scale frequency

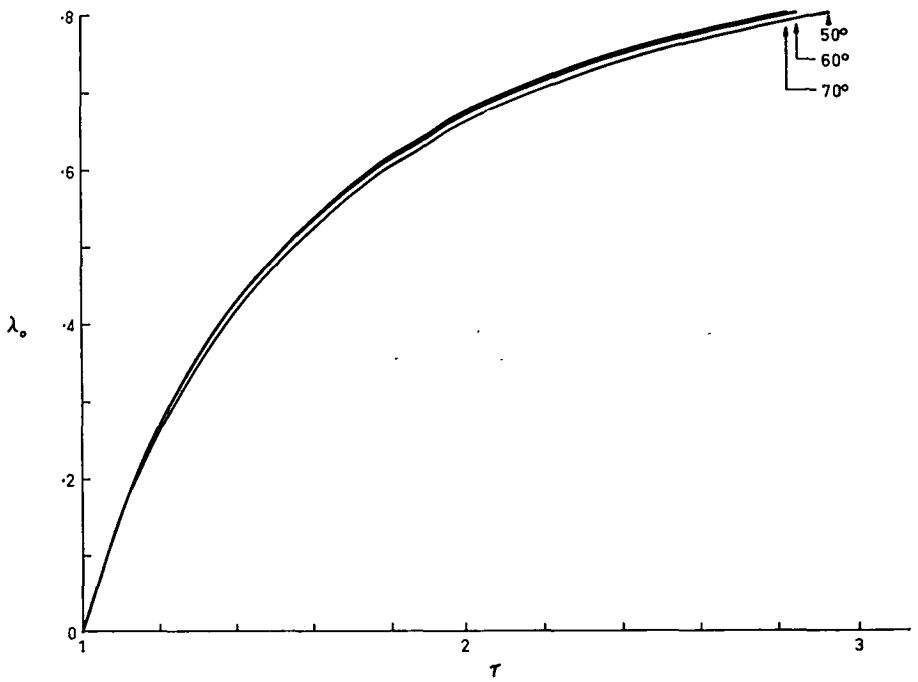

FIG. 9. TRAVEL TIME (τ) NORMALISED TO ITS VALUE AT ZERO FREQUENCY SHOWN AS A FUNCTION OF FREQUENCY (λ_0) NORMALISED TO THE MINIMUM PROTON GYRO-FREQUENCY (g_0) ALONG THE PATH. DISPERSION CURVES ARE SHOWN FOR PATHS TERMINATING AT GEOMAGNETIC LATITUDES $L = 50°$, 60° AND 70° (THE LAST TWO ARE BARELY RESOLVED WITH THIS LINE THICKNESS).

is constant along a field line (so-called gyro frequency model of plasma density). For a dipole field

$$\sigma = (1 + 3\sin^2\ell)^{1/2}\cos\ell$$

and

$$g/g_0 = \sigma \sec^7\ell$$

The terms outside the integral can be avoided by normalising the travel time to its value at $\lambda_0 = 0$:

$$\tau(\lambda_0) = t(\lambda_0)/t(0)$$

The normalised time as a function of normalised frequency λ_0 is shown in Fig. 9 for geomagnetic latitudes $L = 50°$, 60° and 70°. Note that τ is virtually independent of latitude for latitudes greater than 60° or even 50°. The frequency range over which micropulsations of this type are observed suggests that only these high latitudes are involved.

Consider now the zero frequency ($\lambda_0 = 0$) propagation time. The integral of (6) is now a function of L only. Expressing R_0 in terms of g_0 we get

$$t(0) = a^{1/2} g_0^{-5/6} T(L) \text{ sec} \tag{7}$$

where a is in Mc/s and g_0 in c/s. Other numerical factors have been absorbed into $T(L)$

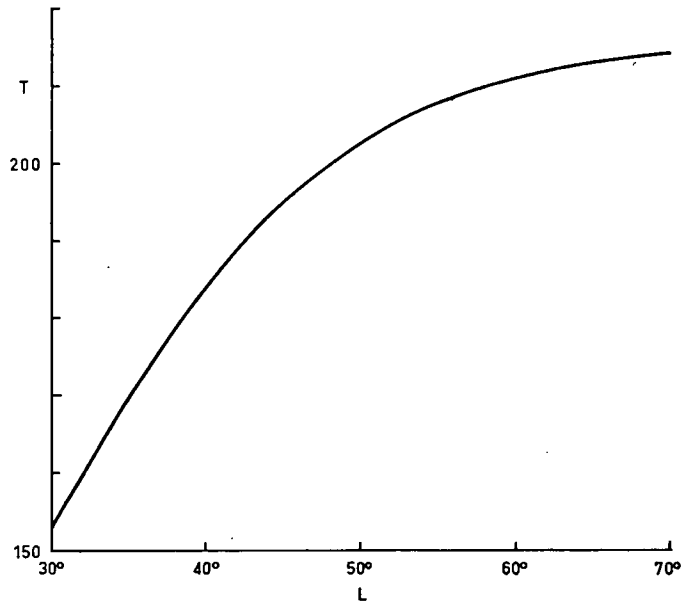

FIG. 10. THE PARAMETER $T(L)$ REQUIRED IN (7) FOR CALCULATION OF ZERO FREQUENCY TRAVEL TIME $t(0)$.

which is shown in Fig. 10. The slope of the $T(L)$ curve is small at high latitudes so that $T(L > 50°) \simeq 210$ to within 3%.

5. DISCUSSION

We need to justify the assumption in the analysis above that in the regions of interest the relevant dimensions are always large compared with a wavelength. Suppose we consider the field line terminating at latitude 65° (for which $g_0 = 2{\cdot}6$ c/s), a constant scale frequency $a = 1$ Mc/s and a signal frequency $f = 1{\cdot}5$ c/s. At the top of the path the refractive index (n) is of the order of 1000 so that the wavelength is about 200 km. This corresponds to about one third of a degree of latitude angle ℓ or 0·2% of the total path length. The choice of field line is not important for the wavelength and scale of the field line change in nearly the same ratio. Thus, in the upper regions of the magnetosphere at least, the ray approach appears justified.

In the lower regions of the magnetosphere and in the ionosphere the refractive index decreases ($n \sim 200$) and the wavelength increases to about 1000 km. In these regions a ray approach would not be justified. However this is of no great consequence for nearly all the travel time and dispersion takes place where the refractive index is large (wavelength small) in the upper regions. This is apparent from Figs. 9 and 10. These lower regions cannot change the dynamic spectral shape or travel time significantly, but can affect the amplitude

(a function of f and θ). For instance, the large change of refractive index at the ionosphere–atmosphere boundary may impose restrictions on the allowable values of θ as would be predicted by a ray approach.

Finally, it is perhaps interesting to mention here a possible "wave" effect which does not appear as such in whistlers. VLF whistlers and, to some extent, emissions often show fine structure due to small differences in path length and so small differences in travel time. Now for the micropulsation signal and path discussed above the total path length in wavelengths (given by ft_p where t_p is the phase travel time) is about 200. For slightly different paths this number would be different so that the signals as observed on the ground would arrive in and out of phase depending on frequency. This may explain the typical modulation of intensity along the rising tones seen in dynamic spectra as shown in Fig. 1. For VLF whistler mode propagation the number of waves in each path is some two orders of magnitude greater so that the fine structure is unresolved in frequency but resolved in time.

6. CONCLUSIONS

It has been shown that the dispersion and travel times are given reasonably by the strictly longitudinal expressions even though the wave normal angles may be large, particularly in the lower regions of the magnetosphere. If the frequency and travel times are expressed in terms of their normalised values (λ_0, τ) the resulting dispersion (for high latitudes) is "universal", that is independent of other parameters. The ray path in the regions of interest is well confined to a magnetic field line by magneto-ionic ducting. Trapping by field aligned columns of ionisation may also occur though the ducting effect alone seems adequate.

Acknowledgement—I would like to thank Professor G. R. A. Ellis for stimulating discussion and for bringing to my attention reference[1].

REFERENCES

1. J. A. Jacobs and T. Watanabe, *J. Atmos. Terr. Phys.* **26,** 835 (1964).
2. R. L. Smith, SEL Technical Report No. 6, July 11, 1960, Stanford University.
3. E. Aström, *Ark. Fys.* **2,** 443 (1950).
4. R. L. Dowden, *Nature, Lond.* **195,** 984 (1962).
5. R. A. Helliwell and E. Gehrels, *Proc. Inst. Radio Engrs* **46,** 785 (1958).
6. Harold B. Liemohn, *Radiation from Electrons in a Magnetosphere* (to be published).
7. R. L. Dowden, *Nature, Lond.* (submitted 1965).

Резюме—Рассматривается распространение волн весьма низкой радиочастоты (~1 ц) вдоль полевых линий в магнитосфере, «способом микропульсации». Воспроизводятся выражения для фазового и группового показателя преломления для любого направления нормали волны. Несмотря на возможно-большие углы нормали волны, продольные выражения могут быть с достаточной точностью применены для вычислений времен пробега и дисперсии. Среда вызывает сильное гидирование без выравниваемых полем столбцев. Повидимому, максимальное отклонение траектории луча от полевой линии—весьма незначительно.

Planet. Space Sci. 1965, Vol. 13, pp. 773 to 779. Pergamon Press Ltd. Printed in Northern Ireland

THE USE OF MICROPULSATION "WHISTLERS" IN THE STUDY OF THE OUTER MAGNETOSPHERE

R. L. DOWDEN and M. W. EMERY
Physics Department, University of Tasmania, Australia

(*Received* 8 *March* 1965)

Abstract—Certain types of micropulsation dynamic spectra show a series of rising tones thought to be caused by dispersion in the magnetosphere. Based on this idea and a previous analysis it is shown that these spectra can be used to evaluate the plasma density in the outer magnetosphere (five to eight Earth radii) in a way analogous to that used for VLF whistlers. The method is applied to micropulsations observed at Hobart in April, 1964. The results indicate a substantial decrease in plasma density beyond about five Earth radii in broad agreement with previous VLF work.

1. INTRODUCTION

It has been suggested[1] that the sequence of rising tones observed in dynamic spectra of certain types of geomagnetic micropulsations might be an expression of dispersion of a hydromagnetic wave packet guided by a magnetic field line through the magnetosphere in a way similar to VLF whistlers. Dynamic spectra calculated on this hypothesis show good agreement with observed spectra.[1] This suggests that it should be possible to obtain plasma density ($N_0 - R_0$) profiles from information contained in observed dynamic spectra.

A method of doing this is developed here. This method is based on a study of propagation in the "micropulsation mode" given previously[2] (referred to here as Paper 1). It was shown there that the observed dispersion should be that of a single "universal" dispersion if frequency and time is suitably normalised. The problem is to find these two normalisation factors which then determine the path (or R_0) and the plasma density (N_0) at the top of the path respectively.

It should be stressed that the dispersed times have been determined by the time intervals (as a function of frequency) between successive echoes and not the spectral shapes of the rising tones themselves which may depend on an emission process.

2. DETERMINATION OF PATH (g_0)

It was shown in Paper 1 that if travel times are normalised to their value at zero frequency and frequencies normalised to the minimum proton gyrofrequency along the path (g_0), the frequency-time ($\lambda_0 - \tau$) dispersion curve is "universal" for latitudes greater than about 50°. This means that, in principle at least, observed dispersion curves obtained from dynamic spectra of micropulsations can be used to determine the paths (field lines) along which the micropulsations were propagated. Measurement of travel time at zero frequency and at frequency f would give τ and consequently λ_0 at f, and hence g_0.

However, observed micropulsations do not extend down to zero frequency so that modified methods have to be devised.

2.1 Method 1

The first method is based on one devised by Smith and Carpenter[3] for the similar problem of determining the path travelled by VLF whistlers which do not extend up to the

nose frequency. Measurements of travel time ((t_U, t_L) are made at two frequencies f_U and f_L. The best accuracy is obtained if these frequencies are the highest and lowest at which accurate measurements can be made. Then since $t(0)$ is common to both t_U and t_L, and since τ is "universal":

$$t_U/t_L = \tau_U/\tau_L = S(f_L/f_U, f_U/g_0)$$

The function S which has been deduced from Paper 1 (Fig. 9) is shown in Fig. 1. From this set of curves the measured ratios f_L/f_U and t_U/t_L determine f_U/g_0 and thus g_0.

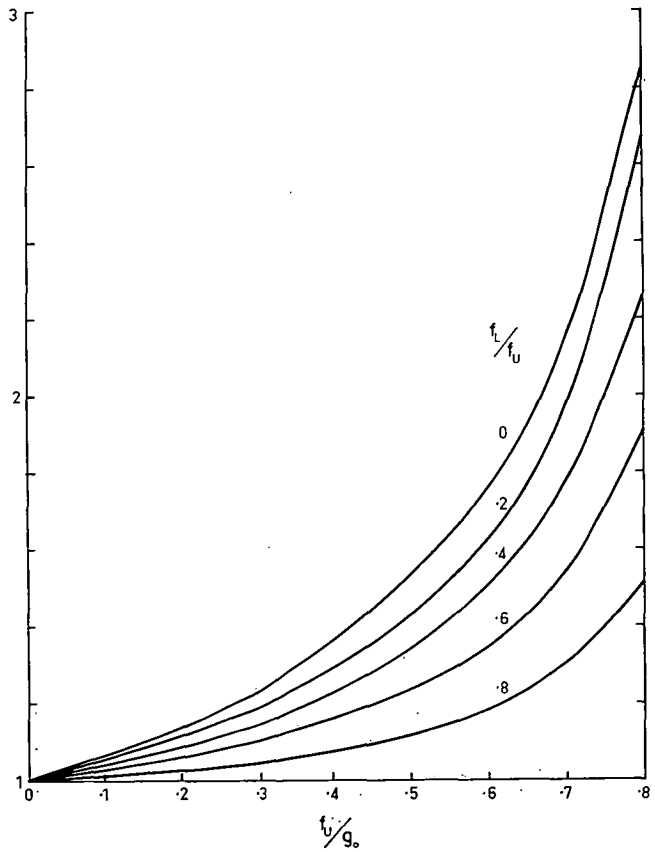

FIG. 1. THE UNIVERSAL PARAMETER S USED IN METHOD 1 SHOWN AS A FUNCTION OF f_U/g_0 FOR VARIOUS VALUES OF f_L/f_U.

2.2 *Method 2*

Many events have a restricted range of frequency. For these Method 1 is difficult to use. Usually the total number of hops is large so that the dispersion or incremental increase in travel time Δt over a small range of frequency Δf is easily measured. If these are expressed in terms of the average travel time and frequency we get:

$$\frac{\Delta t}{t} \Big/ \frac{\Delta f}{f} = \frac{\lambda_0}{\tau} \frac{d\tau}{d\lambda_0} = \xi(\lambda_0)$$

The universal function $\xi(\lambda_0)$ has been calculated by graphical differentiation of the universal $\tau(\lambda_0)$ curve derived in Paper 1. This is shown in Fig. 2.

2.3 Method 3

For some events dispersion may not be measurable. VLF nose whistlers have an upper cut-off frequency at about $1\frac{1}{4}$ times the nose frequency.* At high latitudes (65°, say) this would correspond to $\lambda_0 \simeq 0{\cdot}55$. If this is caused by thermal broadening of the electron cyclotron resonance[4] then an analogous cut-off for micropulsations caused by protons would be expected[5] at about $\lambda_0 \simeq 0{\cdot}6$. If the highest observed frequency (f_{max}) is limited only by this process then $g_0 = 1{\cdot}7\, f_{max}$. This "method", though of doubtful validity, is useful as a last resort.

3. DETERMINATION OF PLASMA DENSITY

For latitudes greater than about 50° the scale frequency is given by equation (7) of Paper 1, rearranged to the form:

$$a = 5{\cdot}7 t^2(0) g_0^{5/3} \times 10^{-6} \text{ Mc/s} \qquad (1)$$

where $t(0)$ is the zero frequency travel time in seconds for one complete (there and back) trip and g_0 is in cycles per second. The quantity $t(0)$ is not measured directly but deduced from the measured value $t(\lambda_0)$ and $\tau(\lambda_0)$ as given in Fig. 9 of Paper 1.

The concept of scale frequency is used because it is quasi-constant in the magnetosphere. The plasma density N_0 at the top of the path in particles per cm^3 is numerically equal to $23\, a g_0$ for a in Mc/s and g_0 in c/s. The radial distance of the top of the path is equal to $7{\cdot}8\, g_0^{-1/3}$ in Earth's radii. For a non-dipole field this (R_0) can be regarded as a convenient parameter.

The main errors in the determination of scale frequency will be caused by uncertainty of λ_0 (and consequently τ) at which the travel time is measured. If (1) is differentiated with respect to λ_0, it can be shown:

$$\frac{\Delta a}{a} = -\frac{\Delta \lambda_0}{\lambda_0}(2\xi + 5/3)$$

Thus travel time should be measured at a low frequency where ξ is small (see Fig. 2). Note that for $\lambda_0 \sim 0{\cdot}5$ the percentage error in scale frequency is about three times that of λ_0.

4. RESULTS

Dynamic spectra have been made of 15 micropulsation events recorded near Hobart, Tasmania during April, 1964. The spectrum of No. 13 is shown in Fig. 1 of Paper 1. Some of the data scaled from each event is shown in Table 1. Values deduced from this, and additional data not shown, are shown in Table 2. In most cases all three methods have been used.

Some of the extreme values of scale frequency (a) seem to correspond with extreme values of deduced normalised maximum frequency λ_0(max). This is probably caused by errors in deducing λ_0 as discussed above. Since the deduced value of g_0 (and R_0) depends on the measured f(max) and the deduced λ_0(max), such errors would tend to produce a spurious variation of a with R_0. Values determined by method 3 would not show this

* This is based on ratios calculated by one of us (R.L.D.) from published[4] data scaled from all available (57) nose whistlers of high quality. The ratio appeared to be independent of nose frequency over the range 3·5 kc/s to 13 kc/s and had a median of $1{\cdot}23 \pm 0{\cdot}05$ (quartile range).

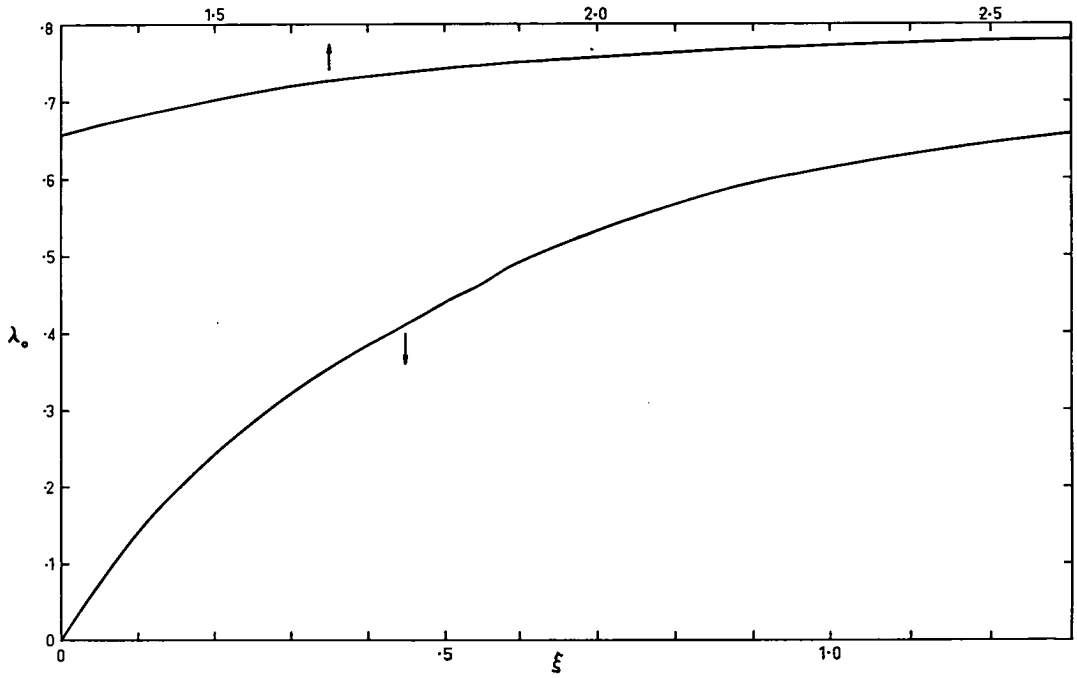

FIG. 2. THE UNIVERSAL PARAMETER ξ USED IN METHOD 2 AS A FUNCTION OF NORMALISED FREQUENCY λ_0. THE UPPER CURVE IS AN EXTENSION: ITS SCALE IS SHOWN AT THE TOP.

error. To test this the $a(R_0)$ values were plotted in Fig. 3. It is seen that the distribution of values deduced by methods 1 and 2 is similar to that of the method 3 values. Thus the dependence of a on R_0, which does not appear in VLF whistler measurements of the lower magnetosphere ($R_0 \sim 2$ to 5 Earth radii), seems to be a real effect.

Values of $N_0(R_0)$ deduced from the $a(g_0)$ values in Table 2 are shown plotted in Fig. 4. Also shown is Smith's[6] distribution derived from VLF nose whistler which fits a model of

TABLE 1. EXPERIMENTAL DATA

Event No.	Date (April '64)	Time (U.T.)	f_{max}* (c/s)	f_{min}* (c/s)	$t(f_{max})$ (sec)
1	4th	0945	0·7	0·5	130
2	4th	1025	0·8	0·6	100
3	4th	1320	1·1	0·5	110
4	4th	1405	1·3	0·8	75
5	4th	1454	1·4	1·0	95
6	4th	1705	1·8	1·6	60
7	4th	2038	1·4	—	80
8	5th	1440	1·6	1·2	90
9	6th	1240	1·0	0·7	170
10	6th	1415	1·1	0·9	120
11	6th	1748	1·5	1·0	120
12	—	—	0·7	0·6	135
13	10th	1750	1·4	0·9	125
14	15th	1940	1·4	—	125†
15	15th	1030	1·5	1·0	140

* Highest and lowest frequencies reached
† Measured at 1·2 c/s

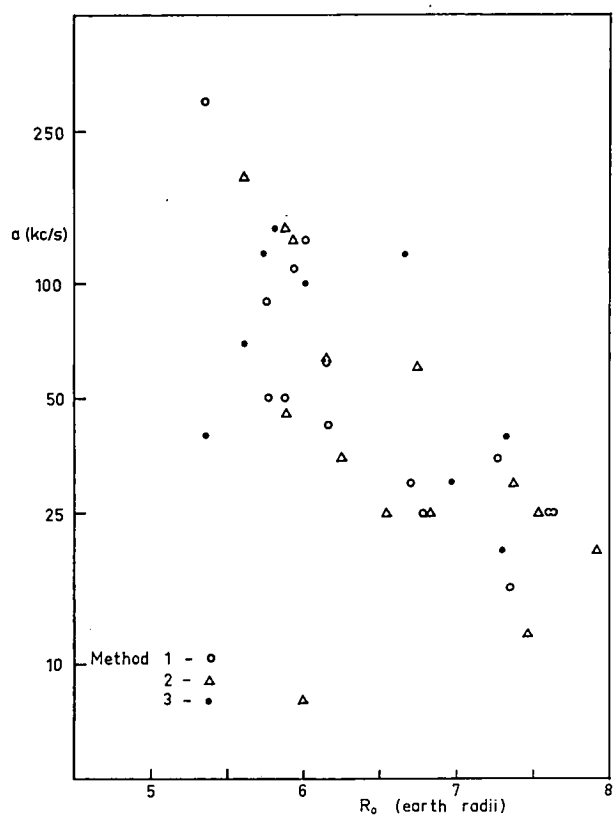

FIG. 3. SCALE FREQUENCY VALUES FROM TABLE 2 PLOTTED AS A FUNCTION OF R_0.

constant scale frequency ($a \simeq 1$ Mc/s). Our results do not fit such a model and in addition the N_0 values are about an order of magnitude lower than an extrapolation of Smith's.

5. DISCUSSION

We now propose to show that our results are in broad agreement with VLF whistler measurements. This is necessary to give an experimental basis to this theory of "micropulsation whistlers" so that it can be used with some confidence in later work.

Recent observations of VLF "knee" whistlers show[7] "that the magnetospheric ionisation profile often exhibits a 'knee', that is, a region at several Earth radii in which the ionisation density drops rapidly from a relatively normal level to a substantially depressed one". The reduction in plasma density is about one order of magnitude.[7] There is evidence[7] that "the knee exists at all times in the magnetosphere, and that its position varies, moving inward with increasing magnetic activity". Thus our data can be reconciled to VLF whistler data by assuming a "knee", at $R_0 \simeq 5$ as shown (dashed curve) in Fig. 4.

Dynamic spectra of high latitude VLF whistlers of unusually low nose frequency (corresponding to $R_0 \sim 7$) have been published recently by Carpenter.[8] Assuming that these are "short" whistlers we have deduced (by a technique described in reference[3]) scale frequencies of the order of 100 kc/s. This is in reasonable agreement with our measurements in this region as shown in Fig. 3.

TABLE 2. DEDUCED DATA

Event No.	Method	λ_0(max)	g_0 (c/s)	$t(0)$ (sec)	a (kc/s)
1	1	0·67	1·1	76	25
	2	0·76	0·95	58	20
	3	0·60*	1·2	74	20
2	1	0·70	1·2	44	16
	2	0·74	1·1	42	12
	3	0·60*	1·4	54	30
3	1	0·44	2·5	60	90
	2	0·71	1·5	72	60
4	1	0·76	1·7	44	25
	2	0·80	1·6	46	25
5	1	0·61	2·3	48	60
	2	0·61	2·3	52	60
6	2	0·84	2·2	18	8
	3	0·60*	3·1	34	40
7	3	0·60*	2·3	46	50
8	1	0·65	2·4	45	50
	2	0·69	2·3	45	45
	3	0·60*	2·7	50	70
9	1	0·78	1·2	67	35
	2	0·82	1·2	65	30
	3	0·60*	1·6	98	120
10	1	0·51	2·2	40	130
	2	0·48	2·3	40	140
11	1	0·74	2·0	24	45
	2	0·78	1·9	24	35
	3	0·60*	2·5	34	120
12	1	0·68	1·1	24	25
	2	0·66	1·1	31	25
	3	0·60*	1·2	38	40
13	1	0·86	1·6	30	30
	2	0·80	1·7	20	25
	3	0·60*	2·3	36	110
14	1	0·66	2·2	42	100
	2	0·64	2·3	38	130
	3	0·60*	2·4	38	140
15	1	0·49	3·1	45	300
	2	0·56	2·7	41	190

* Assumed for method 3.

6. CONCLUSIONS

We have shown that there is broad agreement between plasma density measurements deduced from micropulsation dynamic spectra and those from VLF whistler measurements. A more crucial test would be the comparision of measurements made from simultaneous observations of micropulsations and high latitude VLF whistlers from the same region of the magnetosphere.

It should be pointed out that the accuracy of measurements from micropulsations is considerably less than that obtained from VLF whistlers. This is largely due to the limit* in dynamic spectral detail imposed by the uncertainty principle $\Delta f . \Delta t \sim 1$. On the other hand micropulsations have certain advantages: the very low tape speeds required

* We have gone beyond this limit by measuring times over many echoes in each event.

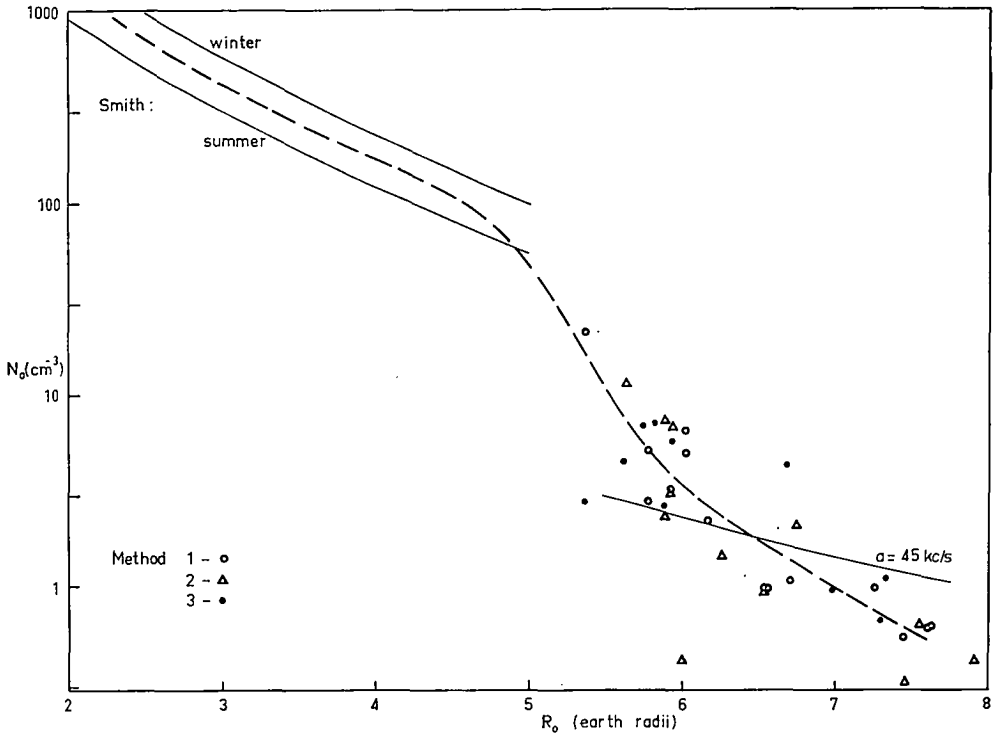

FIG. 4. PLASMA DENSITIES IN THE EQUATORIAL PLANE (N_0) DEDUCED FROM TABLE 2 PLOTTED AS A FUNCTION OF R_0. THE TWO PARALLEL CURVES CORRESPOND TO SMITH'S[6] VLF WHISTLER MEASUREMENTS. THE CURVE LABELLED $a = 45$ KC/S IS AN ATTEMPT TO FIT OUR DATA TO A MODEL OF CONSTANT SCALE FREQUENCY. THE BROKEN CURVE IS AN ATTEMPT TO RECONCILE BOTH SETS OF DATA BY A "KNEED" DISTRIBUTION[7].

(we record at $6\frac{3}{4}$ in per hr) allow continuous recording and, as our results appear to show, high latitude phenomena ($R_0 \sim 8$) can be observed at low latitudes.

REFERENCES

1. J. A. JACOBS and T. WATANABE, *J. Atmos. Terr. Phys.* **26**, 835 (1964).
2. R. L. DOWDEN, *Planet. Space Sci.* **13**, 761 (1965).
3. R. L. SMITH and D. L. CARPENTER, *J. Geophys. Res.* **66**, 2582 (1961).
4. H. B. LIEMOHN and F. L. SCARF, *J. Geophys. Res.* **69**, 833 (1964).
5. R. L. DOWDEN, Cyclotron emission in the "micropulsation mode" (to be published).
6. R. L. SMITH, *J. Geophys. Res.* **66**, 3709 (1961).
7. D. L. CARPENTER, *J. Geophys. Res.* **68**, 1675 (1963).
8. D. L. CARPENTER, *J. Geophys. Res.* **68**, 3727 (1963).

Резюме—Известные виды микропульсации в динамических спектрах обнаруживают ряд наростающих тонов, производимых, как полагают, дисперсией в магнитосфере. На основе такой предпосылки и предыдущих ананлизов указывается, что эти спектры могут быть использованы для оценки плотности плазмы во внешней магнитосфере (от пяти до восьми радиусов Земли) посредством того же приема, который применяется для атмосферных свистков весьма низкой радиочастоты. Этот метод прилагается и к микропульсациям, наблюдаемых в Гобарте, в апреле 1964г. Результаты указывают на значительное сокращение в плотности плазмя за пределом прибл. пяти радиусов Земли, что согласуется, в общих чертах, с предыдущими изысканиями на предмет весьма низкой радиочастоты.

(Reprinted from Nature, Vol. 207, No. 4996, pp. 493–495, July 31, 1965)

AN AUTOMATIC DYNAMIC SPECTRUM ANALYSER FOR TAPE-RECORDED SIGNALS

By Dr. R. L. DOWDEN and M. W. EMERY
Department of Physics, University of Tasmania

A DYNAMIC spectrum analyser provides amplitude or intensity as a function of both frequency and time of transient signals such as music, speech, atmospheric 'whistlers', geomagnetic micropulsations, etc. Typically, for such phenomena, one requires a frequency resolution Δf corresponding to 1 per cent or less of the frequency range of the phenomena and a time resolution limited only by the uncertainty relation $\Delta f \cdot \Delta t \simeq 1$. Two types of analyser are commercially available. The first uses a bank of several hundred narrow band-pass filters. This type has the advantage of 'real-time' analysis but is expensive and inflexible. The second type uses a single narrow band which is tuned (usually by a heterodyne system) over the desired range. However, in order to obtain the maximum available time resolution the signal must be passed several hundred times through the filter. In fact, it is easily shown by the uncertainty principle that the number of passes required is about equal to the number of filters required in a filter bank analyser. Its advantages follow from the use of only one filter. Thus it is relatively inexpensive and highly flexible in that its frequency range and frequency resolution are easily adjusted manually or automatically to follow a pre-set

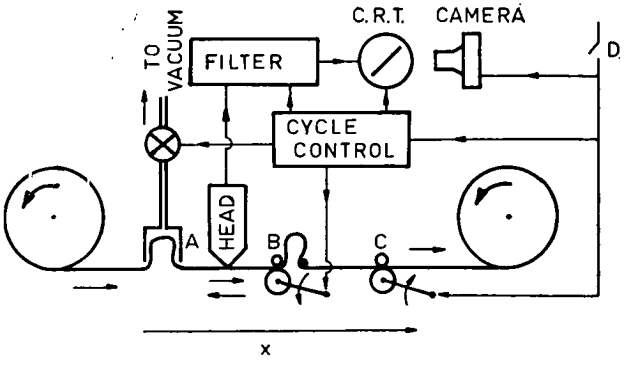

Fig. 1. The complete spectrum analyser, showing details of the multiple pass system

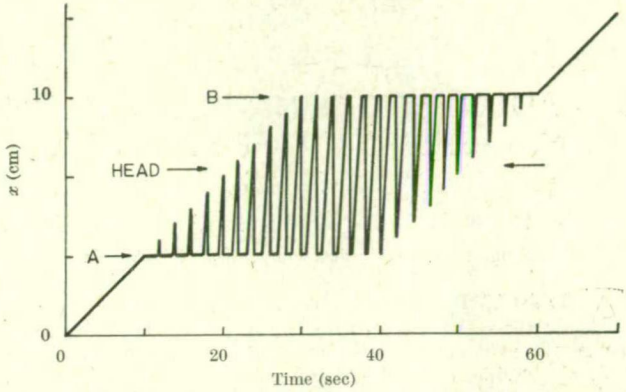

Fig. 2. The locus of a point on the tape as it passes through a 16-pass system. The slopes correspond to the slow capstan, playback and flyback speeds. The x direction is as shown in Fig. 1

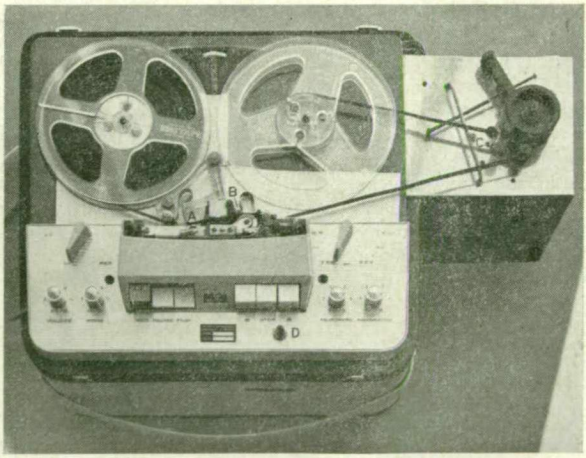

Fig. 3. A photograph of the tape deck showing the modifications. *A*, *B*, *C* and *D* correspond with the points so marked in Fig. 1. The filter and display are not shown

programme. Its obvious disadvantage is related to the large number of passes. Even for high-speed replay, continuous analysis of long signals is very tedious.

Some ingenious methods (for example, ref. 1) have been devised to overcome this, even to the extent of providing 'real-time' analysis. However, in our case the phenomena are already recorded on tape. What we required was an analyser which would provide continuous analysis of any length of tape completely automatically. A long analysis

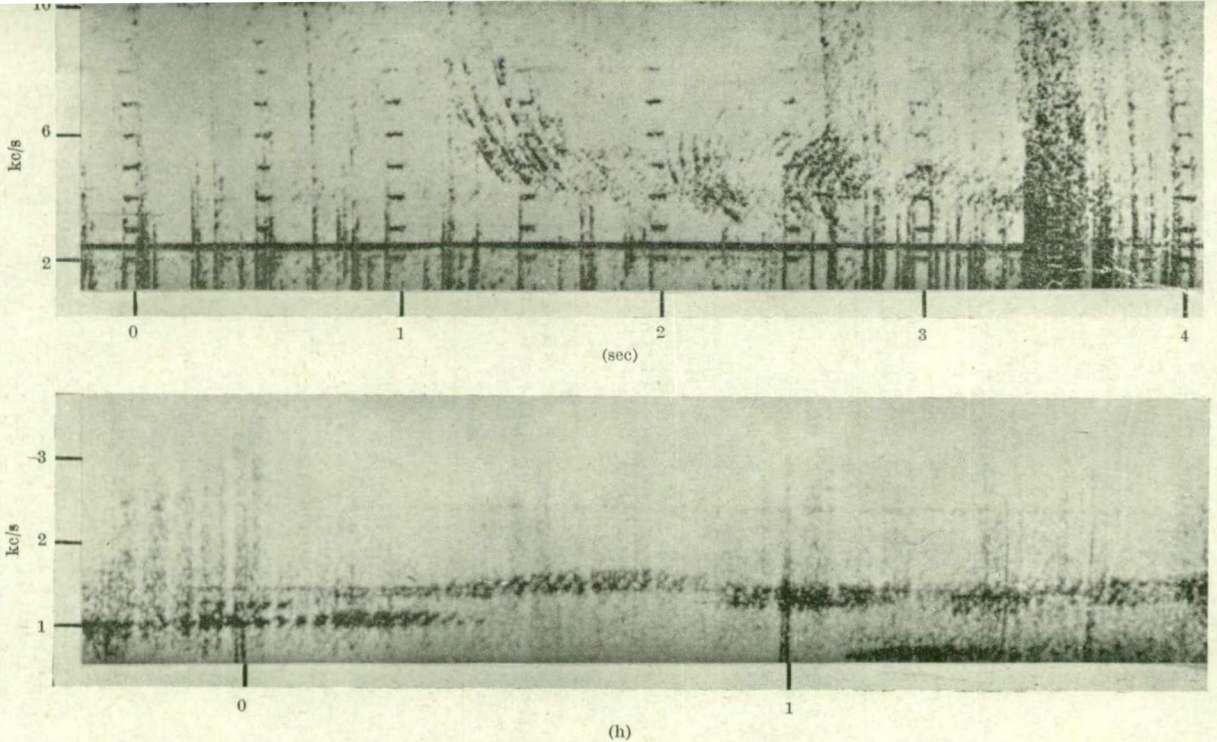

Fig. 4. Continuous spectrograms produced by the analyser in Fig. 1. The upper one shows a very-low-frequency 'nose whistler' and the lower one a train of 'micropulsation whistlers' (both phenomena were recorded at Hobart)

time, provided the operator's time was not involved, was quite acceptable.

The principle of operation is illustrated in Fig. 1. Between A and B the tape travels at the normal playback speed (4·75 cm/sec) controlled by the capstan B, or very much faster in the reverse direction when vacuum is applied at A and the capstan B is disengaged. Thus the tape executes an oscillatory 'saw-tooth' motion past the pick-up head. The forward travel is determined by the programmed duration of a pass (since the speed is fixed). The extent of the 'flyback' is determined by the size of the loop at B. However, since part of this loop has been pulled out by the slow speed capstan C during a pass, the flyback travel is slightly less than the forward travel. Thus the sample of tape passed is changed slightly after each pass. It will be seen that the number of times a given point on the tape passes through the head is equal to the velocity ratio of capstans B and C. The position x of such a point as a function of time is shown in Fig. 2, for a capstan velocity ratio of sixteen. A photograph of the tape deck taken during operation is shown in Fig. 3.

A saw-tooth voltage synchronized to the tape motion controls the frequency of the filter and provides the frequency-time base trace for the display cathode ray tube. The detected output of the filter is applied to the cathode-ray tube as intensity modulation. The modulated trace is recorded on continuously moving film. Note, however, that since the analyser scans in both frequency and time, the trace must be inclined at a certain angle relative to the film direction in order to obtain orthogonal frequency and time axes on the resulting spectrogram. The film speed is adjusted for slight overlap of successive traces. The frequency-time aspect ratio is then controlled by the slow capstan (C) speed. This is made adjustable so as to provide only the required aspect ratio (and time resolution) with a consequent saving in both film and analysis time.

Examples of dynamic spectrograms made by this analyser are shown in Fig. 4. When referred to the playback speed (4·75 cm/sec) the frequency range in each case was 0–10 kc/s, the filter band width (frequency resolution) 80 c/s, and aspect ratio about 10 kc/s = 1 sec. The real time or record speed values depend on the play-back/record speed ratio, which was very high for the long period phenomena. The capstan velocity ratio (or pass number) was 385 in each case, which was somewhat greater than necessary. Note that the analysis time is less than 'real-time' when the capstan velocity ratio is less than the play-back/record ratio. Note also that tape recordable phenomena in any frequency range can be analysed by suitable choice of the latter ratio.

The method described here provides automatic and continuous spectrum analysis in a relatively simple way.

The instrument involved only minor alterations to a standard commercial tape recorder. In fact if the recycling programme is switched off and the slow capstan disengaged it will operate as a 'normal' tape recorder. As an additional refinement our slow capstan is engaged by a solenoid. Thus at any time during 'normal' operation for aural monitoring, analysis can be started immediately by pressing switch *D* shown in Figs. 1 and 3.

[1] Gill, J. S., *Nature*, **189**, 117 (1961).

Printed in Great Britain by Fisher, Knight & Co., Ltd., St. Albans.

(*Reprinted from Nature, Vol. 207, No. 5000, pp. 963–964, August 28, 1965*)

Ordinary Mode Whistlers observed in Satellites

SMITH *et al.*[1] recently published dynamic spectra of a very interesting phenomenon observed in the satellites *Alouette I* and *Injun III*. One of these is reprinted here as Fig. 1*A*. This shows a whistler (rapidly falling part) produced by (extraordinary mode) dispersion of an atmospheric propagated upwards to the satellite. The whistler is followed by a rising trace which flattens out at a frequency which could correspond to the ion gyrofrequency.

Although such a sequence of events may suggest a 'triggering' process for the rising trace[1], I would like to show that the spectral (frequency-time) shapes of both traces can be closely matched if both are interpreted as dispersed forms ('whistlers') of the original atmospheric. Thus the falling trace is an extraordinary mode whistler and the rising part an ordinary mode whistler.

The ordinary mode can propagate only below the ion (proton) gyrofrequency. For frequencies very much less than the electron gyrofrequency, the refractive indices (for longitudinal propagation) become[2]:

$$n^2 = a(g \pm f)^{-1}$$

where g is the proton gyrofrequency, f the wave frequency, and a the scale frequency (ratio of plasma frequency squared to the gyrofrequency, for either protons or electrons). The plus and minus signs correspond to the extraordinary and ordinary modes respectively ($f < g$ for the latter). I have assumed a neutral plasma of electrons and protons only. The group refractive indices are then (signs as above):

$$n_G = a^{1/2}(g \pm \tfrac{1}{2}f)\,(g \pm f)^{-3/2}$$

The travel times of waves in the two modes can be calculated from this with an appropriate model. Fig. 1*B* shows the result of such a calculation using parameters (a,g and path length) to fit the observed dynamic spectrum in Fig. 1*A*.

The agreement for both modes is quite reasonable. Effectively only two independent parameters can be chosen to obtain a fit. These determine the time and frequency scale. The shape is mainly determined by the refractive index expression given here and only slightly by the model or form of the plasma density and magnetic field variation. The effects of other ions do not appear to be important.

Jacobs and Watanabe[3] have suggested that certain types of micropulsations which have dynamic spectral shapes like the rising part shown in Fig. 1*A* might be such ordinary mode whistlers (they used the term

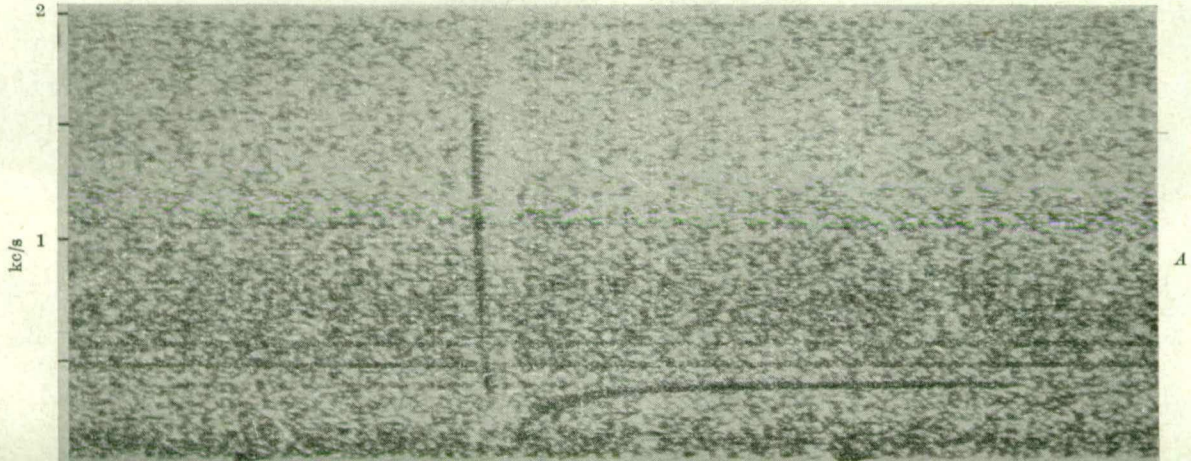
2
kc/s
1
A

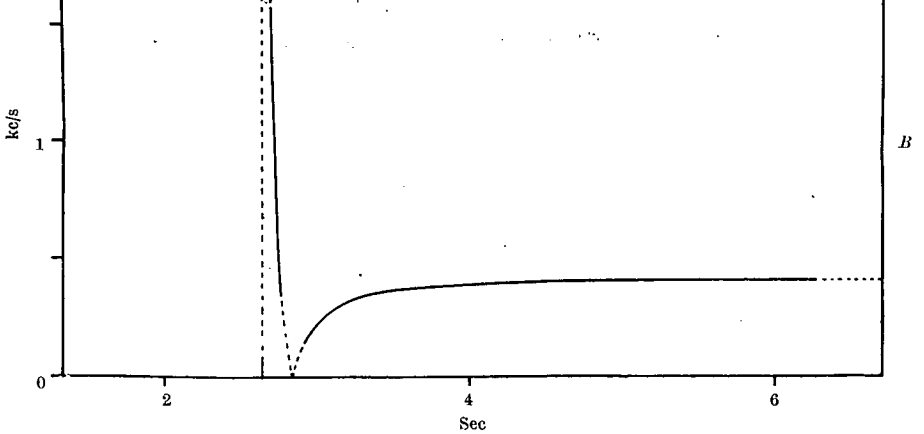

Fig. 1. *A*, Event observed by *Injun III* (after Smith *et al.*[1]). *B*, An attempt to match the event shown in *A* by the two-mode whistler hypothesis. The solid curves correspond to the portions actually observed. The time of the initiating atmospheric is shown by the vertical broken line

'micropulsation whistlers'). This adds considerable weight to their theory and is perhaps the first direct evidence that these can be initiated by an atmospheric impulse.

Note added in proof. Since this letter was submitted the same idea has been presented by Gurnett *et al.*[4]

R. L. DOWDEN

Physics Department,
University of Tasmania,
Australia.

[1] Smith, R. L., Brice, N. M., Katsufrakis, J., Gurnett, D. A., Shawhan, S. D., Belrose, F. S., and Barrington, R. E., *Nature*, **204**, 274 (1964).

[2] Dowden, R. L., '*Micropulsation Mode*' *Propagation in the Magnetosphere* (to be published).

[3] Jacobs, J. A., and Watanabe, T., *J. Atmos. Terr. Phys.*, **26**, 835 (1964).

[4] Gurnett, D. A., Shawhan, S. D., Brice, N. M., and Smith, R. L., *J. Geophys. Res.*, **70**, 1665 (1965).

Printed in Great Britain by Fisher, Knight & Co., Ltd., St. Albans.

Planet. Space Sci. 1966, Vol. 14, pp. 1273 to 1280. Pergamon Press Ltd. Printed in Northern Ireland

MICROPULSATION "NOSE WHISTLERS"
A HELIUM EXPLANATION

R. L. DOWDEN
Physics Department, University of Otago, New Zealand

(*Received* 30 *June* 1966)

Abstract—Occasionally micropulsation dynamic spectra show a series of nosed tones in place of the more usual purely rising tones. These are explained in some detail if, at times, some 3–10 per cent of the ionic content in the outer magnetosphere is helium (He^+). Although this is one or two orders of magnitude greater than expected from diffusive equilibrium theory, it is in broad agreement with recent Ogo-A measurements.

1. INTRODUCTION

Micropulsation or hydromagnetic whistlers consist of a series of rising tones of frequency of the order of 1 c/s and repetition rates of the order of 1/min. It is thought[1] that this is an expression of dispersion of a hydromagnetic wave packet guided by a magnetic field line through the magnetosphere in a way similar to VLF whistlers. Agreement with observed dynamic spectra is obtained in most cases assuming an impulsive source, propagation in the proton-cyclotron or "micropulsation" mode and suitable models of the proton density distribution along a field line (the spectral shape is relatively insensitive to changes in this model). The observed rising tones would then correspond to dispersion produced over many hemispheres to hemisphere hops. The origin of the hydromagnetic wave packet is unknown, and so may not be strictly impulsive (like a VLF "sferic") but if the original emission is generated over a path length short compared with the total path length of many (50, or so) hops the resulting dynamic spectrum would be indistinguishable from one produced by an impulse.

It is therefore of interest to look for the cause of departures from the calculated dynamic spectral shape such as that shown in Fig. 1. These tones show a well developed "nose" at about 1·5 c/s. Although this was the best example observed in fifteen micropulsation whistler trains observed[2] during April 1964, one or two other trains showed some evidence of a nose near or somewhat below the minimum observed frequency. Similar trains showing weak nose effects appear in the published spectra of other workers (for example, Fig. 3 of reference 3).

One acquainted with the history of VLF whistlers might suspect that the answer lay in oversimplifications used in deriving the dispersion equation. However, this does not appear to be the case. Another possibility might be dispersive group retardation during ionospheric propagation across the surface of the earth from the entry point to the observer. However, observed velocities in this mode are of the order of 1000 km/sec,[4] so that even for great distances (~10,000 km) group delays would be of the order of 10 sec. In Fig. 1, on the other hand, there is a *differential* delay over a frequency range of only 0·3 c/s of about one minute.

It occurred to the writer at the time that the effect could be produced if helium ions were present in sufficient quantity near the top of the path (i.e. in the vicinity of the equatorial plane). This would mean that the observed dispersion is produced during propagation at

frequencies between the proton and helium ion gyrofrequencies. Since the observed frequencies are much less than helium ion gyrofrequency in the vicinity of the earth, the wave packet must pass through a stop region in the vicinity of the local helium ion gyro frequency at least twice per hop. For appreciable tunnelling (since the attenuation per hop seems very small) the helium ion concentration would have to be low in these regions. Such a model, requiring appreciable quantities of helium near the top of the path but not in the lower regions, seemed contrary to current ideas. According to diffusive equilibrium theory[5] proton density to helium ion density (R) should increase monotonically from about unity at an altitude of 3000 km to about 1000 in the regions of interest (altitudes beyond about 20,000 km).

Recent measurements by Ogo-A,[6] however, indicate that the required helium ion densities do exist in the regions of interest. Thermal hydrogen and helium ion (H_e^+) densities were measured at altitudes from 1500 km to about 30,000 km. Over most of this range the hydrogen/helium ratio was of the order of 100, and in general this ratio (R) *decreased* with altitude. Data were given for three satellite passes in the region of interest (above 20,000 km). These showed minimum ratios (R) between 10 and 50.

These results show that the model required for a helium explanation of nosed tones is plausible, particularly if the model need apply relatively infrequently.

2. REFRACTIVE INDEX

For a medium of electrons, protons and helium ions (H_e^+), the refractive index for longitudinal propagation at frequency f is given by:[7]

$$n^2 = 1 + \frac{{p_1}^2}{g_1(g_1 \pm f)} + \frac{{p_2}^2}{g_2(g_2 \mp f)} + \frac{{p_3}^2}{g_3(g_3 \mp f)}$$

where p_i are the plasma frequencies and g_i the gyrofrequencies for the electrons (1), protons (2) and helium ions (3), respectively. For the micropulsation mode (ion cyclotron or Alfven "slow" mode) the upper signs are to be taken. For frequencies $f < g_2$; the first two terms may be neglected, giving:

$$n^2 = \frac{{p_2}^2}{g_2(g_2 - f)} - \frac{{p_3}^2}{g_3(f - g_3)}$$

Substituting

$$\lambda = f/g_2,\ R = N_2/N_3 = \tfrac{1}{4}{p_2}^2/{p_3}^2,\ \tfrac{1}{4} = g_3/g_2$$

We get:

$$n = n(0, \infty)\left[\frac{1}{1 - \lambda} - \frac{4}{R(4\lambda - 1)}\right]^{1/2}$$

where $n(0, \infty) = p_2/g_2$ is the refractive index at zero frequency ($\lambda = 0$) in the absence of helium ($R = \infty$). This is shown in Fig. 2 for several values of R, the ratio of proton to helium ion concentration. Note that the refractive index is zero at the frequency:

$$\lambda_c = \frac{1}{4} \cdot \frac{R + 4}{R + 1}$$

For frequencies $\frac{1}{4} < \lambda < \lambda_c$, the refractive index is imaginary.

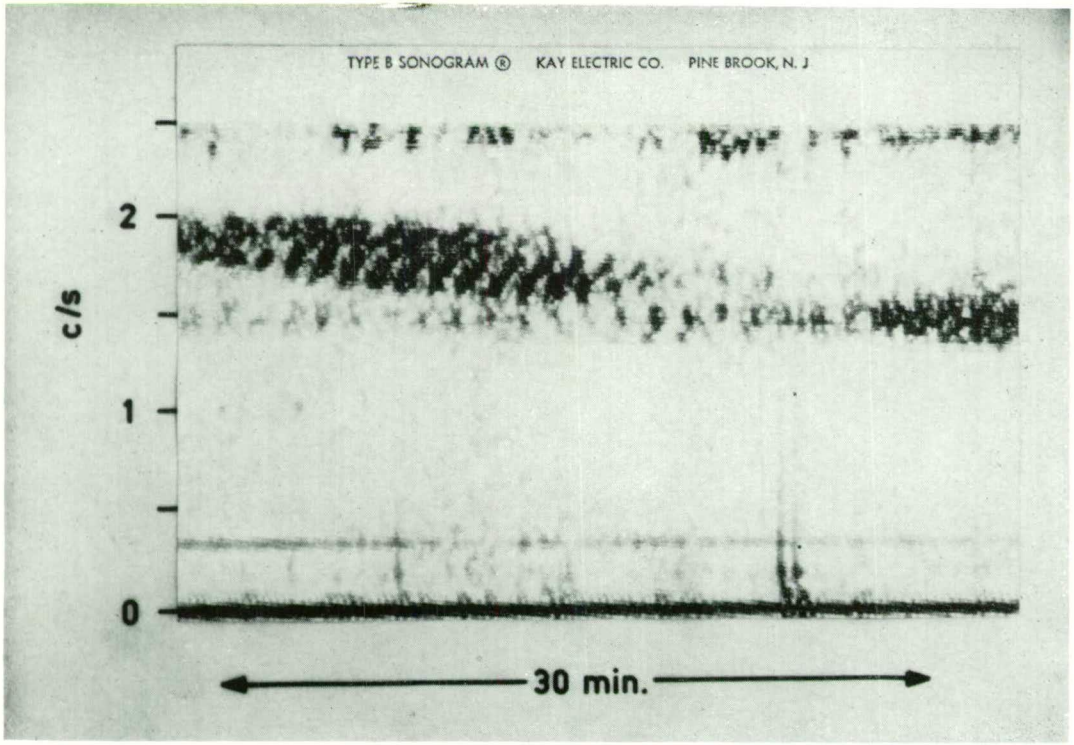

FIG. 1. MICROPULSATION "NOSE-WHISTLERS" RECORDED AT HOBART AT 0150 L.T., 6TH APRIL, 1964.

For calculation of signal travel times we require the group refractive index given by:

$$n_G = \frac{\mathrm{d}}{\mathrm{d}f}(nf) = \frac{\mathrm{d}}{\mathrm{d}\lambda}(n\lambda) = n_G(0, \infty)\left[\frac{1 - \frac{1}{2}\lambda}{(1-\lambda)^2} - \frac{8\lambda - 4}{R(4\lambda - 1)^2}\right]\left[\frac{1}{1-\lambda} - \frac{4}{R(4\lambda - 1)}\right]^{-1/2}$$

where $n_G(0, \infty) = n(0, \infty) = p_2/g_2$.

This is shown in Fig. 3 for several values of R. Note that small amounts of helium (large R) affect the group refractive index more than the phase refractive index. Note also that the group refractive index is infinite at $\lambda = \lambda_c$.

For short distances (i.e. constant p_2, g_2 and R) the travel time or group delay is directly proportional to the group refractive index, so that frequencies for which n_G is least would correspond to nose frequencies.

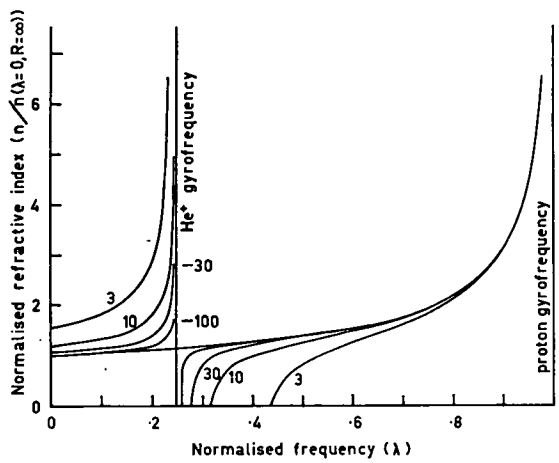

FIG. 2. NORMALIZED PHASE REFRACTIVE INDEX AS A FUNCTION OF FREQUENCY NORMALIZED TO THE PROTON GYROFREQUENCY SHOWN FOR SEVERAL VALUES OF R, THE PROTON–HELIUM ION DENSITY RATIO.

3. DYNAMIC SPECTRUM

As pointed out in the introduction the observed signal becomes "nosed" by dispersion during propagation between the helium and proton gyrofrequencies near the top of the path. However, to be observable on the earth each frequency component must pass through the helium gyro-frequency at some lower point of the path. This is illustrated in Fig. 4. This refers to a field line of $L = 5{\cdot}6$ or terminal geomagnetic latitude 65° (the event in Fig. 1 probably occurred on a slightly lower latitude line). The signal range (λ_0 refers to values in the equatorial plane) is shown by broken lines. In order to avoid computational difficulties at frequencies λ close to λ_c, the helium is considered to be strictly confined to a region near the top of the path. Later an estimate will be made of the allowable helium concentration in the lower regions.

Dynamic spectra are calculated for two models. One for $R = 10$ within latitude angles $\pm 10°$, or within about 6000 km of the equatorial plane, and the other for $R = 30$ within $\pm 14°$ or about 9000 km of the equatorial plane. For both models $R = \infty$ outside this range. The stop regions (imaginary refractive index) corresponding to these models are shown in Fig. 4 as shaded areas.

The group delay or travel time per hop is given by

$$t(f) = \frac{2}{c}\int_0^s n_G(f)\,\mathrm{d}s$$

At least for $R = \infty$, the expression for $n_G(f)$ for strictly longitudinal propagation can be used without incurring significant error.[8] This time can be normalized[8] to its value at zero frequency for $R = \infty$:

$$\tau(\lambda_0) = t(f)/t(0, \infty)$$

Dynamic spectra calculated in this way for the two models of helium distribution defined above as well as one for no helium ($R = \infty$) are shown in Fig. 5 as $\tau - \mathrm{v} - \lambda_0$.

The solid portions of the curves have been drawn to correspond with the observed frequency range in Fig. 1. It is seen that the dynamic spectral *shape* (neglecting for the moment the absolute scales of Fig. 5) of these curves shows good agreement with the observed noses.

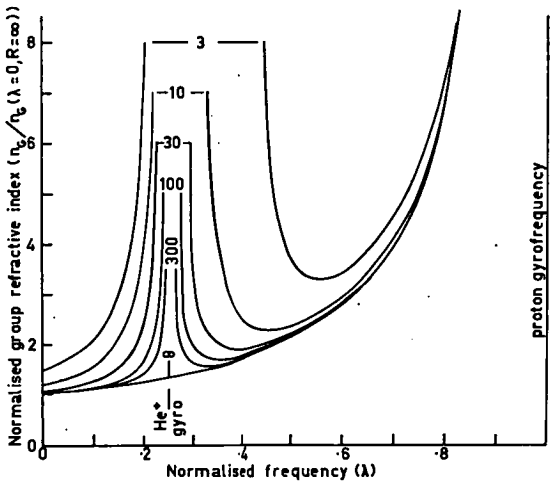

FIG. 3. NORMALIZED GROUP REFRACTIVE INDEX AS A FUNCTION OF NORMALIZED FREQUENCY FOR SEVERAL VALUES OF R.

Using methods developed for deducing data from micropulsation spectrograms[2] the minimum proton gyrofrequency along the path is about $3{\cdot}5 \pm 0{\cdot}5$ c/s. This determines the absolute frequency scale shown in Fig. 5 and locates the nose frequency at about 1·5 c/s as observed. The L-value of the field line is then 5·1 (geomagnetic terminal latitude of 64°). The proton density near the top of the path can then be calculated[2] from echo times measured from Fig. 1. This is about 8 cm^{-3} so that the helium ion density is about 0·5 cm^{-3}.

To find the absolute time scale from τ we need to know the echo order or total number of hemisphere to hemisphere hops. To make the calculated noses fit the nose in the centre of Fig. 1, this nose should have been produced by dispersion over forty-three hops and so be the twenty-first or twenty-second echo observed at Hobart. This is not clear from Fig. 1 (or the original records) though eleven echoes can be traced back in time before the earlier echoes become obscured by superposition of an earlier event.

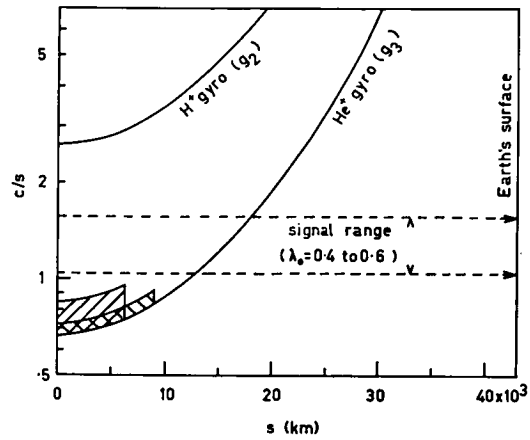

FIG. 4. PROTON AND HELIUM ION GYROFREQUENCY AS A FUNCION OF DISTANCE DOWN FROM THE EQUATORIAL PLANE ALONG A FIELD LINE OF TERMINATING GEOMAGNETIC LATITUDE 65° ($L = 5{\cdot}6$).

The band of frequency within the broken lines represents the observed signal. This must pass through the helium ion gyrofrequency to be observed on the Earth. The shaded portions correspond to the stop regions for two models of helium ion distribution down the field line.

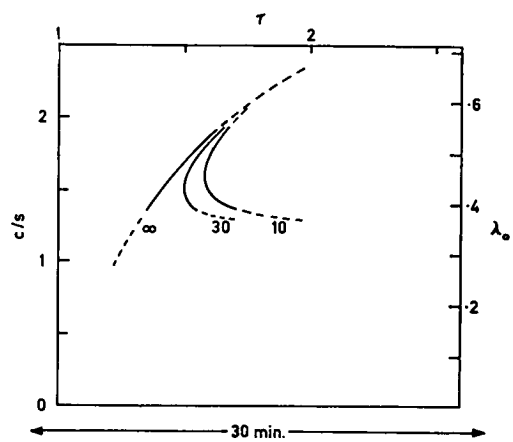

FIG. 5. DYNAMIC SPECTRA CALCULATED FOR NO HELIUM ($R = \infty$), APPROXIMATELY 3 PER CENT HELIUM OVER THE LATITUDE RANGE $\pm 14°$ ($R = 30$) AND ABOUT 10 PER CENT HELIUM OVER THE RANGE $\pm 10°$ ($R = 10$).

These may be compared with observed spectra in Fig. 1.

It is seen that a helium ion density of 3–10 per cent of the proton density ($R = 10$–30) can explain the event observed in some detail. At lower concentrations the nose would occur at a lower frequency and be sharper. A few other spectra from the Hobart events and some spectra published by other workers[3] seem to show this near the lower frequency limit. A rough estimate of R made by comparing the trend in Fig. 5 with that in Fig. 3 indicates that $R \sim 100$ or 1 per cent helium would produce these.

4. STOP REGION TRANSMISSION

So far a purely ray approach has been used. In the calculations above for the field line of Fig. 4 the region from about 12,000 km to 18,000 km (along the field line) where the

local helium ion gyrofrequency sweeps through the observed range of frequencies was assumed to be devoid of helium ions. This is unlikely to be true literally, so it is of interest to estimate the tolerable concentration of helium. This may require a full wave approach using the refractive index for a hot plasma with collisions. Coupling between the "micropulsation" or ordinary mode and the extraordinary ("fast" Alfvén) mode may also be important. However, an estimate will be made here using the W.K.B. approximation for micropulsation mode waves in a cold, collisionless plasma.

At a given frequency f, the refractive index will be imaginary over the path s_1 to s_2 where

$$\lambda_c g_2(s_1) > f \geqslant \tfrac{1}{4} g_2(s_2)$$

In this region the spacial part of the signal wave function has the form of a decreasing exponential. Using the W.K.B. approximation this has the form:

$$b \propto \exp\left(-\int_{s_0}^{s} \gamma(s)\, \mathrm{d}s\right)$$

where b is the amplitude of the perturbation magnetic field (i.e. the signal amplitude), s_0 corresponds to an arbitrary constant, and $\gamma(s)$ is given by

$$\gamma(s) = \frac{2\pi f}{c} n(0, \infty) \left[\frac{1}{R(\lambda - \tfrac{1}{4})} - \frac{1}{1-\lambda}\right]^{1/2}$$

The amplitude decrease in nepers across the stop region is then approximately:

$$\log [b(s_2)/b(s_1)] = \int_{s_1}^{s_2} \gamma(s)\, \mathrm{d}s$$

The variation of $\gamma(s)$ over this range is caused by variation of g_2 and hence λ. The important term is $(\lambda - \frac{1}{4})^{-1}$ which becomes infinite at $s = s_2$. However, for the values of R of interest the distance $s_2 - s_1$ is short so that we can treat $(1 - \lambda)^{-1}$ as a constant and assume $\lambda(s)$ is a linear function of s, so that

$$\frac{\mathrm{d}\lambda}{\mathrm{d}s} = \alpha \text{ (assumed constant)}$$

Expanding $\gamma(s)$ by the binomial theorem and integrating term by term from $\lambda = \lambda_c$ to $\lambda = \frac{1}{4}$ corresponding to the range $s = s_1$ to s_2, we find:

$$\int_{s_1}^{s_2} \left[\frac{1}{R(\lambda - \tfrac{1}{4})} - \frac{1}{1-\lambda}\right]^{1/2} \mathrm{d}s \approx 0{\cdot}79\, R^{-1/2} \frac{2}{\alpha} (\lambda_c - \tfrac{1}{4})^{-1/2} = \frac{1{\cdot}37}{b\sqrt{[R(1+R)]}}$$

using $\lambda_c = \dfrac{1 + R/4}{1 + R}$

Substituting typical values for $n(0, \infty)$ and f, g_2 and α deduced from Fig. 4 we find, for large R, that the amplitude decrease across the stop region is approximately $1500/R$ dB. This does not change significantly over the frequency range of interest because changes of g_2, α, and $n(0, \infty)$ at the relevant levels down the field line are counter balanced by the changes in f.

Since the stop region is transversed twice each hop, taking $R = 1000$ as a maximum likely value (as predicted by diffusive equilibrium theory)[5], we find a loss of 3 dB per hop.

This would seem to prohibit trains of some twenty or so echoes (forty hops). However, there is evidence that the echoing wave packet is amplified along the path since during the first half of many observed echo trains the echo amplitudes increase with order.[9] Thus for 30 dB amplification a stop region loss of this order could be sustained so that allowable values of R might be as low as 100. Finally, it might be noted that the assumption of a cold, collisionless medium and propagation in the longitudinal ordinary ("micropulsation") mode only may have lead to an over estimate of the stop region loss so that under favourable conditions a medium of relatively constant $R \sim 30$ might produce observable nosed forms.

5. DISCUSSION

The micropulsation nose whistler in Fig. 1 seems to imply a helium ion density at the time of about 3–10 per cent of the proton density. This would be required in the vicinity of the equatorial plane to produce the observed dispersion. A helium ion density of about 1 per cent of the proton density would probably produce the relatively sharp but less noticeable noses near the lower cut off frequency which are more commonly observed. The estimate of attenuation in the stop regions made above seems to require lower densities in these regions to allow observation of any micropulsation whistlers. A more complete treatment of this, however, may show that a uniform density of about 1 per cent of the proton density along most of the path is allowed.

The Ogo-A measurements are consistent with these results. Over most of the observed region (1500–30,000 km altitude) the helium ion density was of the order of 1 per cent of the proton density, and up to 10 per cent along portion of one orbit. However, the limit of detection of helium by Ogo-A[6] was about 1 cm^{-3} so that Ogo-A measurements of helium were confined to the "plasmasphere" or the magnetosphere within the knee of the radial density distribution. Micropulsation whistlers on the other hand propagate outside the knee, so that these two methods of estimating the proton–helium ion density ratio (R) refer to different regions.

It seems then that on both sides of the knee the helium ion densities are of the order of 1 per cent of the proton density. Even when observable noses are not produced, absorption by this helium may be the main factor which limits the downward frequency extent of observed micropulsations. The energy absorbed by the helium ions would mainly appear as an increase in transverse velocity since the absorbed wave is circularly polarized in the same sense as the gyration of the helium ions. This would increase the pitch angles and so tend to trap the helium ions between the absorption region and the top of the path. Since the absorption region will be near the top of the field line path, this suggests that perhaps the micropulsations are responsible for increasing the helium ion density above that expected from diffusive equilibrium theory.

An order of magnitude estimate of this could be made in the following way. Suppose the missing part of an observed signal from $\lambda_0 = 0{\cdot}25$ to $\lambda_0 = 0{\cdot}4$ (a range of 0·4 c/s for the field line of Fig. 4) is absorbed by helium. Magnetometer measurements from Ogo-1[10] indicate a micropulsation energy density in the magnetosphere of about 1 eV/cm^3 for this frequency range. For an initial helium ion density of about 10^{-2} cm^{-3} ($R \sim 10^3$) and mean thermal energy of about 0·2 eV ($T \sim 1500°K$) the transverse to longitudinal velocity ratio would be increased to about twenty corresponding to pitch angles of about 87°. This would seem quite adequate to trap the initial amount of helium. Fresh helium diffusing upwards along the field line from lower levels would tend to be trapped also. As the helium ion density increased however, the energy available from the wave per helium ion would

decrease. The final density might be limited by the finite duration of the micropulsations or might represent an equilibrium between gain by this process and loss by various scattering processes. If the former is true we might expect to observe micropulsation nose whistlers after a relatively long series of the more usual micropulsation whistlers if these occurred on the same field line.

Acknowledgements—My thanks are due to the staff of the Physics Department, University of Tasmania, from which I transferred during the course of this work. In particular to Mr. M. W. Emery who recorded and analysed the event shown in Fig. 1, and to Professor G. R. A. Ellis for stimulating discussions.

REFERENCES

1. J. A. Jacobs and T. Watanabe, *J. atmos. terr. Phys.* **26**, 835 (1964).
2. R. L. Dowden and M. W. Emery, *Planet. Space Sci.* **13**, 773 (1965).
3. Lee Tepley, *Radio Sci.* **69D**, 1089 (1965).
4. R. C. Wentworth, Lee Tepley and K. D. Amundsen, *J. geophys. Res.* **71**, 1492 (1966).
5. J. J. Angerami and J. O. Thomas, *J. geophys. Res.* **69**, 4537 (1964).
6. H. A. Taylor, Jr., H. C. Brinton and C. R. Smith, *J. geophys. Res.* **70**, 5769 (1965).
7. E. Astrom, *Ark. Fys.* **2**, 443 (1950).
8. R. L. Dowden, *Planet. Space Sci.* **13**, 761 (1965).
9. J. A. Jacobs and T. Watanabe, *J. atmos. terr. Phys.* **28**, 235 (1966).
10. R. E. Holzer, M. G. McLeod and E. J. Smith, *J. geophys. Res.* **71**, 1481 (1966).

Резюме—Динамические спектры микропульсации по временам выявляют ряд носовых тонов, вместо более обычных, чисто-усиливающихся тонов. Таковые объясняются довольно детально при условии, что иногда от 3 до 10% содержания ионов во внешней магнитосфере, являются гелием (He^+). Несмотря на то, что это одним или двумя порядками величины больше, нежели предвиделось на основании теории диффузивного равновесия, это в общих чертах согласуется с недавними измерениями Ого-А.

Letters

Possible Helium Ion Effects in Micropulsation Spectrograms

R. L. DOWDEN

Physics Department, University of Otago, New Zealand

Spectrograms of micropulsation 'pearls' (Pc typically show a series of rising tones of frency of the order of 1 cps and repetition es of the order of 1/min. According to curt ideas [e.g. *Jacobs and Watanabe,* 1964], is an expression of dispersion of a hydrognetic wave packet guided by a magnetic d line through the magnetosphere in a way ilar to VLF whistlers. Agreement with obved dynamic spectra is obtained in most es assuming an impulsive source, propagation the proton-cyclotron or 'micropulsation' de, a pure hydrogen magnetosphere, and able models of the proton density distribu- along a field line (the spectral shape is tively insensitive to changes in this model). observed rising tones would then corrend to dispersion produced over many hemiere-to-hemisphere hops. The origin of the romagnetic wave packet is unknown, and it may not be strictly impulsive (like a F 'sferic'), but, if the original emission is erated over a path length short compared n the total path length of many (50, or so) s, the resulting dynamic spectum would be stinguishable from one produced by an imse.

However, if the magnetosphere contains ion- helium (He^+) in concentrations (particle sity) of, say, 3% of the proton number sity, the dispersion of the wave packet ld be significantly different in the vicinity he local helium ion cyclotron frequency. Re- measurements by OGO-A [*Taylor et al.,* 5] at altitudes from 1500 km to about 30,000 showed helium ion number densities of ut 1% of the proton density over most of range and some values up to about 10% nerally at the greatest altitudes). It should pointed out that these measurements were fined to the inner magnetosphere, that is, the region inside the knee of the plasma density distribution, whereas micropulsations appear to propagate in the outer magnetosphere. However, the solar wind is about 10% helium and may even be the source of the unexpectedly large concentrations of helium measured in the inner magnetosphere. Thus it is worthwhile to examine the effects of (say) 3% helium in the outer magnetosphere on micropulsation spectrograms. One such effect has been considered recently [*Dowden,* 1966]. In view of recent observations by *Heacock* [1966] this work is extended here.

The refractive index expression for longitudinal propagation in the micropulsation mode (ion cyclotron or Alfvén 'slow' mode) in a hydrogen-helium magnetosphere is given elsewhere [*Dowden,* 1966]. For a hydrogen-helium ion number density ratio of 30 (i.e. 3% helium), the behavior of both the phase and group refractive indices is shown in Figure 1. The group refractive index becomes infinite at the helium ion cyclotron frequency and at the frequency where the phase refractive index passes through zero. The band defined by these two frequencies is a stop region since the phase refractive index is imaginary.

The dynamic spectrum (delay time versus frequency) produced by dispersion of a hypothetical impulse propagating in a medium of constant magnetic field and constant proton and helium ion densities would have the shape of the group refractive index curve in Figure 1. This is because the travel or delay time at any frequency would be equal to the group refractive index at that frequency multiplied by the distance travelled in light-seconds. Note that the spectrum is split into an upper and lower band separated by a stop band where the refractive index is imaginary. In the real case of interest (propagation in the magnetosphere)

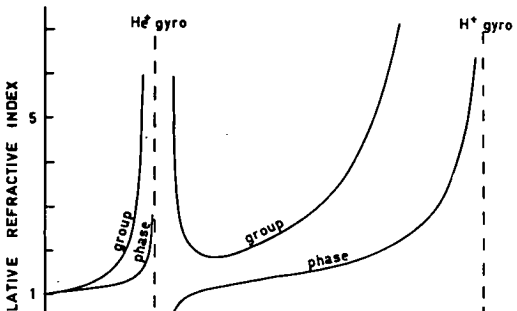

Fig. 1. Phase and group refractive indices, relative to zero frequency values, for longitudinal propagation in a magnetosphere of 3% helium (He^+) and 97% hydrogen (H^+).

the magnetic field strength changes along the path so that a component of the wave packet at a frequency greater than the minimum helium-ion cyclotron frequency along the path (the geomagnetic field line) must encounter a stop region somewhere along the path. This would seem to remove the possibility of observing an upper band. We will avoid this difficulty here by supposing that the helium is appreciable only within about 15° of the equatorial plane that corresponds to about 20% of the field line path length. This limitation may be unnecessary if coupling to the electron cyclotron mode or wave 'tunneling' through a short stop region is appreciable.

The dynamic spectra shown in Figure 2 have been calculated for a field line of about $L = 8$ (minimum proton cyclotron frequency of 1 cps), a proton density model for which the density is proportional to the magnetic field, and a helium ion density of 3% of the proton density along the outermost 20% of the field line path and zero over the remainder. The series of progressively dispersed traces shown corresponds to a train produced by many hemisphere-to-hemisphere hops of the wave packet. Note that the micropulsation spectrum is split into an upper and lower band. The upper limit of the lower band is the minimum helium ion cyclotron frequency along the path (0.25 cps). The upper band extends from the minimum proton cyclotron frequency (1 cps) down to the maximum frequency for which the phase refractive index passes through zero along the path. This frequency is determined by t latitudinal extent, along the path, of heli (0.35 cps for the model used here). As seen Figure 1 this frequency at any level is sligh greater than the local helium ion cyclotron f quency, so that if the helium ion density alo the path is significant beyond about 33° fr the equatorial plane, then the upper band v not be observed at all (unless wave tunneli or mode coupling is appreciable). If losses considered, the upper limits will be below t minimum cyclotron frequencies. The over- lower limit (i.e. lower band) may be determin by the emission or amplification process or propagation.

Little is known about the distribution a time variation of helium in the outer magne sphere. If we suppose that both the spac distribution and the relative concentration helium varies in time (perhaps with magne disturbance or solar wind variation), we wou expect normal Pc 1 micropulsations when helium is insignificant, a two-band structure in Figure 2 when the helium ion concentrat is significant only in the upper regions or n the equatorial plane, and the lower band alo when the helium ion concentration is signific at lower levels also.

To what extent do these ideas fit the prop ties of the 4-sec period band and the occ ionally associated Pc 1 micropulsations scribed by *Heacock* [1966]? The spectrogra of events when both bands occur simultaneou [Figure 7, *Heacock*, 1966] do not appear

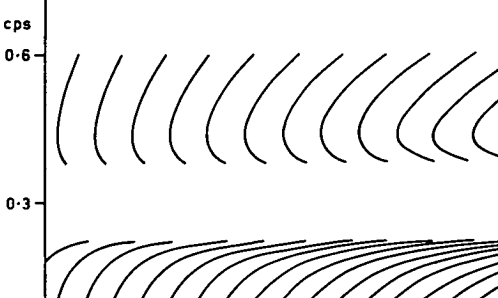

Fig. 2. Dynamic spectra expected from persive propagation in a hydrogen-helium m netosphere.

y as the calculated one in Figure 2. How-
, it is of interest to see nosed forms in his
er band as expected and also that the fre-
ncies of the upper and lower bands occur
bout the same ratio as those shown in Fig-
2. Heacock's observation that the lower
d (4-sec) activity is most prominent at
es of higher K_p, while the upper band ac-
ty is most prominent at lower values of K_p,
simultaneous occurrence is relatively rare,
in with the above ideas if the helium ion
centration and distribution increases with
On the other hand, Heacock's observation
the structure repetition period in the
er band is often shorter than in the lower
d is difficult to explain in these terms unless
the lower part of the upper band and the
ermost part of the lower band is observable
also Figure 1).

he purpose of this letter has been to point
the dispersion effects of helium ions in the
r magnetosphere. The evidence that Hea-
k's 4-sec period band is the lower band dis-
ed here is only suggestive. The evidence for
elium explanation of the nosed forms in the upper band is stronger [*Dowden*, 1966]. A theoretical investigation should be made to determine the maximum allowable helium ion concentration in the lower parts of the path for adequate transmission through the stop region. If these ideas can be placed on a sound footing, micropulsation spectrograms could be used for investigating the proton and helium ion distributions in the outer magnetosphere, which are not easily obtainable by other means.

References

Dowden, R. L., Micropulsation 'nose whistlers'. A helium explanation, *Planetary Space Sci., 14,* 1273–1280, 1966.

Heacock, R. R., The 4-second summertime micropulsation band at College, *J. Geophys. Res., 71,* 2763–2775, 1966.

Jacobs, J. A., and T. Watanabe, Micropulsation whistlers, *J. Atmospheric Terrest. Phys., 26,* 825–829, 1964.

Taylor, H. A., H. C. Brinton, and C. R. Smith, Positive ion composition in the magnetoionosphere obtained from the Ogo-A satellite, *J. Geophys. Res., 70,* 5769–5781, 1965.

(Received October 24, 1966;
revised December 16, 1966.)

Dotted Pearl Micropulsations

R. L. DOWDEN

Physics Department, University of Otago, New Zealand

Spectrograms of pearl (Pc 1) micropulsations show dotted rising tones. It is suggested here that the dot structure is due to interference between the two components of a double tone or 'hook.' The observed dot structure could be produced by a nonconvective cyclotron instability of protons of about 100-kev energy and 60° pitch angle.

1. INTRODUCTION

'c 1 or 'pearl' micropulsations appear on amic spectrograms as dotted rising tones at quencies of the order of 1 Hz spaced about a ute apart. This is believed [e.g., *Jacobs and tanabe*, 1964] to be produced by dispersion n impulsive wave packet, propagating in the ton-cyclotron or L mode along a field line in magnetosphere over several hemisphere-to-isphere hops. However, little is known about generation of the initial wave packet or the se of the dot structure. In this paper, I gest a process of generation of an initial wave ket that would be observed after dispersion a dotted rising tone, as though a 'dotted ulse' had occurred at the top of the field

2. DOT STRUCTURE

typical dotted pearl event is shown in Fig- 1. It is seen that the frequency interval be- en dots is of the order of 0.1 Hz. To find the ribution of this interval, measurements were de from a large number of spectrograms. A ogram of this is shown in Figure 2. The k occurs at about 0.07 Hz. There is some ht evidence of subsidiary maxima at twice three times this frequency. This would be duced if dots are occasionally missed, so that measures the interval over two or three s.

n making these measurements, a few other perties were noticed. In general, as one looks n one rising tone to the next, the dots ap- r at very nearly the same frequencies. There ns to be a general tendency, when scanning in frequency along a given rising tone, for dot interval to decrease; that is, the dot structure becomes finer with frequency. Also, on the average, the holes between dots span about the same frequency interval as the dots themselves.

The following properties have been noted by *Kenney and Knaflich* [1967]. If the same pearl event is observed at widely spaced stations, the dot structure is identical; therefore, the dots cannot be produced by ionospheric duct propagation. The dot structure seems peculiar to pearls, for the structured elements of rising tones in irregular pulsations of diminishing periods (IPDP) are continuous, not dotted. A consistent harmonic relationship between the dot frequencies has not been found so far.

Various suggestions to explain dotting, based on generation or propagation of a set of discrete frequencies, have been discussed recently by *Jacobs and Watanabe* [1967]. In an earlier paper [*Dowden*, 1965], I suggested that dotting might be an interference effect. In this paper, I will discuss interference effects produced by two wave packets arriving at the observer's receiver at slightly different times, that is, within a time interval less than the time resolution of his spectrograph.

3. TIME INTERVAL INTERFERENCE

Consider two short 'dc' pulses occurring at time zero and at time T. If these are idealized as delta functions, the total function can be represented by

$$F(t) = \delta(0) + \delta(T)$$

The Fourier transform (unnormalized) of this is given by

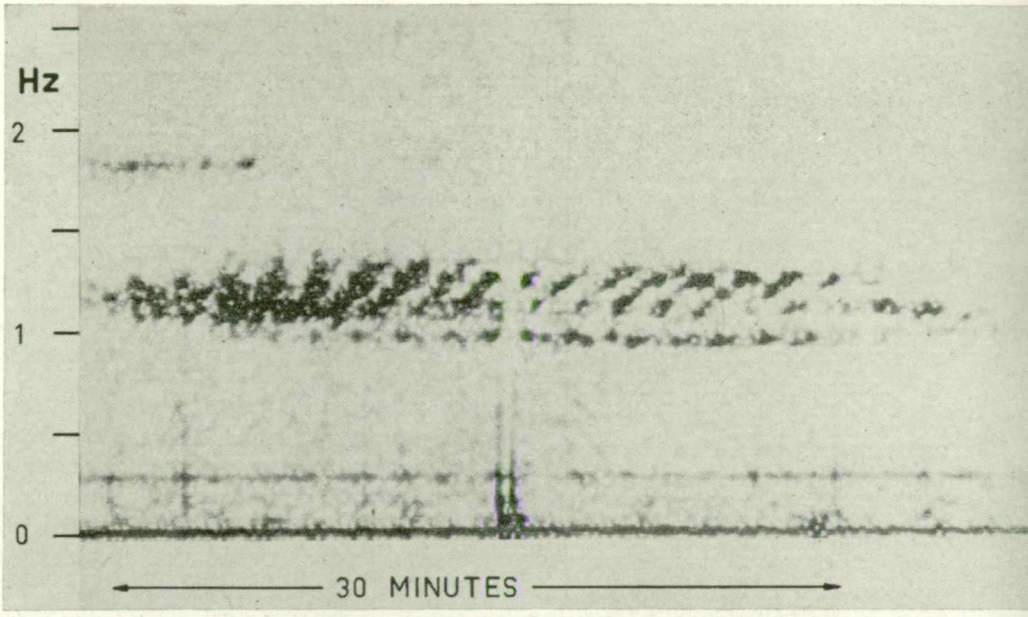

Fig. 1. Pearl event recorded at Hobart (April 10, 1964). An hour mark (1800 UT) appears as a double impulse near the middle of the event.

$$G(f) = \int_{-\infty}^{\infty} F(t) \exp(-i2\pi ft)\, dt$$

$$= 1 + \exp(-i2\pi fT)$$

So the real part of $G(f)$, $1 + \cos 2\pi fT$, is maximum for integral values of the product fT and zero when this product is integral plus one half.

From this we see that the dynamic spectrum or frequency-time spectrogram of a single such pulse is a vertical line (i.e., parallel to the frequency axis). Two such pulses separated by time T will appear as two vertical lines, if T is large, and a single dotted line, if T is small. In the latter case, the frequency interval between dots is $1/T$. If the dynamic spectrograph has frequency resolution Δf and time resolution Δt, it will resolve the vertical lines if $T > \Delta t$, and it will resolve the dots if $1/T > \Delta f$. For a good spectrograph, $\Delta f \cdot \Delta t \approx \frac{1}{3}$, and, therefore, for some such double pulses both the time structure (vertical lines) and the frequency structure (dots) can be resolved.

This is illustrated in Figures 1 and 3. The hour marks have been produced by passing a 40-second 'pulse' of current into a loop that was inductively coupled into the antenna loop. This produced in the receiver two voltage spikes (actually of opposite sign, but this is not relevant here) 40 seconds apart. The sonogram Figure 1 was made with $\Delta f = 0.03$ Hz $\Delta t = 10$ seconds, so that the double pulse pears as two vertical lines without resolved structure. For Figure 3, the micropulsation was played at double speed, so that here Δ 0.015 Hz and $\Delta t = 20$ sec. In this case, the vertical lines and the dot structure of 0.0 Hz spacing are resolved. VLF spectrogr usually show dotted sferics as in Figure 4. T would occur whenever two lightning impu arrive at the receiver within a few millisec of one another.

It is interesting to look at the phy process. A dynamic spectrograph effecti consists of a large number (a few hundred narrow band filters that span the freque range of interest. The 'rayspan' is of just

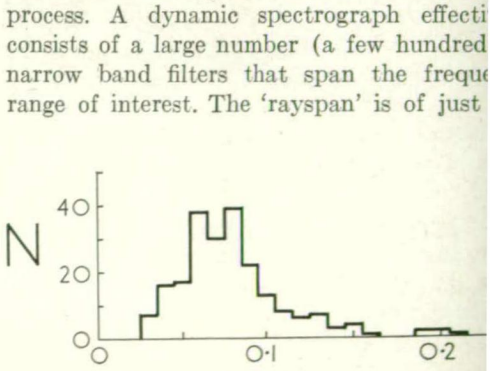

Fig. 2. Histogram of the frequency interval tween dots.

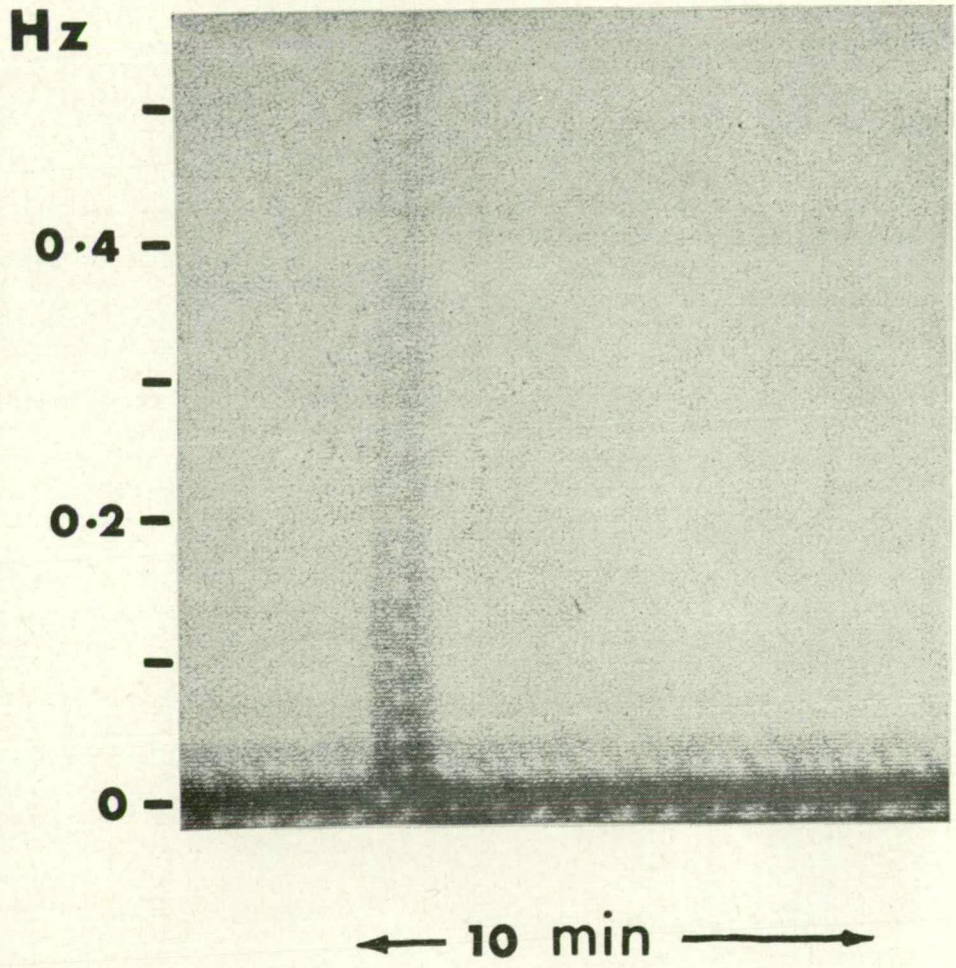

Fig. 3. Enlarged portion of a sonogram of the hour mark played at double speed. Note that the second impulse is dotted.

ı, and the 'sonograph' synthesizes this by g a single filter a few hundred times. Con- the response of such an array of filters to louble pulse discussed above. The first pulse set all the filters ringing for a time of the r of the time resolution Δt. This on its own d produce a continuous vertical line (paral- o the frequency axis) on the display system. ıe second pulse arrives after time $T \gg \Delta t$, ı the filters have stopped ringing, this sec- pulse will produce a similar line. If the nd pulse arrives while the filters are still ng ($T < \Delta t$), it will augment the ringing ome and reduce it in others, depending on phase of the ringing in each filter when the second pulse arrives. This will produce a dotted line on the display.

Consider now the more general case of two gliding tones that can be represented by WKB solutions:

$$F(t) = \cos\left(2\pi \int_{t_0}^{t} f_a \, dt\right) + \cos\left(2\pi \int_{t_0}^{t} f_b \, dt\right) \quad (1)$$

where f_a and f_b are the instantaneous frequencies at time t, and we suppose that the two signals were in phase at some time t_0. This can also be put in the form

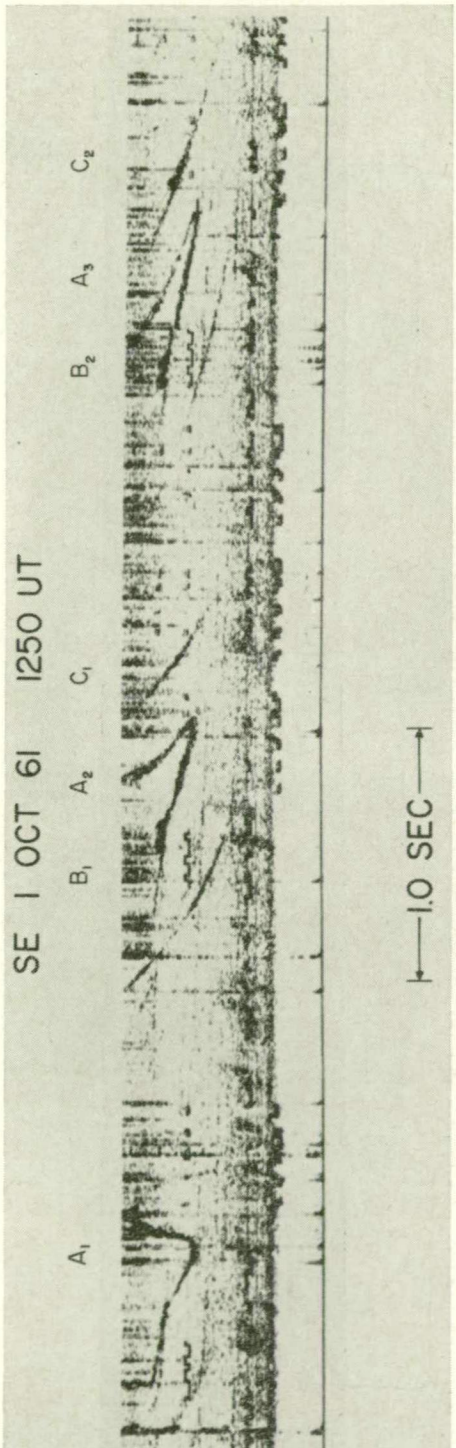

Fig. 4. VLF hooks (*A1*, *A2*, *A3*) and whistlers (*B1*, *B2* and *C1*, *C2*) echoing in the whistler mode over the same path (figure with caption after *Brice* [1962]). Note also dotted sferics.

$$F(t) = 2 \cos\left(2\pi \int_{t_0}^{t} \bar{f}\, dt\right) \cdot \cos\left(\pi \int_{t_0}^{t} \delta f\, dt\right)$$

where $\bar{f}$ is the mean frequency and δf is
difference frequency at time t. This is in the f
of an amplitude modulation of the mean
quency. Maxima (dots, in our case) occur
the times for which

$$\int_{t_0}^{t} \delta f\, dt = \text{an integer}$$

This integral is the phase difference (in cyc
at time t between the two signals, which
accumulated since time t_0. Maximum amplit
(dots) will occur near those times for w
the phase difference is an integral numbe
cycles.

Figure 5 shows two time-varying tones star
from a common point, and hence clearly in ph
at time t_0. Since 'area' in the frequency-
plane has dimensions of phase (units of cyc
the phase difference accumulated up to time
the area enclosed by the two tones up to tir
At time t_1, this is unity; that is, the phase
ference is one cycle, so that a dot will occu
the mean frequency curve. The frequency
this dot is approximately $\bar{f}(t_1)$.

The dot frequencies can be determined
more direct way. A narrow band filter at
set ringing by the first tone it encounters
the second tone arrives exactly in phase
this ringing, this filter will be augmented r
than adjacent ones. That is, a dot will o
centered on f_1. The phase condition is that
phase enclosed by the closed path BOAB i
integral number (unity for f_1) of cycles.
can be determined by equation 3, or more
veniently by integrating in the frequency d
tion, giving the condition

$$\int_{f_0}^{f} T\, df = \text{an integer}$$

where $T(f)$ is the time interval between the
tones at frequency f, and f_0 is some other
phase frequency (in this case the point of
mon origin). Since the dot frequencies are
changed by arbitrary dispersion, this is a ge
condition applying also in cases where the di
ence frequency δf is not definable, as in the
of the two impulses considered above.

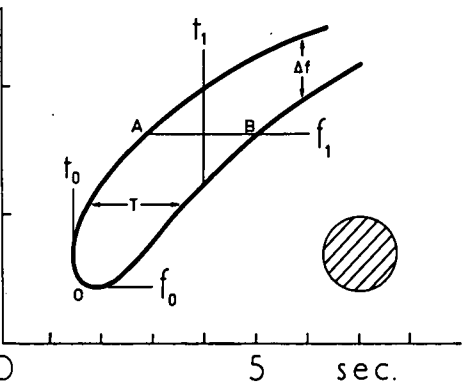

g. 5. Arbitrary double rising tone that di-
es from a common point. The enclosed
se between t_0 and t_1, or between f_0 and f_1, is
cycle. A dot of at least the size shown by
shaded circle (⅓ cycle enclosed phase) will
r near f_0, t_0, and f_1, t_1, etc.

we define the mean interval $\bar{T}$ between two
s over the frequency range from one dot
uency (f_n) to the next (f_{n+1}) as

$$\bar{T} = \int_{f_n}^{f_{n+1}} T\, dt/(f_{n+1} - f_n)$$

since the phase integral is unity,

$$\bar{T} = (f_{n+1} - f_n)^{-1}$$

s means a smoothed form of $T(f)$ can be
ıced from the observed dot frequencies.
e, from Figure 2, the dot spacing is typically
Hz, then T is typically 15 seconds.
he size of a dot in a spectrogram will be at
that determined by the bandwidth and
ing time of the spectrograph filters. Such a
mum size ($\Delta f \cdot \Delta t \sim$ ⅓ cycle) is indicated
the shaded circle in Figure 5. It will gen-
y extend along the direction (in the fre-
ıcy-time plane) of the mean frequency (or
) curve a distance of about half the dot
ing.
ıppose (as in section 4 below) we wish to
ılate the phase difference, $\Delta\phi(f)$, at fre-
ıcy f between two signals originating from
mpulse at point $s = 0$, which have traveled
different paths (1 and 2) to the observer.
n (4) we find

$$\Delta\phi(f) = \int_{f_0}^{f} T\, df \qquad (5)$$

re $T(f)$ is the interval between the arrival of the two wave packets, that is, the difference between the two *group* travel times. This interpretation of T is consistent with the way (4) was derived, though it may seem odd to determine phase from group travel time. It would seem more appropriate to say that the phase length (in cycles) along path 1 is ft_p, and that along path 2 is ft_p, where t_p is the *phase* travel time, so that at the observer

$$\Delta\phi(f) = (t_{p_1} - t_{p_2})f = T_p f \qquad (6)$$

However, these two expressions (5 and 6) are equivalent. The phase and group travel times for each path are

$$t_p = \frac{1}{c}\int_0^s n_p\, ds, \quad \text{and} \quad t_g = \frac{1}{c}\int_0^s n_g\, ds$$

where

$$n_g = \frac{d}{df}(n_p f)$$

or

$$n_p f = \int_{f_0}^{f} n_g\, df$$

Then the phase length along path 1 using (5) is

$$\phi_1 = \int_{f_0}^{f} t_{g_1}\, df$$
$$= \frac{1}{c}\int_{f_0}^{f}\int_0^{s_1} n_{g_1}\, ds\, df = \frac{1}{c}\int_0^{s_1} n_{p_1} f\, ds$$
$$= t_{p_1} f$$

From a similar expression for ϕ_2, we see

$$\Delta\phi(f) = \int_{f_0}^{f} T\, df = T_p f$$

Either (5) or (6) may be used, depending on convenience, provided f_0 is appropriately chosen.

4. Double Tones

If dotted rising tones can be described precisely by expression 2, they can also be described by the mathematical equivalent expression 1. That is, dotted tones and double tones are equivalent, so that we might look for a physical process that inherently produces double tones rather than one that directly modulates a single tone. Such a double tone might be pro-

duced by double generation or double propagation (i.e., two paths) in the magnetosphere.

Consider the latter first, that the double tone (and ultimately the dot structure) is produced by a single impulse that propagates along two slightly different paths in the magnetosphere. This might be justified by supposing that trapping in field-aligned columns of ionization is important and that the impulse seeks out the two nearest columns on either side of it.

The two wave packets will then propagate along slightly different field lines and so have slightly different propagation times. With each successive hemisphere-to-hemisphere hop, the interval (T) between the arrival times at the receiver of the two wave packets will increase, so that the dot structure will become progressively finer. The dot frequencies will change progressively from riser to riser. Eventually the wave packets will arrive at opposite hemispheres simultaneously giving an in-phase relationship between conjugate receivers and 'structure doubling' at both.

The deduced properties of two path propagation do not seem to fit those observed. Also, it is difficult to justify two paths. Theoretical considerations [*Dowden*, 1965] indicate that the wave packet is adequately guided along field lines in the absence of field-aligned columns.

Many insights into the understanding of ULF phenomena have been gained by analogy with VLF phenomena. However, the possible resolution and hence information in spectrograms of ULF phenomena is much less than that in VLF phenomena. As pointed out above, the minimum grain size, $\Delta f \cdot \Delta t$, on a spectrogram has an 'area' (enclosed phase) of about $\frac{1}{3}$ cycle. A typical ULF rising tone, as in Figure 1, has a frequency range of about 10 Δf and an interval between rising tones of about 10 Δt. The dispersive periodic VLF emission (A_1, A_2, A_3) shown in Figure 4 [*Brice*, 1962], on the other hand, has a frequency range of about 60 Δf (3 kHz) and echo interval of about 300 Δt (2 seconds), so that fine structure is easily observable.

The emission in Figure 4 is of the type known as a 'hook.' After successive dispersion (A_2, A_3), it becomes a double falling tone of the same general shape as the lightning-flash-initiated whistlers (B_1, B_2 and C_1, C_2) also shown. Perhaps dotted pearl micropulsations are the counterpart of periodic VLF hooks. In the VLF regime, the double falling tones are resolved such, whereas in the micropulsation or U regime the sense of the dispersion is reversed and the double tones would be observed as equivalent dotted rising tones. Note that dot frequencies would be constant from rising tone to the next, and the dot spacing al a rising tone would decrease as observed. the next section, I discuss processes that mi generate such ULF hooks.

5. Generation of Hooks

Theories that have attempted to desc the detailed dynamic spectral (frequency-ti shape of VLF hooks are based on movemen a relatively localized emission source alon geomagnetic field line. [*Gallet and Helliw* 1959; *Dowden*, 1962*a*, *b*; *Helliwell*, 1967]. the first two of these three, the emission sou is an isolated bunch of charged particles (e trons) that therefore moves with velocity eq to the average longitudinal component of p ticle velocity. In the third [*Helliwell*, 1967] emission source is a localized interaction reg in a continuous stream of particles. This in action region tends to drift in the direction the particles, though generally at a slower sp

Consider then a localized emission sou (whether a bunch or interaction region o stream), moving along a geomagnetic field with velocity v_t. Suppose that the local plas and gyrofrequencies, f_p and f_H, at a point s o field line have the same values at the conjug point s^*, where s and s^* are at equal distan from the midpoint (equatorial plane) of field line, O, as shown in Figure 6. If the sou travels from one hemisphere to the other,

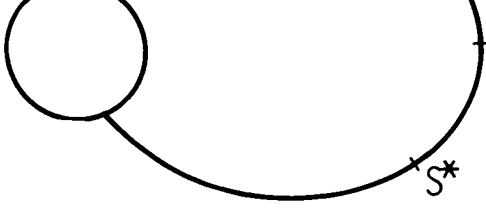

Fig. 6. Localized particle bunch (dot) tra ing in the direction sOs^* and emitting a wav the opposite direction.

conservation of magnetic moment of the rticles holds, then the longitudinal velocity the particles, $\beta_{\parallel}c$, will be the same at s and s^*. this is also true of the emission angle θ, then emission frequency f will be the same at nd s^*.

Suppose then, an emission source traveling up field line toward the equatorial plane emits the backward direction (down the field line ward the earth) the frequency f at point s l again at point s^*. From s downward, both issions at frequency f travel the same path, that the time interval $T(f)$ between recep- n on the earth of these two components is sum of the times taken by the emission rce to travel from s to s^* and the wave ket (at frequency f) to travel from s^* to s. on the other hand, the source emits in the ward direction, $T(f)$ would be the difference ween the source and wave packet travel es for the trip s to s^*. In both cases, $T(f)$ is hook 'width' at frequency f. This determines dot structure of an unresolved hook.

We now need to see what determines the pe of an unresolved hook, that is, the fre- ncy-time shape of a ULF rising tone. Sup- e for the moment that the velocity of the ission source v_i is either constant or at least mmetric about O, so that $v_i(s) = v_i(s^*)$ for points s, s^*. This would produce a symmetry the emission times also, so that the com- ent at frequency f of a hypothetical impulse urring at O, at the instant the source passes ough O, would be received on the earth at a e halfway between the times of reception of real emissions at this frequency f generated s and s^*. This is true for all frequencies gen- ted (and corresponding points s, s^*), so that curve that bisects the two halves of the k will have the form of a hypothetical im- se at the midpoint O dispersed during propa- ion in the appropriate mode from O to the erver. That is, the bisector of the first hook arrive at the earth is a ½-hop whistler. ltiple echoes of this hook will show disper- ns of this bisector in the ratio $\frac{1}{2} : 2\frac{1}{2} : 4\frac{1}{2}$ one end of the field line, and $1\frac{1}{2} : 3\frac{1}{2} : 5\frac{1}{2}$ he other end.

f $v_i(s)$ does not vary symmetrically about the dispersed impulse would not bisect the k, though for a moderate degree of asym- ry it would still lie within the hook. In the ULF case, the hooks are not resolved, so that the sequence of rising tones should have the frequency-time shapes of an impulse dispersed in the ratos given above.

It should be noted here that observed events may be considerably modified by amplification and attenuation in the magnetosphere and ionosphere. The first few echoes in many pearl events show increasing amplitudes that suggest an amplification process. *Liemohn* [1967] has shown that suprathermal protons can produce amplification of ULF signals in the magnetosphere. Thus, it seems likely that in many events the first rising tone observed has already been dispersed by several hops. Also the frequency span observed may be less (but not more) than that generated.

6. Emission Instability

In general, the emission frequency is given by [*Eidman*, 1958]

$$f = m\gamma f_H'/(1 - n_{\parallel}\beta_{\parallel}) \qquad (7)$$

where $n_{\parallel} = n \cos \theta$ is the longitudinal component of the refractive index of the medium for propagation at frequency f and at wave normal angle θ in the appropriate mode. This is simply the Doppler-shifted frequency of an oscillator in motion. The oscillator frequency, $\gamma f_H'$, is the relativistic cyclotron frequency of the emitting particles. The type of instability is determined by m, which takes integral values: $0, \pm 1, \pm 2, \cdots$, etc.

We require emission and propagation in the ULF L mode at frequencies $f < f_H$. For negative values of m (anomalous Doppler shift), we may need relativistic electrons. For positive values of m, the conditions are met by protons of reasonable energy for $m = 1$, and $m = 0$, but considerably greater for $m > 1$. Since low-energy particles are much more abundant than high-energy particles, I shall consider only $m = 1$ and $m = 0$ for which the relativistic term γ is very close to unity. These two values correspond to backward cyclotron and Cerenkov instabilities, respectively.

For $m = 1$, since $f < f_H$, the product $n_{\parallel}\beta_{\parallel}$ must be negative, which means that the particles and the generated wave travel in opposite directions (backward emission). Substituting in (7), taking $n_{\parallel}$ and $\beta_{\parallel}$ as positive quantities, we get

$$f = f_H/(1 + n_\parallel\beta_\parallel)$$

or the condition on $n_\parallel$

$$n_\parallel = \left(\frac{f_H}{f} - 1\right)/\beta_\parallel \qquad (8)$$

For $m = 0$, and $f \neq 0$, we require

$$1 - n_\parallel\beta_\parallel = 0$$

or

$$n_\parallel = 1/\beta_\parallel \qquad (9)$$

In this case, the particles and generated wave travel in the same direction (forward emission). The emission frequency in each case is given by substituting in (8) and (9), respectively, $n_\parallel$ for the ULF L mode, given by *Dowden* [1965]:

$$n_\parallel^2 = \frac{(f_p/f_H)^2 \cos^2\theta}{1 - \frac{1}{2}\sin^2\theta - [\frac{1}{4}\sin^4\theta + (f/f_H)^2\cos^2\theta]^{1/2}} \qquad (1$$

At the highest frequency of interest ($f/f_H \sim 0.6$), $n_\parallel(\theta)$ varies by only 30% over the whole range of θ. At lower frequencies the variation is even less.

For protons of the appropriate energy, the emission and growth will occur in whatever combination of m and θ that produces the strongest instability or most rapid growth. For $m = 1$ (cyclotron), the emission frequency is almost independent of θ, being always within 8% of the value for $\theta = 0$. This is not so for $m = 0$ (Cerenkov), though the velocity ($\beta_\parallel$) required for resonance varies with θ only slightly (<30%). Also the generated wave is strongly guided for all values of θ [*Dowden*, 1965]. So for both instabilities, effects (dotted pearls) calculated for $\theta = 0$ will be reasonably similar to those for other values.

For $\theta = 0$ then, (10) becomes

$$n_\parallel^2 = (f_p/f_H)^2/(1 - f/f_H)$$

Substituting in (8), the generated frequency for the cyclotron instability is given by

$$(1 - f/f_H)^3/(f/f_H)^2 = (\beta_\parallel f_p/f_H)^2 \qquad (11)$$

And similarly from (9) the Cerenkov frequency is given by

$$f/f_H = 1 - (\beta_\parallel f_p/f_H)^2 \qquad (12)$$

Although we might determine the relative importance of the two instabilities ($m =$ or 0), it is of interest to see if either or bo can produce the observed dot structure.

Using the appropriate models for f_p and the generated frequency in each case can found as a function of position (s) along a fi line. The wave packet and source travel tin from s to s^* (the two points where frequer f is generated) determine the interval $T(f)$ tween the arrival at the earth of the emissic from these two points. For backward cyclotr emission ($m = 1$), $T(f)$ is the sum of the t travel times; whereas for Cerenkov emissi which is forward, $T(f)$ is the difference of th times (assuming positive source velocities).

As shown in section 3 above, the emissions a their multiple hop echoes would be observed

dotted risers, the frequency interval betwe consecutive dots being $1/\bar{T}(f)$. However, it is interest to examine first the equivalent hoo for the two instabilities. The hook is determir by its 'width' $T(f)$ at each frequency and bisector curve that has the form of a 1/2-h ULF whistler.

Figure 7 shows such a hook for each ins bility. I used a dipole model for f_H and model $f_p^2 \propto f_H$ (plasma density proportional magnetic field) for f_p. At the top (equator) the field line I chose $f_H = 2$ Hz and $f_p = 300$ These are typical of values deduced from pe dispersion measurements [e.g., *Dowden* & *Emery*, 1965]. To obtain a reasonable f

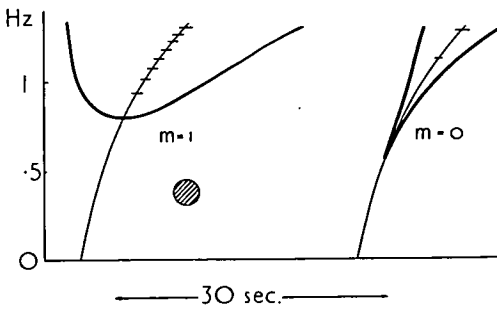

Fig. 7. Calculated spectrograms of a cyclot hook and a Cerenkov hook. The ticks on the sector curves indicate dot frequencies. The sha circle indicates the resolution grain size.

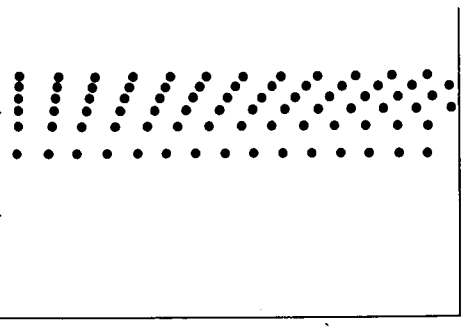

15 min.

g. 8. The cyclotron hook and its echoes
n to a frequency-time aspect ratio similar to
of Figure 1, so that the hooks appear as dot-
ising tones. The dots have minimum size (⅓
).

ıcy span and time width ($T \sim 15$ seconds),
ose protons of 100-kev energy and mini-
ı (i.e., at the top of the field line) pitch
e of 60° for the cyclotron hook. For the
nkov hook, I chose proton energy and
ı angle (15 kev, 20°) to produce a wide
, though it is not wide enough to produce
ical dot structure.

or calculation of $T(f)$ and hence dot struc-
I have assumed $v_t(s) = \beta_{\parallel}(s)c$ for both
bilities. In the case of VLF emission by
rons through the cyclotron instability,
well [1967] regards this as an upper limit
$_t$ expected only under conditions of very
particle fluxes. In the ULF case, this as-
ption can be regarded as a simplifying one
first approximation that should be investi-
d more thoroughly later. Note, however,
if the ULF instability is cyclotron, this
mption gives the dot structure typically
rved (see below). If the source velocity v_t
uch less than this, the hooks would be re-
d, and the dot structure would be unre-
d.

ıe dot frequencies deduced from the phase
gral (4) are shown by ticks on the bisector
es. Note that for the Cerenkov hook only
appear, the first at over twice the minimum
ıency generated. For the cyclotron hook,
dot frequency intervals range from 0.14 to
Hz, which are typical values as seen in
re 2. Since T increases with frequency, the
interval decreases. Figure 8 shows the
l (½ hop) cyclotron dotted riser and sub-

sequent echoes. The dots are shown as circles of size $\Delta f \cdot \Delta t \sim \frac{1}{3}$ cycle. The lowest dot may be elongated slightly up the rising tone, and the top few may be elongated in the time direction (since $T \sim 20$ seconds).

It seems that if ULF emissions are produced by a nonconvective instability in the magnetosphere, the cyclotron instability rather than the Cerenkov explains the observed dot structure. It is interesting to note that the *proton* energies and pitch angles required to match the observed features of typical ULF emissions are remarkably close to the *electron* energies and pitch angles required to match those of typical VLF emissions (hooks), if both are produced by the cyclotron instability [*Dowden*, 1962*a*, *b*]. In both cases, if the generation is as outlined above, the energy and pitch angle of the particles could be determined from measurement of $T(f)$ and the minimum frequency generated, f_0 [*Dowden*, 1962*c*]. In the ULF case (dotted pearls), $T(f)$ could be estimated from the dot frequencies, f_0, f_1, ... , if these are observed and identifiable. One might be able to check from the form of $T(f)$ whether the lowest frequency observed is f_0 (the lowest frequency generated).

References

Brice, N. M., Discussion of paper by R. L. Dowden, 'Doppler-shifted cyclotron radiation from electrons: A theory of very low frequency emissions from the exosphere,' *J. Geophys. Res., 67*, 4897, 1962.

Dowden, R. L., Doppler-shifted cyclotron radiation from electrons: A theory of VLF emissions, *J. Geophys. Res., 67*, 1745, 1962*a*.

Dowden, R. L., Cyclotron theory of VLF discrete emissions, *Nature, 195*, 1085, 1962*b*.

Dowden, R. L., Method of measurement of electron energies and other data from spectrograms of VLF emissions, *Australian J. Phys., 15*, 490, 1962*c*.

Dowden, R. L., 'Micropulsation mode' propagation in the magnetosphere, *Planetary Space Sci., 13*, 761, 1965.

Dowden, R. L., and M. W. Emery, The use of micropulsation 'whistlers' in the study of the outer magnetosphere, *Planetary Space Sci., 13*, 773, 1965.

Eidman, V. Ia., The radiation from an electron moving in a magnetoactive plasma, *J. Exp. Theoret. Phys. USSR, 34*, 131, 1958.

Gallet, R. M., and R. A. Helliwell, Origin of very low frequency emissions, *J. Res. NBS, 63D*, 21, 1959.

Helliwell, R. A., A theory of discrete VLF emissions from the magnetosphere, *J. Geophys. Res., 72,* 4773, 1967.

Jacobs, J. A., and T. Watanabe, Micropulsation whistlers, *J. Atmospheric Terrest. Phys., 26,* 826, 1964.

Jacobs, J. A., and T. Watanabe, Theoretical notes on whistlers and periodic emissions in the hydromagnetic regime, *Planetary Space Sci., 15,* 799, 1967.

Kenney, J. F., and H. B., Knaflich, A system study of structured micropulsations, *J. Geop Res., 72,* 2857, 1967.

Liemohn, H. B., Cyclotron-resonance ampli tion of VLF and ULF whistlers, *J. Geop Res., 72,* 39, 1967.

(Received November 3, 1967;
revised December 22, 1967.)

Location of Generation Regions (in L and λ) of Midlatitude VLF Discrete Emissions by Dispersion Analysis of Ground Station Observations

RICHARD L. DOWDEN*

Cooperative Institute for Research in Environmental Sciences
University of Colorado, Boulder 80302

Dispersion analysis of emission echoes, triggering whistlers, and associated whistlers determines the minimum gyrofrequency (and hence L shell) and the plasma density along the path for each event. These measurements and comparison with the plasmapause $-Kp$ relationship indicate that midlatitude emissions are generated and propagate near the plasmapause, usually just inside the plasmasphere. Evidence for generation at or about the equatorial plane is that the dynamic spectrum of hook emissions is closely symmetrical about minimum frequency if the appropriate amount of path dispersion to the observer (½ or 1½ hop) is subtracted.

Very-low-frequency discrete emissions (risers, falling tones, hooks, etc.) occur in about the same frequency range and often in association with whistlers. Although discrete emissions have been recorded and studied for some twenty years, comparatively little was learned about the location of the emission regions until fairly recently. These recent studies, using in situ satellite observations [*Burtis and Helliwell*, 1969; *Bullough et al.*, 1969] indicate that these discrete emissions, which are usually nonguided and thus not observable on the ground, originate in the magnetosphere near the equatorial plane.

This paper shows that location of the geomagnetic field lines along which ground-observed discrete emissions travel (and presumably were generated), as well as location of the emission regions along these field lines, can be deduced from dispersion analysis of ground-based recordings of dispersed events.

The most obviously useful events for such location would be an emission clearly triggered by a nose whistler, since the nose frequency is simply related to the minimum magnetic field along the path, which thereby locates, or at least labels, the field line of origin. In most cases of interest the nose frequency does not appear within the observed frequency range. However, the nose frequency can still be determined if one can measure the group propagation time (t) per hop versus frequency (f) over a reasonable frequency range. The standard method of *Smith and Carpenter* [1961] uses measurements of $t(f)$ at the highest and lowest frequencies observed. The method used here [*Dowden and Allcock*, 1970] uses as many $t(f)$ points as can be measured. Although more tedious, this method considerably reduces the effect of individual reading errors.

Examples of dispersed events for which this is possible are shown in Figure 1. These fall into three categories: discrete emissions with whistler mode echoes (Figure 1*A*), whistlers that trigger emissions (Figure 1*B*), or whose echoes trigger emissions (Figure 1*D*), and 'associated' whistlers (Figure 1*C*). The last can be identified as echoing on the same path as the emissions. The identification is possible if both the whistler and the discrete emissions have the same propagation time per hop over the frequency range common to both.

It is important to note that location is based on the dispersion of whistlers or on the extra 2-hop dispersion encountered by an emission between its first, second, and later appearances at the ground. This is, of course, independent of the emission process. However, we do make the reasonable assumption that the field line of

*On leave from Department of Physics, University of Otago, Dunedin, New Zealand.

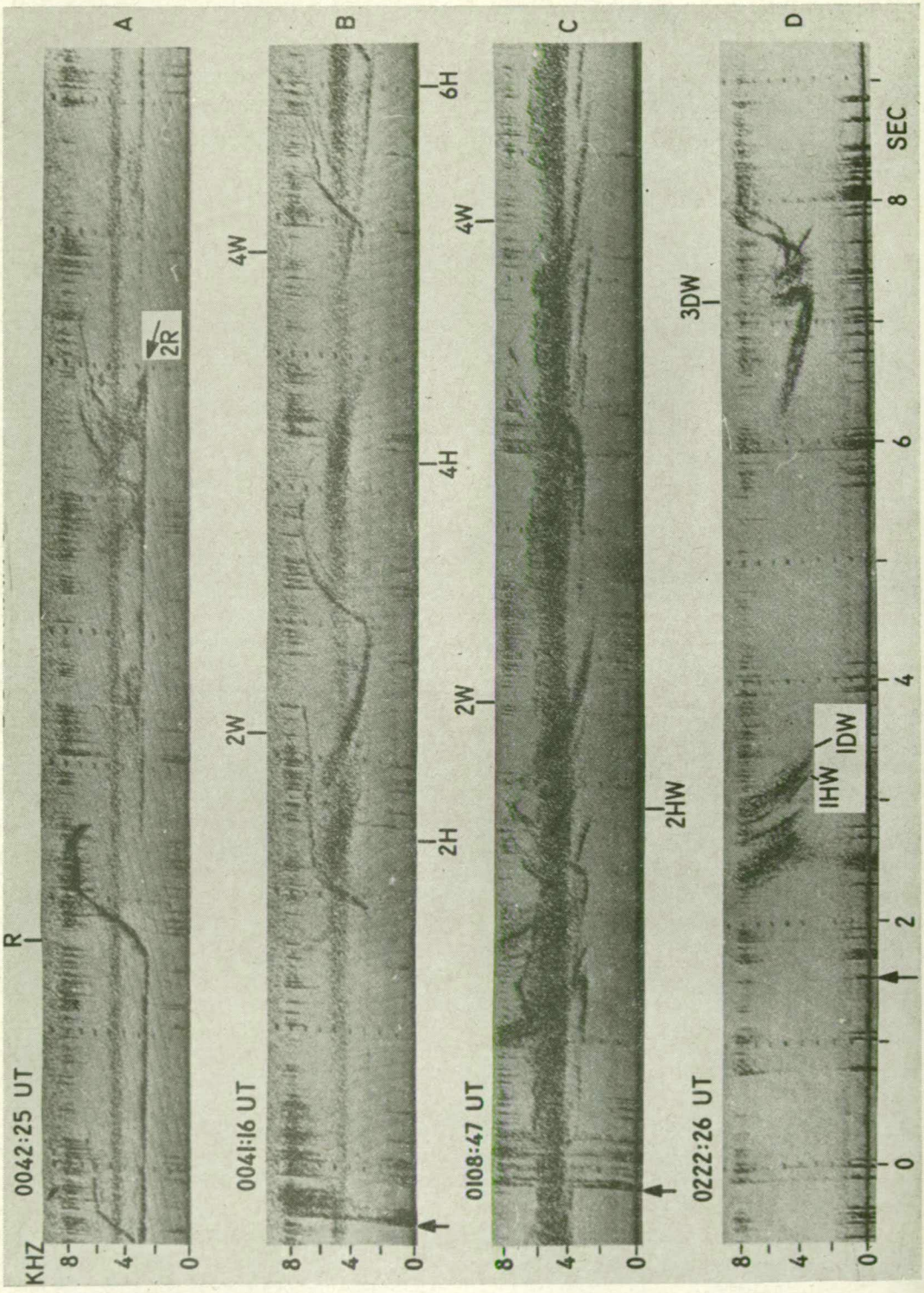
A
B
C
D
KHZ
8
4
0
0042:25 UT
R
2R
0041:16 UT
2W
4W
2H
4H
6H
0108:47 UT
2W
4W
2HW
3DW
0222:26 UT
IHW
IDW
0
2
4
6
8 SEC

propagation so located is also the field line where the emission was generated.

DISPERSION ANALYSIS OF DISCRETE EMISSIONS

The total number of available independent events amenable to dispersion analysis was relatively small. Very few of the sample spectrograms in the published literature and the private collections were usable because the spectrograms were either too short in duration to show whistler source (i.e., epoch) or whistler mode echoes of the emission illustrated, or too low in time resolution for dispersion measurements. On the other hand, long-duration schedules of high resolution were ideal but gave only one independent location per schedule.

Several 2-min schedules showed an abundance of emissions but no echoes at all, and one presumably synoptic 2-min schedule of a conjugate pair (Baie St. Paul and Eights) showed strong and similar emissions at both stations without even 1-hop echoes.

In searching for examples, we noted that nose whistlers often triggered short-duration (sometimes only a few milliseconds) emissions at the whistler cut-off frequency (half the minimum gyrofrequency). In many single-source multipath events several of the nose whistlers showed such triggering. On the other hand, in all cases examined, discrete emissions of appreciable duration (hooks, risers, etc.) and long trains of emissions were always single-path. (Hiss, however, may occur on a different field line as seen by the different propagation time per hop in Figure 1*B*.) So in the analysis below these very short emissions triggered by nose top were excluded, though some of the 'normal' emissions considered here were triggered by nose top.

Field line location. Measurement of the nose frequency (f_n) uniquely determines the field line path, which can be labeled by f_n or by the derived parameter (f_n in kHz):

$$L_B = (325/f_n)^{1/3}$$

The second is more usual, since for a centered dipole magnetic field L_B is equal to the invariant L and is also the geocentric distance, in earth radii, to the top of the field line.

Measurements from fifteen separate discrete emission events gave L_B values ranging from about 2.5 to 4.5. This suggests that emissions might be generated at or near the plasmapause, particularly since recent ideas [*Cole*, 1970] suggest a high concentration of suprathermal particles in this region. Unfortunately, simultaneous measurements of plasmapause position (L_B) are not available. Plasmapause position is related to magnetic indices, however,

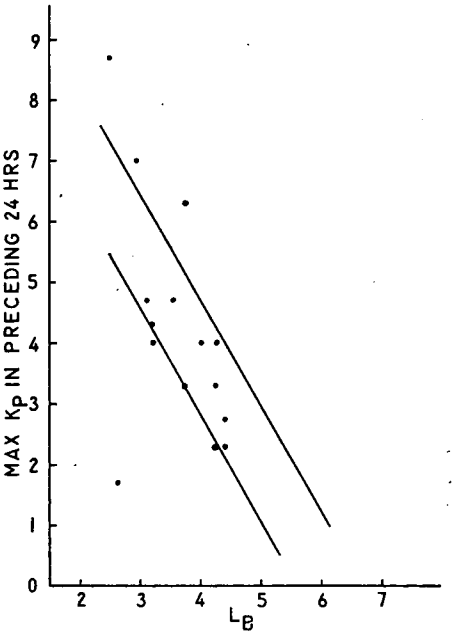

Fig. 2. The equivalent L shells on which discrete emissions were generated (dots) versus maximum 3-hour Kp value in the 24 hours preceding the measurement. The band defined by the two lines represents the relationship between plasmapause L shell and this same index [*Carpenter*, 1967].

Fig. 1. Examples of events suitable for dispersion analysis, March 1, 1969. (*A*) Riser (*R*) with 2-hop whistler mode echo (2*R*). (*B*) Riser triggered by 2-hop whistler (2*W*) with initiating sferic (arrow) and 4-hop echo (4*W*). Hiss burst (2*H*, 4*H*, 6*H*) appears to have been triggered by a whistler from the same sferic but followed a shorter path. (*C*) Associated 2-hop (2*W*) and 4-hop (4*W*) whistler originating at arrow and traveling in the discrete emission path. Note also the whistler confined to the hiss band (2*HW*), which appears to be traveling in the hiss path. (*D*) One-hop multipath whistlers originating at arrow traveling in the hiss path (1*HW*) and discrete emission path (1*DW*). The latter triggers risers on its second (only observable near Dunedin's conjugate) and third hop (3*DH*), as deduced from the riser shapes.

so it is interesting to compare emission position determination with the same indices.

This is shown in Figure 2. The magnetic index (maximum *Kp* in the preceding 24 hours) is that used by *Carpenter* [1967] for comparison with plasmapause position. The band defined by the two lines represents the trend of Carpenter's data. A little over half of his plasmapause points lay within this band, although they tended to cluster along the two lines, as he stated. We note that most of the emission points also lie within this band. The worst deviant is the measurement of $L_B = 2.75$ within 24 hours of a maximum *Kp* of only 2^-, although *Kp* was 4^- in the preceding 27 hours and reached 8^- three days previous to this measurement. Since the magnetosphere takes 5 or more days to recover from a magnetic disturbance [*Park*, 1970], this point might also correspond to the plasmapause.

There is, then, evidence of emission near the plasmapause, although simultaneous emission and plasmapause location would be more convincing. For about theree quarters of these events the nose delay (t_n) indicated propagation on the high-density side of the plasmapause and the other quarter on the low-density side. *Carpenter* [1963] noted emission triggering by whistlers on the low-density side of the plasmapause. Thus, it seems that emissions can propagate on either side. It is conceivable, however, that emissions could be generated on one side but could propagate in ducts on the other side.

Location of source region along field lines. Having determined the field line paths, we next try to locate the position along the field lines where the emissions are generated. This is not so straightforward when using dispersion analysis, for, unlike a whistler's sferic, we have no a priori knowledge of the true or intrinsic dynamic spectral shape of the emission before it is dispersed on its way to the observer. A more fruitful approach is to postulate a likely emission point, subtract the corresponding fractional hop dispersion on the basis of the dispersion per hop that we have already determined, and then look for evidence that what remains is indeed the true or undispersed shape.

There is already strong evidence that emissions are produced near the equator or point of minimum gyrofrequency. For instance, the multipath nose top triggering mentioned above shows that triggering is particularly effective at half the minimum gyrofrequency, even when conditions along the path are not conducive to enduring emissions, and strong triggering action is expected at half the local gyrofrequency at the point of generation [*Helliwell and Burtis*, 1969]. Also, satellites Ogo 1 and 3 observe discreate emissions in a single, variable frequency band. The frequency of this 'banded chorus' is related not to the satellite local gyrofrequency but to the minimum gyrofrequency along the field line passing through the satellite [*Burtis and Helliwell*, 1969]. Similarly, the polar orbiting Aeriel 3 observed in both hemispheres that emissions at 3.2 and 9.6 kHz decrease greatly in intensity as it moved to higher L shells, along which the minimum gyrofrequency falls below the observing frequency [*Bullough et al.*, 1969].

For equatorial generation, then, the fractional hop dispersion to be removed is just half that for 1 hop, provided the emission came to the observer directly. An ambiguity arises, since it is not immediately clear whether an isolated emission, or first of a series of whistler mode echoes, has come to the ground observer directly with ½-hop dispersion or has arrived via reflection at the observer's conjugate with corresponding 1½-hop dispersion. The ambiguity is resolved if synoptic observations from conjugate stations are available, because the first appearance on the ground must be the direct or ½-hop emission [*Brice*, 1962]. An example of this is shown in Figure 3*B*. The ambiguity can also be resolved from single station observations if both types are observed, however, since the dynamic spectral shape of emissions of a given type observed within seconds or minutes of one another varies little from one to the next. Thus the ½-hop hooks in Figure 3*B* have nearly vertical rising parts, whereas the 1½-hop hooks are similar to one another, but the 'rising' parts now have negative slope. On this basis the hooks labeled *H*8 and *H*9 in Figure 3*D* must be ½ hop, whereas the hook labeled *T*, which has just the slope expected for the extra 1-hop dispersion, must be 1½ hop. If the ambiguity cannot be resolved in either of these ways, we must perform the exercise for both ½-and 1½-hop dispersion. The hook in Figure 3*A* and those in Figure 4 have been typed on the basis of the results discussed below.

Figure 5 shows the shape of hook 1 (labeled *H* in Figure 3*A*) after removal of ½-hop dispersion. The 2-hop dispersion was determined

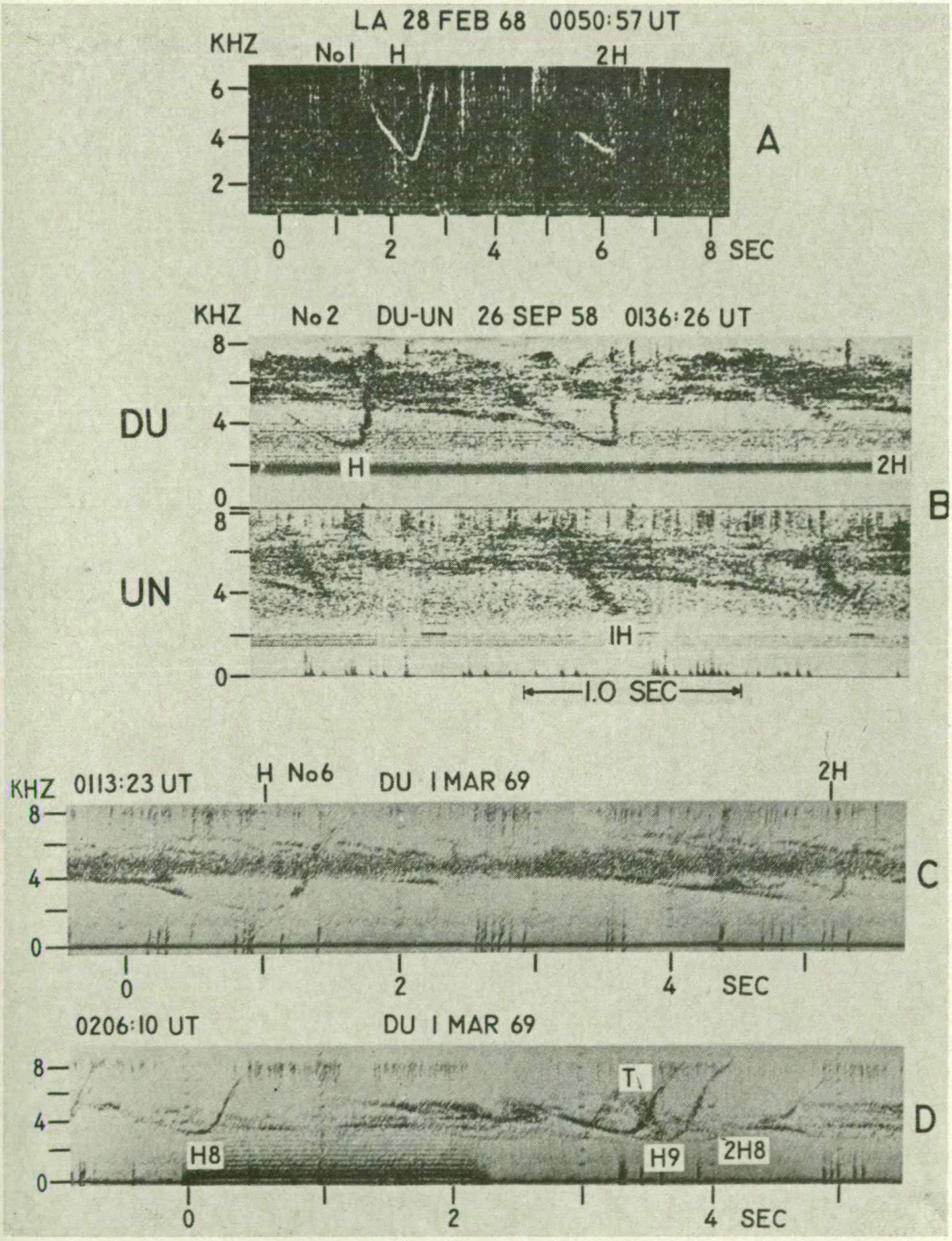

Fig. 3. Hooks that have come to the observer directly without reflection. (*A*) Unusually deep hook (*H*) with 2-hop echo (2*H*). (*B*) Synoptic conjugate observation of a hook that appeared first (*H*) at Dunedin, with 1-hop echo observed (1*H*) at Unalaska and 2-hop echo observed (2*H*) at Dunedin (after *Brice* [1964]). (*C*) Wide hook (*H*) with 2-hop echo (2*H*). (*D*) Direct hooks (*H*8 and *H*9). Comparison of the shape of hook *T* with either *H*8 or *H*9 shows that it has traveled one more hop. It appears that the leading edge of *H*8 triggered *T* as it traveled away from Dunedin after one reflection and triggered *H*9 on its way back. Its 2-hop echo is 2*H*8.

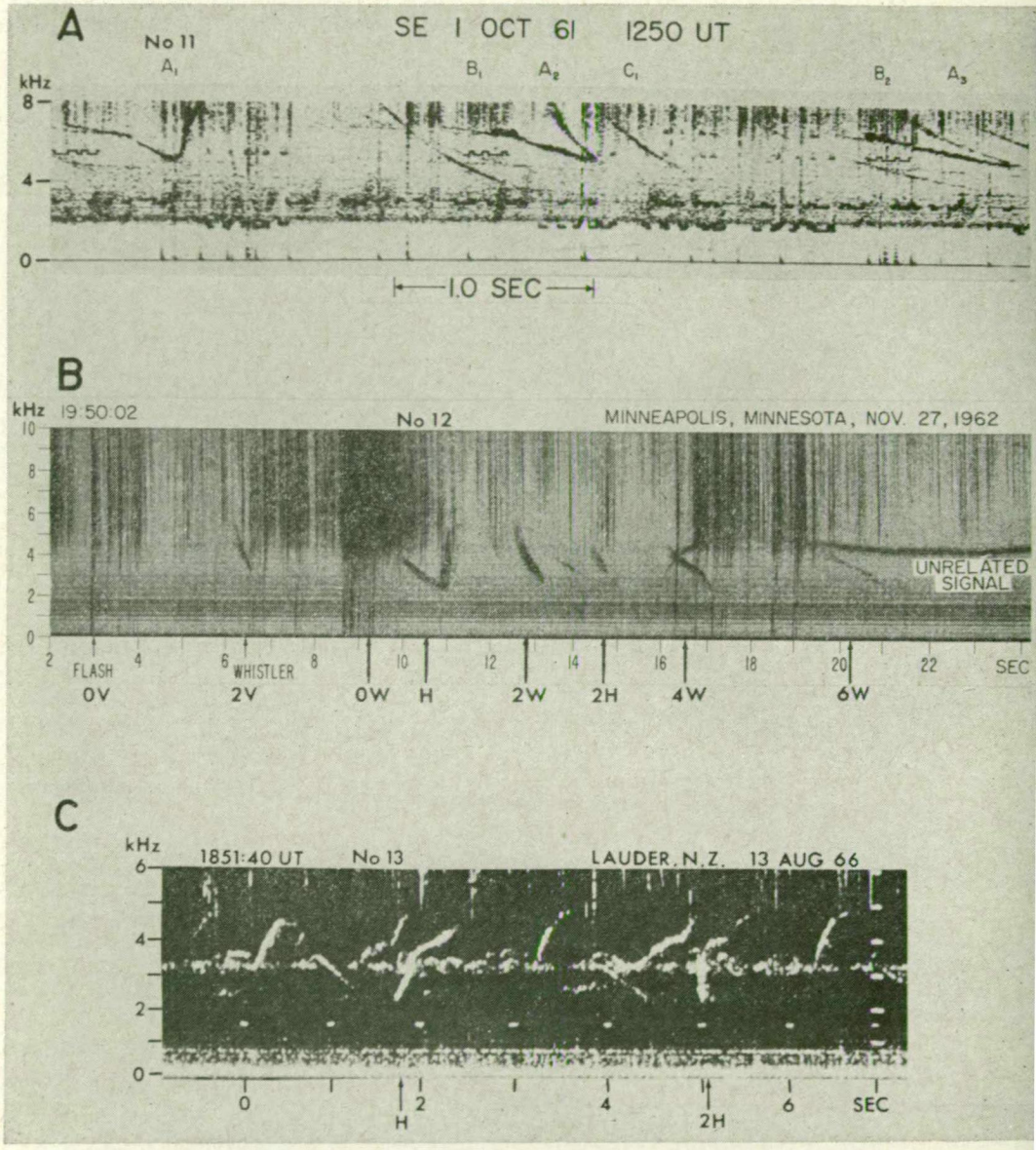

Fig. 4. Hooks that have come to the observer after one reflection in the opposite hemisphere. (*A*) Hook (A_1) with whistler mode echoes (A_2, A_3) and associated whistlers (B_1, B_2, and C_1) traveling in the same path (after *Brice* [1962]). (*B*) Hook (*H*) with echo (2*H*). The train of whistler echoes (0*W* to 6*W*) follows the same path. (*C*) Hook (*H*) with echo (2*H*). These emissions occur near the nose frequency, so that apparent dispersion is small. Note the narrow band of activity at the triggering frequency.

by its echo (2*H*) and also by a nearby associated whistler (not shown). The 'corrected' shape (solid curve) is remarkably symmetrical about the central vertical line, as shown by the 20 points midway between the rising and falling parts. The maximum departure of these points is 13 msec (at 5 kHz), and the median departur (i.e., half are more and half are less) is 4 msec The observed or uncorrected shape is shown b the broken curve.

A large number of hook emissions wer digitized and tested for symmetry, after sub

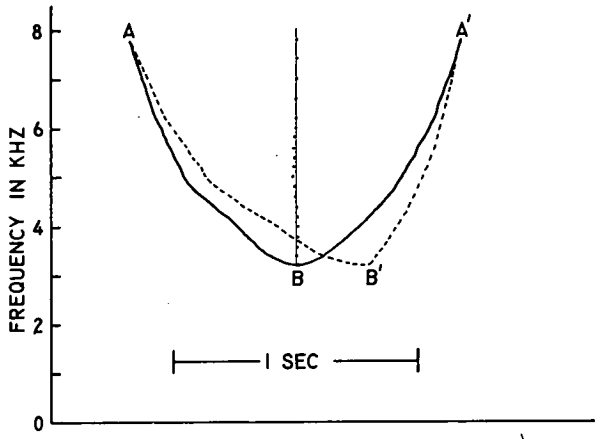

Fig. 5. Hook 1 (of Figure 3*A*) with ½-hop dispersion (corresponding to travel from the equatorial plane) removed (solid curve) and as observed (broken curve). The 20 dots are midway points between the two halves (*AB* and *A'B*) at each frequency. The maximum departure of these points from exact symmetry (vertical line) is 13 msec and half are less than 4 msec.

traction of the appropriate ½- or 1½-hop dispersion, by using a computer program. The results for some of these are displayed schematically by using only the extreme points *A*, *A'*, *B*, *B'* (defined in Figure 5) joined by straight lines. These are shown in Figure 6, where again the corrected forms are shown by solid lines and the original or observed forms by broken lines. The numbers on the hooks are used for identification in Table 1 and for the selection of these shown in Figures 3 and 4. Numbers 1 to 10 are direct or ½-hop hooks, and for all but the first of these the ambiguity was independently removed in one of the two ways described above. Table 1 also gives the maximum time separation between falling and rising parts or width (*A A'*), the skew (*B B'*), or amount by which the hook is straightened out by dispersion removal, and the median of the moduli of the departures (up to 20 points used for each hook) from exact symmetry.

Recalling that the spectrogram time resolution is about 3 to 10 msec and the emission trace thickness is 20 to 50 msec, the dynamic spec-

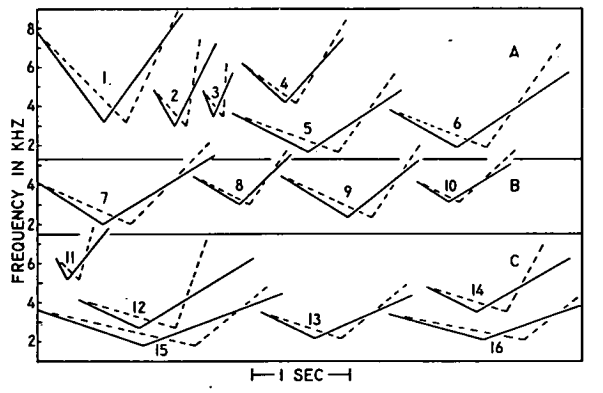

Fig. 6. Schematic drawing of hooks corrected for dispersion (solid lines) and as observed (broken lines). For simpler presentation the hooks are drawn as straight lines *ABA'* and *AB'A'* where these points are defined in Figure 5. The frequency scales in each of the panels *A*, *B*, and *C* are offset to save space. The dispersion removed was ½ hop for the first 10 (panels *A* and *B*) and 1½ hop for the remaining 6 (*C*). The numbers can be used for cross reference to Figures 3 and 4 and Table 1.

TABLE 1. Median Deviation from Symmetry after Removal of Dispersion (½ Hop for 1–10, 1½ Hop for 11–16)

Number	Date	Time ,UT	Recording Station	Width (AA'), sec	Skew (BB'), sec	Median Deviation, msec
1	Feb. 28, 1968	0051:00	[1]Lauder, N. Z.	1.350	0.246	4
2	Sept. 26, 1958	0136:31	[2]Dunedin/Unalaska	0.394	0.133	7
3	Sept. 26, 1958	0135:48	[2]Dunedin/Unalaska	0.221	0.095	10
4	Sept. 6, 1969	0123:18	Dunedin, N. Z.	0.788	0.152	10
5	Mar. 1, 1969	0106:05	Dunedin, N. Z.	1.387	0.391	29
6	Mar. 1, 1969	0113:24	Dunedin, N. Z.	1.291	0.366	12
7	Mar. 1, 1969	0204:46	Dunedin, N. Z.	1.391	0.278	20
8	Mar. 1, 1969	0206:10	Dunedin, N.Z.	0.778	0.186	16
9	Mar. 1, 1969	0206:14	Dunedin, N. Z.	1.215	0.324	28
10	Mar. 1, 1969	0223:36	Dunedin, N. Z.	0.615	0.096	3
11	Oct. 1, 1961	1250:00	[2]Seattle	0.282	0.084	9
12	Nov. 27, 1962	1950:11	[3]Minnesota	1.098	0.432	16
13	Aug. 13, 1966	1851:41	[1]Lauder, N. Z.	1.136	0.236	19
14	Sept. 6, 1969	0124:46	Dunedin, N. Z.	0.958	0.339	10
15	Apr. 4, 1967	1251:12	[1]Lauder, N. Z.	2.068	0.586	28
16	Apr. 4, 1967	1251:16	[1]Lauder, N. Z.	1.734	0.529	28

Spectrograms for these events were supplied by [1]G. McK. Allcock, [2]N. M. Brice, and [3]R. M. Gallet

tral shapes of hooks are fairly symmetrical when dispersion corresponding to travel from the equatorial plane is removed. That any special feature should appear after this exercise is evidence of equatorial generation. Moreover, since the equatorial plane is an extremum for the parameters likely to be relevant to the generation process (gyrofrequency, plasma density, fast particle and wave velocity, etc.), symmetrical generation might be expected. It should be noted that symmetrical generation does not require that the whole emission be generated at the top of the path, but only that the generation be symmetrically disposed in time and space about the equatorial plane.

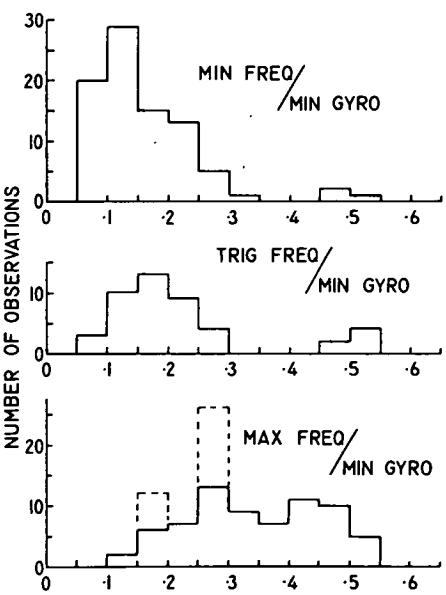

Fig. 7. Histograms of minimum, trigger, and maximum frequencies of discrete emissions in units of the minimum gyrofrequency along their field lines. The two boxes defined by broken lines contain values limited by the spectrogram frequency span.

Emission frequencies in terms of the local gyrofrequency. If emissions are generated at the top of the path, then the gyrofrequency in the region of generation is the field line minimum given by (for a diffusive equilibrium model):

$$f_{HO} = f_n/0.37$$

where f_n is determined by direct observation or by dispersion analysis. It is interesting to relate the emission frequencies to this frequency, because the ratios are likely to be relevant to the generation process.

Histograms of these ratios for the minimum, maximum, and triggering frequencies for many individual emissions are shown in Figure 7. Note that for an appreciable number, emission frequencies were sometimes an order of magnitude less than the gyrofrequency. For cyclotron emission this would require electron velocities of about 10 times the wave phase velocities,

esponding to electron energies of about 100 kev, depending on ambient plasma den-

riggering appears to occur mainly in a ad region (0.15 to 0.25 f_H) usually near the imum frequency. Although the statistical ead of trigger frequencies is large, the trigger uency during an event lasting several min- is often remarkably well defined and stable. is sometimes marked by a thin band of dual activity as in Figure 4*C*. (It is not essarily related to a hiss band, because, as ed above, the hiss band present during the nedin event of March 1, 1969 (Figures 1 and was generated on a different field line.) s suggests that the trigger frequency is re- d to the velocity distribution of the particles onsible for the emission, rather than to the frequency. However, the secondary peak at f_H, which would have been much bigger if all very short emissions had been included, is obably due to the focusing effect at that fre- ncy described by *Helliwell and Burtis* [1969]. he maximum frequencies show a broad dis- ution limited to about 0.5 f_{Ho}, as expected propagation to the ground from or beyond top of the field line. The additional blocks vn as broken lines represent values limited he spectrogram span, so these values should distributed further up the frequency scale. many cases the maximum frequency was a over point rather than an apparent cutoff. and the rather broad distribution suggest the maximum frequency is usually deter- ed by factors other than, or at least in ition to, the gyrofrequency.

cknowledgments. I wish to thank Mr. G. K. Allcock and Dr. R. M. Gallet for original trograms from their stations and Mr. N. R. mson for preparing the spectrograms from my on (Dunedin). I gratefully acknowledge films prints supplied by Mr. G. McK. Allcock, R. M. Gallet, and Professor N. M. Brice used igures 3 and 4, and Professor R. A. Helliwell helpful discussions.

he Dunedin field station and analysis equip- t was financed by a grant from the NZUGC Research Committee, and the data analysis computer time was financed by CIRES.

* * *

The Editor wishes to thank D. L. Carpenter and D. A. McPherson for their assistance in evaluating this paper.

REFERENCES

Brice, N. M., Discussion of paper by R. L. Dowden, 'Doppler-shifted cyclotron radiation from electrons: A theory of very low frequency emissions from the exosphere,' *J. Geophys. Res., 67,* 4897–4899, 1962.

Brice, N. M., Discrete very low frequency emissions from the upper atmosphere, *Rep. SEL 64-088, Radiosci. Lab., Stanford Electron. Lab.,* 1964.

Bullough, K., A. R. W. Hughes, and T. R. Kaiser, Satellite evidence for the generation of VLF emissions at medium latitude by the transverse resonance instability, *Planet. Space Sci., 17,* 363–374, 1969.

Burtis, W. J., and R. A. Helliwell, Banded chorus—a new type of VLF radiation observed in the magnetosphere by Ogo 1 and Ogo 3, *J. Geophys. Res., 74,* 3002–3010, 1969.

Carpenter, D. L., Whistler evidence of a 'knee' in the magnetospheric ionization density profile, *J. Geophys. Res., 68,* 1675–1682, 1963.

Carpenter, D. L., Relations between the dawn minimum in the equatorial radius of the plasmapause and D_{st}, *Kp*, and local *K* at Byrd Station, *J. Geophys. Res., 72,* 2969–2971, 1967.

Cole, K. D., The relationship of geomagnetic fluctuations to other magnetospheric phenomena, *J. Geophys. Res., 75,* 4216–4223, 1970.

Dowden, R. L., and G. McK. Allcock, Determination of nose frequency of non-nose whistlers, submitted to *J. Atmos. Terr. Phys.*, 1971.

Helliwell, R. A., and W. Burtis, Enhancement of discrete VLF emissions at one half the electron gyro frequency, paper presented at *USNC/URSI-IEEE Spring Meeting,* Washington, April, 1969.

Park, C. G., Coupling of thermal magnetospheric plasma with the ionosphere, paper presented at 51st Annual Meeting, AGU, Washington, April, 1970.

Smith, R. L., and D. L. Carpenter, Extension of nose whistler analysis, *J. Geophys. Res., 66,* 2582–2586, 1961.

(Received May 19, 1970;
Revised October 26, 1970.)

Electron Energy Spectrum and Structure Deduced from Analysis of VLF Discrete Emissions by Using the Helliwell Criterion

R. L. DOWDEN[1]

Cooperative Institute for Research in Environmental Sciences
University of Colorado, Boulder, Colorado 80302

Helliwell's [1967] theory of VLF discrete emissions is based on cyclotron resonance between energetic streaming electrons and waves in a localized interaction region near the equator. Maximum wave–electron coupling requires that the emission frequency change at a rate determined by the position, relative to the equator, of the interaction region. In general the interaction region drifts along the field line; the drift velocity is determined by equilibrium between the input electron flux and the output radiation. This criterion is used in this paper to derive a method to determine the electron stream properties from ground-observed VLF emission spectrograms. This method is applied to the analysis of 75 discrete emissions from a single 3-hour event. Over the range of resonant longitudinal energies scanned by the emissions, 6–60 kev, the average energy spectrum was of the form $E^{-2.2}$, in general agreement with satellite measurements in the same region ($L = 3.3$). The relative stream density, as deduced for this energy spectrum, showed spikes similar to electron microbursts observed in satellites. A further test of Helliwell's requirement for internal consistency, that the interaction drift should never overtake either the emitted wave or the resonant electrons ($-v_g < v_i < v_\parallel$), was performed for about a thousand such v_g, v_i, $v_\parallel$ triplets. With four exceptions that were within the probable error, all satisfied this test.

discrete VLF emission usually consists of ingle sharply defined tone that varies in quency in a complicated but fairly charac- stic manner ('falling tone,' 'riser,' 'hook,'). These emissions appear to be generated r the equatorial plane on L shells near the smapause [*Dowden*, 1971] and are observed the ground via whistler mode propagation in d-aligned ducts.

lthough several theories have been suggested e *Helliwell*, 1965, 1967], the most promising based on backward Doppler-shifted cyclo- n radiation from energetic electrons. This s first proposed by the writer [*Dowden*, 2], who showed that the basic dynamic ctral shapes (riser, hook, etc.) could be pro- ed by a single electron traveling along the d line near the equatorial plane. However, obtain observable intensities as well as nar- band tones, discrete bunches of mono- rgetic electrons were required. To avoid these iculties, *Brice* [1963] suggested the cyclotron or transverse resonance instability. In this process, Doppler-shifted cyclotron radiation from electrons, traveling back along the electron stream, phase bunches incoming electrons to sustain a coherent oscillation. Brice noted that this feedback allows the interaction to remain fixed in space like a localized backward wave oscillator. Since this acts as a runaway amplifier, a discrete tone can be sustained, once started, by a continuous stream of electrons of broad energy spectrum. The discreteness is produced by a discrete or localized interaction region remaining at the equatorial plane (where the magnetic field is uniform).

The next step, the explanation of the detailed spectral forms, was taken by *Helliwell* [1967]. He showed that if the interaction region was not a region of uniform field, that is, not precisely in the equatorial plane, the feedback would be altered in a very interesting way. For now the Doppler-shifted cyclotron frequency from a given group of electrons would change slightly as these electrons traverse the interaction region. New electrons entering the interaction region would then be phase bunched by this changed frequency. By considering this frequency change produced by the field gradient

[1] On leave from Department of Physics, University of Otago, Dunedin, New Zealand.

and the feedback delay produced by the finite wave and electron velocities, Helliwell showed that this produces a characteristic rate of change of frequency that, for a given field line and ambient plasma, depends mainly on the instantaneous (and hence initial) frequency and position of the interaction region and is almost independent of the electron spectrum and structure. It is then the Helliwell criterion and the movement of the interaction region, which does depend on electron spectrum and structure, that determine the detailed spectral shapes of discrete emissions.

Helliwell's theory is the only one that can explain the detailed features without requiring unsupported assumptions. However, it is difficult to test, for, unlike the original bunch idea [*Dowden*, 1962], the constraints on the motion of the interaction region are rather wide. Also one can never be sure, on theoretical grounds, that the Helliwell criterion (and not another as yet unrecognized) is the dominant criterion controlling the process. On the other hand, if this theory can be verified, it would not only clear up a problem of long standing, but it would also provide a very useful tool for studying the spectrum and structure of energetic electrons in the magnetosphere.

In this paper we apply this theory to the analysis of a large number of emissions recorded during a single 3-hour period of observation and then examine the electron spectrum and structure so determined for consistency with direct measurements. (In the following all reference to Helliwell means *Helliwell* [1967] unless specified otherwise.)

EXTENSION OF THEORY

In this section we extend Helliwell's theory by using his principles to derive an expression giving the electron energy spectrum in terms of the motion of the interaction region. As Helliwell showed, this motion is determined from the way the rate of change of frequency of an emission (after dispersion correction) varies with time.

The first principle stems from his conclusion that the wave amplitude (wave magnetic field B_w) grows in the interaction region to a limiting value (Helliwell's equations are prefixed by H in the following)

$$B_w = \frac{\pi}{8}\frac{m}{q}\frac{\lambda}{v_\perp}\frac{v_\parallel^2}{L^2} \qquad \text{(H31)}$$

where m and q are the electron mass and charge, λ is the wavelength, $v_\parallel$ and $v_\perp$ are the parallel and transverse velocities of the resonant electrons, and L is the effective length of the interaction region. The corresponding limiting power is

$$\begin{aligned} P_m &= (B_w^2/\mu_0^2)(377/c)v_p \\ &= [(\pi/8)(m/q)]^2(1/\mu_0^2)(377/c) \\ &\quad \cdot(\lambda^2/v_\perp^2)(v_\parallel^4/L^4)v_p \qquad W\,m^{-2} \end{aligned}$$

where μ_0 is the permeability of free space and v_p is the wave phase velocity.

If the interaction region is moving with velocity (positive in direction of electron stream) v_i, we assume, following Helliwell, that P_m determined by the limiting value of B_w remains independent of v_i. Then the power radiated out of the interaction region is

$$P_{out} = P_m(v_g + v_i)/v_g \qquad W\,m^{-2} \qquad (1)$$

where v_g is the wave group velocity. Thus, as noted by Helliwell, when the interaction region drifts backward at the wave group velocity ($v_i = -v_g$), no power flows out of the interaction region.

On the other hand, the electron kinetic power flowing into the interaction region is

$$P_{in} = \tfrac{1}{2}mv_\parallel^2(v_\parallel - v_i)\cdot dN(v_\parallel)$$

where $dN(v_\parallel)$ is the density of resonant electrons, that is, those having velocities within $dv_\parallel$ of the resonant velocity $v_\parallel$. It is more convenient to label these electrons by the equivalent resonance energy (or rather parallel component of energy) E and range dE, and so to replace $dN(v_\parallel)$ by $dN(E)$, where

$$dN(E) = N(E)\,dE = N(E)mv_\parallel\,dv_\parallel$$

We can estimate the range of resonant velocities ($dv_\parallel$) by following the argument that Helliwell used to estimate the Doppler-broadening bandwidth due to this range. Expressing this bandwidth (H24) in terms of $dv_\parallel$ using equation H2,

$$dv_\parallel = \frac{f_H v_p}{f^2}\frac{v_\parallel}{L}$$

where f is the Doppler-shifted cyclotron frequency and f_H is the cyclotron or gyrofrequency.

We then have the usable input power

$$P_{in} = \eta \tfrac{1}{2} m^2 v_\parallel{}^4 N(E)(f_H v_p / f^2)(v_\parallel - v_i)/L \quad W m^{-2} \qquad (2)$$

where η is an efficiency factor that we will assume to be constant.

The second principle is that the interaction region moves so that $P_{in} = P_{out}$. Hence equating (1) and (2) we get an expression for the differential energy spectrum (density per unit energy interval)

$$N(E) = [(\pi^2/32q^2)(377/\mu_0{}^2 c)(1/\eta)](1/f_H) \cdot (1/L^3)(v_p{}^2/v_g v_\perp{}^2)(v_g + v_i)/(v_\parallel - v_i) \qquad (3)$$

where the brackets enclose constant quantities. We can simplify this further by using Helliwell's relation between the interaction length L and the resonant velocity $v_\parallel$

$$L^3 \propto v_\parallel \qquad \text{(H21)}$$

which involves constants that we can place inside the brackets of equation 3. We also use the Doppler-shifted cyclotron resonance conditions to express v_p and v_g in terms of $v_\parallel$ (from H3, H4, and H7)

$$v_p = \Lambda/(1 - \Lambda) v_\parallel$$

$$v_g = 2\Lambda v_\parallel$$

where

$$\Lambda = f/f_H$$

For a given resonant value of $v_\parallel$ there will be a whole spectrum of $v_\perp$ values determined by the pitch angle and energy distribution. However, following Helliwell, we assume that the effective value is

$$v_\perp = v_\parallel \tan \alpha$$

where α is an effective or characteristic pitch angle that is independent of $v_\parallel$. Thus the corresponding constant can also be included in the brackets of equation 3. Hence, we get

$$N(E) = K(\Lambda/(1 - \Lambda)^2)(1/v_\parallel{}^2) \cdot (2\Lambda v_\parallel + v_i)/(v_\parallel - v_i) \qquad (4)$$

where K contains only constant quantities and v_i is taken as positive in the direction of $v_\parallel$.

Analysis Method

The analysis procedure follows that of Helliwell with the addition of equation 4 as follows.

1. It is assumed that one has a sequence of discrete emissions on a long spectrogram and that by dispersion analysis of echoing emissions or triggering whistlers one has determined the field line path parameters (for example, minimum gyrofrequency and plasma frequency) and has determined whether the emissions have arrived directly or after one reflection in the opposite hemisphere. The rest of the procedure is performed for each individual discrete emission, f versus t, trace (for example, a single hook or rising tone).

2. Since the path parameters are known, each $f(t)$ trace can be corrected for dispersion encountered in traveling (½ hop or 1½ hop as determined above) from the equatorial plane to the observer. Since all of the emission trace is produced near the equator, the slope at each point along the corrected trace $f(t)$ is nearly the intrinsic rate of change of frequency. Helliwell gives the relation

$$\dot{f} = Cs\Lambda^{3/2}(1 - \Lambda)^{3/2}(1 + 2\Lambda)^{-2} \qquad \text{(H15)}$$

where C is a constant determined by the path parameters, s is the distance along the field line from the equator to the interaction region center $\Lambda = f/f_H$, and the pitch angle term in equation H15 has been neglected. In deriving this expression, which depends on the local gyrofrequencies and plasma frequencies and their spacial gradients, Helliwell has assumed a dipole field and a constant plasma frequency within the range of s involved. By taking f_H as the equatorial or minimum value, one can then compute $s(t)$ for each point $\dot{f}(f, t)$ along the trace.

3. Having found $s(t)$, we make a further correction to the propagation time from the interaction region to the observer, since in the previous step we had to assume $s = 0$. The sign of this correction depends on the sign of s, that is, on whether the interaction region is on the observer's side (negative s) or on the far side (positive s) of the equator. This correction is particularly important, since we require the time derivative of $s(t)$ in the next step. However,

for the short distances involved (of the order of 1000 km) a simple model of constant gyro and plasma frequency in this region is quite adequate. We could at this point iterate back through step-2 to get a better dispersion correction for f and a better value of f_H for Λ. However, since s is usually small (see below), this was not done here.

4. The time derivative of $s(t)$ is $v_\iota(f)$, the interaction region drift velocity. Since we now know $s(t)$ and hence $f_H(s)$, etc., we can compute $v_\parallel$ and v_φ for each point in s or time and make the test of Helliwell's theory that $-v_\varphi < v_\iota < v_\parallel$.

5. By substituting these values into equation 4 we get $N(E)$ as a function of time as seen from the center of the interaction region. Since we find interesting temporal variations in $N(E)$, it is convenient to make a further time correction $(-sv_\parallel)$ to get these temporal variations of the electron stream as would be seen by an observer at the equator.

6. At each point, that is, for each value $N(E)$, we can calculate the corresponding resonant energy E (or rather the parallel component of energy) from $v_\parallel$ for that point. A single emission that scans through a range of frequency thus scans through a range of E. We cannot get $N(E)$ versus E from a single emission, since $N(E)$ may also vary in time. However, we can presumably get this energy spectrum by averaging over a large number (75 in this study) of emissions in one event. Having found this energy dependence of $N(E)$ we can then find the temporal fluctuations in $N(E)$, or electron stream density, provided that the energy spectrum is not also dependent on time or s.

ANALYSIS OF OBSERVED EMISSIONS

An event lasting nearly 3 hours (0030 to 0330 UT) was recorded on magnetic tape at Dunedin, New Zealand, on March 1, 1969, and later a continuous high-resolution (10 kHz per second aspect ratio) spectrogram was prepared from this tape by using a spectrum analyzer previously described [*Dowden and Emery*, 1965]. This event contained a few hundred discrete emissions together with whistler mode echoes, triggering whistlers, and other whistlers traveling in the same path. Dispersion analysis of these [*Dowden*, 1970] gave the field line parameters, nose frequency (9.9 kHz), and group delay (1.47 sec), and hence the derived ones, minimum gyrofrequency (27 kHz) and plasma frequency (214 kHz). Both ½-hop emissions (direct arrival) and 1½-hop emissions (arrival after one reflection in opposite hemisphere) were observed so the latter were readily distinguishable by the addition 1-hop dispersion.

For analysis, 75 well-developed, ½-hop emissions were selected. Several of these consisted of hooks with branching risers (like those shown in Figure 5).

The f versus t traces of these emissions were sampled at about 20 points at intervals of either 40 or 80 msec, depending on the structure of the trace. The various quantities, s, v_ι, $v_\parallel$, v_φ, E, and $N(E)$, were computed at each point for each emission giving about 1000 values for each quantity.

In addition, a 20-channel energy spectrum analyzer was synthesized within the computing program. These channels were spaced logarithmically spanning the range 2.5 to 250 kev. For all emissions, as each value of $N(E)$ was calculated, it was placed in the appropriate energy channel, so that, at the end of the analysis of all 75 emissions, the mean value of $N(E)$ for each channel was obtained. This set of $N(E)$ versus E was fitted to the power expression

$$N(E) = AE^{-n} \tag{5}$$

Using the average intensity A and exponent n so obtained, the whole program was run through again, normalizing each value of $N(E)$ by equation 5 to obtain the instantaneous relative intensity. This assumes that the fluctuations in the electron stream are due to changes in intensity A rather than to changes in spectral index n. As a check for variation in spectral index, the $N(E)$ versus E data were divided into two sets in time separated by a relative lull in activity at about 0130 UT.

DISCUSSION

An example of the analysis for one of the 75 emission traces is shown in Figure 1. This trace was chosen because parts of it were scaled and digitized two or three times (the computer program was limited to 20 $f(t)$ points per run). Each scaling used 75 msec intervals, two at the same times and one at intermediate times. The

scaling and computation errors can be judged by the difference between values computed for the same time. We note that the errors in v_i are much larger than those in $v_\parallel$ and v_g. This is because the errors in $v_\parallel$ and v_g are due essentially to errors in frequency measurement, whereas those in v_i are due to errors in the second derivative of frequency or curvature of the $f(t)$ trace.

The main constraint that the data must satisfy on Helliwell's theory is that $-v_g < v_i < v_\parallel$. This is clearly true for all points in the trace analyzed in Figure 1. Of the total (from all 75 emission traces) 1000 or so values of v_i computed, all satisfied the lower constraint v_g, but four points (one in two traces and two in a third trace) were slightly greater than the corresponding $v_\parallel$. However, these deviations from a possible $v_i = v_\parallel$ were well within the errors expected for v_i as discussed above.

We notice from Figure 1 that a single emission typically scans through a large range of $v_\parallel$ and thus through a large range of corresponding electron energy (6.4 to 54 kev in this case).

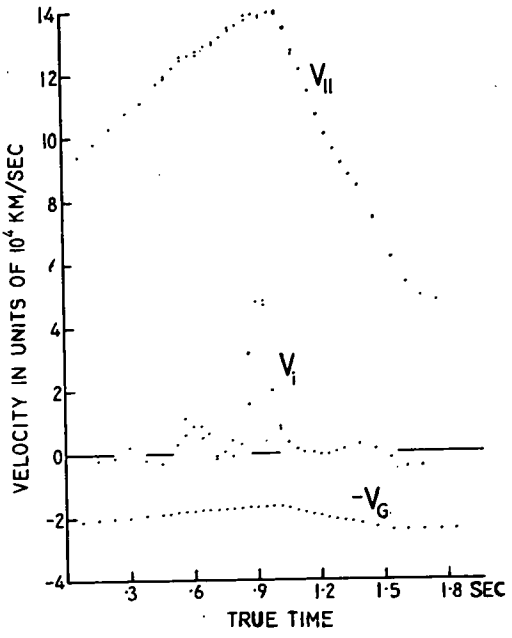

Fig. 1. Parallel, group, and interaction region drift velocities versus true time. Parts of the emission trace (0103:57 UT) were scaled three times giving some scatter in the points computed, particularly in v_i.

However, the random errors and real temporal fluctuations in v_i, and hence $N(E)$, make it difficult to get a meaningful $N(E)$–v–E electron energy spectrum from a single emission. The average spectrum from all emissions is discussed later.

A histogram of the minimum (shaded) and maximum values of the interaction drift velocity v_i of each emission trace is shown in Figure 2. The ranges of the corresponding values of group velocity v_g and parallel component of electron velocity $v_\parallel$ are also shown. Three of the four exceptions noted above (two were adjacent values in one trace) are also shown as shaded. It is interesting to note that, apart from these exceptions, the extreme drift velocities approached but stayed within the constraints and that the ratio of positive to negative values is approximately the ratio of $v_\parallel$ to v_g (about 5 : 1).

The extreme values of the interaction distance s are shown as histograms in Figure 3. We notice that the extremes were usually between −1000 km (south) and +2000 km (north) and nearly always within ±3000 km. Since the geocentric distance to the top of this field line was about 21,000 km, this corresponds to generation within about 10° of the equatorial plane.

Also shown in Figure 3 is a histogram of the interaction region position near the start of each emission (corresponding to the second point of the digitized trace). This indicates a preference for triggering or spontaneous start near the equatorial plane.

The average energy spectrum determined from the 20-channel system described above is shown in Figure 4 where $N(E)$ versus E is plotted on log–log scales. This average spectrum, using all 1000 or so $N(E)$ determinations (solid and open circles denote means of over 100, and over 20 values, respectively), shows a significant power-law type trend. The line shown corresponds to $N(E) \propto E^{-2.2}$. Dividing the data into two sets about 0130 UT gave spectral indices of 2.14 and 2.22, respectively, thus indicating no significant change in spectral index during the 3-hour event.

We gain some insight as to the dynamics of the emissions by examining the variation of the computed quantities during individual emissions. For convenience, five emissions were selected that showed most of the features noticed in the

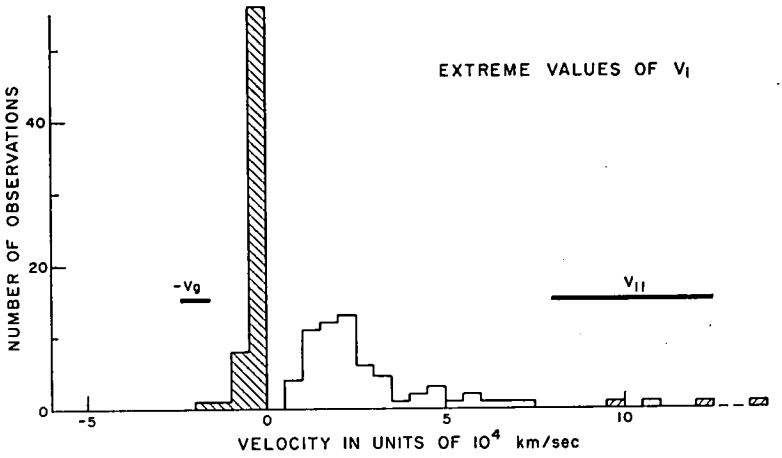

Fig. 2. Histogram of the minimum (shaded) and maximum values of the interaction drift velocity (v_i) of each emission trace. The ranges of the corresponding values of group velocity (v_g) and parallel component of electron velocity ($v_{||}$) are shown as horizontal bars. The three values of v_i shown with different shading (one is off scale) are the exceptions $v_i > v_{||}$.

whole group. The original spectrograms of these five are shown in Figure 5 and the detailed analyses of these in Figure 6 (first two) and Figure 7 (other three).

The top panels in Figures 6 and 7 show the frequency versus time trace plotted from the digitized samples to show the interpretation and the amount of detail 'seen' by the computer. The second panel shows the motion of the interaction region in true time, that is after correction for propagation delay from the interaction region to the observer.

During a single emission, variations in $N(E)$ may be due to variations in energy, energy spectrum, or electron stream density. If we assume that the energy spectrum is constant ($E^{-2.2}$), we can remove the energy dependence by using equation 5 to get the relative stream density $N(E)/\bar{N}(E) = A/\bar{A}$. This is shown in the bottom panel, versus the time that these electrons would be expected at the equatorial plane, that is, time corrected by $v_{||}$ (usually only a few tens of milliseconds). The time scale is the same for all three panels, but, as the corrections

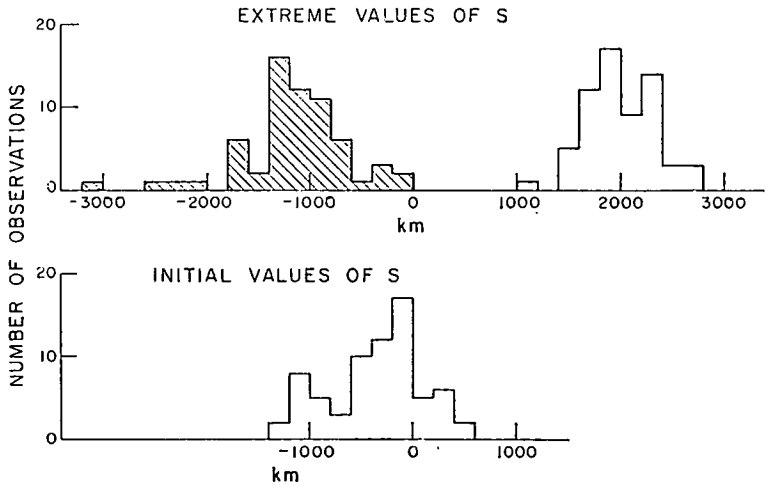

Fig. 3. Histograms of the extreme and initial positions of the interaction region during each emission, as distance along the field line from the equator.

involved make point to point correspondence less obvious, the panels have been centralized to show best correspondence of the important features.

The most striking features are the sharp breaks in the interaction drift from slow and often negative velocities to velocities that occasionally approach the electron stream velocity. These sharp breaks correspond to the sharp peaks in stream intensity in the bottom panels. It is seen from equation 4 that variations in deduced stream density are produced primarily by variations in deduced v_i, since the other quantities vary slowly and are more directly deduced. Comparison with the plot of v_i points of the multiply scaled event in Figure 1 indicates that at least the main peaks in $N(E)/\bar{N}(E)$ in the lower panels of Figures 6 and 7 are real.

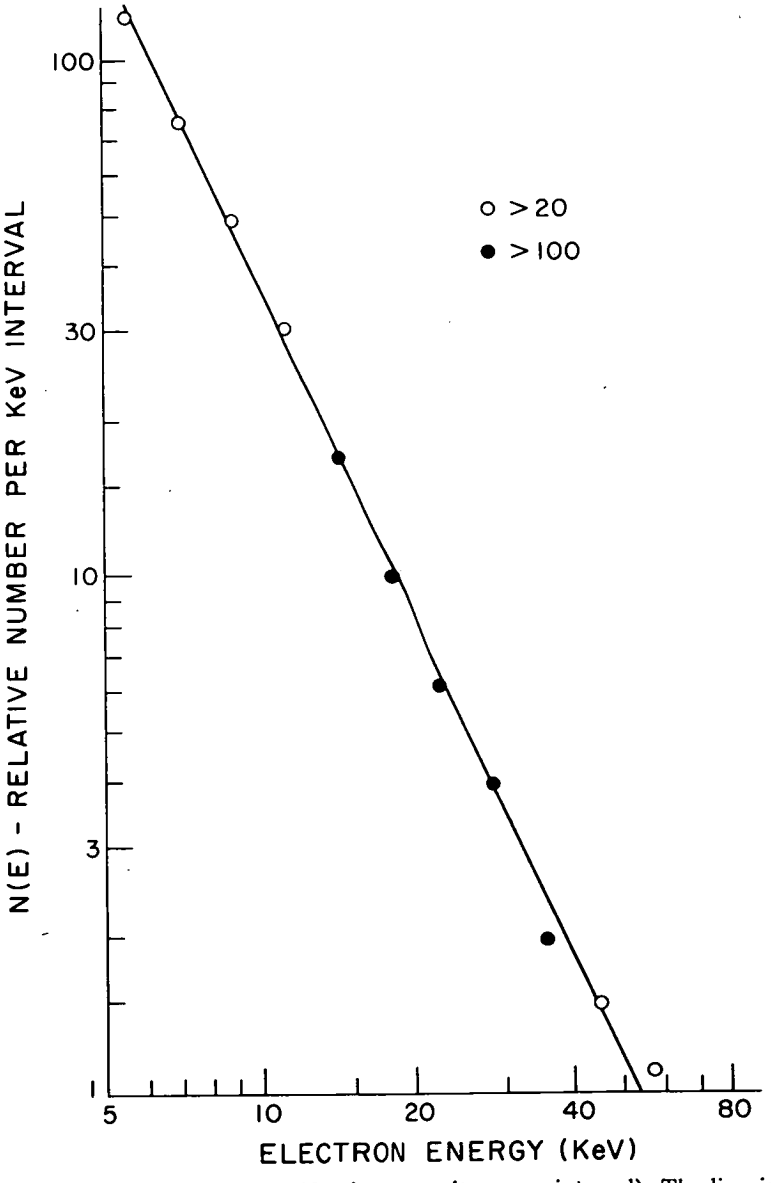

Fig. 4. Differential energy spectrum (density per unit energy interval). The line is a power law fit with spectral index of 2.2.

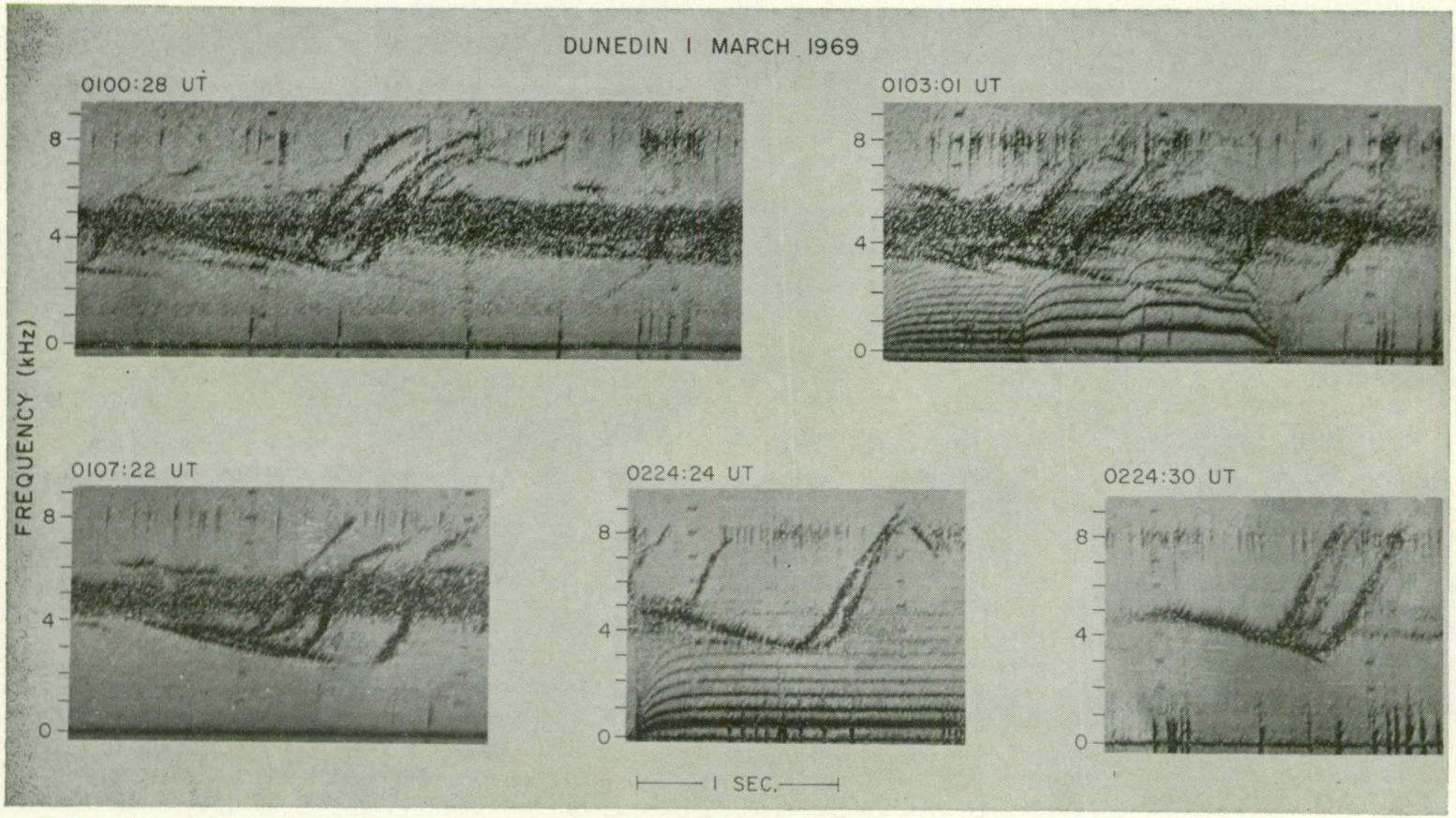

Fig. 5. Hooks with branching risers. Detailed analyses of these are shown in Figures 6 and 7.

These peaks or spikes in stream density, which show resemblence to electron microbursts as discussed below, appeared in most of the hooks analyzed. In $f(t)$ spectrogram, they appear as sharp increases in curvature, or d^2f/dt^2. If a falling tone is in progress, a microburst will tend to bend it up into a rising tone, making a hook. An initially rising tone is not so obviously affected. However, a microburst is not essential for a hook (see below).

It is interesting to note here that the hook analyzed by *Helliwell* [1967] showed a peak in v_t also. This hook appeared with a large number of other artificially (morse pulse) stimulated emissions, or ASE's, as seen in Figure 7–66 of *Helliwell's* [1965] book. Most of the other ASE's were monotonically rising or falling tones, as would be expected for a constant electron stream and triggering slightly to one side or other of the equator, or for equatorial triggering when the electron stream density was slightly above or below a critical value. An occasional microburst would thus change an initially falling tone into a hook like this one.

Although they are relatively rare, it is not clear how the hooks with branching risers in Figure 5 are produced in this theory, since branching implies branching or splitting of the interaction regions upon the arrival of a microburst. One possibility is that the interaction region has a lateral extent across field lines somewhat larger than the lateral extent of the microbursts, which are then able to take over one side of the interaction region, leaving the other side under control of the relatively steady electron steam adjacent. Another possibility is

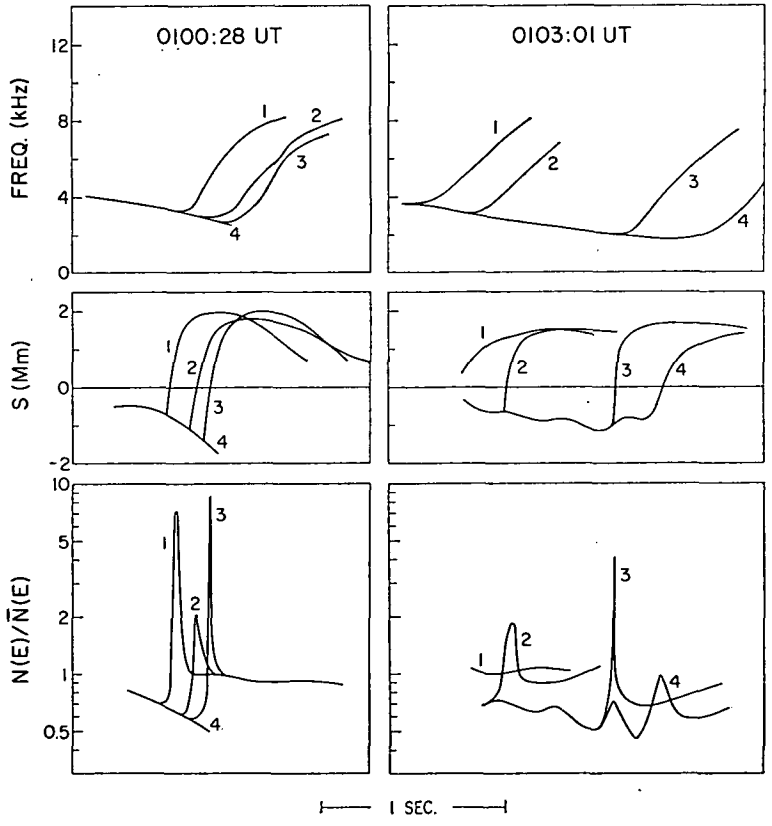

Fig. 6. Analysis of the two emissions shown in the top half of Figure 5. Top panel: Frequency versus (observed) time plotted from the digitized samples. Middle panel: Position of interaction region (distance s from equator) versus true time. Bottom panel: Normalized electron stream intensity versus time of equatorial crossing. Time scale shown is the same for all three, but the panels have been offset (centralized) to show correspondence of main features.

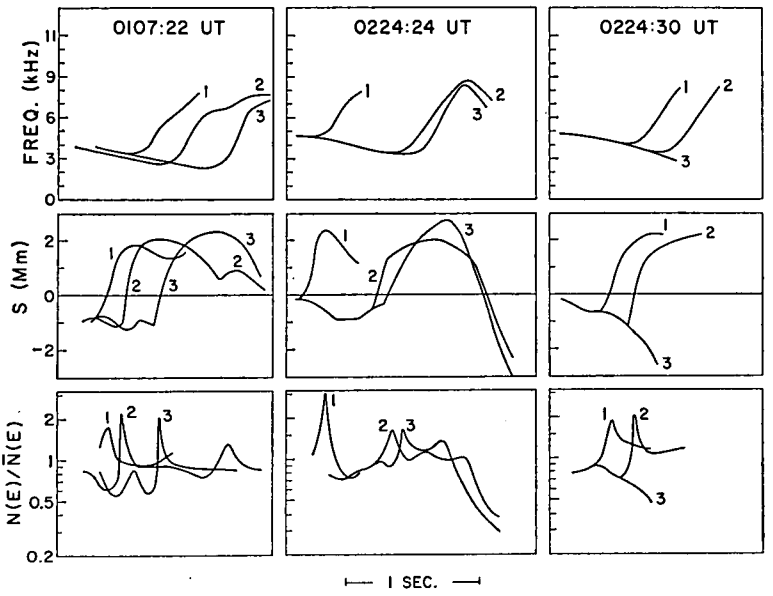

Fig. 7. Analysis of the three emissions shown in the bottom half of Figure 5. The arrangement is as in Figure, 6.

that the microburst electrons are triggered to emit by radiation from the first interaction region before they reach it. If the microburst spectrum is also peaked and is not, as assumed, the same as that of the steady stream, the first interaction region would not 'see' the microburst electrons when they arrive if this energy peak is not near the first interaction resonant energy at this time. Also, this second interaction region could then pass through the first without effect if the emission frequencies and hence the resonant energies are sufficiently different.

A feature of the emissions in this study, as seen in the middle panels of Figures 6 and 7 (particularly for the event at 0224:24 UT), is that the interaction region is inherently equator seeking. It tends to start near the equator and if it drifts upstream it tends to return even in the absence of microbursts. This appeared from some emissions that did not involve microbursts and is also seen in the traces produced here by the part of the interaction that was left behind when a microburst swept through. When the interaction is taken downstream across the equator by a microburst it also tends to return. The reason for this is outlined below.

From equation 4, the condition for zero drift velocity is

$$N(E) = K(2\Lambda^2/(1 - \Lambda)^2)(1/v_\parallel{}^2)$$

and if $N(E)$ can be represented by

$$N(E) = AE^{-n}$$

we get the critical stream intensity A_0

$$A_0 = K(2\Lambda^2/(1 - \Lambda)^2)(E^n/v_\parallel{}^2)$$

Since $E \propto v_\parallel{}^2$,

$$A_0 = K_2(\Lambda/(1 - \Lambda)^2)v_\parallel{}^2E^{n-2}$$

Then, using the resonance condition (H6) to express $v_\parallel$ in terms of frequencies and placing constant quantities together,

$$A_0 = K_3f(f_H - f)E^{n-2}$$

Since v_t is determined by $N(E)$ according to equation 4, the interaction region drifts upstream or downstream depending on whether the electron stream intensity A is smaller or greater than A_0. For $n \sim 2$, as in this case, the energy term is almost constant, so A_0 increases with frequency up to $\frac{1}{2}f_H$, which is also the duct guiding cut off. So we see that in the absence of any special fluctuations in A this produces an equatorward acceleration, for when s is negative (interaction upstream of the equator) the frequency must be falling and so v_t must be increasing, whereas when s is positive

the frequency must be rising and so v_t must be decreasing. In general we would expect overshoot of the equator and hence oscillation because the drift velocity will tend to increase or decrease monotonically during the whole time the interaction region spends in one hemisphere.

This implies that an emission, once triggered, should continue through many such oscillations whereas more than one or two oscillations are rarely observed, and emissions seem to stop without obvious reason, although usually at an upper or lower frequency limit. However, for emissions to occur and be sustained we also require a velocity distribution that can provide signal amplification or radiative instability. An appropriate distribution would confine the emission to a frequency band, and temporal fluctuations in this velocity distribution might occasionally stop (and possibly start) emissions within this band.

The effects discussed above can be seen in the five emissions shown. Thus traces 2 and 3 in the one at 0224:24 show a complete drift oscillation with the beginnings of a second. These both end within the normal emission band. The risers of the other emissions seem to have ended at the upper limit of the band, although the falling tones (or aborted hooks) in the emissions at 0100:28 (4) and 0224:30 (3) seem to have ended at the lower limit. Some apparent cutoffs are produced by the receiver (built-in at 1 kHz and 10 kHz for interference suppression), which might explain the missing low-frequency part of the deep hook (not processed) at 0100:28 in Figure 5. But if there was no natural cutoff we would expect to see the emission when it was returned to the observable range.

Comparison with Direct Measurements

It would be very interesting to compare the energy spectrum and microburst structure deduced from analysis of VLF emissions with those measured simultaneously in the same place by direct methods. Such simultaneous measurements are not yet available for this event. However, spectrum measurements in the same region (afternoon sector, geocentric distance $\sim 3.4\ R_E$, latitude $\sim 20°$) by Ogo 3 [*Frank*, 1967] showed a power law spectrum for $N(E)$ over the range 300 ev to 50 kev with spectral index $n \sim 2.3$. The index obtained above ($n \sim 2.2$) is in very good agreement with this and (although possibly fortuitous) it is in general agreement with typical values of 2–3 found by *McDiarmid et al.* [1963] and the general range 2–4 for trapped outer zone electrons in the energy range $40 < E < 250$ kev [*Hess*, 1968].

The spikes in normalized $N(E)$ in Figures 6 and 7 show a general resemblance to electron microbursts observed in satellites [*Oliven et al.*, 1968] and, via X-ray bremsstrahlung, in balloons [*Venkatesan et al.*, 1968]. Thus both involve about the same electron energies (tens of kev), about the same time scale (~0.1–0.2 sec), and often show faster rise times than fall times (particularly those in Figure 6). On the other hand, microbursts occur generally before noon and on L shells above 4 (usually 6–8.5) [*Oliven et al.*, 1968], whereas this VLF event occurred just after local noon at about $L = 3.3$.

A direct comparison between microbursts and VLF emissions has been made by *Oliven and Gurnett* [1968]. They found that microbursts are always accompanied by VLF emissions, but emissions are not necessarily accompanied by microbursts. While emissions without microbursts may be due to uninteresting effects (e.g., weaker guiding of emissions) it is interesting to note that a few of the emissions in this event were not accompanied by apparent microbursts. They also noted that it is not generally possible to find a one-to-one (burst-to-burst) correspondence between individual microbursts and VLF chorus bursts. However, the theoretical considerations above show that microbursts do not cause (i.e., initiate) emissions, but rather they change the spectrogram shape of emissions in progress. A detailed correspondence would be expected between the electron intensity deduced from emission structure analysis and that measured directly for those times when a discrete emission happened to be in progress. Such a test could be regarded positive if there was some close one-to-one correspondence, since it would be difficult to ensure that all of the emissions and the electrons directly observed followed the same paths.

Conclusions

Analysis of a large number of VLF discrete emissions, based on Helliwell's theory, showed that $-v_e < v_t < v_0$, as required by this theory,

about a thousand such tests (neglecting 4 tances of $v_t > v_{\parallel}$, probably due to scaling ors). An interesting interaction drift oscilla- n deduced from these emissions is shown to predicted by the theory for relatively steady ctron streams.

The deduced electron energy spectrum and nporal structure (microbursts) show general reement with nonsimultaneous, direct meas- ements. Clearly the next step should be to simultaneous comparisons of VLF-deduced d direct measurements of normalized $N(E)$ h appropriate time corrections for point-to- nt correspondence.

An apparent affinity for triggering at the uator ($s = 0$) at a frequency or time (i.e., iting for the 'right' electron intensity) to e low initial drift velocities is allowed by the ory, but since it is not specifically predicted might be worth further investigation. After ggering, the typical motion of the interaction ion appears to be a slow drift ($v_t \sim 0$) until nicroburst arrives that abruptly increases the ft velocity to near the upper limit ($v_t \sim v_{\parallel}$). us the 2 earlier extreme models, a stationary eraction region at the equator [*Brice*, 1963] d an interaction region moving with the elec- ns [*Dowden*, 1962], are often reasonably id at different times even in a single emission.

Acknowledgments. I wish to thank Mr. N. R. omson for preparing the spectrograms, Dr. H. Campbell for use of his scaling facilities, Professor R. A. Helliwell for helpful discus- ns.

The Dunedin field station and analysis equip- nt were financed by a grant from the w Zealand University Grant Committee Re- rch Committee and the data analysis com- ter time was financed by CIRES.

* * *

The Editor wishes to thank T. F. Bell and D. Shawhan for their assistance in evaluating s paper.

References

Brice, N. M., An explanation of triggered very-low-frequency emissions, *J. Geophys. Res., 68,* 4626–28. 1963.

Dowden, R. L., Doppler-shifted cyclotron radiation from electrons: A theory of very low frequency emissions from the exosphere, *J. Geophys. Res., 67,* 1745–50, 1962.

Dowden, R. L., Location of generation regions (in L and λ) of VLF discrete emissions by dispersion analysis of ground station observations, *J. Geophys. Res., 76,* 1729–1737, 1971.

Dowden, R. L., and M. W. Emery, An automatic dynamic spectrum analyzer for tape recorded signals, *Nature, 207,* 493–95. 1965.

Frank, L. A., Several observations of low energy protons and electrons in the earth's magnetosphere with Ogo 3, *J. Geophys. Res., 72,* 1905–1916, 1967.

Helliwell, R. A., *Whistlers and Related Ionospheric Phenomena,* Stanford University Press, Stanford. Calif., 1965.

Helliwell, R. A., A theory of discrete VLF emissions from the magnetosphere, *J. Geophys. Res., 72,* 4773–89, 1967.

Hess, Wilmot N., *The Radiation Belt and Magnetosphere,* Blaisdell, Waltham, Mass., 1968.

McDiarmid, I. B., J. R. Burrows, E. E. Budzinski, and M. D. Wilson, Some average properties of the outer radiation zone at 1000 km, *Can. J. Phys., 41,* 2064–2079, 1963.

Oliven, M. N., and D. A. Gurnett, Microburst phenomena, 3, An association between microbursts and VLF chorus, *J. Geophys. Res., 73,* 2355–62, 1968.

Oliven, M. N., D. Venkatesan, and K. G. McCracken, Microburst phenomena, 2, Auroral-zone electrons, *J. Geophys. Res., 73,* 2345–53, 1968.

Venkatesan, D., M. N. Oliven, P. J. Edwards, K. G. McCracken, and M. Steinbock, Microburst phenomena, 1, Auroral-zone X rays, *J. Geophys. Res., 73,* 2333–43, 1968.

(Received July 30, 1970;
accepted November 25, 1970.)

VLF Discrete Emissions Deduced from Helliwell's Theory

R. L. DOWDEN[1]

Cooperative Institute for Research in Environmental Sciences
University of Colorado, Boulder 80302

An iterative procedure based on R. A. Helliwell's theory is used to compute frequency-versus-time spectral shapes of VLF discrete emissions for various field line and electron stream parameters. A quasi-constant stream produces symmetrical emissions (symmetrical generation about the equator), and superimposed microbursts produce hooks with branching risers. Parameters appropriate to quiet and storm conditions produced the observed characteristics of *Q* chorus and *S* chorus, respectively. A general feature of the computed position of the interaction region for constant electron streams of low spectral index is an almost sinusoidal motion of the interaction position about the equatorial plane. An analytic expression derived for the period of this motion shows that such periodic motion will occur for electron spectral indices less than about 2.4. A mechanism for nondispersed, multiphase periodic emissions is suggested in terms of this periodic drift motion.

LF discrete emissions consist of rising and ng tones at frequencies of the order of a kilohertz [*Helliwell*, 1965]. It is generally ght that these are produced in the mag-sphere near the equatorial plane by back-l Doppler-shifted cyclotron interaction with getic electrons.

ne most promising mechanism explaining -defined discrete emissions in terms of inter-on with a continuous stream of wide-band getic electrons is that given by *Helliwell* 7]. By considering the interaction resonance itions and their gradients along the field he showed that if the interaction is localized e will be a characteristic rate of change of uency determined essentially by the instan-ous emission frequency and the position of interaction region. In general the inter-on region will drift along the field line with ift velocity determined by the instantaneous nsity and energy spectrum of the energetic rons. The detailed frequency-time shape of ete emissions is therefore determined by ield line parameters (nose frequency f_n and p delay t_n at this frequency, or the derived , base field and plasma density), the elec-tron intensity and energy spectrum, and the initial conditions (e.g., trigger frequency, and initial position and velocity of the interaction region).

As a general test of this theory, a method was derived and applied to determine the energetic electron spectrum and intensity structure by analysis of observed VLF discrete emissions [*Dowden*, 1971*b*, referred to here as paper B]. This showed general agreement with satellite measurements and showed other interesting but unexpected features.

In this paper these features are examined further by the reverse procedure, that is, by synthesizing emissions for given field line parameters, energetic electron properties, and initial conditions.

ITERATIVE COMPUTATIONS

The stepwise procedure outlined by *Helliwell* [1967] and developed for analysis in paper B is even more amenable for synthesis, because synthesis involves integration rather than differentiation and so is well suited to iterative summation by computer.

The steps are these. For an assumed field line and plasma, we choose the position of the interaction region and the instantaneous emission frequency. The cyclotron resonance condition determines the resonant velocity (v_0) at this frequency, and the group velocity (v_g) is determined by the ambient plasma and gyrofrequency.

[1] Permanent and present address: Department hysics, University of Otago, Dunedin, New nd.

The instantaneous rate of change of emission frequency (df/dt) required for matching the spatial variations of gyrofrequency and Doppler-shifted wave frequency, for the chosen interaction position and frequency, is determined by the relations given by *Helliwell* [1967].

We now require the drift velocity of the interaction region (v_i). Following *Helliwell* [1967], we use the criterion that the interaction region drifts so that the resonant electron kinetic power into the interaction region equals the electromagnetic power radiated out. The first of these depends on the relative velocity ($v_\parallel - v_i$) of the resonant electrons to the interaction drift as well as on the relative abundance of resonant electrons or the differential energy spectrum, $N(E)$, where E is the corresponding resonant energy. The radiated power is proportional to the relative velocity ($v_i + v_g$) of the wave packet to the interaction region (the positive sign is a consequence of backward emission). Equating these two powers, it was shown in paper B that $N(E)$ and v_i are related by

$$N(E) = K \frac{\Lambda}{(1 - \Lambda)^2} \frac{1}{v_\parallel^2} \frac{v_i + v_g}{v_\parallel - v_i} \qquad (1)$$

where Λ is the ratio of the emission frequency f to the local gyro frequency f_H, and K is unknown but is assumed to be constant. If we assume that $N(E)$ has the form

$$N(E) = AE^{-n} \qquad (2)$$

we can choose the spectral index n and the initial value of v_i to determine the ratio A/K. In future iterations, v_i is given by equations 1 and 2 for this ratio.

Calculation of the arrival time at the ground (T_G) of this emission component at frequency f completes the first iteration.

For the second iteration, after an increment of time (ΔT), the change in interaction position is given by $v_i \Delta T$, so that new values can be calculated for all quantities. The time increment was either 0.05 sec or else reduced to ensure a frequency increment of less than 200 Hz.

Up to 200 iterations were made unless the emission frequency or duration went beyond preset limits. After each iteration, all relevant values were printed, and after the complete calculation selected pairs (usually emission frequency versus 'ground' or observer time, and interaction position versus true time) were plotted by the computer Calcomp plotter.

Figure 1 shows an emission calculated in this way for a uniform electron stream and with dispersion corresponding to its first appearance at the ground. The field line parameters ($f_n = 10$ kHz, $t_n = 1.5$ sec) and spectral index ($n = 2.25$) are those deduced from an observed series of emissions in paper B. Also shown is the motion of the interaction region which is closely sinusoidal for this uniform stream. The interesting growth in the amplitude of the interaction drift turns out to be a spurious computer effect related to the iteration increment, for halving this increment reduced the apparent growth rate to less than half. When this is removed, the emission process is symmetrical; that is, the generation is symmetrically disposed in time and space about the equatorial plane. In particular, the same frequency is emitted at the two extremes (B and D in Figure 1) of the interaction drift oscillation. This symmetric generation is a general tendency for observed emissions ([*Dowden*, 1971*a*] referred to here as paper A).

This synthetic emission has shape, frequency range, and oscillation period (~2 sec) similar to those observed in paper B, though both random and impulsive (microburst) fluctuations in the real electron streams produced less regular drift motions.

The relative intensity (w m^{-2} Hz^{-1}) along the trace is shown in the bottom panel of Figure 1. This involves the limiting amplitude of the interaction given by *Helliwell* [1967], the motion of the interaction, and the effect of compression or spreading of energy by dispersion on the way to the observer. Frequency-selective losses have been neglected. The rising part of the emission is much stronger than the falling part, as is usually observed. The weakest parts, AB and EF, are often not observed at all.

ELECTRON STREAM VARIATIONS

The emission in Figure 1 was calculated for a non-varying electron stream by holding the stream density A in equation 2 constant. We now consider the effect of varying the electron stream. In general, an increase in stream density produces an algebraic increase in the interaction drift velocity (equation 1). Since the rate

of change of emission frequency depends on the interaction position, such an increase will increase the curvature or d^2f/dt^2 of the emission trace. In view of this double integration effect, a randomly varying stream, or even an impulsive stream, will still produce a smoothly varying emission trace.

It is interesting to compute the effects of an impulsive increase in stream density corresponding to an electron microburst. Although there is no direct (satellite or balloon) evidence of microbursts on the L shells where discrete emissions occur (2.5 to 4), analysis of emissions in paper B indicated their presence. Microbursts can be simulated by superimposing a time-dependent term on the electron stream intensity:

$$A(t) = A_0\{1 + C \exp[-(t - t_0)^2/t_d^2]\}$$

where t_0 is the time the microburst peak passed through the equatorial plane, t_d determines the duration, and C determines the (1 + C)-fold increase above background (A_0) at the peak. Figure 2 shows a composite emission for microbursts occurring at intervals of 0.3 sec, each with duration (to half peak) of 0.1 sec, and strength corresponding to a fourfold increase in stream density (A) at the peak. A microburst produces a sharp increase in the interaction drift velocity that lasts somewhat longer than the microburst duration (as measured at a fixed point), since the drift velocity (v_t) approaches the electron stream velocity ($v_\parallel$). This in turn produces a sharp increase in emission trace curvature, changing a possibly falling tone into a rising tone. If the microburst is felt by only part of the interaction region, then each microburst will peel off a rising tone. The remaining part produces the parent emission, which has the same form (since the same parameters were used) as the one in Figure 1.

Although the microbursts are all the same, their effect (the form of the branching riser) depends on the state of the interaction when they arrive. Since the microburst produces an impulse to the oscillating motion of the interaction region, the lower the emission frequency at this time of arrival, the higher the upswing of the branching riser. A microburst arriving when the emission frequency is already rising has relatively little effect.

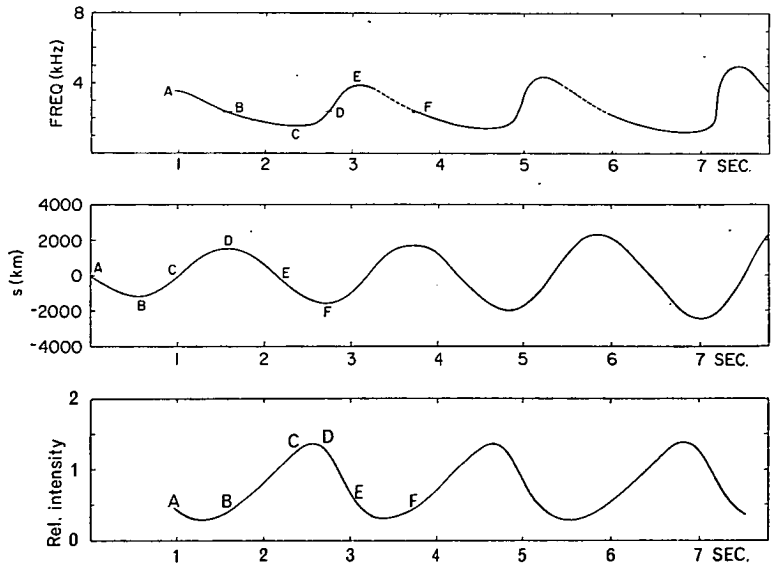

Fig. 1. Emission calculated for a uniform electron stream of energy spectral index $n = 2.25$ and field line parameters $f_n = 10$ kHz, $t_n = 1.5$ sec. *Top*: Frequency versus 'ground' time for the emission's first appearance at the ground (½ hop). Parts that are often not observed and expected to be relatively weaker are shown by the broken curves. *Center*: Position of the interaction region versus true time (i.e., at the interaction region). Correspondence with the spectrogram above is indicated by A, B, C, D, E, F. Positive positions are downstream of the equator (origin), that is, in the hemisphere opposite the observer. *Bottom*: Relative ground intensity (W m^{-2} Hz^{-1}), neglecting propagation losses.

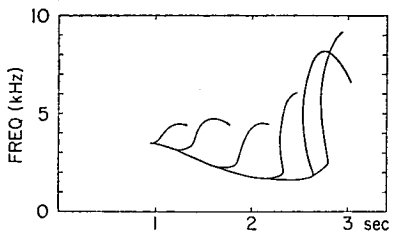

Fig. 2. Emission calculated using the same parameters as in Figure 1 but with superimposed electron spikes or microbursts. These have maximum intensity (stream density) of 4 times background, duration (half intensity) of 0.1 sec, and are spaced 0.3 sec apart.

MAGNETIC DISTURBANCE EFFECTS

Recently *Allcock and Mountjoy* [1970] showed that discrete emissions or chorus can be classified into two distinct types, Q and S, with two intermediate types, IQ and IS. The Q chorus is characterized by the invariable presence of inverted hooks, usually with bandwidths less than 1 kHz and often accompanied by other emissions such as quasi-constant tones and normal hooks. The slopes of the rising parts are about 1 kHz/sec. Q chorus occurs during quiet magnetic conditions (local K index, 0–2). The S chorus, on the other hand, consists of straight tones rising very rapidly (~50 kHz/sec) that are occasionally vertical or even tilting backward. These typically occur in bursts of rising tones, giving the appearance of a rising band starting at ~1 kHz and rising to 7 kHz or higher. S chorus occurs during disturbed conditions (local K index, ~6–8).

Now it will be interesting to see whether our synthetic emissions calculated using field line and electron stream parameters appropriate to quiet and disturbed conditions have the characteristics of Q chorus and S chorus, respectively. In paper A, a relation was found between the location of the field line along which emissions are generated and magnetic index. From this a typical L value during quiet conditions would be ~3.9, corresponding to a nose frequency $f_n = 5.5$ kHz, and for disturbed conditions typical values would be $L = 2.6$ or $f_n = 18$ kHz. These values indicate generation near the plasmapause, though this has no special relevance here. For typical conditions in the plasmasphere, the corresponding values of t_n are 2 sec (for Q) and 0.8 sec (for S). There appear to be few direct (satellite) measurements of the electron parameters A and n in the energy ranges of interest (~5 kev for Q and 30–200 kev for S). However, for energies above 280 kev, *Williams and Smith* [1965] found $n \sim 1.5$–2 during relatively quiet conditions and $n \gtrsim 4$ during disturbed conditions, particularly for the field lines ($L < 3$) where S chorus would be expected. Thus for this exercise we might choose $n = 1.5$ for Q and $n = 4$ for S. In the absence of better information, we will leave A constant for both types. For the initial conditions, we will assume triggering at the equator with initial interaction drift velocity of 2000 km/sec for both.

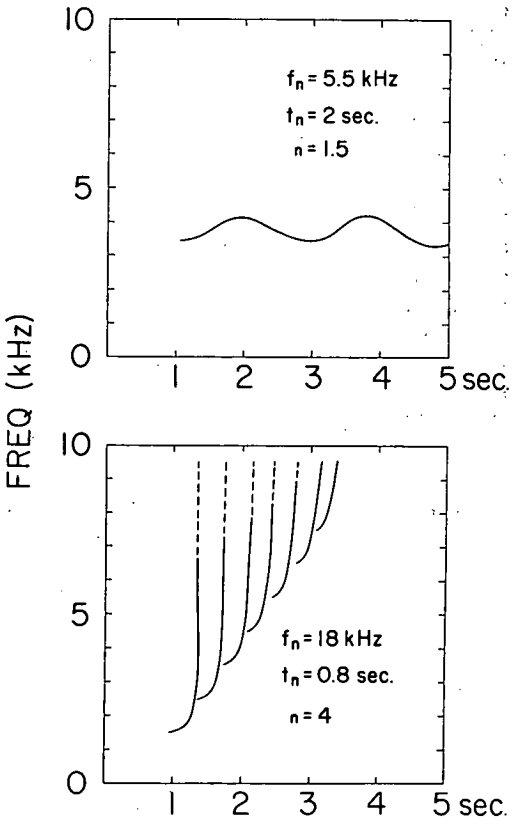

Fig. 3. Emissions calculated using parameters appropriate to quiet (Q chorus, top panel) and disturbed (S chorus, bottom panel) conditions. The S-chorus emissions are calculated for several trigger frequencies and are arranged in time as though each is triggered by the previous one. Calculations were taken up to 9 kHz, but broken curves were drawn to indicate parts that often do not appear in observed events.

Figure 3 shows the emissions calculated from these parameters. For Q chorus a trigger frequency of 3.5 kHz was chosen to place the emission in the typically observed frequency band. A continuous emission is shown, though one generally observes pieces of this as hooks and inverted hooks. Important features that appear are the low slopes and narrow bandwidth. Also, as will be shown later, low spectral indices ($n < 2$) should always produce an oscillating drift motion so that risers produced by microbursts will always bend over to produce inverted hooks. Lower values of initial drift velocity would produce quasi-constant tones for quasi-constant stream intensity A. For the S chorus, a set of trigger frequencies was chosen in 1-kHz steps from 1.5 kHz. The individual risers were spaced out in time as though each was triggered by the previous one. This is possible, since each riser is produced in the hemisphere opposite the observer and so must pass back through the triggering region (assumed here to be the equator) again on its way to the observer. If triggering is much more active during disturbed conditions, we might expect it to occur over a wide range of frequencies and it might be effective over a wider distance from the equator. If so, the risers would trigger new ones before reaching the equator, which would produce larger initial slopes (df/dt). The general features of this synthetic S chorus are the large slopes, the absence of turnover or inverted hooks, and the large over-all bandwidth. This is largely a consequence of high spectral indices that produce interaction drift motions that are always unstable or exponential for $n > 3$, as is shown below. Thus microbursts, which might be prevalent during disturbed conditions, would have little effect on rising tones, but rapidly falling tones, for which v_i is negative, could be changed to rapidly rising tones with hooklike beginnings.

INTERACTION REGION DRIFT STABILITY

One of the most interesting consequences of applying *Helliwell's* [1967] theory to discrete emissions is that the localized region of electron-wave interaction drifts back and forward along the field line about the equator. This oscillatory drift motion was suggested by *Helliwell* [1967] for a rather special electron energy spectrum, but it now appears more general.

In physical terms, what happens is this. Suppose the interaction region is downstream of the equator. Regardless of the drift motion, the emission or interaction frequency will be rising so that resonance will require progressively lower electron energies. If the electron energy spectrum is soft enough (large n), the electron flux at the falling resonant energies will be increasing. Consequently, the drift velocity will be increasing; that is, the interaction region will be accelerated away from the equator. Similarly, for hard enough spectra (small n), the interaction region will be accelerated toward the equator. We reach the same conclusion if we suppose instead that the interaction region is upstream of the equator. For now the emission frequency will be falling and the resonance energy rising. Thus soft spectra will produce decreasing, and hard spectra increasing, drift velocities, corresponding to acceleration, respectively, away from and toward the equator as before. So we see that the drift stability, that is, whether the motion is oscillatory or exponentially divergent, should depend largely on the energy spectral index.

To obtain an analytic expression for the drift stability and drift oscillation period, we note from Figure 1 that the motion computed by successive iterations turns out to be closely sinusoidal. If we denote the position of the interaction region by s, the distance along the field line from the equator, this implies that

$$\ddot{s} = -\omega^2 s \tag{3}$$

where ω is at least quasi-constant and is the drift oscillation frequency. From equation 1, we have

$$v_i = v_\parallel \frac{B\alpha^{-n} - 2K\Lambda^2(1-\Lambda)^{-2}\alpha^{-1}}{B\alpha^{-n} - K\Lambda(1-\Lambda)^{-2}\alpha^{-1}} \tag{4}$$

where we have used $\alpha = v_\parallel^2$ and have expressed $N(E)$ in terms of $v_\parallel$:

$$N(E) = AE^{-n} = B(v_\parallel^2)^{-n} = B\alpha^{-n}$$

then

$$\ddot{s} = (d/dt)v_i$$

The general differentiation of v_i is complicated, but since ω is approximately constant during the drift oscillation we can choose a convenient point to do this. This is one of the extremes

where the drift velocity is zero. The drift acceleration is then produced entirely by the frequency drift (df/dt) and is independent of the gradients along the field line of the gyrofrequency f_H and plasma frequency f_p except where these are already incorporated in the equation for df/dt. Thus we need to find:

$$\ddot{s}_0 = \left(\frac{df}{dt}\cdot\frac{dv_i}{df}\right)_{v_i=0} \tag{5}$$

Writing equation 4 as

$$v_i = v_\parallel x/y$$

we get

$$\frac{dv_i}{df} = \frac{x}{y}\frac{dv_\parallel}{df} - \frac{xv_\parallel}{y^2}\frac{dy}{df} + \frac{v_\parallel}{y}\frac{dx}{df}$$

If $v_i = 0$, then $x = 0$, and so only the last term is nonzero. For this we need α from the Doppler-shifted cyclotron resonance condition:

$$\alpha = v_\parallel{}^2 = c^2\frac{f_H{}^2}{f_p{}^2}\frac{(1-\Lambda)^3}{\Lambda} \tag{6}$$

and its derivative:

$$\frac{d\alpha}{df} = -c^2\frac{f_H}{f_p{}^2}\frac{(1-\Lambda)^2(1+2\Lambda)}{\Lambda^2}$$

and also:

$$\frac{d}{df}\left[\frac{2\Lambda^2}{(1-\Lambda)^2}\right] = \frac{1}{f_H}\frac{4\Lambda}{(1-\Lambda)^3}$$

Then

$$\frac{dx}{df} = \frac{1}{f_H}\left\{\left[-\frac{n}{\alpha}(B\alpha^{-n}) + \left(\frac{K}{\alpha}\frac{2\Lambda^2}{(1-\Lambda)^2}\right)\frac{1}{\alpha}\right]\frac{d\alpha}{d\Lambda} - \frac{K}{\alpha}\frac{4}{(1-\Lambda)^3}\right\}$$

The two terms in the square brackets are related by the condition $x = 0$, giving

$$\frac{dx}{df} = -\frac{2K}{\alpha^2}c^2\frac{f_H}{f_p{}^2}[3 - n - 2\Lambda(n-1)] \tag{7}$$

The same condition gives

$$y = \frac{K}{\alpha}\frac{\Lambda(1-2\Lambda)}{(1-\Lambda)^2} \tag{8}$$

Then using *Helliwell's* [1967] equation 15:

$$\frac{df}{dt} = \frac{54cf_H{}^2}{R_m{}^2 f_p}s\frac{\Lambda^{3/2}(1-\Lambda)^{3/2}}{(1+2\Lambda)^2}$$

We get, finally, from equations 3, 5, 6, 7, 8, and Helliwell's 15:

$$\omega^2 = 108\left(\frac{cf_H}{R_m f_p}\right)^2\frac{\Lambda(1-\Lambda)^2}{(1+2\Lambda)^3}\cdot[3 - n - 2\Lambda(n-1)] \tag{9}$$

where R_m is the geocentric distance to the field line in the equatorial plane, and all units are mks.

For $n > 3$, ω^2 is negative for all frequencies. In this case the drift motion is unstable, for if the interaction region is displaced from the equator the drift speed $|v_i|$ and distance s will increase monotonically and exponentially.

For $n < 2$, ω^2 is positive for all frequencies less than the observed cutoff for guided emissions: $f = \frac{1}{2}f_H$. In this case the drift motion is stable so that displacement from the equator will produce an oscillating drift motion. The drift motion is even more stable (large positive ω^2) for negative spectral indices or 'spectral inversions,' should these occur.

For $3 > n > 2$, ω^2 is positive and the drift motion stable, provided that

$$\Lambda \leq \frac{3-n}{2(n-1)}$$

Satellite measurements in the appropriate region ($L = 3 \sim 4$) reviewed in paper B indicate that spectral indices are typically in this range, as was the spectral index deduced in paper B from emission analysis. Thus this case of conditional stability may be fairly common. However, if we take (from paper A) $\Lambda = 0.2$ as typical, then the drift motion is generally stable below $n \sim 2.4$ and generally unstable for a higher spectral index. The frequency Λ used in equation 9 for calculation of ω^2 must be the frequency emitted where $v_i = 0$. For a stable emission, this is approximately the midfrequency. Equation 9 cannot be used to find how the stability ω^2 varies with frequency during a given emission.

The period of the interaction drift motion can be obtained from equation 9. However, the field line parameters in that expression (R_m, f_H, f_p) are more conveniently expressed in terms of the 1-hop nose delay (t_n), since for a 'gyrofrequency' model along field lines:

$$t_n = 1.2\frac{S}{c}\cdot\frac{f_p}{f_H}$$

where S, the total length of the field line, is approximately 2.2 R_m in the region ($L \sim 3$–4) of interest. Consequently, the interaction drift period from this and equation 9 is:

$$T_i = 0.23 t_n \frac{(1 + 2\Lambda)^{3/2}}{\Lambda^{1/2}(1 - \Lambda)} \cdot [3 - n - 2\Lambda(n - 1)]^{-1/2}$$

The interaction drift period is shown in Figure 4 as a function of midfrequency (more precisely, the frequency for $v_t = 0$) for various values of n. Also shown is a 2-hop nose whistler, that is, the wave-packet bounce period. The left and bottom scales apply for typical field line parameters, whereas the normalized scales (right and top) apply generally.

The interesting feature is that, for all field line parameters, the interaction drift period (T_i) and the 2-hop group delay (T_g) are of the same order of magnitude. This suggests a mechanism to explain nondispersed periodic emissions, particularly the multiphase ones, in terms of harmonic relationships between T_i and T_g. The ratio T_g/T_i depends on frequency, but the trigger frequency in a long series of emissions is often very well defined and only slowly varying (paper A).

Suppose, for example, this ratio is approximately 3. An emission triggered at time $t = 0$ would tend to produce similar parts (risers, say) at intervals of T_i as sketched in Figure 5. At $t = T_g$, a new but similar emission would be triggered by the whistler mode echo of the first producing a new interaction region a little upstream or downstream of the first, if T_g were not precisely $3T_i$. The two interaction regions would tend to merge to a single one, for the downstream one would have an electron stream somewhat depleted of usable kinetic power by the upstream one, and so it would have a lower drift velocity, enabling it to catch up to or be caught up by the upstream one. Alternatively, taking into account the finite length of the interaction region, the second triggering lengthens the original interaction region, which tends to contract to the optimum length given by *Helliwell* [1967].

Thus, for $T_g \sim 3T_i$, we would expect 3-phase periodic emissions. If interaction regions sharing the same resonant electrons attract strongly, the harmonic relationship need not be very close, and by the same token, high-order multiphase periodic emissions would not occur. If the ratio T_g/T_i slowly decreased, either through an increasing trigger frequency or changing spectral index, we would expect 2-phase periodic emissions for $T_g \sim 2T_i$ and 3-phase ones again for $2T_g \sim 3T_i$, with perhaps single-phase ones in between when the harmonic relationships are unfavorable. Thus two ratios T_g/T_i can produce 3-phase versus one for 2-phase. Similarly, if higher orders are possible, four different ratios can produce 5-phase versus two for 4-phase.

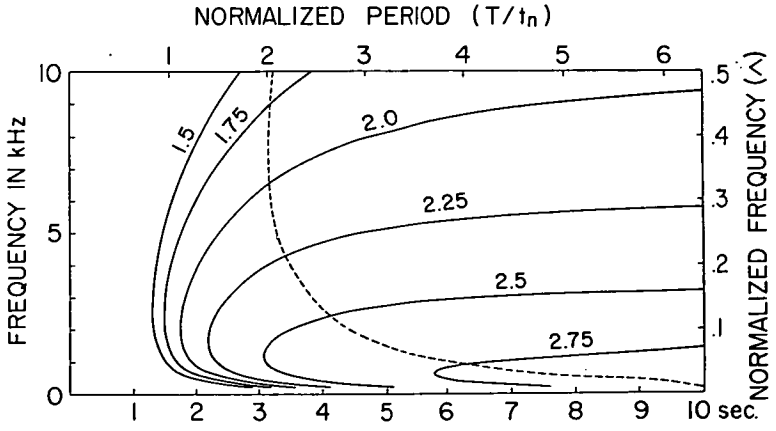

Fig. 4. The interaction drift period versus emission midfrequency for the values of electron energy spectral index shown. The broken curve is a 2-hop nose whistler. The left and bottom scales apply for typical field line parameters, whereas the normalized scales (right and top) apply generally.

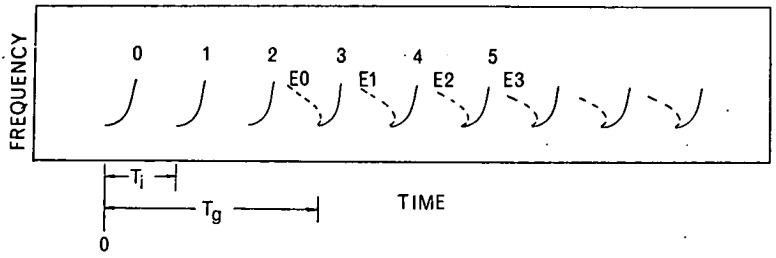

Fig. 5. Spectrogram sketch illustrating a mechanism for generation of 3-phase, nondispersed, periodic emissions. The risers 0, 1, 2 are the strongest parts of a single emission produced by the oscillation motion of the interaction region. Later risers (3, 4, etc.) are triggered by the 2-hop echoes ($E0$, $E1$, etc.) of these, which synchronize the oscillation motion so that $T_i = T_g/3$.

This may explain the observed preference for odd phases over even phases.

A difficulty with this idea is that we would expect such multiphase periodic emissions to consist of a continuous wavelike emission (like that in Figure 1), whereas we often observe only a series of short risers. Perhaps only the rising parts are strong enough to be observed, as was discussed above, whereas the complete emission, though undetected, determines the periodicity relation for the multiphase period. Part of this problem has been with us a long time, for it is generally accepted that single-phase periodic emissions are produced by triggering by whistler-mode echoes, even though these triggering signals are usually not observed.

CONCLUSIONS AND SUGGESTIONS FOR FUTURE WORK

Helliwell's theory is able to explain the features of VLF discrete emissions in terms of quasi-constant electron streams with occasionally superimposed intensity spikes or microbursts. The characteristic forms observed during disturbed and quiet periods are explained in terms of the field line and stream parameters expected during these periods. The periodic nature of the interaction drift motion observed in paper B is predicted by the theory for electron spectral indices less than about 2.4, and this effect may also explain nondispersed multiphase periodic emissions.

Though this agreement does not establish the theory, it does establish the worth of further work, both experimental and theoretical.

Experimental tests might be external or internal. In an external test, one would find the electron stream parameters and possibly also the field-line parameters from external measurements, such as satellite measurements, and either compare these with those deduced from discrete emissions or use these parameters to synthesize emissions that can then be compared with those observed. Internal tests using only VLF data can also be made. For example, does the energy spectral index n deduced from spectral f-v-t shapes of emissions give the right interaction drift period for multiphase periodic emissions in the same event?

Further theoretical work is needed on the microscopic aspects of the interaction, particularly the initiation or triggering. Thus, should triggering occur preferentially at the equatorial plane and often at a characteristic frequency? Can a microburst split the interaction region, one part 'seeing' the microburst and the other ignoring it, as was suggested by the analysis of hooks with branching risers? Can interaction regions pass through one another when the emission frequencies are different and attract one another and coalesce when these frequencies are close, as was suggested in the discussion of multiphase periodic emissions?

Acknowledgments. I wish to thank Professor R. A. Helliwell for helpful discussions and the Cooperative Institute for Research in Environmental Sciences for providing computer time.

* * *

The Editor wishes to thank F. V. Coroniti and R. A. Helliwell for their assistance in evaluating this paper.

REFERENCES

Allcock, G. McK., and J. C. Mountjoy, Dynamic spectral characteristics of chorus at a mid-latitude station, *J. Geophys. Res., 75,* 2503–2510, 1970.

Dowden, R. L., Location of generation regions (in L and λ) of VLF discrete emissions by dispersion analysis of ground station observations, *J. Geophys. Res., 76*(13), 1971*a*.

Dowden, R. L., Electron energy spectrum and structure deduced from analysis of VLF discrete emissions using the Helliwell criterion, *J. Geophys. Res., 76*(13), 1971*b*.

Helliwell, R. A., *Whistlers and Related Ionospheric Phenomena,* Stanford University Press, Stanford, California, 1965.

Helliwell, R. A., A theory of discrete VLF emissions from the magnetosphere, *J. Geophys. Res., 72,* 4773–4789, 1967.

Williams, D. J., and A. M. Smith, Daytime trapped electron intensities at high latitudes at 1100 kilometers, *J. Geophys. Res., 75,* 541–556, 1965.

(Received September 15, 1970;
accepted January 29, 1971.)

Planet. Space Sci. 1971, Vol. 19, pp. 374 to 376. Pergamon Press. Printed in Northern Ireland

DISTINCTIONS BETWEEN MID LATITUDE VLF HISS AND DISCRETE EMISSIONS*

(*Received in final form* 21 *October* 1970)

1. INTRODUCTION AND SUMMARY

Mid latitude VLF emissions fall broadly into two types: band limited noise called hiss and relatively pure rising and falling tones called chorus or discrete emissions. Both appear at frequencies of a few kilohertz at medium latitudes (50°–60° invariant) and have much the same diurnal variations and relationship with magnetic activity. The question arises, is discreteness or diffuseness the only distinction between the two types, hence is hiss merely the result of a sufficient density of overlapping, unresolved chorus?

The purpose of this note is to show another essential distinction between these two types which was observed at Dunedin, New Zealand, during an event lasting about 2 hr on 1st March, 1996. The hiss and discrete emissions were uncorrelated on the short term (minutes) and were found by dispersion analysis of associated whistlers to be propagating along quite different paths. Whereas whistlers travelling along the discrete emission path were characterized by triggering, the hiss path whistlers were characterized by strong

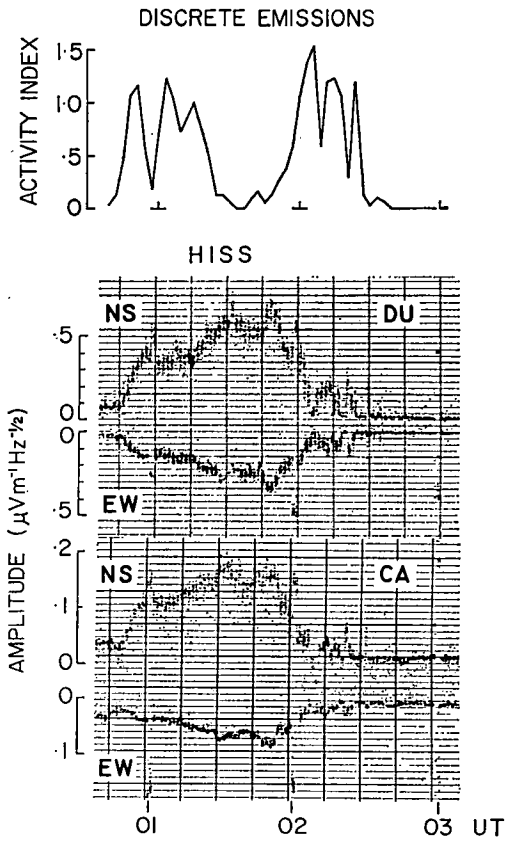

FIG. 1. HISS AMPLITUDE RECORDINGS IN THE BAND 4–5 kHz USING N–S AND E–W LOOP ANTENNAS (TIME SHARING) FROM DUNEDIN AND CAMPBELL ISLAND.
Also shown for comparison is the relative discrete emission activity during this period.

* This work was carried out during the tenure of a Visiting Fellowship awarded by the Cooperative Institute for Research in Environmental Sciences, University of Colorado, Boulder, Colo. 80302, USA.

2. DETAILS

The whole event was recorded wide band on magnetic tape for later spectrum analysis and on medium band hiss amplitude recorders at Dunedin ($L = 2{\cdot}7$) and Campbell Island ($L = 4$), about 800 km to the south. Hiss amplitudes in the band 4–5 kHz using N–S and E–W loop antennas are shown for the two stations in Fig. 1. The relative amplitudes at the two stations and two antennas plus a direction finding from Dunedin indicated that the hiss reached the ground just south of Dunedin at about $L = 3$. This is consistent with location by dispersion analysis discussed below.

Sample spectrograms of the event are shown in Fig. 2. In panel A, whistlers 2W and 4W echoing in the discrete emission path (since both trigger risers) are initiated by the sferic at the arrow. This sferic also appears to be the source of the train of hiss bursts. Thus the hiss is either triggered by a whistler from this sferic or is itself a multihop swishy whistler of limited band width. Despite the fuzziness of the hiss, the period or 2-hop delay at 5 kHz can be measured accurately because this train and others in this event persisted for about twenty or thirty such periods. Note that the 2-hop delay is quite different from that for 2W, 4W, implying that the hiss is echoing in a path different from the discrete emissions.

amplification limited to the hiss frequency band. It is suggested here that hiss may be strong, band limited amplification of the ever present wide band background of whistlers and incoherent electron noise. Thus hiss appears to be produced by an amplifier type or convective instability whereas, as usually proposed, discrete emissions are produced by an oscillator type or non-convective instability. However, the radiative instability (transverse or electron cyclotron) may be the same for both since it is shown here that cyclotron resonance amplification by electrons having energy and pitch angle distributions consistent with satellite measurements could produce both the hiss amplitude and spectrum observed.

Panel B also shows whistlers 2W and 4W echoing in the discrete emission path initiated by the indicated sferic. The same sferic initiated the intense whistler 2HW which is identified as hiss path by the 2-hop delay at 5 kHz. This whistler is barely detectable outside the hiss band but quite intense within the band. On the other hand the discrete emissions and their associated whistlers are not augmented by the hiss band.

A large number of whistlers initiated by sferics from both hemispheres were recorded during the event. Identification of discrete path whistlers was relatively simple since they usually triggered risers. However since whistlers occurred every minute or so throughout the event with very little change in delay and dispersion it was also possible to identify the hiss path by comparison with the previous hiss path whistler starting from that shown in Panel B. This was easier for 2-hop whistlers for fewer paths appeared—usually only the discrete and hiss paths, and a few much shorter (less delay) ones. An example which occurred near the end of the event is shown in Panel C. The discrete path path whistler which appears at 1DW after its first hop triggered risers on its second and third hop. These are the negative slope (1½ hop dispersion) and normal risers (½ hop) which appear at 3DW. The one hop hiss path whistler 1HW still appears to be augmented in the band previously occupied by hiss, although by this time the hiss is detectable only on the more sensitive hiss amplitude recorders (Fig. 1).

Dispersion analysis of 22 whistlers and 14 whistler mode echoes of discrete emissions gave a quality weighted average of the discrete path parameters in terms of nose frequency, $f_n = 9{\cdot}9$ kHz, and group delay per hop at this frequency, $t_n = 1{\cdot}47$ sec. Similarly the hiss path parameters determined from 14 whistlers were $f_n = 12{\cdot}8$ kHz and $t_n = 1{\cdot}25$ sec. Thus the discrete emissions occurred on a path near $L = 3{\cdot}2$ and the hiss at about $L = 3{\cdot}0$. During the main part of the event (0100–0200 UT) both paths drifted towards the Earth by about $\Delta L = 0{\cdot}2$.

Further evidence of the mutual independence of discrete emissions and hiss is shown in Fig. 1. The activity index for discrete emissions was based on their accumulated length in the spectrograms. Thus if all the discrete emissions in a three minute interval just spanned the interval when straightened out and placed end to end, the index would be unity. Comparison of the discrete activity and the hiss amplitude for any of the station and antenna combinations in Fig. 1 shows that the discrete-vs.-hiss correlation is zero or less (i.e. slight indication of anticorrelation). A scatter diagram using three minute averages of both showed this also. We would expect a positive correlation for averages taken over much longer periods if only because both are related to magnetic activity.

The evidence above suggests that hiss occurs whenever conditions are suitable for strong band limited amplification. The original signal might be the ever present wide band background of whistlers and incoherent electron noise. If so the hiss spectrum would be determined by the amplification which must also be quite large, for the maximum hiss level in Fig. 1 is at least 40 dB above that during the quiet periods at Dunedin (after 0230 UT). Hiss appears to exist quite independently of discrete emissions and may be merely a special case of normal whistler amplification. The disturbed conditions which lead to strong amplification may also be those which provide the right conditions for chorus so we would expect a general correlation on the long term.

Doppler shifted cyclotron resonance amplification by electrons having energy and pitch angle distributions of the form $E^{-n} \sin^m \alpha$ has been considered by Liemohn (1967). The hiss path parameters, f_n, t_n, deduced above give the path minimum gyro and plasma frequencies of 34 kHz and 250 kHz respectively. The hiss center frequency normalised to this minimum gyro frequency is then 0·15 and the normalised band width is

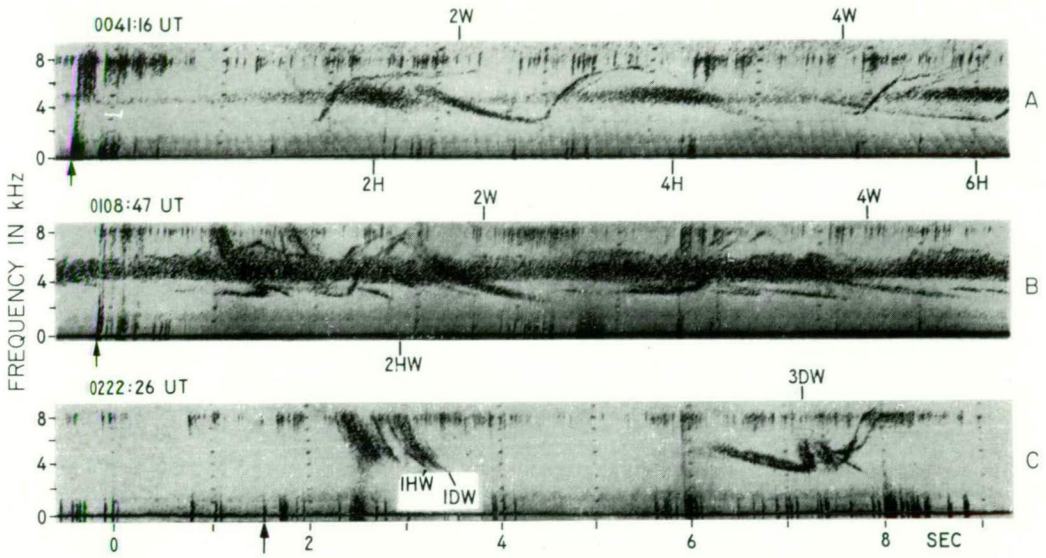

FIG. 2. SAMPLE SPECTROGRAMS FROM DUNEDIN DURING THIS EVENT.
Panel A: Riser triggering whistlers (2W, 4W) and a train of hiss bursts (2H, 4H, 6H), both originating from the sferic at the arrow. The different 2-hop group delays imply different paths. Panel B: Discrete emission path whistlers (2W, 4W) and a short but intense whistler (2HW) from the same sferic (arrow). This whistler (2HW) is strongly amplified in the hiss band and has the same 2-hop group delay as the hiss bursts in Panel A. Panel C: Short or single hop multi path whistlers, including the discrete emission path whistler (1DW), which triggers the emissions seen at 3DW on later hops, and the hiss path whistler (1HW), which is still augmented in the band previously occupied by hiss.

about 0·05. If we assume that during quiet periods the amplification is around 30–40 dB (observable whistlers but no hiss) and at least 40 dB more than this during disturbed periods (for hiss), then we require 70–80 dB amplification. From the curves given by Liemohn (1967), electrons with energy and pitch angle indices of around $n \sim 3$–4 and $m \sim 0{\cdot}3$ would produce adequate amplification with about the right center frequency and band width.

Most of the amplification would be produced in the general vicinity of the equator, so the resonant electron energies would be of the order of 20 keV. Suitable satellite measurements in this energy range do not seem to be available, but for energies above 280 keV, Williams and Smith (1965) found $n \sim 3$–5 for $L = 3$ during disturbed periods.

Department of Physics R. L. DOWDEN
University of Otago
Dunedin, New Zealand

REFERENCES

LIEMOHN, H. B. (1967). Cyclotron-resonance amplification of VLF and ULF whistlers. *J. geophys. Res.* **72,** 39–55.

WILLIAMS, D. J. and SMITH, A. M. (1965). Daytime trapped electron intensities at high latitudes at 1100 km. *J. geophys. Res.* **70,** 541–56.

Journal of Atmospheric and Terrestrial Physics, 1971, Vol. 33, pp. 1125–1129. Pergamon Press. Printed in Northern Ireland

SHORT PAPER

Determination of nose frequency of non-nose whistlers

R. L. DOWDEN
Department of Physics, University of Otago, Dunedin, New Zealand
and
G. McK. ALLCOCK
Physics and Engineering Laboratories, D.S.I.R., Lower Hutt, New Zealand

(*Received* 26 *October* 1970)

Abstract—A method is described for determining nose frequency (f_n) and minimum group delay (t_n) from measurements of group delay at many frequencies along the observed whistler trace. It is primarily intended for the analysis of whistlers which do not reach the nose frequency, but the multipoint sampling may give improved accuracy for nose whistlers also, particularly if the traces are ill-defined. It is well suited to digital computation since only algebraic manipulations are involved.

1. INTRODUCTION

THE STANDARD extension method (SMITH and CARPENTER, 1961) used to determine the nose frequency of whistlers whose recorded dynamic spectra do not reach the nose frequency uses measurements at the points (f_1, t_1, and f_2, t_2) at each end of the observed trace. The nose frequency (f_n) and minimum group delay (t_n) are then determined from the ratios f_1/f_2 and t_1/t_2 by reference to a set of standard curves. By contrast, the method described here uses as many points (f, t) on the observed trace as desired and f_n, t_n are calculated from these using only algebraic manipulations. This has the advantage that full use can be made of the available data and the effect of random reading errors is considerably reduced.

2. EMPIRICAL RELATIONS FROM OBSERVED WHISTLERS

Consider the quantity (the reciprocal of the 'dispersion')

$$Q(f) = (t\sqrt{f})^{-1}$$

where t is the group propagation time per hop at frequency f. Figure 1 shows Q as a function of frequency for a well-defined nose whistler. The $Q(f)$ points fit closely a straight line which intercepts the $Q = 0$ axis at $f_0 = 41$ kHz, or 3·06 times the observed nose frequency (13·4 kHz). This linearity of Q–v–f has been found in about 100 non-nose whistlers measured. Measurements of 19 well-defined nose whistlers gave a mean ratio* of zero-Q frequency (f_0) to observed nose frequency of $3{\cdot}09 \pm 0{\cdot}04$ (standard deviation).

Consequently one can use this property to determine the nose frequency (f_n) of whistlers, which do not exhibit the nose by extrapolation of the $Q(f)$ regression line obtained from $t(f)$ measurements within the available frequency range. The value

* This factor includes the effect of the ionosphere so ionospheric dispersion should not be removed from data when using this method.

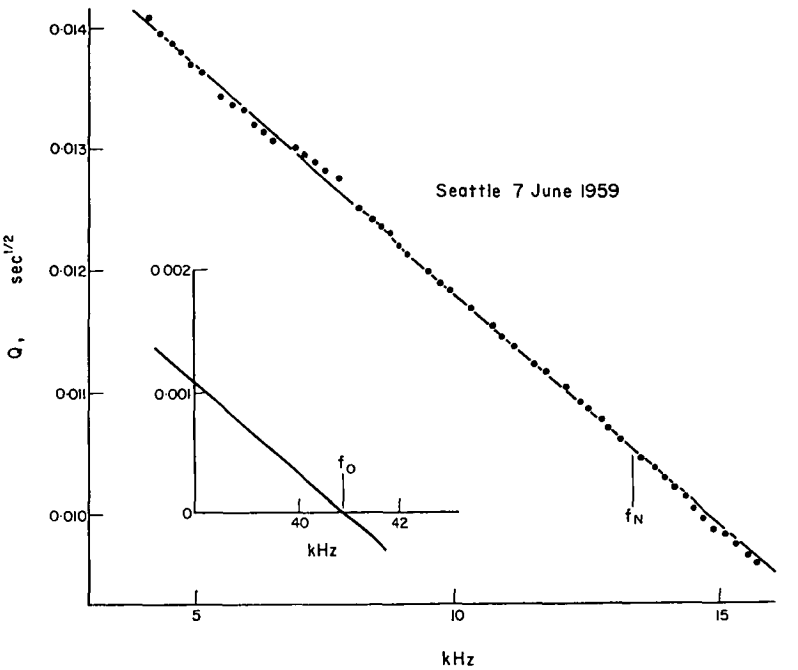

Fig. 1. $Q(f)$ plot of a well-defined nose whistler. (This whistler is shown in Fig. 4-17b of HELLIWELL (1965) and the $f(t)$ data was taken from his Fig. 4-18.) The Q and f scales used here have been offset and expanded to show up any non linearity. Extrapolation of the regression line (see inset) shown gives f_0 = 41 kHz, or 3·06 times the observed (arrow) nose frequency, at Q = 0.

of Q at f_n then also allows calculation of t_n, the group propagation time per hop at the nose frequency. In terms of f_0 and the slope:

$$Q' = \mathrm{d}Q/\mathrm{d}f \tag{1}$$

We get

$$f_n = f_0/3{\cdot}1 \tag{2}$$

$$t_n = -(2{\cdot}1\ Q' f_n^{3/2})^{-1}. \tag{3}$$

3. Systematic and Random Errors

The 19 well-defined nose whistlers used to determine $\alpha = f_0/f_n$ had nose frequencies ranging from 3 kHz to 20 kHz. There was no evidence of α dependence on f_n. Also the spread in α values ($\sim$1 per cent) could be entirely due to errors in direct measurement of f_n.

Another systematic error would arise (if not allowed for) if Q–v–f is not strictly linear. This can be estimated by comparing values of f_n calculated using different portions of a single whistler. For example, Table 1 shows these for the whistler of Fig. 1.

If group delay measurements (t) are made at N different frequencies (f) the effect of random errors (Δt) on deduced f_n can be determined by standard least squares

Table 1

Range (kHz)	f_n (kHz)	error (per cent)	t_n (sec)	error (per cent)	$f_n + \Delta f_n$	error (per cent)
Observed	13·4	–	0·822	–	13·4	–
4–16	13·3	−1	0·822	<0·1	13·3	−1
4–8	13·9	4	0·818	−0·5	13·4	0
8–12	13·5	1	0·818	−0·5	13·5	1
12–16	12·7	−5	0·816	−0·7	13·2	−1

The errors in t_n are less than the whistler trace width or spectrogram resolving time (about 5 msec). The errors in f_n show a barely significant trend which is removed to below significance by an updating correction (last two columns) discussed later.

regression theory:

$$\Delta f_n/f_n = \gamma \Delta Q/Q$$
$$= \gamma \Delta t/t$$

where $$\gamma^2 = N^{-1}(\beta + 1)/(\beta - 1)$$

where β is the frequency mean square to square mean ratio:

$$\beta = \overline{f^2}/\bar{f}^2.$$

For a typical case involving 20 independent measurements over a 2:1 frequency range (e.g. 5–10 kHz), $\gamma \sim 1{\cdot}6$, giving an error in f_n ranging from about 1–2 per cent for a well defined whistler to perhaps 20–30 per cent for a diffuse whistler. Note that for measurements in the range f_1–f_2, the effect of random errors depends (through γ) essentially on the ratio f_2/f_1 and not on f_n/f_2, the degree of extrapolation required. Thus the method works equally well for both extrapolation to f_n from either below (non-nose whistlers) or above ('nose-top' whistlers), and for interpolation to f_n (ill defined or partly obscured nose whistlers).

4. Consideration of Theoretical Models

It should be emphasised that the relationships above are derived entirely from the properties of observed nose whistlers, and not by considering the dispersion expected from a model of electron density distribution along the field line path. The method above merely gives f_n, t_n. Standard methods (which require such a density model) for deducing, say, the minimum gyrofrequency and electron density along the path in terms of observed f_n, t_n, already exist and will not be discussed here.

However it is worth investigating to see if the observed properties, linear Q and $\alpha = 3{\cdot}1$, are to be expected from realistic models.

A realistic model (diffusive equilibrium in the magnetosphere with a small correction for the ionosphere) is not tractable, so two simpler models, which correspond to extremes on either side of a realistic one, will be considered here.

A constant density model with certain other approximations (Helliwell, 1965) gives a linear Q relationship and $\alpha = 3{\cdot}0$. For a 'gyrofrequency' model (electron density proportional to gyrofrequency) the dispersion or $Q(f)$ can be expressed in terms of complete elliptic integrals of the second kind (Smith and Carpenter, 1961). For this model $Q(f)$ is not strictly linear so that the value of f_0 deduced from $Q(f)$

values in a restricted range of frequencies centered on $\bar{f}$ depends on $\bar{f}$. Hence the value of α needed to give the correct f_n also depends on $\bar{f}$. This value of α calculated from elliptic integrals is shown in Fig. 2 as $1/\alpha$ versus $\bar{f}/f_{HO}$ (the sample mean frequency normalised to the path minimum gyrofrequency). The 19 nose whistlers used to determine α experimentally had mean frequencies of about three quarters of the observed nose frequency ($\bar{\Lambda} \approx 0{\cdot}75\Lambda_n$). For this case the gyrofrequency model predicts a value of α close to that observed.

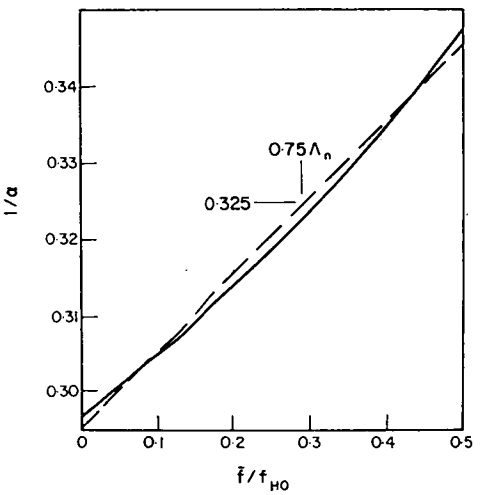

Fig. 2. $1/\alpha$ versus $\bar{f}/f_{HO}$ (solid curve). The broken line is a linear approximation of $1/\alpha$ used to derive equation (4). Note that $\alpha \approx 3{\cdot}1$ at $0{\cdot}75$ times the nose frequency in agreement with the value derived empirically from observed whistlers for this average frequency.

From the above it appears that the properties predicted by these two extreme models are not significantly different from those observed. However Table 1 shows some slight experimental evidence that α varies with $\bar{f}$. This is to be expected if the plasma density is not strictly constant. However the effect will be small even for a gyrofrequency model, so we might use the latter to determine a correction. This would have the additional advantage of bringing our method into line with the Smith–Carpenter method which is also based on this model.

Using the straight line in Fig. 2 as a reasonable approximation to the $1/\alpha$ curve, we get

$$\Delta f_n = 0{\cdot}12(\bar{f} - 0{\cdot}75f_n). \tag{4}$$

This correction is quite small (a few per cent) but does appear to give a significant improvement in Table 1. If a computer program is used for this Q-analysis method the correction is a simple update statement. The corresponding correction to t_n would involve both this updated f_n value and a different 'constant' (instead of 2·1) derived from a corrected α. It turns out however that these two corrections are nearly equal and opposite. So the correct procedure is to calculate f_n from equation (2), t_n from equation (3) and then, if desired, update f_n according to equation (4).

Acknowledgement—The work by R. L. DOWDEN was carried out during the tenure of a Visiting Fellowship awarded by the Cooperative Institute for Research in Environmental Sciences, University of Colorado.

REFERENCES

SMITH R. L. and CARPENTER D. L. 1961 *J. geophys. Res.* **66**, 2582.

HELLIWELL R. A. 1965 *Whistlers and Related Ionospheric Phenomena*. Stanford University Press, Stanford.

Trigger Delay in Whistler Precursors

R. L. DOWDEN[1]

Cooperative Institute for Research in Environmental Sciences
University of Colorado, Boulder, Colorado 80302

Detailed dispersion analysis of about thirty precursor events showed that the associated long whistlers traveled in the plasmasphere, at $L \sim 2.5$–3.8, and probably in the same duct as their precursors. Measurement of the f, t trigger points of the precursors showed that the time of triggering (t) was generally more than halfway between the initiating lightning flashes and the associated two-hop whistlers by an amount (Δt) that generally decreased with trigger frequency (f). Because of apparent objections to triggering by hybrid whistlers, three alternative eplanations are investigated. Since all these are subject to serious objections, the hybrid explanation is re-examined. It is shown that the hybrid signal is expected to be quite weak (and hence rarely, if ever, observed) and that weak trigger signals should give, according to R. A. Helliwell's 1967 theory, both a delay and a frequency shift that account for the observed trigger points quite well.

Precursors are VLF discrete emissions that are observed before the whistlers with which they appear to be associated. Several examples are shown by *Helliwell* [1965, Figure 7–53] and *Laaspere and Wang* [1968] (these two references are abbreviated to H and LW in what follows). A schematic drawing is shown in Figure 1.

Relevant properties of precursors seem to be:

1. Precursors are associated only with long whistlers (H and LW).
2. Echoing precursors show the same round-trip delay as their associated whistlers, implying similar paths (H and LW).

The first and most straightforward explanation (H) is that the precursor is triggered by the short component of a hybrid whistler, which results when part of the energy from a lightning flash in the observer's hemisphere travels in the earth-ionosphere waveguide to the opposite hemisphere before entering the magnetosphere. However, further observed properties present difficulties:

3. The expected hybrid whistler is not observed (H and LW).
4. The precursor begins at a time not halfway between the causation impulse and the associated long whistler, but a little later (Δt, as shown in Figure 1) (LW).
5. Simultaneous observations at spaced stations show differences in the relative intensities of precursor traces and the associated whistler, implying, contrary to property 1, different propagation paths (LW).

A few alternative explanations occurred to the writer, and so it was decided to make detailed dispersion analyses of available observations to determine the properties of precursors more precisely and to examine these explanations in the light of these properties.

OBSERVATIONS

From available data (see *Acknowledgments*), about thirty events were selected as sufficiently well defined for detailed analysis. Dispersion analysis [*Dowden and Allcock*, 1971] of the non-nose whistlers (some showed noses) gave the nose frequency f_n and delay per hop t_n for each. Nose frequencies ranged from about 6 to 20 kHz, corresponding to L shells of propagation in the range 2.5–3.8. The 'scale' frequency [*Dowden*, 1962], obtained by dividing the square of minimum plasma frequency (obtained from f_n, t_n) by the minimum cyclotron frequency (from f_n), is relatively constant in the inner magnetosphere or plasmasphere at about

[1] Permanent and present address: Department of Physics, University of Otago, Dunedin, New Zealand.

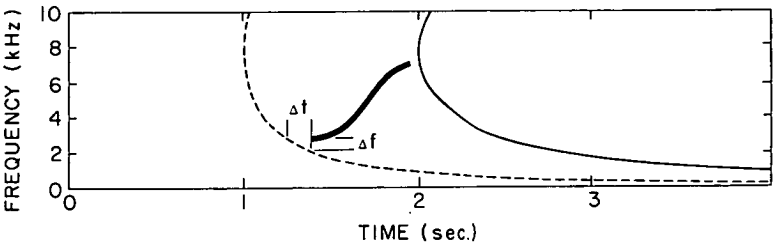

Fig. 1. Schematic drawing of a precursor event. A lightning flash at time origin produces the observed two-hop whistler. The precursor (thick trace) begins a little after (Δt), the halfway curve (one-hop whistler) shown as broken. An alternative interpretation is that it is initiated with a frequency shift (Δf) or a combination of the two.

one megahertz, and also in the outer magnetosphere or plasma trough at a few tens of kilohertz. Values measured from these whistlers were in the range 850 to 1700 kHz, indicating that the whistlers and precursors propagated within the inner magnetosphere, though perhaps just inside the plasmapause.

In events showing echoing precursors, there was no detectable difference between the round trip delays of the precursors and their associated whistlers. Since a delay difference of 1% to 2% would usually have been detectable, this implies propagation paths within about 0.1 of L and 0.5° of invariant latitude, so that the north-south separation of the exit points should be less than about 50 km. Since whistler measurements also show east-west gradients in the magnetosphere [*Park and Carpenter*, 1970; *Bullough and Sagredo*, 1970], the east-west separation of exit points should be within a few hundred kilometers. Although not conclusive, the evidence thus suggests that both precursor and whistler travel in the same duct and that property 5 (above) is not due to different magnetospheric paths.

Contrary to property 3, one of the thirty events (shown by R. M. Gallet at the Conjugate Point Symposium, Boulder, 1967) clearly showed the short hybrid whistler extending down to within about 500 Hz of the precursor trigger frequency. Simultaneous observation at conjugate stations (Cape Sarichef, Alaska, and Waimate, New Zealand) showed both the normal short and long versions of the associated whistler, the hybrid, and the precursor with a one-hop echo; this is adequate information to identify these relationships with confidence.

For all events, the frequency and time of triggering (the trigger point) of the precursor were measured and were compared with the one-hop delay calculated by dispersion analysis of the associated whistler to determine the apparent delay Δt, or frequency shift Δf, defined in Figure 1. These measurements can be displayed in the following way. As is well known, f_n (or the path minimum cyclotron frequency, f_H) and t_n determine the whistler for a given hop number, and so if the frequency-time spectrogram scales are normalized to f_H and t_n, respectively, all the two-hop whistlers appear as a single trace. Thus all the precursor events can be shown in a single diagram as in Figure 2. The precursor trigger points, also scaled in this way, are shown as circles.

Curve A in Figure 2 is the short one-hop hybrid component of the precursor's associated long whistler (thick curve). This should occur as shown with half the delay of the long whistler plus about 30 msec to allow for the earthbound travel of the hybrid initiating pulse, from the observer's to the opposite hemisphere. Even so, most of the trigger points in Figure 2 are to the right or above this curve, implying an additional delay (Δt) or frequency offset (Δf).

Alternative Explanations

Three alternative explanations have been examined in detail. Since all three are subject to serious objections, this work is only briefly summarized here.

1. *Longitudinal resonance.* *Helliwell* [1965] suggested that an electron stream modified through longitudinal resonance by the one-hop whistler might become unstable to transverse

(cyclotron) resonance and so radiate an emission back along the path. However, it is not clear how the longitudinal phase bunching produced by the whistler can induce cyclotron instability, which requires helical bunching. Also, the two resonance conditions show that, for a typical normalized trigger frequency $\Lambda \sim 0.1$, the cyclotron resonance requires electron energies some 2 orders of magnitude above those for longitudinal resonance.

2. *Electron bounce. Cornwall and Shulz* [1970] showed that two particles that have the same three adiabatic invariants recover their initial gyrophase relationship after each bounce period and so a reversed relationship after a half period. It is conceivable, then, that electrons which are cyclotron phase bunched by the one-hop whistler, but which for some reason do not radiate, are phase bunched again, but in the reverse direction, after a half bounce period. Emission this time, if it occurs, would be back along the path and would be observed on the ground with an apparent trigger delay $\Delta t(f)$ corresponding to the half bounce period of electrons resonant at frequency f. The expected (normalized) trigger locus is shown in Figure 2 as curve B. There are other objections to this explanation which will not be discussed, for it is clear that the observed delays do not fit this curve.

3. *Magnetospherically reflected whistler.* Suppose a nonducted whistler (from the same lightning flash that produces the two-hop associated whistler eventually observed on the ground) is 'magnetospherically reflected' [*Smith and Angerami*, 1968] somewhat beyond the equator and triggers an emission (the precursor) on its way back. Again there are other difficulties, but there would be an apparent trigger delay Δt corresponding to the difference between the travel time taken by the nonducted whistler to reach the equator (trigger point?) after one magnetospheric reflection and the half hop travel time of a ducted whistler. The expected trigger locus is shown in Figure 2 as curve C, which, however, clearly does not fit the observed trigger points.

DISCUSSION

Since these alternative explanations raise difficulties and predict trigger delays (Δt) much greater than those observed, we will re-examine the objections to the hybrid whistler explanation. These are properties 3 and 4. Property 5 has been dealt with above.

An apparent exception to property 3, the nonobservance of the short hybrid whistler, is noted above. We would expect such observations to be relatively rare, for although short hybrid whistlers are much weaker than their long com-

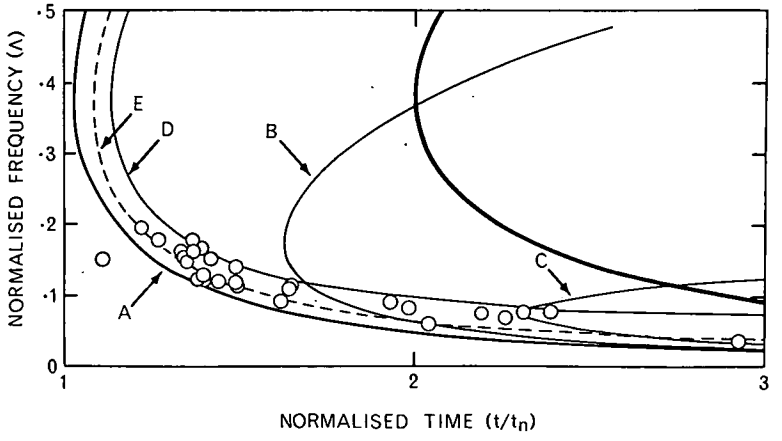

Fig. 2. Precursor starting points (circles) in normalized frequency (f/f_H) and time (t/t_n). For these normalized scales, all the associated two-hop whistlers are represented by the one thick curve. The two curves labeled B and C are the expected loci of trigger points for (B) the 'electron bounce' and (C) 'MR whistler' explanations, respectively. The other three curves are expected trigger loci for hybrid whistler triggering with (A) zero trigger delay and frequency offset, (D) maximum delay and offset, (E) intermediate values.

ponents (H), the precursor's associated long whistler is usually weaker than the precursor (LW) and is sometimes barely detectable, and 'occasionally a riser that follows an impulse and has all the earmarks of a precursor is accompanied by no whistler at all' (LW). It seems that signals strong enough for triggering in the magnetosphere need not be of detectable strength at ground level, for though periodic emissions are satisfactorily explained in terms of triggering by echoes of previous emissions (H), the trigger signals rarely appear. Indeed, it has been suggested that perhaps all 'spontaneous' discrete emissions have invisible triggers.

The other objection (property 4) is that, though normal whistler-triggered emissions seem to branch off the triggering whistlers without any discontinuity, precursors appear to be triggered after a slight delay (Δt). On the other hand, emissions triggered by Morse pulses [*Helliwell et al.*, 1964, 1965] have both a delay $\Delta t \sim 140$ msec and a frequency offset $\Delta f \sim 300$ Hz. Though such effects might conceivably arise because of the very different nature of a Morse pulse compared with a whistler, *Helliwell*'s [1967] interaction theory, which accounts for both the form and magnitude of these effects quite well, predicts them when the triggering signal is of marginal amplitude. This suggests that the rare observance or nonobservance of the hybrid trigger signal and the observed trigger delay are both consequences of the same thing: a weak hybrid signal.

Consider first the delay, Δt. *Helliwell* [1967] gives (in Helliwell's notation)

$$\Delta t = 2L/v_{\parallel} + 2L/v_g$$

where L is the length of Helliwell's resonance region, $v_{\parallel}$ is the cyclotron resonance velocity, and v_g is the wave group velocity. This is the maximum delay corresponding to the interaction time, the time taken for the resonant electrons to go through the complete unbunched, fully bunched, fully debunched cycle. The delay could be zero or very short in the case of a plasma hovering on the threshold of instability, and so in general could be anywhere between these two extremes. The halfway point, the resonance time (when the electrons are fully bunched), might be a likely intermediate value.

Using the various equations in *Helliwell* [1967] to express L, $v_{\parallel}$, and v_g, and so Δt in terms of Λ, f_H, and f_p, and expressing t_n in terms of these same quantities, we find that the delay normalizes quite well, giving:

$$\Delta t/t_n = K_1(1 + 2\Lambda)(1 - \Lambda)^{-1}\Lambda^{-2/3}$$

where K_1 contains only slowly varying quantities (e.g., the 18th root of f_H), so that in the region of interest (L shells of 2½ to 4) we have

$K_1 = 0.02$ (maximum or interaction time)

$K_1 = 0.01$ (resonance time)

The frequency offset Δf in a similar way can be expressed as the maximum value (Helliwell's notation):

$$\Delta f = 4.5 f_H L^2/R_m^2$$

where R_m is the equatorial geocentric distance to the field line. Again under appropriate conditions, Δf might be zero or have an intermediate value of one quarter of this. It can be shown that this expression also normalizes in terms of Λ and a slowly varying factor adequately represented by a constant in the region of interest:

$$\Delta\Lambda = K_2(1 - \Lambda)\Lambda^{-1/3}$$

where

$K_2 = 0.014$ (maximum)

$K_2 = 0.0035$ (intermediate)

Trigger locus curves for the two effects combined (Δf and Δt) are shown in Figure 2 as the solid curve D (maximum K_1 and K_2) and the broken curve E (intermediate K_1 and K_2).

According to this theory, all trigger points should lie between curves A and D. Since all but one do, and this one is displaced only by about the possible error, the agreement is quite good.

Acknowledgments. The percursor measurements in this work were made from events published in *Helliwell*'s [1965] book and from spectrograms kindly provided by R. M. Gallet and T. Laaspere, to whom I am also grateful for helpful discussions.

* * *

The Editor wishes to thank F. V. Coroniti, S. H. Gross, and R. A. Helliwell for their assistance in evaluating this paper.

REFERENCES

lough, K., and J. L. Sagredo, Longitudinal tructure in the plasmapause: VLF goniometer bservations of knee whistlers, *Nature, 225,* 038–1039, 1970.

nwall, J. M., and M. Schulz, Adiabatic preser-ation of gyrophase coherence in the earth's eld, *J. Geophys. Res., 75,* 4339–4342, 1970.

wden, R. L., 'Scale frequency' of the exosphere, *lature, 195,* 984–985, 1962.

wden, R. L., and G. McK. Allcock, Determina-on of nose frequency of non-nose whistlers, *J. tmos. Terr. Phys., 33,* 1125–1129, 1971.

lliwell, R. A., *Whistlers and Related Iono-pheric Phenomena,* Stanford University Press, tanford, Calif., 1965.

lliwell, R. A., A theory of discrete VLF emis-ions from the magnetosphere, *J. Geophys. Res., 2,* 4773–4790, 1967.

lliwell, R. A., J. Katsufrakis, M. Trimpi, and N. Brice, Artificially stimulated very-low-frequency radiation from the ionosphere, *J. Geophys. Res., 69,* 2391–2394, 1964.

Helliwell, R. A., J. Katsufrakis, and I. Kimura, Artificially stimulated VLF emissions, paper presented at URSI Meeting, Washington D. C., April 1965.

Laaspere, T., and C. Y. Wang, Whistler precursors, *Radio Sci., 3,* 213–218, 1968.

Park, C. G., and D. L. Carpenter, Whistler evidence of large scale electron-density irregularities in the plasmasphere, *J. Geophys. Res., 75,* 3825–3836, 1970.

Smith, R. L., and J. J. Angerami, Magnetospheric properties deduced from Ogo 1 observations of ducted and nonducted whistlers, *J. Geophys. Res., 73,* 1–20, 1968.

(Received December 4, 1970;
accepted October 19, 1971.)

Use of Electron and Proton Beams for Production of Very Low Frequency and Hydromagnetic Emissions

R. L. DOWDEN

Physics Department, University of Otago, Dunedin, New Zealand

The feasibility of using helical partical beams (~10 kev, 1 A) fired from orbiting satellites to produce backward Doppler-shifted cyclotron emission (very low frequency from electrons, hydromagnetic or micropulsations from protons) is considered. It is found that the frequency and position of emission can be controlled by choice of particle energy and by gyrophase modulation (or 'rotation') of the beams at the desired frequency. Phase spread of the prephased beams through both natural processes and limitations of accelerators, as well as through radiative instability of the beams, should not be serious. Emitted powers of tens of watts are expected.

A new generation of earth orbital satellites concerned more with active experiments than with passive monitoring is expected in the late seventies and beyond. Active experiments involving, say, 10-kw VLF transmitters, 10-kw particle accelerators (10 kv, 1 amp), and structures (beams, antennas) of about 100-meter dimension should be possible. An experiment is proposed here involving the use of such accelerators to produce phased beams for coherent emission. The VLF emission from electrons is considered in detail, and hydromagnetic (hm) emission from protons is briefly discussed by analogy.

The VLF transmitters on the ground have been used for some time to trigger VLF emissions. However, since the triggered signal travels on the same path, in the same direction, and at very nearly the same frequency, such experiments alone do not determine the position along the field line where triggering takes place or even resolve whether the emission is backward (cyclotron) or forward (Cerenkov), although recent experiments involving monitoring of precipitated electrons as well have indicated backward emission at the equator [*Rosenberg et al.*, 1971]. Also VLF transmitters provide only two variable parameters, frequency and power, and the use of electrically short antennas with high Q tuning places further restrictions on these (carrier frequencies, $\gtrsim 5$ kHz; modulation frequencies, $\lesssim 50$ Hz).

Satellite-mounted electron accelerators, on the other hand, provide four variable parameters, electron velocity, beam current, and two deflection directions. These accelerators make it possible to fire an electron beam that, at some predetermined point s along the field line, takes up the structure and phasing appropriate for coherent emission in the desired emission mode (e.g., cyclotron or Cerenkov) at the predetermined frequency f and emission angle θ. For example, a field-aligned beam velocity-modulated at frequency f would become intensity-modulated at a predetermined point s and so radiate coherently in the Cerenkov mode at frequency f and at an angle θ determined by the appropriate choice of electron velocity and perhaps by broadside phasing also. For backward Doppler-shifted cyclotron emission, on the other hand, one requires a helical beam rotating at frequency f. Appropriate variation of the electron accelerator deflection and voltage (electron velocity) could bring such a phased beam into existence at point s. Coherent radiation would occur at frequency f and at an angle θ determined by the choice of electron velocity (and even at an azimuthal angle determined by broadside phasing).

Associated experiments, such as VLF sounding, would provide the path parameters and so enable calculation of electron and wave travel times for all distances. Measurement of the delay between firing the beam and receiving an emission at the satellite would verify the emission mode and, for backward emission, would

enable postdetermination of s, f, and θ. More detailed measurements of the emitted signal (amplitude, spectrum, and variation of these), perhaps as a function of electron beam current and degree of phasing, could be used to determine radiative stability of the electron beam and nonlinear effects. Prepulses from the VLF transmitter of the satellite, either for 'pumping' natural streams or for arranging a rendezvous (after conjugate reflection) with the fired beam at point s, could be used also.

This paper examines the requirements needed to produce such beams and estimates the likelihood of meeting these requirements, concentrating on beams structured for backward Doppler-shifted radiation at zero emission angle (θ).

Resonance and Coherence Conditions

A single electron spiraling along the field line with velocity $\beta_\parallel c$ parallel to B radiates at frequency $f(\theta)$ in direction θ:

$$f = f_B/(1 + n\beta_\parallel \cos\theta)$$

where f_B is the local electron cyclotron frequency and $n(\theta)$ is the refractive index. This is also called the resonance condition (wave-electron gyrointeraction). Note that the electron can radiate at a range of frequencies and at angles subject to this condition.

Suppose now an electron beam is fired from an electron accelerator up the field but in a fixed direction at some angle to B with a parallel velocity $\beta_\parallel c$. All electrons will follow the same helical path, so the helix appears to 'screw' its way up the field line (the helix phase at any point is constant in time). The pitch of the helix is $l_0 = \beta_\parallel c/f_B$ and varies along the field line, since both $\beta_\parallel$ and f_B vary.

Suppose, instead, a more complicated system is used so that the beam direction is at a fixed angle to B but the beam rotates about B in the direction of f_B at frequency f_r. The helix now rotates (like a twist drill in use) in the sense that the heliphase at any point rotates at frequency f_r. Suppose the new helipitch is l_f. A single electron will move this distance along the field line in time $t = l_f/\beta_\parallel c$ and rotate $\omega_B t$ rad. During this time the heliphase at a fixed point rotates $\omega_r t$ rad. By definition we require 2π rad over distance l_f, so that

$$(\omega_B - \omega_r) l_f/\beta_\parallel c = 2\pi$$

$$l_f = \beta_\parallel c/(f_B - f_r)$$

If the electron accelerator is fired for a few tens of milliseconds, the resulting helix will have a length large in comparison with its pitch (l_f) but small in comparison with the dimension of the magnetosphere (L). As a helical antenna it can radiate in direction θ at frequency f, provided $l_f \cos\theta = \lambda$, i.e., if

$$\beta_\parallel c \cos\theta/(f_B - f) = c/nf \qquad (1)$$

It is not obvious (without invoking the resonance condition) that $f = f_r$, so we investigate the coherence condition from a dynamic point of view. The helix rotates like a twist drill, so that the points of constant heliphase move backward.

The heliphase velocity is

$$v_h = l_f f_r = \beta_\parallel c f_r/(f_B - f_r)$$

For a wave propagating in direction θ at frequency f, the velocity of the point of intersection of wave front and field line is

$$v_p \sec\theta = c/(n \cos\theta)$$

The phase coherence condition is $v_h = v_p \sec\theta$; hence

$$\beta_\parallel c f_r/(f_B - f_r) = c/(n \cos\theta) \qquad (2)$$

From (1) and (2),

$$f = f_r = f_B/(1 + n\beta_\parallel \cos\theta)$$

This is the resonance condition with the additional requirement that coherent emission is only possible (without rephasing the beam) at the rotation frequency f_r.

Note that, as the helical beam segment progresses along the field line (changing f_B, $\beta_\parallel$, n, and so forth), the beam remains phased for coherent emission at $f = f_r$ but at a varying angle θ (sometimes at two angles θ) over an appreciable part of the journey from the electron accelerator to the top of the field line path (equatorial plane). The radiation angle θ is determined by the resonance (and coherence) condition

$$\cos\theta = [(f_B/f) - 1]/n\beta_\parallel$$

where, in Q-L approximation,

$$n^2 = f_p^2/f(f_B \cos\theta - f)$$

(f_p is the electron plasma frequency). Substituting for n gives

$$\cos^2\theta = \frac{(f_B - f)^2}{\beta_\parallel^2 f_p^2 f}(f_B\cos\theta - f)$$

Hence solving for $\cos\theta$ gives

$$\cos\theta = \frac{(f_B - f)^2}{2f\beta_\parallel^2 f_p^2}\cdot\{f_B \pm [f_B^2 - 4f^2\beta_\parallel^2 f_p^2/(f_B - f)^2]^{1/2}\}$$

Toward the top of the field line path, there will be no solution unless

$$f_B > 2f\beta_\parallel f_p/(f_B - f)$$

which, on solving the quadratic for f_B, is

$$f_B > \tfrac{1}{2}f\{1 + [1 + 8\beta_\parallel f_p/f]^{1/2}\}$$

At the critical value of f_B the two solutions (plus and minus signs) of $\cos\theta$ merge to one: $\cos\theta = 2f/f_B$. For large f_B the minus sign solution is $\cos\theta \sim f/f_B$.

At sufficiently low heights where the lower hybrid resonance frequency (LHR) approaches and exceeds frequency f, the Q-L approximation for n (and hence $\cos\theta$) fails, and no minus sign solution exists. The plus sign solution is valid only for $\cos\theta < 1$.

Consequently, as the helical beam segment travels up along the field line, we find that coherent resonant radiation is first possible above the level for which LHR $= f$ at $\theta = \pi/2$. From there the emission angle θ falls as $\cos\theta \sim f/f_B$, and eventually the plus sign solution becomes possible. This happens first at $\theta = 0$. From there on, there are two possible angles of θ that ultimately merge to one, and after that no value of θ satisfies the resonance condition.

The point along the field line where the plus sign solution becomes valid at $\theta = 0$ is of particular interest. For $\theta = 0$, the resonance condition can be expressed as

$$(1 - \Lambda)^3 = \Lambda\beta_\parallel^2 f_p^2/f_B^2$$

where $\Lambda = f/f_B$.

By substituting the resonance condition into the expression for $\cos\theta$ it can be shown that the minus sign solution at this point is simply $\cos\theta = \Lambda/(1 - \Lambda)$.

The refractive index expression can be put in normalized (Λ) form:

$$n^2 = \frac{f_p^2/f_B^2}{\Lambda(\cos\theta - \Lambda)}$$

hence the ratio of refractive index for $\theta = 0$ to that for the other solution is $\Lambda/(1 - \Lambda)$.

Natural VLF emissions are usually triggered at $\Lambda \sim 0.1$–0.2. If we take $\Lambda = 0.2$, for example, the minus sign solution gives $\cos\theta = 0.25$ ($\theta \sim 75°$), and the wavelength for this high angle emission is one quarter that for $\theta = 0$. This finding suggests that one might inhibit (or at least discriminate against) high angle radiation by broadside phasing of parallel helical beams.

MODEL

It will be convenient for the discussion in later sections to have values for relevant parameters. The satellites planned for such active experiments will have low-altitude orbits (150–600 km, 30°–90° inclination). We will suppose that the instantaneous position of the satellite is on the $L = 4$ shell at an altitude of 500 km. The local electron gyrofrequency is then about 1.23 MHz, and the ambient electron density is about 1.3×10^{10} m^{-3}.

The electron accelerator is likely to consist of several electron guns to minimize the beam current density and to provide high total currents. The accelerator used in the artificial aurora experiment [*Hess et al.*, 1971] provided electron energies of up to 10 kev and a total beam current of 0.5 A by using ten guns mounted in a circle of the largest practical radius (~30 cm). We will assume that our accelerator provides 10-kev electrons at a total beam current of 1 A, perhaps by using 20 guns. To obtain useful broadside phasing effects, these guns would need to be distributed in an array of the order of 100 meters in diameter. Although this diameter may be within the design constraints of the planned satellite, it seems an extravagant sophistication for a minor advantage. The width of the electron beam produced by the small array in the artificial aurora experiment was enlarged by lateral diffusion to about 130 meters some 200 km downstream [*Hess et al.*, 1971]. In addition to (or in the absence of) this diffusion, the beam width in our case will

increase as the beam progresses up the field line such that the beam cross section encloses constant magnetic flux. For this model then we will assume that the beam width at any point along the field line not close to the accelerator is given by this flux conservation as if the beam diameter at the accelerator were 100 meters, whether this diameter is produced from a small array by diffusion or by a 100-meter array without diffusion.

The accelerator will be required to inject the electrons at an angle to B (the initial pitch angle ψ_A) and at a sweeping azimuthal angle as discussed later. The transverse kinetic power of the electrons (the usable component for later emission) increases with ψ_A, but the aiming accuracy and later phase spread also increases with ψ_A, and so we will use $\psi_A = 45°$ as a suitable compromise. The accelerated electrons thus have a total velocity v of 6×10^7 m/sec and initially have a parallel $v_\parallel$ and transverse $v_\perp$ velocity of about 4.2×10^7 m/sec and a radius of gyration ρ of 5.5 meters. The effective initial electron beam density is then about 1.3×10^7 m^{-3}. Since both ambient density and beam density vary roughly as $N \propto B$, the beam density will remain of the order of 10^{-3} of the ambient plasma density.

The ratio of beam transverse kinetic energy density to magnetic energy density is

$$(\tfrac{1}{2}N_e m v_\perp^2)/(B^2/2\mu_0) = \mu_0 m(v_\perp^2/B)\cdot(N_e/B)$$

To the extent that the beam density N_e is proportional to B (constant $v_\parallel$), conservation of the first adiabatic invariant ensures that this ratio is constant along the field line at about 1.5×10^{-5}. If the beam electrons have random gyrophase, this ratio is also the fractional perturbation (diamagnetic effect) of the magnetic field by the beam. This is generally negligible ($\nabla \times \mathbf{B} = 0$), though a possible cumulative effect for unphased electrons (not applicable for phased electrons) will be discussed later.

Consider now the system required to rotate the beam about B in the sense described in the previous section. Suppose the electrons from each gun of the array are deflected by angle ψ (the electron pitch angle) from B and by azimuthal angle $\phi(t)$, which is rotated at frequency f_r. This deflection produces the desired effect in that the instantaneous direction of all electrons is the same, so that all electrons make an in phase contribution to the total transverse current. The phase of this current (denoted by the azimuthal angle ϕ) then changes with time and position along the field line, as was discussed in the previous section.

Although successive electrons from a given gun have displaced guiding centers, the displacement is small ($\rho = 5.5$ meters), and it is the electron velocity direction rather than the lateral position in the beam that is of consequence. In fact, if there are mechanical advantages (and if a small correction is made to f_r), the whole array could be rotated on its axis (aligned to B).

PHASE REQUIREMENTS

In principle, the helix phase, or azimuthal direction angle ϕ of the transverse electron current, is determined at all later times and positions along the field line by its initial value at the satellite ϕ_A. However, various processes discussed below will produce both systematic and random deviations from the desired value. We first see what error we can tolerate.

Assume that the electron phases are normally and randomly disturbed about a mean, which, for convenience, we define as 0. The contribution to the wave electric (or magnetic) field E made by $dN(\phi)$ electrons having phase within a range $d\phi$ of phase ϕ is

$$dE = E_e \cos\phi \, dN(\phi)$$

where E_e is the field due to a single electron.

For a normal distribution the fraction of electrons with this phase is

$$\frac{dN(\phi)}{N} = \frac{1}{\phi_E(2\pi)^{1/2}} \exp\left(-\frac{\phi^2}{2\phi_E^2}\right) d\phi$$

where ϕ_E is the standard deviation of phase. The total field, where $E = E_0$ if all electrons are in phase, is

$$E = \frac{E_0}{\phi_E(2\pi)^{1/2}} \int_{-\infty}^{\infty} \exp\left(-\frac{\phi^2}{2\phi_E^2}\right) \cos\phi \, d\phi$$

$$= E_0 \exp(-\phi_E^2/2)$$

Thus for a standard phase error of ϕ_E rad the emitted power is reduced by ϕ_E^2 nepers or 4.3 ϕ_E^2 db. This is approximately true of a systematic distribution of phase deviation, if the deviation is azimuthally symmetric (no new preferred direction) or if the resonance condi-

tions specify the direction. Clearly phase errors of ~ 1 rad are of little consequence, though errors of a few radians are quite serious. We therefore use $\Delta\phi \sim 1$ as the criterion.

To find what this means in terms of fractional error, we require the total phase accumulated by the electron beam from the satellite (ϕ_A) to, say, the equatorial plane (ϕ_0):

$$\phi_0 - \phi_A = \int_0^s \frac{\omega_B}{v_\parallel}\, ds - \omega_r \int_0^s \frac{ds}{v_\parallel}$$

where ω_B and ω_r are the angular gyrofrequency and 'rotational' frequency, s is the distance along the field line, and subscript A is used to denote initial values at the accelerator. Since $v_\parallel$ is always within the range 4.2×10^7 m/sec (initially) to 6×10^7 m/sec (for $B \to 0$), it is convenient to assume it constant. Then

$$\phi_0 - \phi_A \approx (v_\parallel)^{-1} \int_0^s \omega_B\, ds - \omega_r(s/v_\parallel)$$

For a dipole field the first term is

$$\frac{1}{v_\parallel}\int_0^s \omega_B\, ds = \frac{La(\omega_B)_0}{v_\parallel}\int_0^\lambda \frac{1 + 3\sin^2\lambda}{\cos^6\lambda}\, d\lambda = \frac{La(\omega_B)_0}{v_\parallel}\frac{\sin\lambda}{\cos^4\lambda} \tag{3}$$

where $L = 4$, a is the radius of the earth, and λ is the latitude of a point on the $L = 4$ field line. Substituting values appropriate for our case, we find that $\phi_0 - \phi_A$ is approximately $4 \times 10^3 - 0.5\,\omega_r$ rad. The allowable fractional error is then $\Delta\phi/\phi \sim 2.5 \times 10^{-6}$.

We investigate first the accuracy that this error imposes on the electron accelerator array. The azimuthal deflection for phasing is not critical because any errors remain constant. On the other hand, variation in time or between one electron gun to another of acceleration potential V or pitch deflection ψ_A will produce cumulative errors in phase. If variations in V and ψ_A are uncorrelated, we can examine their effects separately.

For V varying by ΔV we have

$$\Delta\phi/\phi = -\Delta v/v = -\tfrac{1}{2}\Delta V/V$$

Thus for phasing near the equator we require $\Delta V/V \sim 5 \times 10^{-4}$ or $\Delta V \sim 0.05$ volt. This criterion could be met if the accelerating potential for all guns is provided from the same supply and if the supply is constant to this order for the duration of firing (tens of milliseconds).

A deviation of $\Delta\psi_A$ in the initial pitch angle ψ_A will produce a change in $v_\parallel$ at any point (denoted by the magnetic field B) by

$$\Delta v_\parallel = -v\frac{B}{B_A}\frac{\sin\psi_A\cos\psi_A}{[1 - (B/B_A)\sin^2\psi_A]^{1/2}}\Delta\psi_A$$

Taking the square root term as approximately 1, we find that two electrons differing only in initial pitch angle will drift apart by Δs in time t where

$$\Delta s \approx \frac{v\sin\psi_A\cos\psi_A\,\Delta\psi_A}{B_A}\int_0^t B\, dt$$

If we use the ratio of gyrofrequencies instead of B/B_A, the integral becomes $\int_0^t \omega_B\, dt = \phi$, and thus

$$\Delta s = \frac{v\sin\psi_A\cos\psi_A}{(\omega_B)_A}\phi\Delta\psi_A$$

This result corresponds to a phase difference in the vicinity of the equator (subscript 0) of

$$\Delta\phi = [(\omega_B)_0/v]\,\Delta s$$

Thus

$$\Delta\phi = (B_0/B_A)\sin\psi_A\cos\psi_A\phi\Delta\psi_A \tag{4}$$

For $\Delta\phi \sim 1$, $\psi_A = 45°$, and $B_0/B_A = 0.010$, this gives $\Delta\psi \sim 0.03°$. A deflection accuracy and individual gun beam width of this order should not be difficult to attain.

If emission in the direction of B is desired, lateral diffusion of guiding centers, such as might be produced by electric field gradients, would be advantageous rather than detrimental. On the other hand, even a small accumulated deflection of electron velocities in the ψ direction could be serious.

From *Spitzer* [1962] the rate of increase of the mean square deviation (in the ψ direction) by Coulomb scattering is given in mksa units by

$$\frac{d}{dt}(\Delta\psi)^2 = \frac{Ne^4}{4\pi m^2 v^3 \epsilon_0^2}\ln\Sigma$$

where N is the ambient plasma density, e and m are the electronic charge and mass, and Σ is the integration cutoff parameter defined and tabulated by *Spitzer* [1962]. From these tables, $\ln\Sigma \sim 33$, and thus

$$d/dt\,(\Delta\psi)^2 = 1.2 \times 10^{-16}\,N$$

For $N = 1.3 \times 10^{10}$ m^{-3}, the rate of increase of the mean square deviation is about 1.6×10^{-6} sec^{-1}. Since the travel time to the equator is about 0.5 sec, the phase spread would exceed 1 rad if this rate were constant. However, the rate is decreasing in time as a typical electron travels up the field line toward the equator. Thus after time t, by which time the electron has reached point C,

$$(\Delta\psi)_C^2 = 1.2 \times 10^{-16} \int_0^t N\,dt$$

It is convenient and not too unrealistic (it gives a slight overestimate of the phase spread) to assume that $N \propto \omega_B$, for then

$$(\Delta\psi)_C^2 = 1.2 \times 10^{-16}\,(N/\omega_B)_0(\phi_C - \phi_A)$$

where $\phi_C - \phi_A$ is the gyrophase accumulated by the electron in traveling from the accelerator to point C.

We can modify (4) to apply to point C by changing the subscripts. Also, since $\psi_c < 45°$, we make the further approximations:

$$\sin\psi_C \sim (B_C/2B_A)^{1/2} \qquad \cos\psi_C \sim 1$$

If the Coulomb scattering is now 'turned off,' the mean square deviation of phase at the equator produced by $(\Delta\psi)_C^2$ is

$$(\Delta\phi)^2 = 1.2 \times 10^{-16}\,N_0 \cdot \frac{B_0}{2B_A}\left[(\phi_0 - \phi_C)^2\,\frac{(\phi_C - \phi_A)}{(\omega_B)_C}\right]$$

where $\phi_0 - \phi_C$ is the gyrophase accumulated by the electron in traveling from point C to the equator. The value of the term in the square brackets depends on the position of C. From (3) it can be shown that this term is largest for C at about $\lambda \sim 50°$. If we neglect the phase spread at this point and the additional phase spread produced by further pitch angle spread at lower latitudes ($\lambda < 50°$), we get $(\Delta\phi)^2 \sim 0.3$. We can tolerate a mean square deviation of phase of at least 3 times this amount, so Coulomb scattering is not likely to be serious.

The finite size of the electron beam will produce a small systematic phase error (if it is not allowed for) in the vicinity of the equator, because the gyrophase paths on opposite sides of the beam will differ slightly. If we neglect 'rotation' (at ω_r) for the moment, this error is

$$\Delta\phi = \Delta\left[\int_0^s (\omega_B/v_\parallel)\,ds\right]$$

Now, since the electron beam does not significantly perturb the magnetic field, the field is essentially curl free or conservative. Our phase reference surfaces at the satellite and elsewhere are surfaces normal to B and so are magnetic equipotentials. Consequently

$$\Delta\left[\int_0^s \omega_B\,ds\right] = 0$$

which physically means that the slightly increased path distance along the outermost side of the beam is exactly compensated by the slightly reduced gyrofrequency. For any short distance ds the fractional error in phase is produced entirely by the fractional change in $v_\parallel$:

$$\frac{d(\Delta\phi)}{d\phi} = -\frac{\Delta v_\parallel}{v_\parallel}$$

From the first adiabatic invariant (subscript m referring to the mirror point),

$$v_\parallel = v[1 - (B/B_m)]^{1/2}$$

We can then express the fractional phase error in terms of the change in B across the beam at the point we are considering (one within ds) and also across the same flux tube extrapolated down to the mirror point of the electron. Thus

$$\frac{d(\Delta\phi)}{d\phi} = \frac{1}{2}\left(\frac{\Delta B}{B} - \frac{\Delta B_m}{B_m}\right)\Big/\left(\frac{B_m}{B} - 1\right)$$

Since $\nabla \times \mathbf{B} = 0$, $(R)^{-1} = -(B)^{-1}\,\partial B/\partial R$, where R is the radius of curvature of the field line. Hence $\Delta B/B = -D/R$, where D is the beam diameter. Since the beam cross section varies to enclose the same magnetic flux,

$$D = D_A(B_A/B)^{1/2}$$

and, for a dipole magnetic field,

$$\frac{1}{R} = \frac{3}{La}\,\frac{1 + \sin^2\lambda}{\cos^4\lambda(1 + 4\tan^2\lambda)^{3/2}}$$

Substituting appropriate values, we find that the fractional change in $v_\parallel$ varies monotonically from about 3×10^{-7} at the equator to about 8.5×10^{-7} at the satellite. If we take the largest value as applying at all points, the upper

limit on the phase error near the equator is about 0.3 rad.

If we now consider the superimposed 'rotation' (at ω_r), we find that the fractional rotation phase error in the vicinity of the equator is approximately

$$\Delta\phi_r/\phi_r = (\Delta s/s) - (\Delta v_{\parallel}/v_{\parallel})$$

The first term is about 100 times the second, and for a dipole field it can be shown to be

$$\frac{\Delta s}{s} = \frac{D_0}{aL} + \frac{D_A L}{s}(1 + 3\sin^2\lambda)^{1/2}\cos\lambda$$
$$= 5 \times 10^{-5}$$

where D_0 and D_A are the beam diameters at the equator and satellite and appropriate values ($\lambda = 60°$, and so forth) have been substituted. Taking $\omega_r = 17 \times 10^3$ rad/sec, which is the resonance frequency for 10-kev electrons near the equator, we find $\phi_r \sim 10^4$, so that $\Delta\phi_r \sim \frac{1}{2}$ rad. These two effects are in the same sense and so are perhaps large enough to warrant a correction. This is readily done by advancing the phase of the rotation signal of the accelerators on the poleward side of the array over those on the equatorward side by this amount.

An alternative mode of operation would be to program or sweep the acceleration potential and both the azimuthal and the pitch deflection so that the electrons would arrive in phase at the desired point. This might help prevent premature emission, for the electrons would not be phased for coherent emission at any angle before reaching the desired point. However, in this case the electrons are moving relative to one another. The resulting mutual magnetic interaction or diamagnetic effect reduces B, and hence ω_B, by about 1.5 parts in 10^5, as was determined in the section on the model. Electrons whose guiding centers stay near the center of the beam throughout the travel from the accelerator to, say, the equator accumulate about 6 rad less gyrophase than those near the periphery of the beam. This value is too large for correction by phase adjustment at the accelerator array. However, both this effect and the systematic effect discussed previously apply only if the guiding centers of individual electrons keep their relative lateral positions within the beam throughout their progress along the field line. If there is appreciable lateral mixing or diffusion, all electrons are treated equally, and both systematic effects vanish.

To sum up this section, none of the phase spreading processes considered appear serious, and the accuracy required of the accelerator is not too demanding. Provided that processes not considered (e.g., scattering by time and spatially varying fields) are also unimportant, phased electron beams appear feasible. This applies for a 'firing' or initial pitch angle of 45°. If instead ψ_A is increased to 90° (satellite at mirror point), the situation is changed greatly. The gyrophase accumulated from satellite to equator increases about twofold, as does the required accuracy of the acceleration voltage. The initial pitch angle error or spread $\Delta\psi_A$ must be held to $<10^{-5}$ rad, and, even if this is technically obtainable, Coulomb scattering will produce about this spread within 60 μsec.

RADIATED POWER

The power flux radiated by the phased electrons is given by *Helliwell* [1967]:

$$W = \int J_{\perp} E \cos\chi \, ds \qquad \text{w/m}^2$$

where $J_{\perp}$ is the transverse current density, E is the intensity of the circularly polarized electric field, and χ is the phase angle between the transverse current and the wave electric field. We will consider only radiation at $\theta = 0$ and assume for the moment zero phase spread ($\phi_s = 0$).

At some preselected point (defined $s = 0$ for convenience) along the field line the beam electrons become resonant and phased for coherent radiation at $f = f_r$ and $\theta = 0$ if we neglect any perturbations of phase produced by the radiated wave. These perturbations of the phase and even of the transverse energy of the electrons may ultimately be quite large and may begin just before the leading edge of the electron beam segment reaches the preselected point ($s = 0$), because the electron heliphase will be nearly right for coherent emission. However, to get an estimate of the radiated power, we will assume that radiation begins only when the leading edge of the electron beam segment reaches the preselected point ($s = 0$), and we will consider only the initial power radiated by resonant electrons as the initial wave sweeps back along the field line and electron beam segment toward

the satellite. We will assume also that the length of the electron beam segment is not a limiting factor, though it will be simple to vary the segment length (through firing duration) for experimental investigations of the processes mentioned above.

For this case then at $s = 0$ the radiated phase velocity v_p and the electron beam heliphase velocity v_h are equal, say, v_0. The expressions for v_p and v_h, given in the section on resonance and coherence conditions, show that these velocities do not remain equal as the radiated wave and the heliphase pattern propagate toward the satellite but are changed by different amounts and in opposite directions, as

$$\Delta v_p/v_p = \tfrac{1}{2}\Delta f_B/(f_B - f)$$
$$\Delta v_h/v_h = -\Delta f_B/(f_B - f)$$

where we have neglected the variation of f_p and $v_\parallel$. Any two reference points of constant heliphase and wave phase initially coincident at $s = 0$ drift apart elsewhere at a relative velocity of

$$\Delta v = v_p - v_h = \Delta v_p - \Delta v_h$$

That is,

$$\Delta v/v = \tfrac{3}{2}\Delta f_B/(f_B - f)$$
$$= \tfrac{3}{2}(f_B - f)^{-1}\, df_B/ds\, s$$

At s the two reference points have drifted apart by

$$\Delta s = \tfrac{3}{4}(f_B - f)^{-1}\, df_B/ds\, s^2$$

If we assume that the wave electric field and the transverse current are in phase ($\chi = 0$) at $s = 0$, the phase difference at s is

$$\chi(s) = (3\pi/2)\, df_B/ds(s^2/v_\parallel)$$
$$= Ks^2$$

where use has been made of the resonance condition $v_\parallel$ and K will be regarded as effectively constant in the region of interest (s is small).

Following *Helliwell* [1967], the power flux radiated from a small slab of the beam at s of thickness ds is given by

$$dW = EJ_\perp \cos(Ks^2)\, ds \qquad \mathrm{w/m^2}$$

But $W = E^2/Z$, where $Z = 377/n$ ohms, so that we can write the expression above with variables separated as

$$\int_0^{W_{max}} \frac{dW}{W^{1/2}} = Z^{1/2} J_\perp \int_0^{s'} \cos(Ks^2)\, ds$$

The integrand on the right is large only for small s, so for mathematical convenience we will set the upper integration limit as $s' = \infty$:

$$W_{max} = \frac{3\pi^2}{64} v_\parallel Z J_\perp{}^2 \left(\frac{df_B}{ds}\right)^{-1} \qquad (5)$$

We wish to find the total power (watts) radiated by the electron beam as a function of the position or latitude of the preselected point. Although the width of the electron beam is not large in comparison with the radiated wavelength, we will assume that this power is given by

$$P_c = W_{max} A \propto J_\perp{}^2 A$$

where A is the beam cross section area at the preselected point. We use subscript c to denote 'calculated power,' for, as we will find below, substitution of the numerical values of our model case gives powers greater than the transverse kinetic power of the electrons.

Now

$$J_\perp{}^2 A = N_s{}^2 e^2 v_\perp{}^2 A$$

From the first adiabatic invariant and the assumption that the beam cross section encloses constant magnetic flux, $v_\perp{}^2 A$ is constant. The beam density is approximately proportional to B; so, for an accelerator current I, an initial pitch angle (firing angle) of 45°, and an initial beam area of A_A,

$$J_\perp{}^2 A = \tfrac{1}{2}(I^2/A_A)(B/B_A)^2$$

Substituting these expressions and the expression for n and making further use of the resonance condition, we get

$$P_c = 123c\left[\frac{\beta_\parallel I}{Df_B}\right]_A^2 f_B \frac{f}{f_B - f}\left(\frac{df_B}{ds}\right)^{-1} \cdot \exp(-\phi_E{}^2)$$

Table 1 shows the calculated powers P_c for our model, for $I = 1$ amp and $\phi_E = 1$ rad, and for various chosen points along the field line. In all cases, P_c is considerably greater than the available transverse kinetic power P_K of the electrons. It appears that we can stand a greater phase spread ($\phi_E \sim 2$ or 3) and still

obtain an appreciable fraction of the kinetic power as radiated power. It is interesting to note that, even if the radiated power is only a few tens of watts, the power flux is still of the order of 10^{-4} w m^{-2}, which is greater than that achievable by ground-based VLF transmitters by some 6 orders of magnitude [*Helliwell*, 1965] and is greater than that of natural VLF emissions by some 8 orders of magnitude [*Helliwell*, 1967]. This suggests that very low beam currents, even as low as those used in television picture tubes (few hundred microamperes), should produce detectable signals and trigger sustained VLF emissions in suitable natural electron streams. Alternatively, with beam currents up to 1 A available, nonlinear effects in both radiation from artificial beams and from triggering of emissions in natural electron streams could be investigated experimentally by varying both the beam current and beam length (firing duration).

RADIATIVE INSTABILITY

In a recent artificial aurora experiment [*Hess et al.*, 1971] involving field-aligned (low pitch angle) electron beams of current and energy similar to those proposed here, plasma instabilities were not evident (no radiation was observed), and any that may have occurred did not appreciably disorganize the beams. Even though our criterion for disorganization (phase spread) is much more stringent than theirs (beam disruption), the amplitude of an instability grows exponentially, so that an amplitude strong enough to produce serious phase spread would, after a few more e folds, produce effects looked for (but not found) by Hess et al. Since, as they pointed out, the calculated growth rates for, say, two-stream instabilities between the beam and the ambient plasma are enormous, their result is an encouraging sign that phase spread is not serious either. Although this does not resolve the point, such general instabilities have received considerable theoretical attention in the past and so will not be reconsidered here.

On the other hand, we might expect helical beams, unlike those used in the artificial aurora experiment, to be particularly prone to radiative instability in the Doppler-shifted cyclotron mode. This instability, if it is significant, would effectively mean that we could not control the emission point by prephasing, for the beam would radiate prematurely and so destroy the phasing, even if it did not appreciably affect the beam in other ways (e.g., beam width, energy, and pitch distribution).

TABLE 1. Calculated Powers P_c for Our Model, for $I = 1$ amp and $\phi_E = 1$ rad, and for Various Chosen Points along the Field Line

λ, deg	f_B, kHz	f, kHz	P_c, kw	P_K, watts
40	100	45	15	400
32	50	18	6	200
18	20	4.6	2	80
10	15	2.9	2	60
5	14	2.7	4	60

Fortunately, our rather special case of a delta function velocity distribution (monoenergetic, monopitched electrons) has been considered by *Fung* [1966]. His treatment strictly applies only in a uniform medium and for streams of unlimited lateral extent and so requires some modification for our case. It also gives only the initial growth rate (small signal or linear approximation), but that is all we need in this study. Since he shows that the growth rate is maximum for $\theta = 180°$ (backward emission at $\theta = 0$ in our convention) and that only frequencies close to the frequency emitted at $\theta = 180°$ are amplified appreciably, we will consider this case only. For narrow streams, this choice is further justified, since only field-aligned emission would stay in the beam.

With this and the further approximation $n^2 \gg 1$, Fung's expression for the temporal growth rate δ (reciprocal of the e folding time) simplifies to

$$\delta = \pi(3)^{1/2}[\beta_\perp{}^2 f_s{}^2 f_B \Lambda(1 - \Lambda)]^{1/3}$$

where f_s is the stream plasma frequency and Λ is the resonance frequency normalized to the local cyclotron frequency. This expression is the same for all electrons at a given point (all have the same $v_\parallel$), so amplification or growth occurs only at a single frequency (for $\theta = 0$) at that point.

When we use the first adiabatic invariant and assume that the beam is confined to a flux tube,

$$\delta = \pi(3)^{1/2}\left(\beta_\perp \frac{f_s}{f_B}\right)_A^{2/3} \Lambda^{1/3}(1 - \Lambda)^{1/3} f_B$$

$$= 0.23 f_B \Lambda^{1/3}(1 - \Lambda)^{1/3}$$

where subscript A refers to values at the satellite and numerical substitution for these values in our case has been made.

We will assume that the only important effect of a nonuniform medium is restriction of the duration of growth. The effect of finite beam width will be considered later, so initially we will assume that the wave energy stays within the beam.

The duration of growth at any given frequency is limited by the rate of change of the resonance condition as the wave propagates along the beam. If the wave is effectively in resonance for time Δt, it travels a distance $v_p \Delta t$ over which the resonance frequency of the electrons changes by

$$\Delta f = df/ds\, v_p\, \Delta t$$

Now, restricting the resonance time to Δt broadens the resonance frequency by Δf, where $\Delta f \cdot \Delta t \sim 1$. Hence the effective resonance (and growth) duration is

$$\Delta t \sim (df/ds\, v_p)^{-1/2}$$

For an electron beam of unlimited lateral extent the power amplification in nepers at frequency f would be $2\delta\Delta t$. In our case the beam width is only of the order of a wavelength, so we need to take account of the diffraction loss of energy from the beam.

Consider a narrow electron beam extending indefinitely in an effectively uniform medium along the field line from any point of interest, which for convenience we will call $s = 0$. The electrons travel in the direction of increasing s, and the wave travels in the opposite direction, i.e., toward $s = 0$. This beam will act as an end fire antenna of indefinite length for which in phase transverse current density (coherent electrons) increases exponentially with distance toward $s = 0$. We wish to find its radiation polar diagram (power emitted versus θ). If we take $s = 0$ as reference, the phase of the contribution from an element at s and for direction θ is

$$\chi(s, \theta) = (\omega/c)s[n(\theta) \cos \theta - n(0)]$$
$$= \alpha s$$

where ω is the angular frequency and $n(\theta)$ and $n(0)$ are the refractive indices for directions θ and $\theta = 0$. The contribution to the field (electric or magnetic) at $s = 0$ from this element of length ds for direction θ is then

$$dE(\theta) = \epsilon\, ds \exp(-\gamma_e s) \cos \alpha s$$

where ϵ contains constant quantities and γ_e is the effective (including diffraction losses) spatial growth rate of the coherent current in nepers per meter. The total field at $s = 0$ for direction θ is then

$$E(\theta) = \epsilon \int_0^\infty \exp(-\gamma_e s) \cos \alpha s\, ds$$
$$= [\gamma_e/(\gamma_e^2 + \alpha^2)]\epsilon$$

Normalized to direction $\theta = 0$,

$$\frac{E(\theta)}{E(0)} = \frac{\gamma_e^2}{\gamma_e^2 + \alpha^2}$$

and the total power emitted within a range of wave-normal angles of θ_c is then proportional to

$$\int_0^{\theta_c} \frac{\sin \theta\, d\theta}{[1 + (\omega/\gamma_e c)^2(n(\theta) \cos \theta - n(0))^2]^2}$$

The term in the square brackets can be rewritten as

$$1 + \left(\frac{\omega}{\delta_e}\right)^2\left(\frac{n(\theta) \cos \theta}{n(0)} - 1\right)^2$$

where δ_e is the effective growth rate in time. Since $\delta \ll \omega$, the integrand is small unless $n(\theta) \cos \theta \sim n(0)$.

This happens at all frequencies for $\theta \sim 0$ and at a higher angle as well for $\Lambda < \frac{1}{2}$. However, the rate of change of the term in θ with θ is relatively fast in the high angle case, so we will neglect the contribution this case makes to the integral. Consequently, we can say that most of the power is radiated within a range of wave normal angles θ_c for which

$$\frac{\delta_e}{\omega} = \left|\frac{n(\theta_c) \cos \theta_c}{n(0)} - 1\right|$$

Substituting the whistler mode refractive index expression and using approximations appropriate for $\theta_c^2 \ll 1$, we get

$$\theta_c^2 = \frac{\delta_e}{\omega} \frac{4(1 - \Lambda)}{|1 - 2\Lambda|}$$

This power is emitted within a cone of semiangle θ_R, where θ_R is the ray direction angle corresponding to θ_c. Again, for small angles,

$$|\theta_R| = \frac{|1 - 2\Lambda|}{2(1 - \Lambda)}\,\theta_e$$

Hence

$$\theta_R^2 = \frac{|1 - 2\Lambda|}{1 - \Lambda}\,\frac{\delta_e}{\omega}$$

Note that δ_e determines the effective length of the electron beam and hence the width of the radiation cone. We now use this expression to estimate the diffraction loss.

Consider a small element ds of the electron beam as shown in Figure 1. Over this distance the net gain in wave power flux is dW. If the electron beam has cross section A, the net gain in power is

$$A\,dW = AW\gamma\,ds - W\,dA$$

where γ is the intrinsic (i.e., for a beam without diffraction loss) growth rate per unit distance and dA is the increase in area over which this power is spread. Expressing dA in terms of θ_R, we find

$$\begin{aligned} A\,dW &= AW\gamma\,ds - 2\pi(A/\pi)^{1/2}W\theta_R\,ds \\ &= [\gamma - 2\theta_R(\pi/A)^{1/2}]\,AW\,ds \\ &= \gamma_e AW\,ds \end{aligned}$$

Hence

$$\gamma_e = \gamma - 2\theta_R(\pi/A)^{1/2}$$

Using $\gamma\lambda/2\pi = \delta/\omega$ and substituting for θ_R, we get a quadratic in δ, for which the first-order (i.e., $\delta \ll \omega$) solution is

$$\frac{\delta_e}{\omega} = \frac{\pi}{2}\,\frac{A}{\lambda^2}\,\frac{1 - \Lambda}{|1 - 2\Lambda|}\left(\frac{\delta}{\omega}\right)^2$$

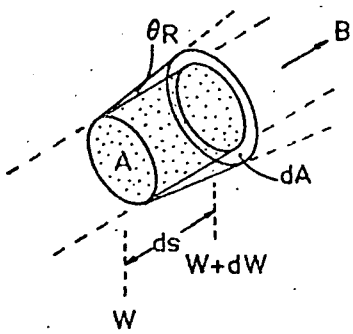

Fig. 1. Short section of electron beam used to determine effective growth rate in terms of the diffraction cone.

TABLE 2. Effective Growth Rate δ_e, Growth Duration Δt, and hence Amplification at Selected Points along the Field Line

Latitude, deg	f_B, kHz	f, kHz	δ_e, sec^{-1}	Δt, msec	Amplification, db
57	1000	800	55	0.1	0.04
51	400	240	53	0.3	0.1
40	100	45	80	1	0.7
32	50	18	24	3	0.6
18	20	4.6	10	8	0.7
10	15	2.9	9	14	1.1
5	14	2.7	8	18	1.3

Substituting for δ, we find

$$\delta_e = \frac{3}{4}\frac{\pi^2}{c^2}\left[(Af_B)\left(\beta_\perp\frac{f_e}{f_B}\right)^{4/3}\right]_A \cdot f_p^2\,\frac{\Lambda^{2/3}(1 - \Lambda)^{2/3}}{|1 - 2\Lambda|}$$

The effective growth rate δ_e, growth duration Δt, and hence amplification in db are given in Table 2 at selected points along the field line.

In order for a passing whistler to rephase the beam electrons completely and thus produce premature emission, the amplification required is of the order of 100 db, except near the point where emission is desired. From Table 2 it would appear that the amplification is always so low that the prephasing will not be significantly affected.

At $\Lambda \sim 0.5$, which occurs a little above 40° latitude, the effective growth rate δ_e, according to the expression above, becomes very large. Although the expression is not valid there, since the assumptions in its derivation are violated, we might assume at worst that the diffraction loss becomes negligible, so that δ_e increases to δ, which is about 1.5×10^4 sec^{-1}. The physical reason for this increase is that a small but finite range of emission or wave normal angles θ about 0 (the diffraction cone) can collapse into a single ray direction of 0, i.e., along the field and electron beam. However, this high value of $\delta_e = \delta$ applies only to $\Lambda = 0.5 \pm 3 \times 10^{-4}$. The beam electrons or a resonant wave (since $v_p = v_\parallel$ at $\Lambda = 0.5$) will traverse this range of Λ in about 0.2 msec, so the amplification is only about 3 nepers or 26 db. If we regard the presence of a strong signal (the appropriate part of a whistler) at the critical time and place

to be an unlikely event, this is probably not serious.

It would appear that cyclotron radiative instability is not a problem, so that prephasing is still feasible. If through neglecting some effect this conclusion is wrong, interesting experiments could still be made. For example, if the stability is marginal, control of the emission point along the field line might be possible by programming $v_\parallel$ at the accelerator to produce a large Δt (the duration of resonance) at a desired point and hence enhanced amplification at that point.

THE HM EMISSIONS BY A PROTON BEAM

Micropulsation pearls or hm emissions are thought to be the proton counterpart of VLF emissions; i.e., hm emissions are produced by backward Doppler-shifted cyclotron resonance of fast protons with waves in the proton cyclotron mode. It will be interesting to see if hm emissions can be produced or triggered artificially by a proton beam of the same energy and current as the electron beam considered for the VLF case, since hm emissions probably cannot be triggered artificially from the ground. Although hm emissions generally occur on L shells of about 4–8 [*Jacobs*, 1970], it will be convenient to consider the same model ($L = 4$, and so forth) that we used above. The proton counterparts of the parameters f_p, v, β, ϕ, and $1/\rho$ are scaled down by the square root of the electron-proton mass ratio (43), though f_B is scaled by the mass ratio (1840). Thus the proton cyclotron frequency f_B ranges from 670 Hz at the satellite to 7.2 Hz at the equator, the proton velocity is 1.4×10^6 m/sec, and the radius of gyration ρ is initially (for $\psi_A = 45°$) 235 meters. A 100-meter diameter array of proton accelerators would produce negligible additional broadside phasing, since the beam diameter using the same method of rotation would be at least 4ρ, so that the beam at all points along the field line is about 10 times the diameter of the electron beam considered above. The beam density and diamagnetic effect are thus lower than the beam density and diamagnetic effect considered in the electron case by about 2 orders of magnitude.

However, the basic processes and the mechanism for production of emissions at a desired point by a prephased beam are the same. We now consider minor differences, mainly in magnitude, under the same section headings.

Resonance and coherence conditions. The formal treatment above still applies (same resonance condition) except that the proton cyclotron mode refractive index is given by [*Dowden*, 1965]

$$n^2 = (f_p/f_B)^2[1 - \tfrac{1}{2}\sin^2\theta - (\tfrac{1}{4}\sin^4\theta + A^2\cos^2\theta)^{1/2}]^{-1}$$

This is more anisotropic than the VLF whistler mode. In particular, $n\cos\theta$ decreases monotonically (and quite slowly) with increasing θ. One effect of this is that a prephased proton beam segment progressing along the field line is phased for coherent emission (at $f = f_r$) at a varying but single angle θ. Another is that the resonance frequency is almost independent of θ, being always within 8% of the value for $\theta = 0$ [*Dowden*, 1968]. In this case ($\theta = 0$), the normalized resonance frequency is given by

$$(1 - A)^{3/2}/A = \beta_\parallel f_p/f_B$$

Thus, at the equator, $f_p = 2.7$ kHz and $f_B = 7.2$ Hz, and thus $A = 0.32$ or $f = 2.3$ Hz.

Phase requirements. The total phase accumulated by the proton beam from the satellite to the equator is only about 10^4 rad. The proton accelerator potentials need only be held to within about 0.02% or 2 volts, whereas the deflection (ψ_A) accuracy and individual gun beam width required is $\Delta\psi_A \sim 1°$. Coulomb scattering and the other phase spreading effects considered above are quite trivial in the proton case.

The phase requirements are thus easily met at $L = 4$ and are not likely to be bothersome at higher L where hm emissions occur naturally.

Radiated power. We can still use (5) to find $P_e = WA$. The parameters are reduced: $v_\parallel$ by 40-fold, $J_\perp A$ by 100-fold, Z by 20-fold, and df_B/ds by about 2000-fold. The total effect of this reduction is to reduce P_e by about 40-fold, which is still several tens of watts and is of the order of P_K, the transverse kinetic power of the protons. Thus we might expect radiated power fluxes of the order of 10^{-4} w m^{-2}, which is greater than those of natural hm emissions by some 2 or 3 orders of magnitude.

Radiative instability. The electron cyclotron instability at VLF is less easily modified to the

proton case. However, since the proton beam diameter is a very small fraction (1/30) of the wavelength, the effective growth rate is probably negligible. Also, the only singularity ($\theta_R = 0$ for a range of θ) equivalent to that at $\Lambda = 0.5$ in the electron case occurs in the limit $\Lambda = 0$ in the proton case and so is not a real problem.

It appears then that artificial production of hm emissions by prephased proton beams is quite feasible. Electron beams (for VLF) and proton beams (for hm), both of 10 kev, might conveniently be fired together, though a firing duration of a few seconds would be more appropriate for protons.

CONCLUSIONS

Production of both VLF emissions at desired points by prephased electron beams and hm emissions by proton beams appears feasible. The phase spread by various factors and the cyclotron radiative instability do not appear to be serious or critically dependent on the model chosen for illustration here. The technology required and the feasibility of other aspects not considered here have been achieved and demonstrated in the artificial aurora experiment of *Hess et al.* [1971]. Broadside phasing by parallel helical beams could be achieved by a large (100 meters) array of guns but may occur naturally through lateral diffusion of guiding centers.

The calculated emitted power levels are larger than the transverse kinetic power by 1 or 2 orders of magnitude, a fact suggesting that there is considerable leeway in phase spread, guiding center diffusion, and so forth. Alternatively, if this power leeway is not needed for this, it could be used to investigate nonlinear effects, effects of degraded phasing, or considerably reduced beam current or firing duration.

Acknowledgments. I wish to thank N. R. Thomson for detailed criticism of the first draft.

* * *

The Editor thanks T. J. Rosenberg and F. L. Scarf for their assistance in evaluating this paper.

REFERENCES

Dowden, R. L., 'Micropulsation mode' propagation in the magnetosphere, *Planet. Space Sci., 13*, 761, 1965.

Dowden, R. L., Dotted pearl micropulsations, *J. Geophys. Res., 73*, 2995, 1968.

Fung. P. C. W., Excitation of backward Doppler-shifted cyclotron radiation in a magneto-active plasma by an electron stream, *Planet. Space Sci., 14*, 335, 1966.

Helliwell, R. A., *Whistlers and Related Ionospheric Phenomena*, Stanford University Press, Palo Alto, Calif., 1965.

Helliwell, R. A., A theory of discrete VLF emissions from the magnetosphere, *J. Geophys. Res., 72*, 4773, 1967.

Hess, W. N., M. C. Trichel, T. N. Davis, W. C. Beggs, G. E. Kraft, E. Stassinopoulos, and E. J. R. Maier, Artificial aurora experiment: Experiment and principal results, *J. Geophys. Res., 76*, 6067, 1971.

Jacobs, J. A., *Geomagnetic Micropulsations*, Springer, Berlin, 1970.

Rosenberg, T. J., R. A. Helliwell, and J. P. Katsufrakis, Electron precipitation associated with discrete very low frequency emissions, *J. Geophys. Res., 76*, 8445, 1971.

Spitzer, L., *Physics of Fully Ionized Gases*, Interscience, New York, 1962.

(Received June 29, 1972;
accepted September 29, 1972.)